

UNCLASSIFIED

AD NUMBER
ADB045248
NEW LIMITATION CHANGE
TO Approved for public release, distribution unlimited
FROM Distribution authorized to U.S. Gov't. agencies only; Test and Evaluation; Jul 1979. Other requests shall be referred to Air Force Materials Laboratory, Attn: AFML/MBC, Wright-Patterson AFB, OH 45433.
AUTHORITY
AFWAL ltr, 3 Aug 1983

THIS PAGE IS UNCLASSIFIED

MLBP/FILE CY.

AFML-TR-79-4115

ADB045 248

OFFICIAL FILE COPY

DO NOT REMOVE

SOLUTION PROCESSING — RODLIKE POLYMERS

G. C. BERRY

C. -P. WONG

S. VENKATRAMEN

S. -G. CHU

CARNEGIE-MELLON UNIVERSITY

4400 FIFTH AVENUE

PITTSBURGH, PENNSYLVANIA 15213

AUGUST 1979

TECHNICAL REPORT AFML-TR-79-4115

Final Report for period April 1977 — April 1979

Distribution limited to U. S. Government agencies only; Test and Evaluation, July 1979.
Other requests for this document must be referred to the Air Force Materials Laboratory
Nonmetallic Materials Division, AFML/MBC, Wright-Patterson Air Force Base, Ohio
45433.

AIR FORCE MATERIALS LABORATORY

AIR FORCE WRIGHT AERONAUTICAL LABORATORIES

AIR FORCE SYSTEMS COMMAND

WRIGHT-PATTERSON AIR FORCE BASE, OHIO 45433

20040226235

BEST AVAILABLE COPY

NOTICE

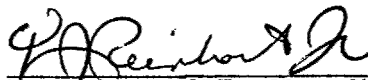
When Government drawings, specifications, or other data are used for any purpose other than in connection with a definitely related Government procurement operation, the United States Government thereby incurs no responsibility nor any obligation whatsoever; and the fact that the government may have formulated, furnished, or in any way supplied the said drawings, specifications, or other data, is not to be regarded by implication or otherwise as in any manner licensing the holder or any other person or corporation, or conveying any rights or permission to manufacture, use, or sell any patented invention that may in any way be related thereto.

This technical report has been reviewed and is approved for publication.




THADDEUS E. HELMINIAK
Project Monitor

FOR THE COMMANDER



T. J. REINHART, JR., Chief
Composites, Adhesives & Fibrous
Materials Branch
Nonmetallic Materials Division


J. M. KELBLE, Chief
Nonmetallic Materials Division

Copies of this report should not be returned unless return is required by security considerations, contractual obligations, or notice on a specific document.

UNCLASSIFIED

SECURITY CLASSIFICATION OF THIS PAGE (When Data Entered)

REPORT DOCUMENTATION PAGE		READ INSTRUCTIONS BEFORE COMPLETING FORM
1. REPORT NUMBER AFML-TR-79-4115	2. GOVT ACCESSION NO.	3. RECIPIENT'S CATALOG NUMBER
4. TITLE (and Subtitle) "Solution Processing--Rodlike Polymers"		5. TYPE OF REPORT & PERIOD COVERED Final Report April 1977-April 1979
		6. PERFORMING ORG. REPORT NUMBER
7. AUTHOR(s) G. C. Berry, Principal Investigator C. -P. Wong S. Venkatramen S. G. Chu		8. CONTRACT OR GRANT NUMBER(s) F33615-77-C-5061
9. PERFORMING ORGANIZATION NAME AND ADDRESS Carnegie-Mellon University 4400 Fifth Avenue Pittsburgh, PA 15213		10. PROGRAM ELEMENT, PROJECT, TASK AREA & WORK UNIT NUMBERS ILIR0093
11. CONTROLLING OFFICE NAME AND ADDRESS Air Force Materials Laboratory (AFML/MBC) Air Force Wright Aeronautical Laboratories Wright-Patterson AFB, Ohio 45433		12. REPORT DATE August 1979
		13. NUMBER OF PAGES 289
14. MONITORING AGENCY NAME & ADDRESS (if different from Controlling Office)		15. SECURITY CLASS. (of this report) UNCLASSIFIED
		15a. DECLASSIFICATION/DOWNGRADING SCHEDULE
16. DISTRIBUTION STATEMENT (of this Report) Distribution limited to U.S. Government agencies only; test and evaluation, July 1979. Other requests for this document must be referred to the Air Force Materials Laboratory, Nonmetallic Materials Division, Composites, Adhesives and Fibrous Materials Branch, AFML/MBC, Wright-Patterson Air Force Base, Ohio 45433.		
17. DISTRIBUTION STATEMENT (of the abstract entered in Block 20, if different from Report)		
18. SUPPLEMENTARY NOTES		
19. KEY WORDS (Continue on reverse side if necessary and identify by block number) Polybenzoxazole (PBO) Polybenzthiozole (PBT) Dry-Jet Wet Spinning Cone-and-Plate Rheometry		
20. ABSTRACT (Continue on reverse side if necessary and identify by block number) The solution processing of polybenzoxazole (PBO) and polybenzthiozole (PBT) to form oriented solids is discussed. The rheological considerations important in solution processing are considered, with special emphasis on the dry-jet wet spinning process used to form fibers. Pertinent rheological time constants and orientation parameters are measured by cone-and-plate rheometry and parallel plate flow birefringence. Solution processing experiments to evaluate the pro- posed process models are presented, along with evaluation of the properties of the formed solid polymers. The study included scale-up of the solution		

DD FORM 1 JAN 73 1473

EDITION OF 1 NOV 65 IS OBSOLETE

UNCLASSIFIED

SECURITY CLASSIFICATION OF THIS PAGE (When Data Entered)

UNCLASSIFIED

SECURITY CLASSIFICATION OF THIS PAGE(When Data Entered)

processing methods from research to development level. It is shown that PBT is more easily processed into oriented solids than is PBO, and reason for this difference are discussed. With PBT, a modulus of 1530 g/d (30×10^6 psi) was achieved in a well oriented material. Void formation has so far limited the overall tenacity to about 12 g/d (2.3×10^5 psi), but it appears that with short sections, tenacities of at least 20 g/d (4×10^5 psi) have been reached. Methods to suppress void formation are proposed.

SECURITY CLASSIFICATION OF THIS PAGE(When Data Entered)

FOREWORD

This report was prepared at Mellon Institute, Carnegie-Mellon University, 4400 Fifth Avenue, Pittsburgh, Pennsylvania 15213, under AF Contract No. F33615-77-C-5061. It was administered under the direction of the Air Force Materials Laboratory, Dr. T. E. Helminiak.

The report covers work conducted from 13 April 1977 to 13 April 1979. It was submitted in July, 1979. Authors are G. C. Berry, Principal Investigator, C.-P. Wong, S. Venkatramen and S.-G. Chu from CMU, and under subcontract to CMU, E. W. Choe and S. N. Kim of the Celanese Research Company, Summit, N.J.

TABLE OF CONTENTS

1.	INTRODUCTION	1
2.	REMARKS ON DRY-JET WET SPUN FIBER FORMATION	3
2.1	Kinematics of the Elongating Dry Jet	3
2.2	Rheology in Elongational Flow for Rod-like Polymer Solution	10
2.3	Mechanism of Jet Breakage	12
3.	COAGULATION STUDIES	20
3.1	Experimental Method	20
3.2	Results and Discussion	22
3.3	Summary	25
4.	RHEOLOGICAL STUDIES ON PBT SOLUTIONS	38
4.1	Experimental	38
	Materials	38
	Apparatus	38
4.2	Results and Discussion	39
4.3	Discussion	42
	a) Type I Behavior	43
	b) Type III Behavior	46
	c) Type II Behavior	47
5.	MOLECULAR ORIENTATION OF ROD-LIKE MOLECULES	62
5.1	Review of Models for Representing PBT Polymer Solution	62
5.2	Elongational Viscosity $\bar{\eta}$ and the Time Constant τ_c	65
5.3	Effect of Length Distribution	68
6.	FLOW BIREFRINGENCE OF SOLUTIONS OF ROD-LIKE POLYMERS	71
6.1	Flow Birefringence Apparatus	71
6.2	Results	76
6.3	Discussion	78

Table of Contents (continued)

7.	FIBER FORMATION BY SOLUTION PROCESSING	89
7.1	Fiber Formation with PBO Solutions	89
7.1.1	Solubility of PBO	89
7.1.2	Fiber Wet-Spin Process	92
7.1.3	Dry-Jet-Wet-Spinning of PBO Solutions	98
	a) Effect of Re	102
	b) Effect of $\langle \bar{\kappa} \rangle_t$	102
	c) Effect of $(t_1 - t_0)$	103
	d) Effect of β	103
7.1.4	Inert Jet-Wet Spinning With a PBO Solution	105
7.2	Fiber Formation With Nematic Solutions of PBT	120
7.2.1	Wet Spinning With a PBT-43 Solution	120
7.2.2	Dry-Jet-Wet-Spinning and Wet-Spinning With a PBT-47 Solution	121
7.2.3	Dry-Jet-Wet-Spinning with a PBT-53 Solution	122
7.2.4	Dry-Jet-Wet-Spinning with a PBT Solution	124
7.2.5	Effects of Spinning Variables	125
	a) Elongation Number and Dry-Jet Length	125
	b) Incursion During Coagulation	128
	c) Conclusion	129
8.	TENSILE CREEP AND THERMAL-MECHANICAL CONDITIONING	141
8.1	Creep and Recovery	141
8.2	Thermal-Mechanical Annealing	144
9.	SCALE-UP OF FIBER FORMATION PROCESS	152
10.	CONCLUSIONS AND RECOMMENDATIONS	155
	REFERENCES	158

Table of Contents (continued)

APPENDIX		PAGE
I	Comments on the Use of Equation 7	160
II	Use of Equation 7 With a 'Power Law Fluid'	163
III	Synthesis and Processing of Rod-like Aromatic Heterocyclic Polymers: Para-Phenylene-Polybenzbisoxazoles and Para- Phenylene-Polybenzbisthiazoles. A Report From the Celanese Research Company	165

LIST OF TABLES

Table		Page
1	Orientation of Dumbbells in Elongational Flow	17
2	Coagulation of 7.62% PBO-5/MSA (5% CSA)	27
3	Coagulation of 7.6% PBO-5/MSA	28
4	Coagulation of 4.76% PBT-20/MSA at Room Temperature . . .	30
5	Coagulation of 9.2% PBT-43/MSA at Room Temperature . . .	32
6	Coagulation of a Solution of PBT-47 in Methane Sulfonic Acid (10.3% Polymer) at Room Temperature	33
7	Rheological Parameters for Solutions of PBT-62A	48
8	Material Constants for Rod-like Models	70
9	Flow Birefringence Data Obtained with Some Solutions of Rod-like Polymers	86
10	Water Content of $\text{CH}_3\text{SO}_3\text{H}$ and a PBO Solution in $\text{CH}_3\text{SO}_3\text{H}$.	90
11	Data on PBO Fibers	107
12	Fibers Dry-Jet-Wet Spun From 8.98% PBO-37/MSA (2.5% CSA).	108
13	Wet Spinning of 9.2% PBT-43/MSA	131
14	Wet Spinning and Dry-Jet-Wet-Spinning	132
15	Dry-Jet-Wet-Spinning of 9.85% PBT-53/MSA	133
16	Dry-Jet-Wet-Spinning of 8.2% PBT-62/MSA	134
17	Creep and Recovery Parameters for PBO Fibers	147
18	Equations for Power-Law Fluid with Constant Tension . . .	164

LIST OF ILLUSTRATIONS

Figure		Page
1	Schematic diagram of dry-jet wet-spinning with PBO solution. Enlarged jet showing breakage mechanism due to capillary wave.	18
2	Logarithm of elongational viscosity due to solute and Herman parameter plotted against reduced elongation rate $\tau_c \bar{\lambda}$ for dilute suspension of rigid dumbbells.	19
3	Coagulation of a 7.6% PBO-5/MSA solution with alcohols: pip down, ethanol; no pip, n-propanol; pip up, t-butanol and pip 4 o'clock, n-hesanol.	34
4	Coagulation rate y/\sqrt{t} plotted against composition of the coagulation mixture MSA/H ₂ O for a 7.6% PBO/MSA solution (circles) and a 4.76% PBT/MSA solution (circles with pip).	35
5	Coagulation rate y/\sqrt{t} plotted against composition of the coagulation mixture MSA/MeOH for a 7.6% PBO/MSA solution (circle with pip) and a 4.76% PBT/MSA solution (circles).	36
6	Coagulation rate y/\sqrt{t} plotted against composition of the coagulation mixture ES/MeOH for a 9.2% PBT/MSA solution.	37
7	Schematic drawing of the cone and plate assembly, showing the guard ring immersed in oil used to seal the sample from moisture.	49
8	Plot showing the combinations of temperature and weight fraction studied with solutions of PBT-62. The symbols are used in subsequent plots to designate a particular T, w ₂ combination. The notations T and N indicate that the fluid was isotropic or nematic at the corresponding T and w ₂ conditions. The approximate boundaries between type I, II and III flow regimes are indicated by the dashed lines.	50
9	a) The viscosity η_{κ} versus shear rate for several PBT solutions at 60 degrees C. b) The recovery R_{κ} versus shear rate for several PBT solutions at 60 degrees C.	51
10	a) The reduced viscosity η_{κ}/η_0 versus reduced shear rate $\eta_0 R_0$ for PBT solutions with type I behavior. b) The reduced recovery R_{κ}/R_0 versus reduced shear rate $\eta_0 R_0 \kappa$ for PBT solutions with type I behavior.	52
11	The viscosity versus temperature for PBT solution with the indicated w ₂ . The limiting viscosity η_0 is used for solution with type I and II behavior. The plateau viscosity η_p is used for solutions with type III behavior.	53

List of Illustrations (continued)

Figure		Page
12	The viscosity η_0 or η_p (see Fig. Captions 1-5) versus temperature for PBT polymer solutions with indicated w_2 .	54
13	Limiting recoverable compliance R_0 versus weight fraction for PBT solutions with indicated temperature.	55
14	Limiting recoverable compliance versus temperature for PBT polymer solutions with indicated w_2 .	56
15	a) The reduced viscosity η_{κ}/η_p versus reduced shear rate $\eta_p R_0 \kappa$ for PBT solutions with type III behavior. b) The reduced recovery R_{κ}/R_0 versus reduced shear rate $\eta_p R_0 \kappa$ for PBT solutions with type III behavior.	57
16	a) The reduced viscosity η_{κ}/η_0 versus reduced shear rate $\eta_0 R_0 \kappa$ for PBT solutions with type II behavior. b) The reduced recovery R_{κ}/R_0 versus reduced shear rate $\eta_0 R_0 \kappa$ for PBT solutions with type II behavior.	58
17	a) The reduced viscosity η_{κ}/η_p versus reduced shear rate $\eta_p R_0 \kappa$ for PBT solutions with type II behavior. b) The reduced recovery R_{κ}/R_0 versus reduced shear rate $\eta_p R_0 \kappa$ for PBT solutions with type II behavior.	59
18	a) Composite curves of η_{κ}/η_0 or η_{κ}/η_p versus $\eta_0 R_0 \kappa$, respectively, for data on PBT solutions with several concentrations at 60° C illustrating the range of behavior in types I, II and III. b) Composite curves of R_{κ}/R_0 versus $\eta_0 R_0 \kappa$, for data on PBT solutions with several concentrations at 60°C illustrating the range of behavior in types I, II and III.	60
19	The rheological time constant $\tau_c = \eta_0 R_0$ or $\eta_p R_0$ versus w_2 for PBT solutions at two temperatures.	61
20	Overall schematic diagram of the flow birefringence apparatus.	87
21	Detailed schematic drawing of the solution chamber of the flow birefringence apparatus.	88
22	X-ray diffraction patterns of PBO fibers. a) Fiber 09273, as spun from a biphasic solution. b) Fiber 09273H2, above after 6% draw at 382°C.	109

List of Illustrations (continued)

Figure		Page
23	Scanning electron micrographs of a PBO fiber. a) Fractured end of fiber 10174. b) Surface of fiber 10174, as spun from a nematic solution.	110
24	X-ray diffraction pattern for PBO fiber 04297H.	111
25	a) X-ray diffraction pattern for as-spun fiber 04297. b) Scanning electron micrograph for a specimen of fiber 04297 fractured at liquid nitrogen temperature.	112
26	Stress-strain data for PBO fibers. △ As-spun fiber 12010 prepared with an isotropic solution. ⊗ Above after 17% draw at 400°C, fiber 12010HS. ○ Fiber 09273H2, spun from a biphasic solution.	113
27	Scanning electron micrographs of PBO fiber. a) Fiber 09273 as spun from a biphasic solution; fractured in liquid nitrogen (x1000). b) Fiber 09273H, above after 6% draw at 382°C, fractured in liquid nitrogen (x1000).	114
28	X-ray diffraction pattern of PBO fiber 12010 prepared from an isotropic solution.	115
29	Logarithm of modulus $E_0 \epsilon_b^{1/2}$ plotted against elongational residence R_e and time-average elongation rate $\langle \dot{\epsilon} \rangle_t$ for PBO dry-jet wet spun fibers.	116
30	Reduced time-average elongation rate $\langle \dot{\epsilon} \rangle_t$. $\bar{\eta} R_0/\alpha$ plotted logarithmically against radius ratio R_0/R_1 for selected values of dry-jet length $(x_1 - x_0)/b$.	117
31	Reduced dry-jet residence time $(t_1 - t_0)/(\bar{\eta} R_0/\alpha)$ plotted against dry-jet length $(x_1 - x_0)/b$ for selected values of radius ratio R_0/R_1 .	118
32	Contribution β of the force due to surface tension to the total force plotted against reduced dry-jet length $(x_1 - x_0)/b$ for selected values of radius ratio R_0/R_1 .	119
33	X-ray diffraction pattern for a dry-jet wet spun fiber #PBT-47-071938.	135
34	X-ray diffraction pattern for heat drawn fiber #PBT-47-071938H2.	136

List of Illustrations (continued)

Figure		Page
35	Logarithm of modulus index plotted against the elongation number N_e for a series of wet-spinning (filled circles) and dry-jet wet spinning (open circles) experiment with PBT-47/MSA solutions.	137
36	Logarithm of modulus index plotted against the dry-jet length for a series of dry-jet wet-spinning experiments with same take-up speeds, with PBT-47.	138
37	Optical microscopy of (a) PBT-47-071938 and (b) PBT-47-071938H1, fiber axis 45° to the cross polars, fiber diameter $\sim 10\mu$.	139
38	Scanning electron microscopy of PBT-47-071930, showing defects due to incursion 1,000X.	140
39	Tensile creep compliance $D(t)$ versus the cube root of time $t^{1/3}$ under a stress of 0.735 gpd for PBO-0429-8 fiber at room temperature. (a) square, (b) circle and (c) triangle refer to first, second and third loading cycles.	148
40	Recovery compliance $D(\theta, t_c)$ versus cube root of recovery time (dotted points); and the function $R(\theta, t_c)$. (Crosses); (a) square, (b) circle and (c) triangle, refer to recovery from the first, second and third loading.	149
41	Extension of PBO-2101-0 fiber under a stress of 0.055 gpd.	150
42	Nonrecoverable strain ϵ_{NR} and initial modulus E_0 of PBO-0429-7 fiber under a stress 0.368 gpd.	151

Nomenclature

A	cross sectional area of a jet	(cm ² or μ ²)
a	= $F/2\pi\alpha$, a fictitious radius with which the force due to surface tension is equal to the external force	(cm)
b	= $\bar{\eta} Q/\pi\alpha R_0$	(cm)
d/dt	travelling derivative with respect to time	(sec ⁻¹)
E ₀	initial tensile modulus	(gpd)
F	external force	(dynes)
F _{fric}	frictional force due to shear stress on the jet boundary	(dynes)
F _{grav}	gravitational force due to the weight of the jet	(dynes)
F _{in}	inertial force due to acceleration of mass	(dynes)
F _{rheo}	rheological force developed in the elongating jet	(dynes)
F _{surf}	force due to surface tension	(dynes)
g	gravitational constant = 980	(cm sec ⁻²)
g	subscript indicating effect of gravitational force	
h	Herman-Stein orientation parameter	
J	= $\pi L^2 \Psi_0$ normalized distribution function at zero elongation rate	
L	length of rigid dumbbell	(cm)
m	power in power law of $\bar{\eta} = \bar{\eta}_0 (\bar{\kappa}/\bar{\kappa}_0)^m$	
p	stress	(dyne cm ⁻²)
Q	throughput velocity = AV	(cm ³ sec ⁻¹)
q ₁ , q ₂	= $1/2[1 \pm \sqrt{2g\rho Q\bar{\eta}/\pi\alpha^2}]$	
R	radius of jet	(cm or μ)
Re	Total elongational residence = $\int_0^t \bar{\kappa} dt$	
S	size of fiber	(denier)
T	tenacity of fiber	(gpd)
t	time	(sec)
u	= $[F + g\rho Q(t_1 - t) - 2\pi\alpha R]/2\pi\alpha R$	
v	velocity of jet in x-direction	(cm sec ⁻¹)
x	coordinate of jet	(cm)
z	variable for integration	
α	surface tension	(dynes cm ⁻²)
β	parameter, the ratio of force due to surface tension and the total external force	
γ	parameter, the ratio of forces other than surface tension and that of the latter	

Nomenclature (continued.....)

δ	perturbation on the radius of the jet	(cm sec ⁻¹)
ϵ	elongation of the jet	
ϵ_b	elongation at break of the fiber	(%)
η	shear viscosity of the jet	(poise)
η'	shear viscosity of the medium	(poise)
$\bar{\eta}$	elongational viscosity	(poise)
$\bar{\kappa}$	elongation rate	(sec ⁻¹)
λ	wavelength of perturbation on the jet	(cm)
μ	$= \frac{15}{2} \tau_c \bar{\kappa}$, parameter	
ν	growth factor for perturbation	(sec ⁻¹)
ξ	$= F/\bar{\eta} Q$ profile decaying factor	(cm ⁻¹)
ρ	density	(gm cm ⁻³)
τ_c	time constant	(sec)
φ	volume fraction of polymer	
Ψ	orientation distribution function	
0	subscript indicating initial condition	
1	subscript indicating the point of quenching into bath	
2	subscript indicating jet rupture	

1. INTRODUCTION

The following is a final report on Contract No. F-33615-77-C-5061, "Solution Processing--Rodlike Polymers," for the period 13 April 1977 to 31 May 1979. The report consists of two major sections:

a) Work carried out at Carnegie-Mellon University, Department of Chemistry, to elucidate the principles of solution processing of rodlike polymers such as poly(benzbisoxazole), PBO, or poly(benzbisthiozole), PBT; and b) Work carried out at the Celanese Research Company, under subcontract to CMU, to prepare PBO and investigate scale-up of methods of fiber formation as an example of solution processing of rodlike polymers.

In the first section, attention is given to fiber formation by solution processing of PBO and PBT as a means to evaluate processing considerations developed for rodlike chains, and to obtain some oriented solid PBO and PBT for physical testing (e.g., moduli, strength, electron microscopy, etc.). Both the wet-spin and dry-jet-wet spin fiber formation processes are explored. The latter is given more attention since the simultaneous orientation and coagulation of rodlike polymers appears to lead to limited final order in the solid state. This limitation apparently results from loss of molecular mobility during coagulation⁽¹⁾. It will be shown that the dry-jet-wet spin fiber formation process leads to superior results with both PBO and PBT, but that the latter is more easily used in solution processing. Other topics considered in the first section deal with the rheology of solutions of rodlike chains, methods to determine the orientation in

solutions of rodlike molecules, and some limited creep and recovery measurements on oriented fibers of PBO.

In the second section, it will be shown that wet-spin fiber formation process can be used with either PBO or PBT solutions, but that the dry-jet-wet spin process is adaptable only with PBT solutions. With the latter, the inherent properties obtainable with flow-free sections are found to be very good--1500 g/denier modulus, and 15-20 g/denier tenacity.

2. REMARKS ON DRY-JET-WET SPIN FIBER FORMATION

Solution processing of PBO by the wet-spin fiber formation process has been discussed elsewhere,⁽¹⁾ and the method will also be used in this study. The wet-spin process suffers, however, by combination of the orientation and coagulation steps in the formation process. In either the wet-spin or dry-jet-wet spin processes, the necessary orientation is induced by elongational flow below the spinnerette. In the wet-spin process, the solution undergoes simultaneous coagulation. With rodlike chains such as PBO and PBT, coagulation is accompanied by substantial decrease in molecular mobility, thereby limiting the extent of orientation possible. In the dry-jet wet-spin process orientation is obtained by elongational flow in an air gap between the spinnerette and the coagulant (see below), removing the coupling between these two operations. The solution must have certain properties in order to develop sufficient elongational flow to obtain the desired orientation without rupture of the fluid column. These properties are barely met with PBO, but are available with PBT. Since the dry-jet wet-spin process involves a delicate balance of forces tending to orient or rupture the fluid column, an analysis of this process is included in the following section.

2.1 Kinematics Of The Elongating Dry Jet.

Consider the polymer solution being extruded from the orifice of a capillary perpendicular to the coagulation bath surface at time $t = t_0$ and coordinate $x = x_0$ with an initial velocity V_0 . The

extruded jet is elongated continuously due to tension in the filament until it reaches the coagulation bath at $t = t_1$ and $x = x_1$ with $v = v_1$, where upon it is quenched to form a solid fiber. This is shown schematically in Figure 1. The force balance along the x direction may be expressed⁽²⁾ as:

$$F = F_{\text{rheo}}(x) + F_{\text{in}}(x) + F_{\text{surf}}(x) + F_{\text{fric}}(x) - F_{\text{grav}}(x) \quad (1)$$

where F_{rheo} , F_{in} , F_{surf} , F_{fric} , F_{grav} and F are the rheological force developed in the elongating jet, the inertial force due to acceleration of the polymer solution, the force due to surface tension, the frictional force that arises from integrating the shear stress on the jet boundary from $x = 0$ to x , the gravitational force and the external force exerted by the take-up device. An estimation of the order of magnitude of the various forces simplifies our analysis quite a lot. In the elongation zone of the jet, the effect of jet swell can be neglected and the first term is given by

$$F_{\text{rheo}} = A \bar{\eta} \bar{\kappa} \quad (2)$$

where A is the cross-sectional area of the jet, $\bar{\eta}$ is the elongational viscosity and $\bar{\kappa}$ is the elongation rate. In our experiment, the time average of this quantity $\langle F_{\text{rheo}} \rangle_t$ ranges from 0.31 to 0.38 dynes.

The second term can be approximated by

$$F_{in} = \rho QV \quad (3)$$

where the density $\rho = 1.5 \text{ gm ml}^{-1}$, the throughput velocity, $Q = 7 \times 10^{-4} \text{ cm}^3 \text{ sec}^{-1}$ and the largest final velocity $V = 33 \text{ cm sec}^{-1}$. This results in a maximum value of 0.03 dynes, negligible with respect to F .

The third term can be expressed by

$$F_{surf} = 2\pi\alpha R \quad (4)$$

where the surface tension $\alpha \approx 51 \text{ dyne cm}^{-1}$ and the radius of the jet R changes from 80μ to about 30μ , resulting in a change of F_{surf} from 1.3 dynes to 0.5 dynes.

The fourth term is given by

$$F_{fric} = 2\pi \int_0^x p_{xr} \cdot R dx \quad (5)$$

where p_{xr} is the shear stress on the boundary which may not be negligible in the case of wet spinning, but is quite small in the case of dry jet. The order of magnitude of F_{fric} is 10^{-5} dynes here.

The fifth term is given, for a vertical jet, assuming the contribution due to the part in the coagulation bath negligible, by

$$F_{grav} = g\rho Q(t_1 - t) \quad (6)$$

where $g = 980 \text{ cm sec}^{-2}$ is the gravitational acceleration. The time average of this term $\langle F_{\text{grav}} \rangle_t$ ranges from 0.064 to 0.072 dynes.

It is rather surprising to find that the effect due to surface tension as the dominating effect in the system under investigation. For most conventional spinning operations, surface tension is quite negligible⁽²⁾. Perhaps this is due to the low rate of spinning and the low viscosity of the PBO solution.

Neglecting the inertial, frictional and gravitational terms in Equation (1), the force balance along the x direction yields

$$F = A \bar{\eta} \bar{\kappa} + 2 \pi \alpha R \quad (7)$$

The elongation rate is defined as

$$\bar{\kappa} = - \frac{1}{A} \frac{dA}{dt} = - \frac{2\pi R}{A} \frac{dR}{dt} \quad (8)$$

where the time derivative $\frac{d}{dt}$ travels along with the moving jet. Substituting Eqn. (8) into Eqn. (7) yields

$$\frac{dR}{dt} = \frac{\alpha}{\bar{\eta}} \left[1 - \frac{F}{2\pi\alpha} \frac{1}{R} \right] \quad (9)$$

Consider the case of isothermal spinning, with an elongational viscosity constant throughout the fiber (to be discussed later), Eqn. (9) can easily be integrated to yield

$$a \ln \frac{a - R}{a - R_0} - R_0 + R = \frac{\alpha}{\bar{\eta}} (t - t_0) \quad (10)$$

where $a = F/2\pi\alpha$, and the dry-jet residence time $(t_1 - t_0)$ is given by

$$t_1 - t_0 = \frac{\bar{\eta}}{\alpha} a \ln \left(\frac{a - R_1}{a - R_0} \right) - R_0 + R_1 \quad (11)$$

Now we define the total elongational residence Re by

$$Re = \int_{t_0}^{t_1} \bar{\kappa} dt = \ln \frac{A_0}{A_1} \quad (12)$$

The time-average elongation rate will be given by

$$\langle \bar{\kappa} \rangle_t = Re / (t_1 - t_0) \quad (13)$$

The latter is a useful measure of the effectiveness of the elongational flow for inducing alignment of the rodlike polymer. It is better than the distance-average elongation rate $\langle \bar{\kappa} \rangle_x$ given by

$$\langle \bar{\kappa} \rangle_x = (v_1 - v_0) / (x_1 - x_0) \quad (14)$$

since the jet is accelerated as x increases.

To solve for the streaming profile and the velocity distribution in the fluid jet, we note that for steady state spinning all partial derivatives with respect to time $\frac{\partial}{\partial t}$ vanishes. Thus the

throughput velocity is constant

$$Q = A_0 V_0 = A_1 V_1 \quad (15)$$

$$\bar{\eta} = - \frac{2Q}{AR} \frac{\partial R}{\partial x} \quad (16)$$

Substituting Eqn. (16) into Eqn. (7) yields

$$\frac{\partial R}{\partial x} = \frac{\pi \alpha}{\bar{\eta} Q} R(R - a) \quad (17)$$

which, again, can be integrated to give

$$\frac{R_0}{R(x)} = \beta + (1 - \beta) \exp \left(\frac{x - x_0}{\beta b} \right) \quad (18)$$

where $\beta \equiv R_0/a$ is the initial fraction of the force due to surface tension to that of the total external force, and $b \equiv \bar{\eta} Q / \pi \alpha R_0$. The streaming profile and the velocity profile are given by

$$A(x) = A_0 [R(x)/R_0]^2 \quad (19)$$

$$V(x) = V_0 [R_0/R(x)]^2 \quad (20)$$

and the elongation rate is obtained by substituting Eqn. (18), (17) into Eqn. (16),

$$\bar{\kappa} = \bar{\kappa}_0 \left[\beta + (1 - \beta) \exp\left(\frac{x - x_0}{\beta b}\right) \right] \exp\left(\frac{x - x_0}{\beta b}\right) \quad (21)$$

where $\bar{\kappa}_0 = 2v_0(1 - \beta)/\beta b \quad (22)$

It should be noted that in our experiment, realization of the external force F is through the change of the take-up velocity V_T . For constant throughput velocity Q , the parameters a and β are varied accordingly, and can be evaluated with Equation (18) knowing the dry-jet length $x_1 - x_0$, the final radius R_1 and the constant b . For the set of experiments described in Table 1, $(x_1 - x_0)/b = 4.86$, and the value of β is very close to unity. An approximate form of Eqn. (18) is attainable by letting $1/\beta = 1 + \gamma$, where γ is a measure of the initial contribution of the forces other than that of the surface tension, normalized by the latter. This results in

$$\frac{1 - \beta}{\beta} = \gamma \approx \frac{(R_0/R_1) - 1}{\exp\left(\frac{x_1 - x_0}{b}\right) - 1} = \frac{\exp\left(\frac{N_u}{2}\right) - 1}{\exp\left(\frac{x}{b}\right) - 1} \quad (23)$$

provided $\gamma < b/(x_1 - x_0)$.

In this case, we substitute $a = R_0(1 + \gamma)$ and Eqn. (23) into Eqn. (11), and obtain

$$t_1 - t_0 \approx \frac{\bar{\eta}}{\alpha} \left[R_0 \ln \frac{R_0 - R_1}{\gamma R_0} - R_0 + R_1 \right] \quad (24a)$$

$$= \frac{\bar{\eta} R_0}{\alpha} \left\{ \ln \left(\exp \frac{x_1 - x_0}{b} - 1 \right) + \frac{R_1}{R_0} + \ln \frac{R_1}{R_0} - 1 \right\} \quad (24b)$$

Therefore, the residence time increases almost linearly with the dry jet length $(x_1 - x_0)$, and it decreases with the square root of the take-up speed V_T since $V_T \propto 1/R_1^2$.

2.2 Rheology In Elongational Flow For Rodlike Polymer Solution.

There have been only a few experimental studies on the rheology in elongational flow. Even more scarce are studies on rodlike polymer solutions. For guidance on the rheological behavior of rodlike polymer solution in elongational flow, we shall invoke the rigid dumbbell model developed by Bird and coworkers^(3,4). This topic will be explored in more detail in a subsequent section. Here, we present a limited discussion adequate for the present purpose. According to Bird et al. for a suspension of dumbbells with Length L in a solvent with viscosity η_s the elongational viscosity $\bar{\eta}$ is given as a function of $\bar{\kappa}$ by:

$$\bar{\eta}(\bar{\kappa}) = 3\eta_s + (\bar{\eta}(0) - 3\eta_s) \left[\frac{1}{2} + \frac{3}{4\mu} (J - 1) \right] \quad (24)$$

where $\mu = \frac{15}{2} \tau_c \bar{\kappa}$, τ_c is the usual time constant given by the product of zero shear viscosity and recoverable compliance, and

$$J = e^{\mu} / \int_0^1 e^{\mu z^2} dz \quad (25)$$

The orientation of dumbbells in the flow has been studied with Kramer's method in a previous report^(1b) to yield the angular distribution function $\Psi(\theta, \phi)$

$$\Psi(\theta, \phi) = \frac{J}{\pi L^2} \exp[-\mu \sin^2 \theta] \quad (26)$$

As a measure of the extent of the alignment of the dumbbell along the flow direction, the Hermans and Stein orientation parameter $h = \frac{3}{2} [\langle \cos^2 \theta \rangle - 1]$ can be evaluated by taking the average $\langle \cos^2 \theta \rangle$ with Eqn. (26) and results in

$$h = \frac{3}{4\mu} (J - 1) - \frac{1}{2} \quad (27)$$

Values of $\bar{\eta}$ and h have been computed for selected values of $\tau_c \bar{\kappa}$. They are listed in Table 1 and plotted in Figure 2. The region of elongation rates that is of our interest in the spinning process includes $\tau_c \bar{\kappa} = 0.1$ to 2 where the Herman's parameter changes from 0.1 to 0.9. In this region, the elongational viscosity $\bar{\eta}$ increases very gradually from $\bar{\eta}_0$ to $2\bar{\eta}_0$, and can be represented conveniently as a power law, as indicated by the dotted line in the Figure,

$$\bar{\eta}(\bar{\kappa}) = \bar{\eta}^* (\bar{\kappa}/\bar{\kappa}^*)^{0.2} \quad (28)$$

where $\bar{\eta}^*$ is the viscosity at a reference elongation rate $\bar{\kappa}^*$.

A more realistic form for Eqn. (9) can be expressed as

$$\left(\frac{dR}{dt}\right)^{1.2} = \frac{0.87 \alpha \bar{\kappa}^{*0.2}}{\bar{\eta}^*} \frac{(a - R)}{R^{0.8}} \quad (29)$$

The reduction of the jet radius R would then be slower than that given by Eqn. (11). The residence time $t_1 - t_0$, as well as the time average elongation rate $\langle \bar{\kappa} \rangle_t$, however, are not affected

significantly. In the region of $\bar{\kappa} > 2/\tau_c$, $\bar{\eta}$ remains closed to a constant value ($2\bar{\eta}_0$) and this effect is even less significant. Therefore, for practical purposes and mathematical simplicity, we shall consider $\bar{\eta}$ constant in our analysis for elucidation of the nature of isothermal dry-jet spinning of PBO solutions.

2.3 Mechanism Of Jet Breakage.

Formally, a purely viscous fluid jet can be elongated continuously to an infinitely small diameter without breakage. In actual practice, the jet ruptures at some point when it is attenuated to a certain diameter or when the tensile stress is increased to a certain critical value. The problem of dry jet rupture is even more serious for PBO solution than other polymer solution. Spinnability of a fluid, as defined by the ability of the fluid to form a jet without breakage, has been investigated quite extensively^(2,4,5,6). Among them, Ziabicki et al. has given a very comprehensive discussion on the subject^(2,7). Two mechanisms are proposed to be responsible for fracture of the fluid jet: the capillary-wave fracture and the cohesive fracture. The former is due to the growth of waves on the surface of the fluid jet. These grow until their amplitude equals the radius of the attenuated jet. This effect is connected with the surface tensions and viscosities of both the fluid jet and the medium in which the jet is immersed. The second rupture mechanism involves the increase of tensile stress until the stored elastic energy equals the cohesive energy density of the material. For PBO solutions, in the dry-jet region, the first mechanism will be the determining one,

especially with low viscosity solutions. On the other hand, in wet spinning, the interfacial surface tension is lower and surface waves are damped out by the surrounding medium, so that the second mechanism dominates. We shall concentrate our attention to the mechanism of capillary-wave fracture in the following discussion on the dry-jet of PBO solution spinning.

Capillary waves are invariably generated on the jet surface for any real steady fluid jet. The perturbation δ on the surface grows with time because of the excess pressure due to surface tension at the nodes of the waves. Following Ziabicki^(7b), it can be expressed as

$$\delta = \delta_0 e^{\nu t} \cos(2\pi x / \lambda) \quad (30)$$

where δ_0 is the amplitude of the initial perturbation on the radius R on the jet at time $t = t_0$, λ is the wavelength of the perturbation and ν the growth factor.

For a free cylindrical jet, Weber⁽⁸⁾ has derived an expression for ν

$$\nu = \frac{\alpha/R}{6\eta + \sqrt{8\rho\alpha R}} \quad (31)$$

relating it with the surface tension α and its viscosity η . For the system under investigation, $\sqrt{8\rho\alpha R_0} / 6\eta = 0.0037 \ll 1$, and Eqn. (31) can be simplified to

$$v = \frac{\alpha}{6\eta R} \quad (32)$$

If the jet is immersed in another fluid of viscosity η' , then v is given by

$$v = \frac{\alpha}{2\eta' R} (1 - \theta^2) \Phi(\theta) \quad (33a)$$

where $\theta = 2\pi x/\lambda$ and $\Phi(\theta)$ is a function of θ , η and η' given by Tomotika⁽⁹⁾. In particular, Tomotika has evaluated the values of $(1 - \theta^2) \Phi(\theta)$ for selected values of η/η' with maximum growth listed below

$$\eta / \eta' \rightarrow \infty \quad v = \alpha / 6 \eta R \quad (33b)$$

$$\eta / \eta' = 0.91 \quad v = \alpha / 30 \eta R \quad (33c)$$

$$\eta / \eta' \rightarrow 0 \quad v = (\alpha / 6 \eta R)(3 \eta / \eta') \quad (33d)$$

If the breakage mechanism is purely capillary-waved, the attenuated jet will rupture at R_2 when $\delta(t_2) = R_2$. (See Figure 1) Since the jet radius R , and consequently v , change with time, the condition of breakage is given by^(7b)

$$\delta_0 \exp \int_{t_0}^{t_2} v \, dt = R_2 \quad (34)$$

Rearranging Eqn. (9), integration yields

$$\int_{t_0}^{t_2} \frac{dt}{R} = \frac{1}{a} [t_2 - t_0 - \frac{\bar{\eta}}{\alpha} (R_2 - R_0)] \quad (35)$$

Substituting Eqn. (35), (11) (replacing subscript 1 with 2) and Eqn. (32) into Eqn. (34), one obtains the breakage condition for the radius R_2 for fiber fracture:

$$\delta_0 \left(\frac{a - R_2}{a - R_0} \right)^{1/2} = R_2 \quad (36)$$

or rearranging to give an expression explicit in R_2

$$R_2 = \frac{\delta_0 \sqrt{\delta_0^2 + 4(1 + \gamma)\gamma R_0^2} - \delta_0^2}{2\gamma R_0} \quad (37)$$

In case of $4(1 + \gamma)\gamma R_0^2 \gg \delta_0^2$, Eqn. (37) reduces to

$$R_2 = \delta_0 \sqrt{(1 + \gamma)/\gamma} = \delta_0 / \sqrt{1 - \beta} \quad (38)$$

For a dry-jet wet spinning operation to be continuous with a dry-jet length $x_1 - x_0$ and an attenuation ratio R_1/R_0 , the condition $R_1 > R_2$ has to be satisfied. The parameter β plays an important role. In other words, we must satisfy the spinnable condition

$$\beta < \left(1 - \frac{\delta_0}{R_0} \cdot \frac{R_0}{R_1} \right)^2 \quad (39)$$

where β is determined by the reduced dry-jet length $(x_1 - x_0)/b$ with fixed ratio of R_0/R_1 according to Eqn. (18). The effect of surface tension is imbedded in the parameter b .

Table 1

Orientation of Dumbbells in Elongational Flow

$\tau_c \bar{\kappa}$	$\cos^{-1} \langle \cos \theta \rangle$	$\langle \cos^2 \theta \rangle$	h	$\bar{\eta} - 3\eta_s / \bar{\eta}(0) - 3\eta_s$
0	60°	0.333	0	1.00
0.3	45.7°	0.560	0.33	1.33
0.6	32.8°	0.737	0.61	1.61
1	23.2°	0.851	0.78	1.78
2	16.3°	0.927	0.89	1.89
6	8.1°	0.979	0.99	1.99
∞	0°	1.000	1.00	2.00

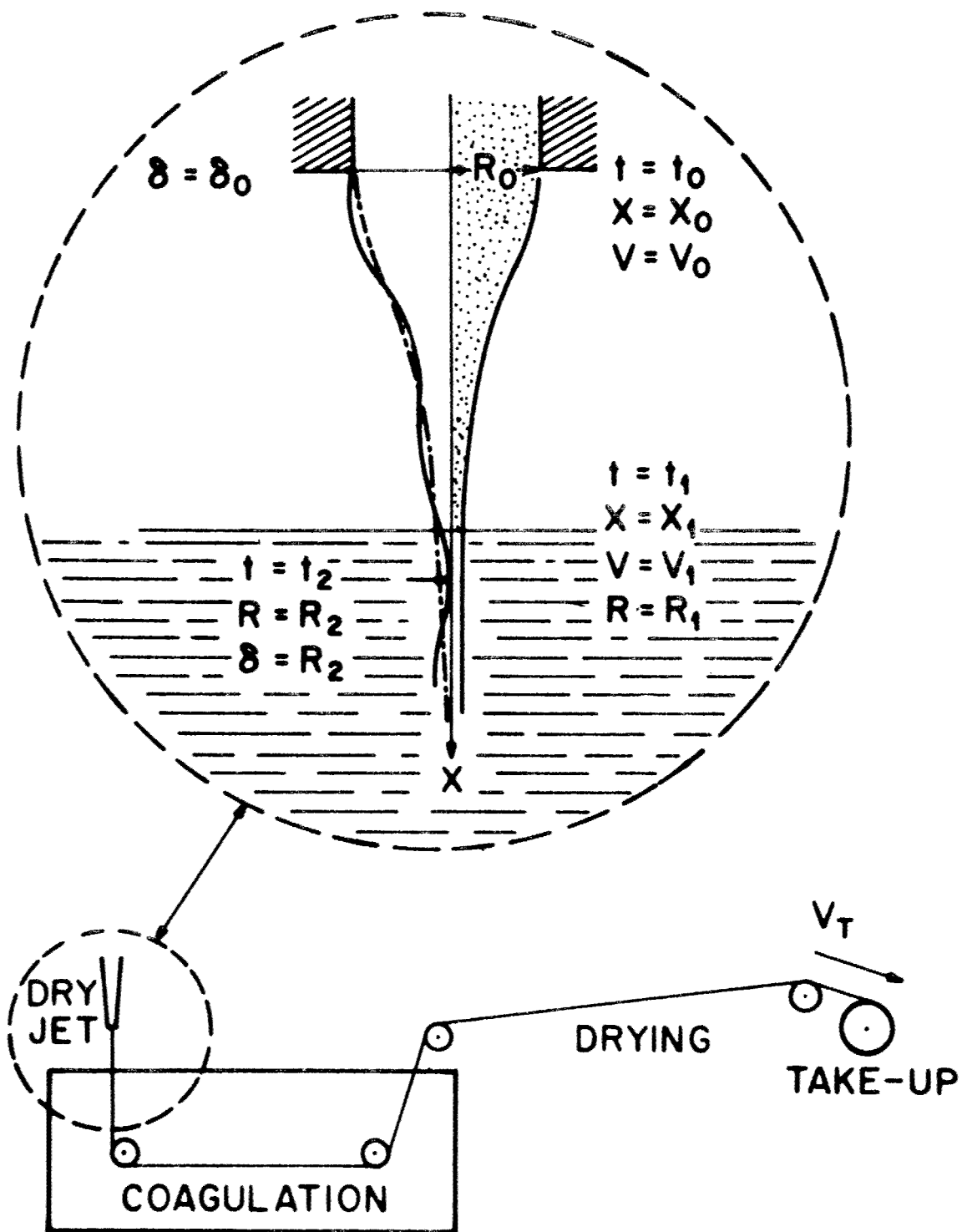


Figure 1 Schematic diagram of dry-jet wet-spinning with PBO solution. Enlarged jet showing breakage mechanism due to capillary wave.

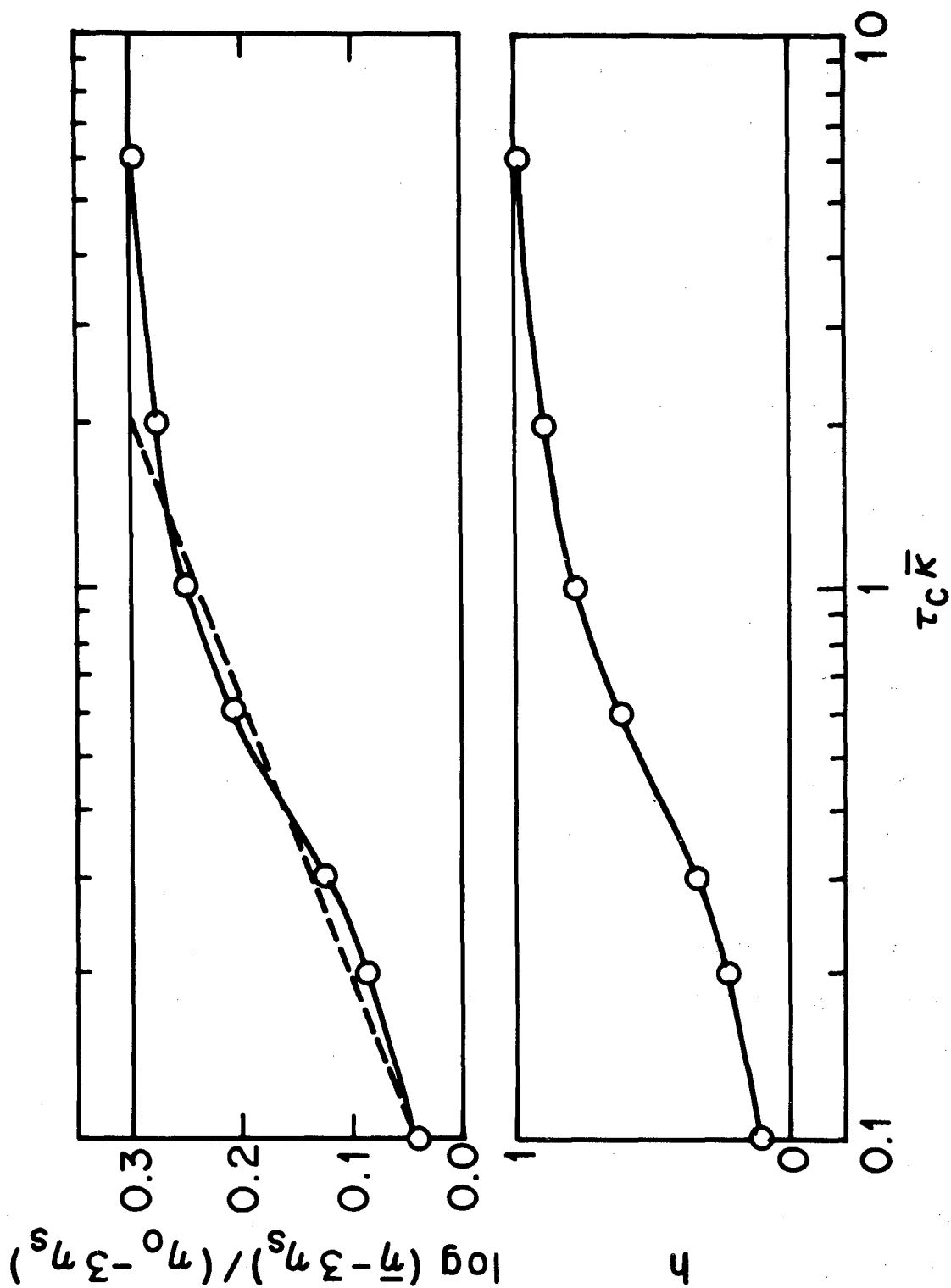


Figure 2 Logarithm of elongational viscosity due to solute and Hermans parameter plotted against reduced elongation rate $\tau_c \bar{K}$ for dilute suspension of rigid dumbbells.

3. COAGULATION STUDIES

The coagulation step in solution processing involves a balance between two opposing rates: a) the coagulation must be fast enough to be effective in maintaining the orientation induced during flow; but b) coagulation must not be so fast that the process distorts the oriented domains, or produces other undesirable artifacts. In fact, as will be seen below, the coagulation process can result in instabilities, producing incursions of the coagulant into the polymer solution. These incursions culminate in voids in the coagulated solid. Since these are important in determining the strength and, to some extent, the modulus of the processed solid, a series evaluate the coagulation properties of a number of nonsolvents inducing mixtures.

3.1 Experimental Method.

A small drop of PBO (or PBT) solution was sandwiched between a dried glass slide and a cover glass, and placed on the stage of a polarizing microscope fitted with a calibrated scale in the eye piece. Immediately, a drop or two of the selected coagulant was introduced at the edge of the cover glass with a disposable pipette. The coagulant proceeded towards and encircled the PBO solution due to capillary action. This took place very rapidly except for highly viscous coagulants such as glycerol. Upon contact between the two liquids, coagulation starts in the PBO solution. Usually a rather sharp coagulation boundary was observable with or without the cross polars, proceeding into the interior of the PBO solution. The advancement of this coagulation boundary could be registered as a function of time with the aid of a tape recorder to

record the boundary location as read from the eye-piece calibration scale. The experiments were usually performed at room temperature.

With experiments run at temperatures other than room temperature, or with coagulants too volatile to maintain an excess supply of coagulant surrounding the PBO solution, the following modification was adopted. The coagulant under investigation was placed inside a closed vessel and equilibrated at the desirable temperature. The sandwich of PBO solution and glass slides was then immersed into the coagulant and the initial time of immersion was noted as that of coagulation. After a sufficiently long time of immersion, the slides were taken out and placed onto a microscope stage for examination of distance of coagulation. The duration of observation on the microscope stage was short in comparison to the total duration of immersion so that no significant change occurred during observation. For another experimental point the process was repeated with a different duration of immersion. Naturally, only the long time behavior of coagulation could be investigated this way.

It was observed that with an 8.98% PBO/MSA (2.5 CSA) solution coagulated by water or methanol, the coagulation mechanism is composed of two simultaneous processes. In addition to the appearance of a sharp coagulation boundary more or less in parallel with the interface between the two liquids, at numerous points of the interface, coagulant incurred into the PBO solution as if it had broken the coagulated boundary originally formed. The lobes of incursion grew rapidly, leaving behind regions diluted with the coagulant and creating coagulation fronts around themselves. This catastrophic mechanism of coagulation,

apparently related to the interfacial surface tension between the coagulant and the coagulated phase, is believed to be undesirable for solution fabrication of the polymer.

3.2 Results and Discussion

Some of the results of a typical coagulation measurement are illustrated in Figure 3. Here a 7.62% isotropic PBO-5/MSA (2.5 CSA) is coagulated with a number of alcohols. The advancement $y(t)$ of the coagulation front is plotted against the square root of the coagulation time t . In general, linear relationships are followed up to 200 microns (μ). This behavior is in accord with Herman's theory on diffusion with immobile trapping chemical reactions. In his analysis, molecules with concentration c diffuse into a medium with trapping sites of concentration m . The change in concentration of molecules with time may be written as

$$\frac{\partial c}{\partial t} = D \frac{\partial^2 c}{\partial x^2} - K cm \quad (40)$$

where D is the diffusion constant, K is the rate constant of reaction and x is the coordinate for one dimensional diffusion.

In the case of coagulation with a sharp boundary, K is very large. One can practically assume that for $x < y, m = 0$ and for $x > y, m = m_0$ where m_0 is the original trapping site concentration. With initial conditions

$$c(0, t) = c_0, \quad c(x, 0) = 0 \text{ for } x > 0 \quad (41)$$

and boundary conditions

$$c(y, t) = 0, \quad -D \frac{\partial c}{\partial x} \bigg|_y = m_o \frac{dy}{dt} \quad (42)$$

The diffusion equation can be solved to yield the advancement of coagulation boundary $y(t)$ as

$$y = 2z \sqrt{Dt} \quad (43)$$

where z is given implicitly by

$$ze^{z^2} \int_0^z e^{-S^2} dS = \frac{c_o}{2m_o} \quad (44)$$

Accordingly, the coagulation boundary y advances linearly with the square root of time and the quantity $y/\sqrt{t} = 2z\sqrt{D}$ can be used as a measure of the coagulation rate. The quantity z increases monotonically with c_o/m_o , the ratio of initial concentration of the coagulant to that of the trapping sites.

Coagulation study has been performed with three rodlike polymer solutions: (1) an isotropic 7.6% PBO-5/MSA (5 CSA) solution, (2) an isotropic 4.7% PBT-20/MSA solution (3) a nematic 9.2% PBT-43/MSA (2.5 CSA) solution and (4) a nematic 10.3% PBT-47/MSA solution. The coagulation rates y/\sqrt{t} , incursion behavior and solution contraction are summarized in Tables 2-6. Some of the coagulants are mixtures of a fast coagulant (e.g. H_2O or MeOH), which unfortunately produce

incursion in the solution, and a noncoagulant (e.g. MSA) or a slow coagulant (e.g. ethyl sulfate). The resulting mixtures in general have intermediate coagulation rates but much more satisfactory incursion and contraction properties. The coagulation rates for these mixtures are plotted in Figures 4-6.

Criteria for selection of a coagulant for a particular spinning operation include several factors. First, the rate of coagulation is to be considered in three respects: (1) complete or nearly complete coagulation should have been attained before the fiber reaches the first godet in the coagulation bath. This is especially true in wet spinning operation; (2) If a rigid skin is formed in the fiber upon quenching into the bath, the time for complete coagulation should be smaller than the relaxation time of the oriented species in the fiber. This may be the case in dry jet wet spinning; (3) in "inert jet" spinning, on the other hand, the fluid chosen as the "inert jet" bath should have zero or very low coagulation rate. For example, in a wet spinning operation with a take-up speed V_T of 15 cm sec^{-1} , a first coagulation length ℓ_1 (the distance between the point of immersion and the first godet) of 30 cm and a fiber radius R_1 of 30μ , the selected coagulant should have a coagulation rate y/\sqrt{t} not smaller than $R_1 \sqrt{V_T/\ell_1} = 21 \mu\text{sec}^{-1/2}$. If on the other hand $\ell_1 = 3 \text{ dm}$, then the required y/\sqrt{t} is increased to $67 \mu\text{sec}^{-1/2}$.

Secondly, as mentioned above, the occurrence of incursion is believed to be unfavorable in solution fabrication of oriented polymers. In wet spinning, the flow field for alignment of molecules in the jet

may be disrupted by the radiating incursion, creating an ill oriented fiber with coarse surfaces. In dry jet wet spinning, the molecular alignment developed in the dry jet is likely to be destroyed or reduced if the incursion proceeds transversely towards the center of the jet. If, on the other hand, the incursion proceeds longitudinally along the impinging jet, it may split the jet into a number of fibrils with finite lengths.

Thirdly, solution contraction has to be considered, especially in wet spinning. In conventional operations, jet swell is always present in coil-like polymers and is diminished by the reaction of the coagulant with the jet. Experiments with PBO and PBT solution spinning reveal, however, a disadvantage for systems with substantial contraction. Coagulants which yield appreciable contraction of the solution gradually creep into the orifice of the spinnerette along the inner wall asymmetrically. Such premature and nonuniform coagulation proves to be disastrous and prevent attainment of high stretch ratio.

3.3 Summary

Based on the limited data listed in Tables 1, 2 and 3, and the aforementioned criteria, candidate coagulants can be suggested for a particular spinning operation. For instance, a 40% MSA/MeOH or a 5% MeOH/xylene may be chosen for wet spinning of a 7.6% PBO/MSA solution, a 40% MSA/H₂O or a 30 ~ 40% MSA/MeOH for a 4.76% PBT/MSA solution, and a 50-70% ES/MeOH or a diethyl ether for a 9.2% PBT/MSA solution. For dry jet set spinning, if the incursion proves to proceed longitudinally so that it does not destroy the molecular orientation, extremely fast

coagulant such as H_2O or MeOH may be used. Otherwise, a 10% MSA/MeOH would be more suitable for a 7.6% PBO/MSA solution, a 50% MeOH/DOP or ether for the PBT solution. For inert jet wet spinning, the inert bath liquid has to be compatible with the subsequent coagulant and be mobile enough to allow immediate and uniform coagulation once the jet leaves the inert bath and enters the coagulation bath. Depending on the nature of the subsequent coagulation bath, 1-chlorooctane, dioctyl phthalate, chloroform or carbon tetrachloride etc. may be used for the inert bath liquid. Finally, it should be remembered that the coagulate measurements were made in a static drop of polymer solution sandwiched between two glass slides. One must be very cautious in translating such information to the spinning process, where the polymer solution is subjected to constant deformation and orientation.

Table 2

Coagulation of 7.62% PBO-5/MSA (5% CSA)

<u>Coagulant</u>	<u>Incursion</u>	<u>Coag. Rate y/\sqrt{t} (μ sec^{-1/2})</u>	<u>Solution Contraction (μ)</u>
H ₂ O	a lot	----	----
CH ₃ OH	a lot	----	----
Ethanol	1	18.9	~ 80
n-Propanol	2 ~ 3	11.5	~ 12
n-Butanol	a lot	----	----
t-Butanol	some	6.67	~ 12
n-Hexanol	some	8.69	~ 12
n-Octanol	a lot	----	----
n-Butyl Acetate	a lot	----	----
Dimethylformamide	a lot	----	----

Table 3. Coagulation of 7.6% PBO-5/MSA

Coagulant	Coagulation rate y/\sqrt{t} ($\mu\text{sec}^{-1/2}$)	Incursion	Contraction (μ)
At room temp.			
20% MSA/H ₂ O	27.5	a lot	46
30% " "	24.4	several	34
40% " "	21.6	3 ~ 4	12
1% MSA/MeOH	26.0	several	80 ~ 50
3% " "	25.8	1	44
5% " "	25.0	some	40
10% " "	25.7	none	34
20% " "	22.2	1	17
30% " "	20.6	several	17
40% " "	18.6	0 ~ 2	12
5% MeOH/xylene	12.3	none	0
10% " "	15.2	3	12
30% " "	24.8	a lot	46
C ₂ H ₅ OH	18.7	v. little	80
n-propanol	10.2	1	12
t-butanol	6.5	v. much	12
n-hexanol	8.6	some	12
cyclohexanol	(slow)	6	0
n-octanol	-	completely	-
laural alc.	(slow)	completely	0
benzyl alc.	(moderate)	3	0
ethylene glycol	(slow)	4	0
glycerol	8.65	0 ~ 2	0
triethanolamine	9.6	0 ~ 1	0
1-chlorooctane	4.5	none	0
n-butyl acetate	-	a lot	-

Table 3. Coagulation of 7.6% PBO-5/MSA cont'd.

Coagulant	Coagulation rate y/\sqrt{t} ($\mu\text{sec}^{-1/2}$)	Incursion	Contraction (μ)
diethyl phthalate	(slow)	completely	-
dibutyl phthalate	(slow)	a lot	0
dioctyl phthalate	~ 0	none	0
DMSO	(moderate)	a lot	-
DMF	-	a lot	-
at 0°C			
MeOH	20.5	v. much	-
3% MSA/MeOH	19.5	v. little	-
5% MSA/MeOH	19.8	v. little	-

Table 4. Coagulation of 4.76% PBT-20/MSA
At Room Temperature

Coagulant	Coagulation rate y/\sqrt{t} (μsec^{-1})	Incursion	Contraction (μ)
H ₂ O	63.1	(v. nonuniform)	69
20% MSA/H ₂ O	41.0	(v. nonuniform)	34
30% " "	32.4	(nonuniform)	34
40% " "	21.2	1	12
50% " "	15.5	several	12
MeOH	50	5	69
3% MSA/MeOH	35 ~ 39	some large	12
10% " "	25.8 ~ 26.6	5	12 ~ 34
20% " "	23.2 ~ 25.2	a few	12
30% " "	20.4 ~ 23.9	none	12
40% " "	18.2 ~ 20.2	none	0 ~ 12
50% " "	16.3	none	0 ~ 12
60% " "	15.2	none	0 ~ 12
5% MeOH/xylene	(incomplete coag.)	none	-
10% " "	19.4	a few	12
10% MeOH/CHCl ₃	(incomplete coag.)	a few	0
10% MeOH/triethanolamine	9.0	some small	0
50% MeOH/triethanolamine	18.4	a lot	12
C ₂ H ₅ OH	27.0	5	34
n-propanol	-	(completely)	-
10% MSA/C ₂ H ₅ OH	16.8	a lot	23
20% " "	16.1	a few	12
glycerol	5.7	some small	0
triethanolamine	8.2	some	0
50% MeOH/glycerol	11	none	12
50% MeOH/CHCl ₃	25.4	(nonuniform)	46

Table 4. Coagulation of 4.76% PBT-20/MSA
at Room Temperature cont'd

Coagulant	Coagulation rate y/\sqrt{t} (μsec^{-1})	Incursion	Contraction (μ)
50% MeOH/ CCl_4	39.0	(v. nonuniform)	35
50% MeOH/dioctyl phthalate	35.2	none	58
diethyl ether	23.8	none	69
dioxane	14.5	a lot	23
acetone	47.1	(nonuniform)	58
MEK	24.8	some	0

Table 5. Coagulation of 9.2% PBT-43/MSA
at Room Temperature

Coagulant	Coagulation rate y/\sqrt{t} ($\mu\text{sec}^{-1/2}$)	Incursion	Contraction (μ)
30% MSA/MeOH	20.9	3 large	-12
30% ES/MeOH*	30.6	(v. nonuniform)	58
40% " "	24.4	some large	34
45% " "	26.0	2 large	23
50% " "	21.3	none	0 ~ 12
55% " "	21.0	1 large	23
60% " "	22.8	several small	0
70% " "	21.0	1 large	0
MeOH:MSA:ES (50:10:40)	24.0	3 medium	12
" " " (50:30:20)	19.8	1 large	12
" " " (50:40:10)	18.2	2 large	0
C ₂ H ₅ OH	16.4	1	12
diethyl ether	23.2	a few small	0
acetone	26.1	a few	12
50% acetone/benzene	16.1	none	12

*ES = ethyl sulfate

Table 6

Coagulation of a Solution of PBT-47 in
Methane Sulfonic Acid (10.3% Polymer)
(Room Temperature)

Component 1	Component 2	Coagulation Rate y/\sqrt{t} ($\mu \text{ sec}^{-1/2}$)	Incursion	Contraction ^a (μ)
50% Methanol	50% Ethyl Sulfate	15.6	None	0
20% Methanol	80% Sulfolane	14.4	None	-11.5
50	50	20.0	None	-1
70	30	23.5	1	-2
80	20	~30	Several	-6
10% Water	90% Sulfolane	11.5	None	-1
20	80	19.4	1(large)	-1
40	60	22.4	None	-1
50	50	22 ~ 24	1(small)	-1
70	30	30.2	few(small)	-5
80	20	26.4	few(small)	-2
40% Water	60 Methane Sulf. Acid	14.6	None	-1
50	50	17.8	None	-1
60	40	20.4	1	-1
70	30	23.4	few(small)	-2
80	20	28.2	few(small)	-3
90	10	25.8	Several	-2
40% Water	60% Methane Sulf. Acid	14.6	None	-1
50	50	17.8	None	-1
60	40	20.4	1	-1
70	30	23.4	few(small)	-2
80	20	28.2	few(small)	-3
90	10	25.8	Several	-4

(a) Radial contraction of solution of about 1 cm diameter

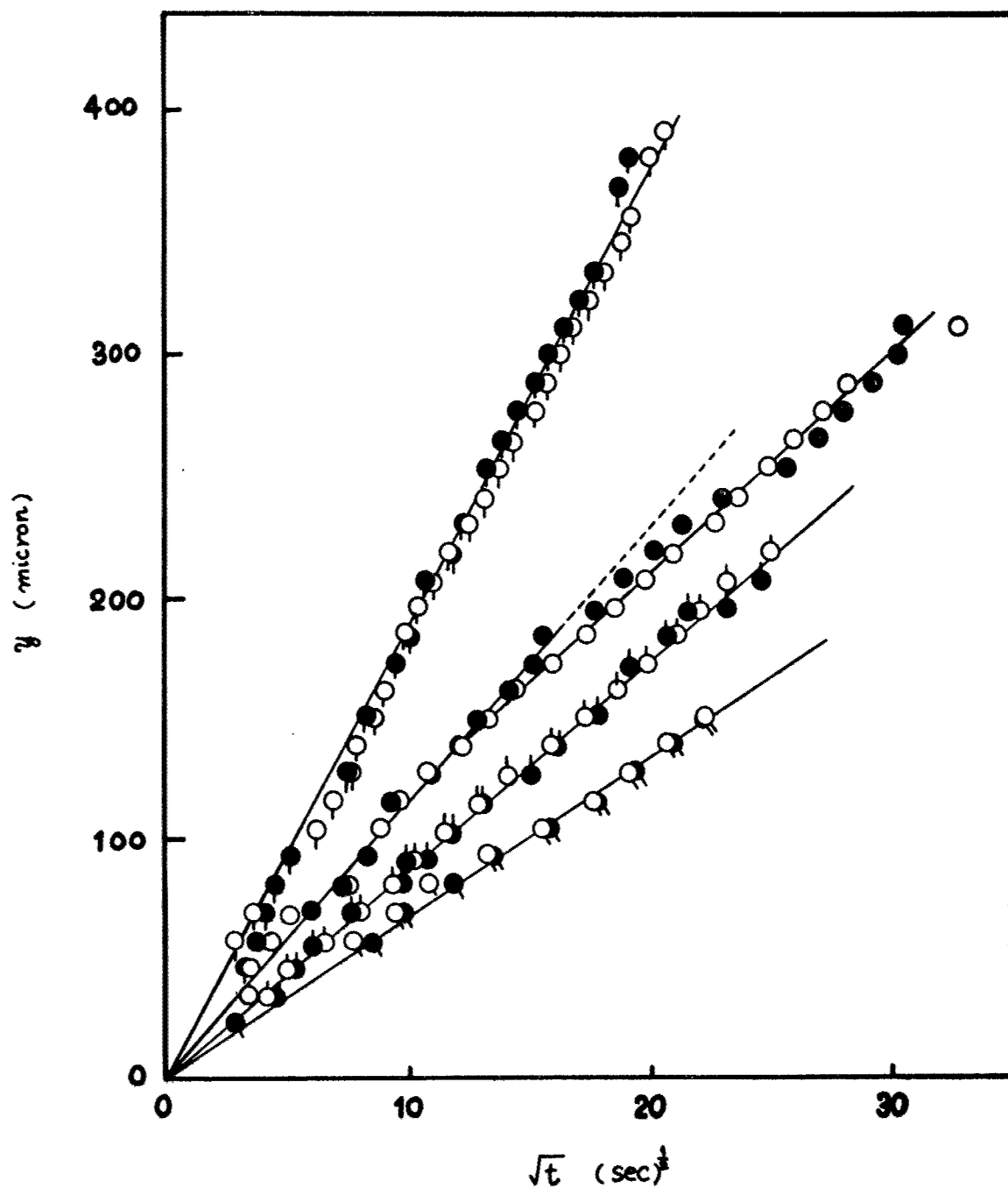


Figure 3 Coagulation of a 7.6% PBO-5/MSA solution with alcohols: pip down, ethanol; no pip, n-propanol; pip up, t-butanol and pip 4 o'clock, n-hexanol.

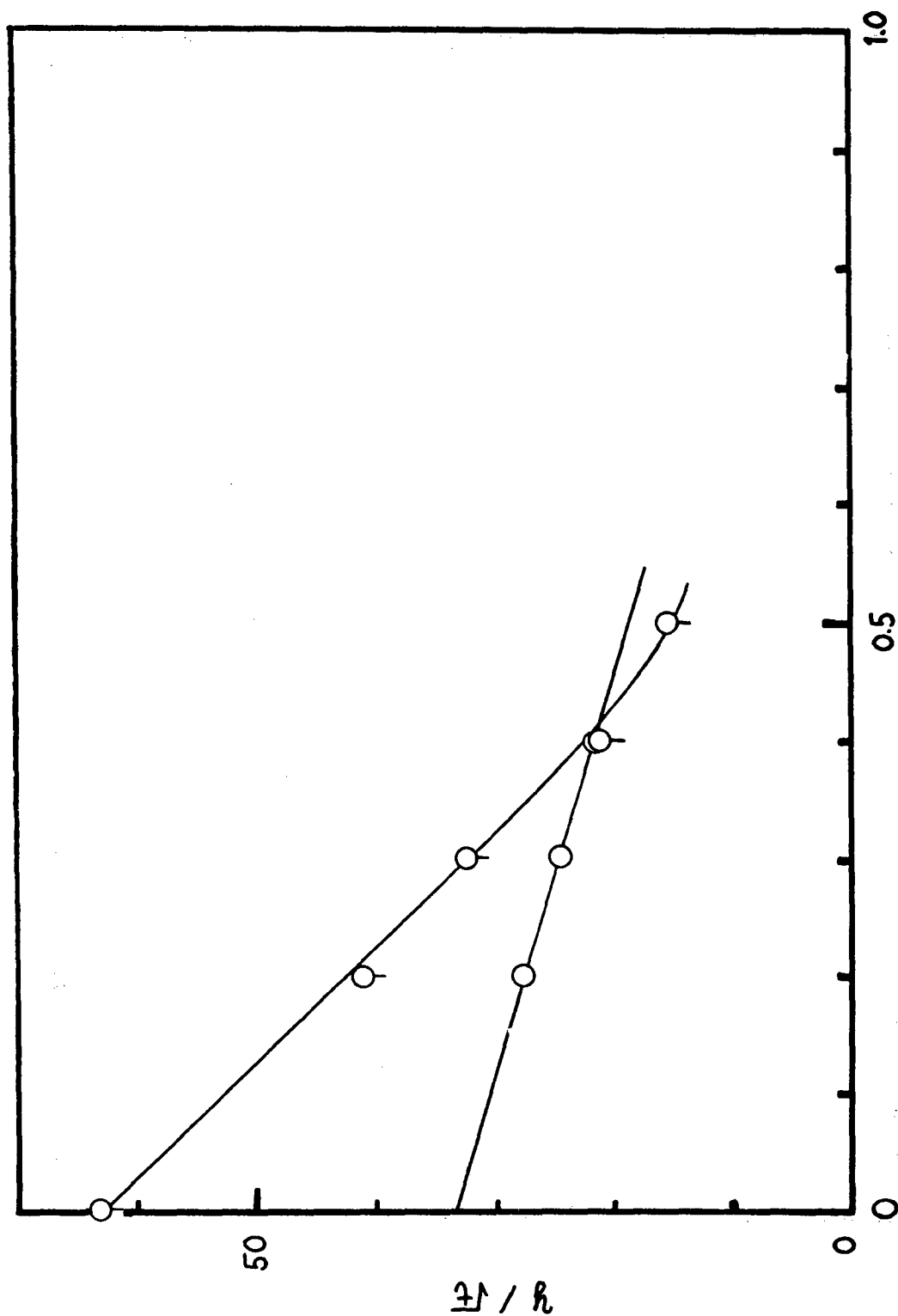


Figure 4 Coagulation rate y/\sqrt{t} plotted against composition of the coagulation mixture $\text{MSA}/\text{H}_2\text{O}$ for a 7.6% PBO/MSA solution (circles) and a 4.76% PBT/MSA solution (circles with pip).

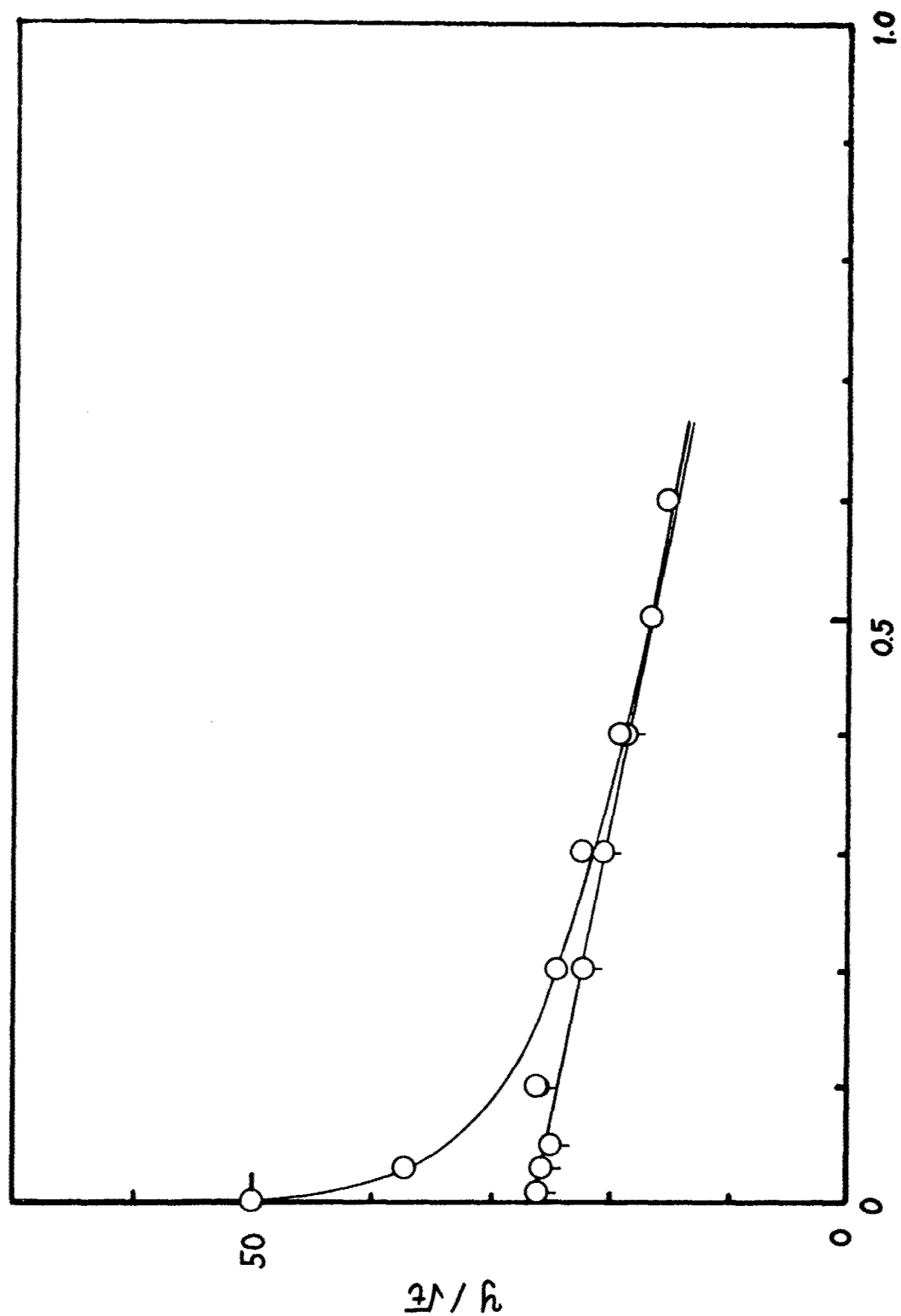


Figure 5 Coagulation rate y/\sqrt{t} plotted against composition of the coagulation mixture MSA/MeOH for a 7.6% PBO/MSA solution (circle with pip) and a 4.76% PBT/MSA solution (circles).

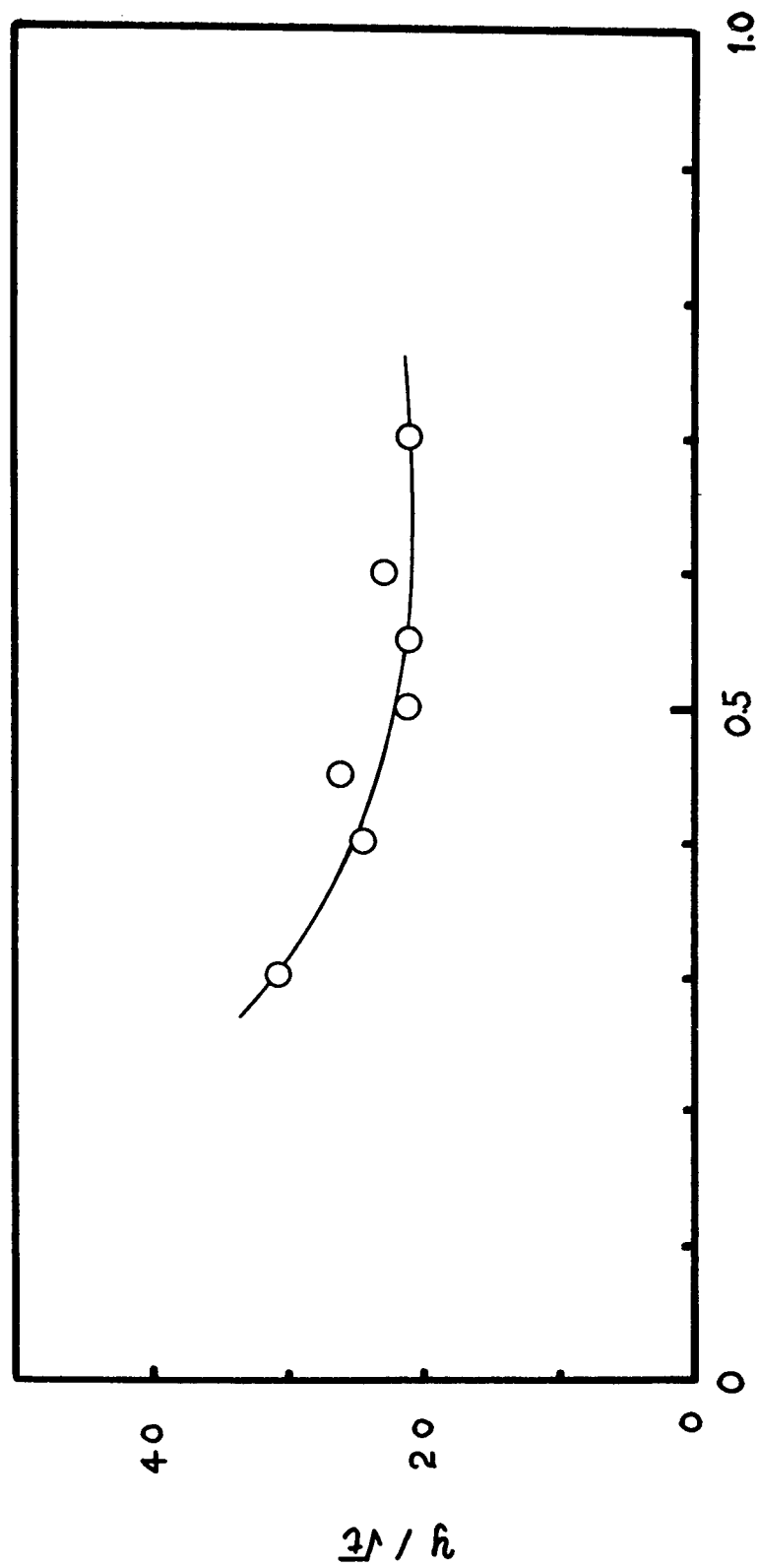


Figure 6 Coagulation rate y/\sqrt{t} plotted against composition of the coagulation mixture ES/MeOH for a 9.2% PBT/MSA solution.

4. RHEOLOGICAL STUDIES ON PBT SOLUTIONS

The rheological properties of rodlike solutions are central to solution processing to develop well oriented materials. In the fiber formation process discussed in Section 2 the elongational flow properties are important. In the film formation process to be discussed in Section 10 the shear flow properties are important. In the following, the properties of isotropic and anisotropic solutions of PBT-62A in MSA (with 2.5% CSA) will be described. The data were determined with a cone-and-plate rheometer described previously¹⁰.

4.1 Experimental

Materials

PBT-62A sample was obtained from SRI International. Its intrinsic viscosity was reported in MSA as 26.5 dl/g. The polymer was dried under vacuum at 60°C for several days prior to use. MSA and CSA were distilled under vacuum and stored in vacuum desiccator. Solution were prepared by mixing dried polymer and acid mixture in a sealed container at 60°C. A Teflon coated magnetic bar was used to slowly stir the solution.

Apparatus

The wire suspension cone and plate rheometer used in this study has been described in detail elsewhere⁽¹⁰⁾. The main problem in this experiment was possible contamination of the sample by moisture. The following procedure was employed to suppress or eliminate this problem. The Rheometer was purged with dry nitrogen for a night at

70°C before the sample was transferred from its sealed container to the sample chamber. The proper amounts of sample (~ 0.7 ml) was transferred from the sealed sample container by dry nitrogen pressure (~ 50 psi) to a 1 ml syringe in a dry glove bag, and injected immediately to the closed rheometer through Teflon tubing. Then, to avoid contamination of sample by moisture during the experiment, the cone plate fixture was sealed by a concentric glass ring resting in dry mineral oil, see Fig. 7. During all these operations, the rheometer was purged with dry nitrogen entering through the bottom and the sample chamber of the rheometer. The sample was well maintained for a week.

4.2 Results and Discussion

In general, the viscosity $\eta_{\dot{\gamma}}$ of polymer solutions approaches a constant value η_0 at each specific temperature, concentration, and composition of polymers at low rate of shear. As the rate of shear $\dot{\gamma}$ is increased, the viscosity departs from η_0 becoming in almost all cases a decreasing function of shear rate. For many fluids, the dependence of the viscosity $\eta_{\dot{\gamma}}$ on the shear rate $\dot{\gamma}$ can be represented in the forms (11,12)

$$\eta_{\dot{\gamma}} = \eta_0 Q(\tau_c \dot{\gamma}) \quad (45)$$

where the time constant τ_c can be evaluated as

$$\tau_c = \eta_0 R_0 \quad (46)$$

with η_0 the zero shear viscosity, the steady state recoverable shear compliance, R_0 defined as the value of the steady state recovery function $R = \gamma_{\dot{\gamma}} / \dot{\gamma} \eta_{\dot{\gamma}}$ in the limit of steady state creep at shear rate $\dot{\gamma}$. In addition for many polymeric fluids, the recovery function $R_{\dot{\gamma}}$ can also be correlated in terms of time constant τ_c ⁽¹²⁾

$$R_{\dot{\gamma}} = R_0 P(\tau_c \dot{\gamma}) \quad (47)$$

In the following, we will discuss the behavior of concentrated solutions of PBT in terms of these relations. It is well known that concentrated solutions of rodlike polymer chains will undergo a phase change from an isotropic to anisotropic state of some molecular dependent concentration. It is also interesting to note that this concentration changes with the temperature and quality of the solvent. In this study, we measured the steady state viscosity $\eta_{\dot{\gamma}}$ function of concentration C and temperature T . The phase change of the polymer solution are also observed by using the polarized microscopy.

Rheological data were collected for solutions of PBT-62 in MSA at the twenty-one combination of concentration and temperature shown in Figure 8. The phase diagram is not yet determined completely for this system, but a few conditions noted as isotropic or nematic phase are also given in the diagram.

The rheological data studied included the steady state viscosity $\eta_{\dot{\gamma}}$ and the recoverable compliance $R_{\dot{\gamma}}$ as functions of the strain rate $\dot{\gamma}$. The data for the six concentrations studied at 60°C are shown in

Figure 9. It may be seen that a rich variety of rheological behavior obtains, including data with a clearly defined limiting viscosity, η_0 at low shear rate, and data for which η_χ appears to increase without bound with decreasing χ at low χ . The behavior noted for the 21 solutions can be separated into three broad classes as illustrated schematically in Figure 8. 1) Type I behavior is observed for isotropic solutions well removed from the phase boundary the data could be correlated by the relations

$$\eta_\chi = \eta_0 Q(\tau_c \chi) \quad (48)$$

$$R_\chi = R_0 P(\tau_c \chi) \quad (49)$$

with $\tau_c = \eta_0 R_0$, and the functions $Q(\)$ and $P(\)$ exhibiting properties similar to those found with other isotropic solutions of rodlike and flexible coil polymers⁽¹²⁻¹⁴⁾. This behavior is illustrated in Figure 10 and Table 1. In this region, η_0 and R_0 are both well defined experimentally--values of η_0 and R_0 are given in Table 7 and Figs. 11-14. 2) Type III behavior is observed for nematic solutions well removed from the phase boundary. The rheological data, shown in Fig. 15, deviate from Eqns. 48 and 49 in at least two ways: a) no limiting value η_0 of the viscosity was found, even for χ as low as 10^{-4} sec^{-1} , and b) the dependence of η_χ and R_χ on a reduced strain rate $\tau_c \chi$ is not universal. For small χ , η_χ is nearly proportional to χ^{-1} . A 'plateau viscosity' η_p equal to the value of η_χ in a plateau is

observed as χ is increased at slightly larger values of χ . Curiously, a well defined limiting value R_0 is observed for the recoverable compliance even though η_χ does not appear to tend to a limiting value for small χ . Type II behavior obtains when the solutions are near a phase boundary. For some of these solutions, it appears that the data can be fitted by Eqns. 48 and 49 as shown in Fig. 16, but the reduced plots do not coincide with the reduced plot for the isotropic solutions. For example, the onset of nonlinearity in η_χ is observed for smaller values of $\tau_c \chi$ than with the isotropic solutions. With these solutions, it is not clear whether the limiting value of η_χ used to compute τ_c corresponds to η_0 or η_p as the limiting behavior did not cover a large span in χ . Values of η_0 (or η_p as the case may be) and R_0 are entered in Table 7 and Figures 11-14.

In two cases, the behavior in region II appears to be a complex blend of the behavior found in regions I and III. As may be seen in Fig. 17 the data obtained at 60 and 40° (with a solution with $w_2 = 0.034$) do not exhibit a true limiting value for η_0 as in region I, or the sharply increasing η_χ at small χ in region III. Rather, η_χ appears to decrease slowly with increasing χ over the range of χ studied. The reason for representing the data as shown in Fig. 17, with the value of η_p given in Table 7 and Figs. 11 and 12 will be discussed below.

4.3 Discussion

Reduced plots for the seven concentrations studied at 60°C are given in Fig. 18 to illustrate the diversity of behavior encountered

in this study. This diverse behavior is conveniently discussed in terms of the three behavior classes described above. It may be noted here that in future work we will attempt to correlate these domains with those observed in the phase equilibria between the isotropic and nematic states.

a) Type I Behavior

The reduced curves given in Fig. 10 for the isotropic solutions are very similar to behavior for flexible chain polymers. Indeed, the reduced flow curve is nearly identical with that for a 6% solution of a high molecular weight polyisobutylene in a mineral oil. The reduced recovery curve is similar to that for other polymer with a molecular weight distribution showing nonlinearity at values of $\tau_c \chi$ for which the flow curve is still linear. The similarity of flow curves for diverse systems has been noted previously in our work. By analogy with other systems studied in our laboratory, the curve for R_χ vs. $\tau_c \chi$ is probably very similar to the function $R_0(\theta)$ versus τ_c/θ where $R_0(\theta)$ is the linear recoverable compliance at time θ after cessation of steady-state flow (e.g., $R_0(\theta) = R_\chi$ for $\chi = \theta^{-1}$). The latter may conveniently be expressed in terms of a spectrum $L(\tau)$ of retardation times τ :

$$R_0(\theta/\tau_c) = R_g + \int_{-\infty}^{\infty} L(\tau/\tau_c) [1 - \exp(-t/\tau)] d\ln(\tau/\tau_c) \quad (50)$$

where R_g is the glassy recoverable compliance. For a thermorheologically simple fluid, $L(\tau/\tau_c)$ is independent of temperature. The data on the isotropic solution indicate a rather broad spectrum, with a

peak at long times approximately in the range 10-100 times τ_c . This is similar to the retardation spectra for other polydispersed polymers.

As may be seen in Fig. 12, η_0 is a strongly increasing function of w_2 for the isotropic solutions.

It is of interest to compare the rheological behavior observed with isotropic solutions with the theoretical calculations of Doi and Edwards^(15,16) for some properties of rodlike molecules. These authors report results of the form

$$\eta_\kappa = \eta_0 [1 + A_\eta (\tau_r \kappa)^2]^{-0.525} \quad (51)$$

$$S_\kappa = S_0 \frac{[1 + A_s (\tau_r \kappa)^2]^{-0.874}}{[1 + A_\eta (\tau_r \kappa)^2]^{-1.050}} \quad (52)$$

where S_κ is determined from the first normal stress difference $N_{1,\kappa}$ as

$$S_\kappa = \frac{N_{1,\kappa}}{2\kappa^2 \eta_\kappa^2} \quad (53)$$

Here τ_r is $(6D_r)^{-1}$, where D_r is the rotational diffusion constant at the concentration (and temperature) of measurement. With the model used for non-dispersed rodlike molecules, $A_\eta = 2.556$, $A_s = 2.009$ and

$$\eta_0 = \sqrt{kT/10} D_r \quad (54)$$

$$S_0 = \frac{5/3}{\sqrt{kT}} \quad (55)$$

so that

$$\eta_0^{S_0} = \eta_0^{R_0} = (6D_r)^{-1} \quad (56)$$

and

$$D_r = \beta D_r^0 / (\nu L^3)^{-2} \quad (57)$$

$$D_r^0 = kT \ln (L/d) / 3\pi \eta_s L^3 \quad (58)$$

where ν is the number of rods per unit volume, β is of order unity, and L is the length of the rodlike molecule.

These relations are meant to apply in the concentration range

$$1/L^3 \ll \nu \ll 1/dL^2 \quad (59)$$

or, in terms of the weight fraction concentration units used here, where M_L is the mass per unit length and ρ_1 is the solvent density, with lengths expressed in Angstrom units. With d and L taken to be 10 and 10^3 Å, respectively for an order magnitude calculation, it may be seen that the concentration range is

$$2 \times 10^{-5} \ll w_2 \ll 2 \times 10^{-3} \quad (60)$$

or far below the range covered in our experiments. It may be reasonable then that the dependence of η_0 on concentration is much greater than the proportionality with ν^3 predicted by these relations. In addition, the calculated decrease of η_x/η_0 with increasing $\tau_r x$ is greater than is

observed experimentally in the range of concentrations studied here. Nonetheless, the general picture presented by the Doi-Edwards calculation to explain the large values of $\tau_c = \tau_r = (6D_r)^{-1}$ must be qualitatively useful. In this picture D_r decreases with increasing ν owing to intermolecular 'entanglement effects'. These intermolecular interactions greatly reduce motions in which the chain moves laterally to its long dimension, but do not much alter motions of the chain along its length axis. Hence the term entanglement, Doi and Edwards have applied the same sort of consideration to the flow of coil chain polymers.

b) Type III Behavior

The type III rheological behavior of the nematic phase reveals the effects of orientation of the ordered domains in the flow field. The behavior at low χ , with η_χ nearly proportional to χ^{-1} is believed to originate with this orientation. The data show that orientation develops at even the smallest values of χ used (about 10^{-4} sec^{-1}). The relative mobility of these domains is advantageous in the formation of well oriented fibers and films by solution processing. The rheological time constant $\tau_c = \eta_p R_0$ is not large for these nematic PBT fluids, in contrast to the situation with PBO for which it appeared that τ_c increased appreciably for the nematic fluid. The data in Fig. 19 show that τ_c reaches a maximum near the phase boundary, then falls by about ten-fold as the solution becomes fully nematic. The small values of τ_c for the nematic fluid indicate that the quenching step in a solution processing method will have to be rapid to preserve fluid induced orientation.

The plateau observed in η_κ for $\eta_p R_0 \kappa \sim 1$ may indicate that the domain orientation is essentially complete, with flow occurring by slippage of the rods along their long axis. The origin of the non-linear effect observed for $\eta_p R_0 \kappa > 1$ with type III behavior is not understood, but must indicate that κ^{-1} has become comparable to or larger than the longest time constants for motion in the oriented nematic fluid.

c) Type II Behavior

The behavior in type II flow is more complicated, and may involve an isotropic to nematic phase transition under the influence of the flow field. Thus, the gradual decrease of η_κ at low κ may involve the creation and orientation of a nematic phase in addition to any that may exist for the stagnant fluid. The data do not exhibit any pronounced plateau, but an inflection is used to estimate a value for η_p to give the reduced plot shown in Fig. 17. Perhaps by happenstance, this plot coincides with the general reduced curve for type I behavior for $\eta_p R_0 \kappa > 1$. In future work, we will correlate the flow birefringence with the rheological data to provide an assessment for this model.

Table 7

Rheological Parameters for Solutions of PBT-62A

Conc.	Temp.	η_0	R_0	$\tau_c = \eta_0 R_0$	$\frac{1}{\tau_c}$	Remarks
1.5 w%	60°C	0.63×10^3	1.06×10^{-3}	0.67	1.5	R_0 calculated from master curve
	45°C	1.25×10^3	1.07×10^{-3}	1.33	0.75	
	20°C	3.20×10^3	1.42×10^{-3}	4.54	0.22	
2.52 w%	60°C	5.2×10^4	1.5×10^{-3}	78	1.28×10^{-2}	$\eta_0 R_0$ experimental data
	23.5°C	4.2×10^5	1.25×10^{-3}	525	1.90×10^{-3}	
	4°C	1.4×10^6	0.78×10^{-3}	1092	9.15×10^{-4}	
3.0 w%	80°C	0.52×10^5	1.8×10^{-3}	93.6	1.07×10^{-2}	R_0 extra-polated data
	60°C	0.95×10^5	1.6×10^{-3}	152	6.58×10^{-3}	$\eta_0 R_0$ experimental data
	40°C	3×10^5	1.4×10^{-3}	420	2.38×10^{-3}	
	20°C	9×10^5	1.2×10^{-3}	1080	9.26×10^{-4}	
	10°C	1.7×10^6	1.05×10^{-3}	1785	5.60×10^{-4}	
	-1°C	2.5×10^6	0.85×10^{-3}	2125	4.70×10^{-4}	
3.43 w%	60°C	3.0×10^4	0.82×10^{-3}	246	4.06×10^{-3}	$\eta_0 \Rightarrow \eta_{\text{plateau}}$
	40°C	6.5×10^4	0.60×10^{-3}	390	2.56×10^{-3}	$\eta_0 \Rightarrow \eta_{\text{plateau}}$
	20°C	3.5×10^4	1.0×10^{-3}	350	2.85×10^{-3}	$\eta_0 \Rightarrow \eta_K = 10^{-4}$
	10°C	4.8×10^4	0.78×10^{-3}	374	2.67×10^{-3}	$\eta_0 \Rightarrow \eta_K = 10^{-4}$
4.73 w%	60°C	2.2×10^3	1.8×10^{-2}	39.6	2.52×10^{-2}	$\eta_0 \Rightarrow \eta_{\text{plateau}}$
	20°C	6.0×10^3	2.1×10^{-2}	126	7.9×10^{-3}	
6.11 w%	60°C	3.4×10^3	3×10^{-2}	102	9.8×10^{-3}	$\eta_0 \Rightarrow \eta_{\text{plateau}}$
8.2 w%	60°C	3.0×10^3	4.0×10^{-2}	120	8.3×10^{-3}	$\eta_0 \Rightarrow \eta_{\text{plateau}}$
	23.5°C	4.8×10^3	4.5×10^{-2}	216	4.6×10^{-3}	

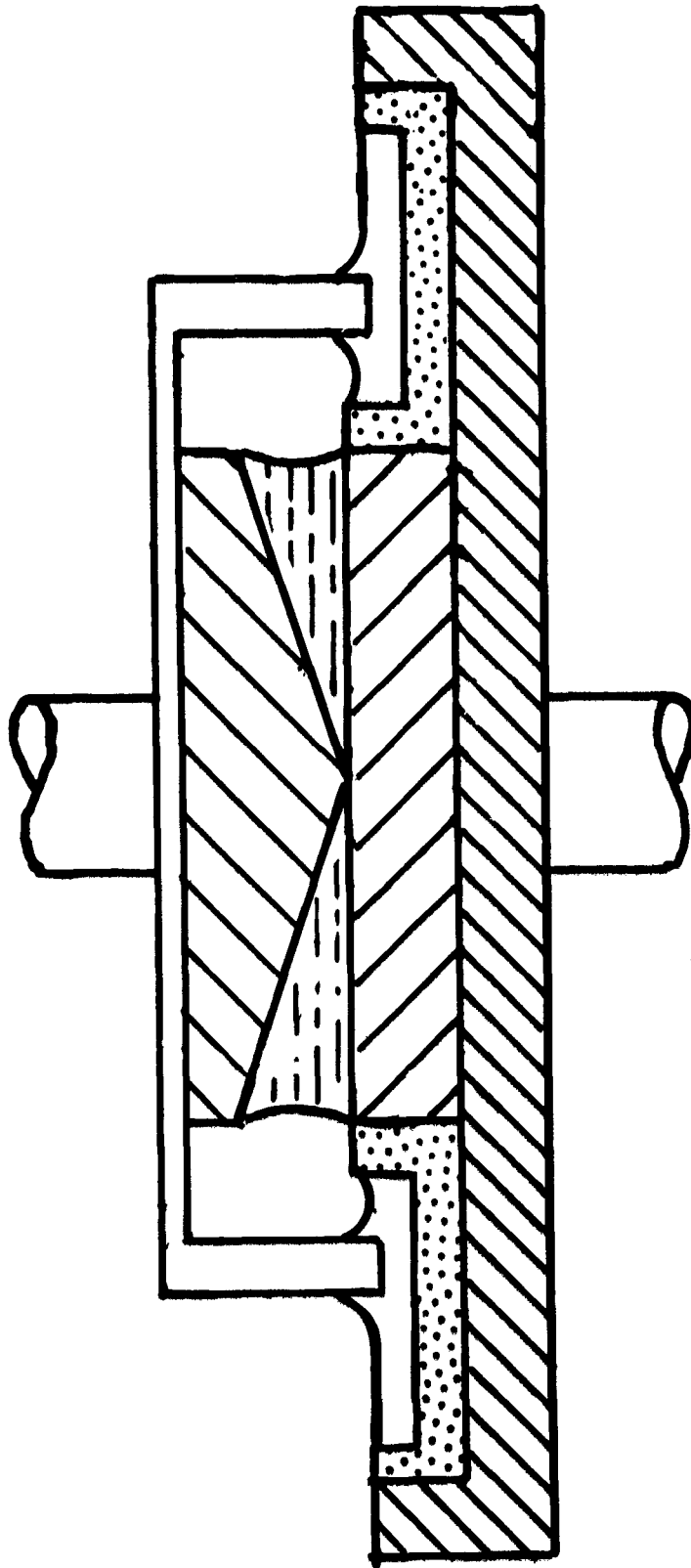


Figure 7 Schematic drawing of the cone and plate assembly, showing the guard ring immersed in oil used to seal the sample from moisture.

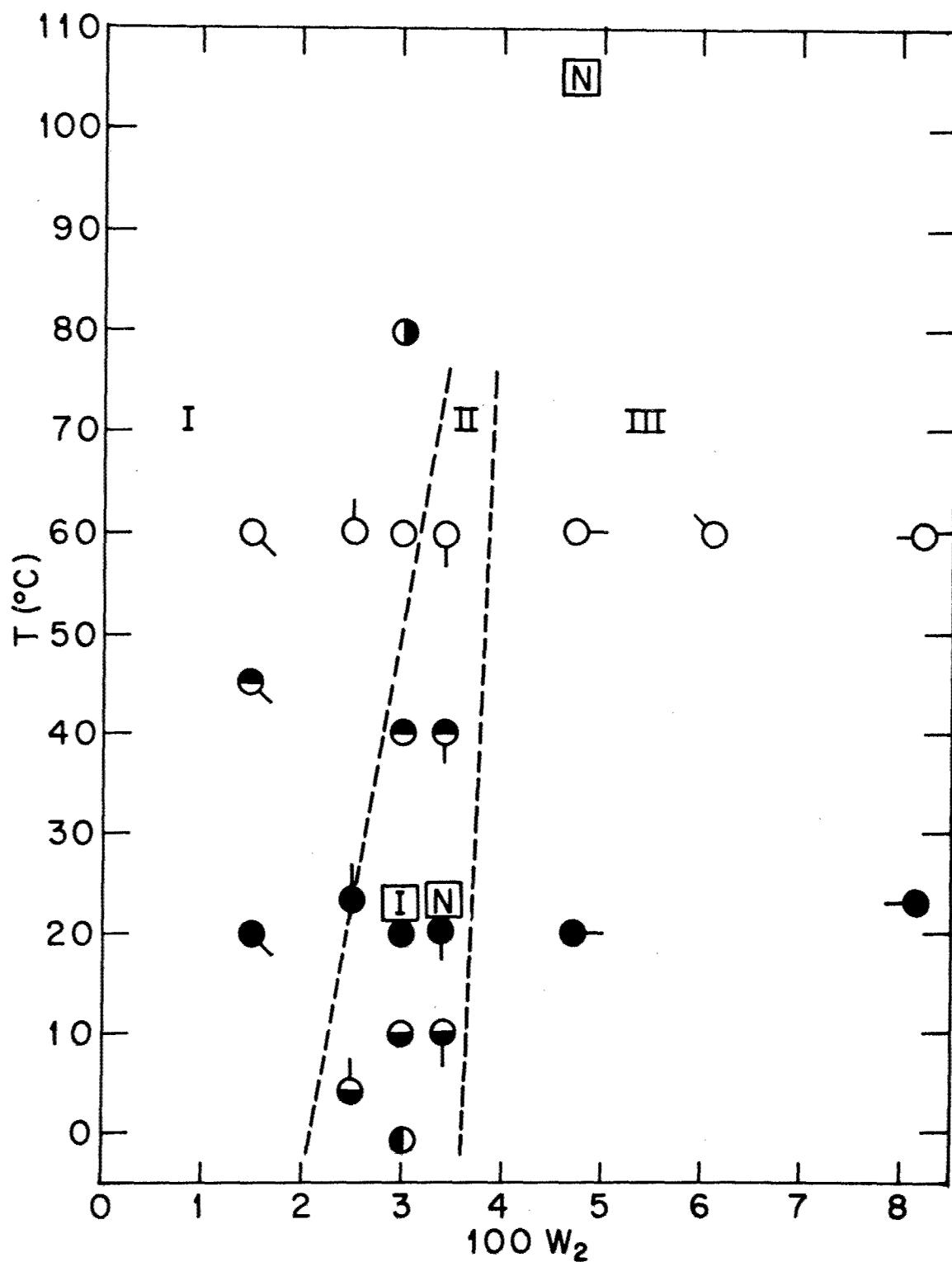


Figure 8

Plot showing the combinations of temperature and weight fraction studied with solutions of PBT-62. The symbols are used in subsequent plots to designate a particular T , w_2 combination. The notations [I] and [N] indicate that the fluid was isotropic or nematic at the corresponding T and w_2 conditions. The approximate boundaries between type I, II and III flow regimes are indicated by the dashed lines.

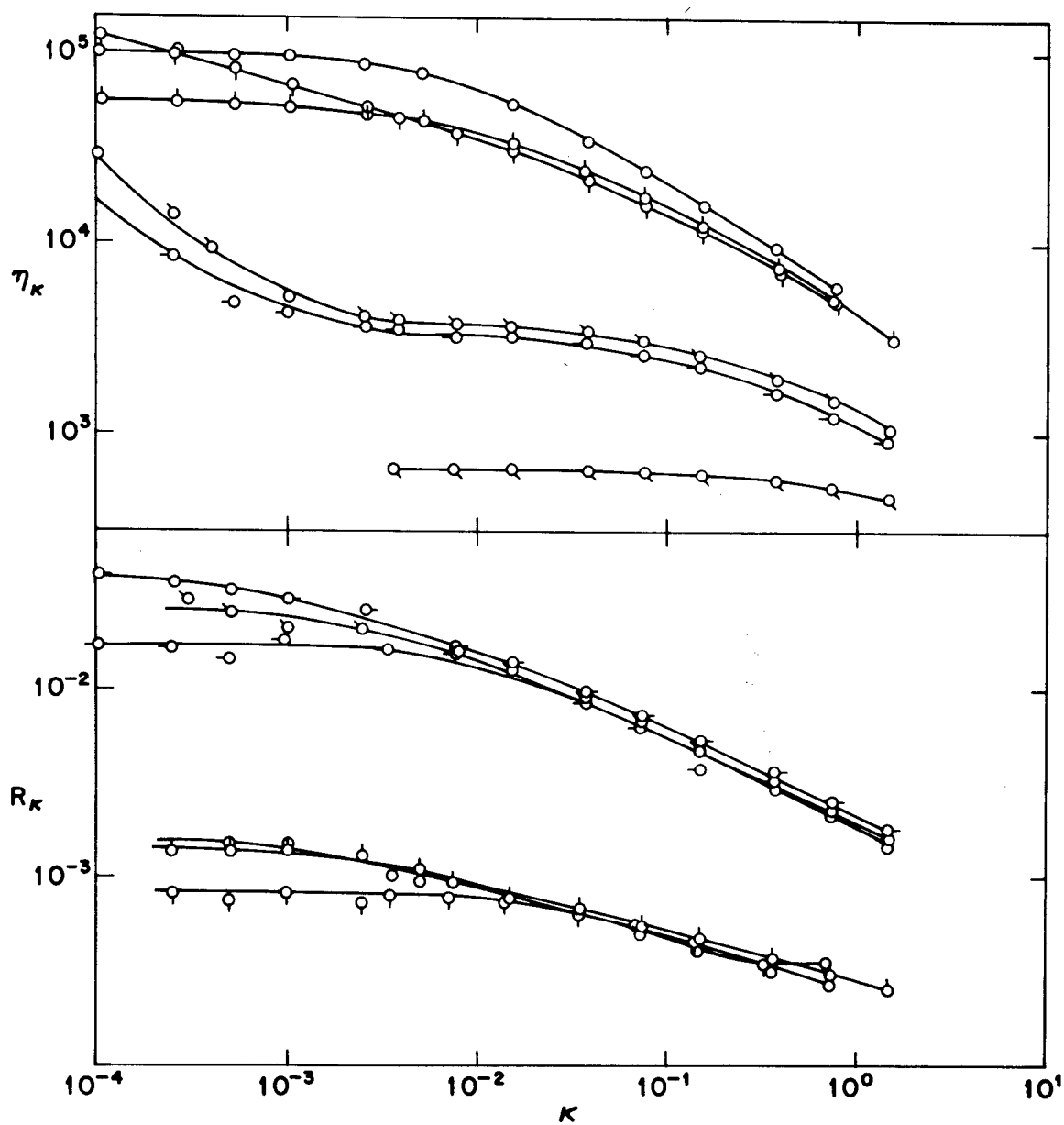


Figure 9 a) The viscosity η_κ versus shear rate for several PBT solutions at 60 degrees C.
 b) The recovery R_κ versus shear rate for several PBT solutions at 60 degrees C.

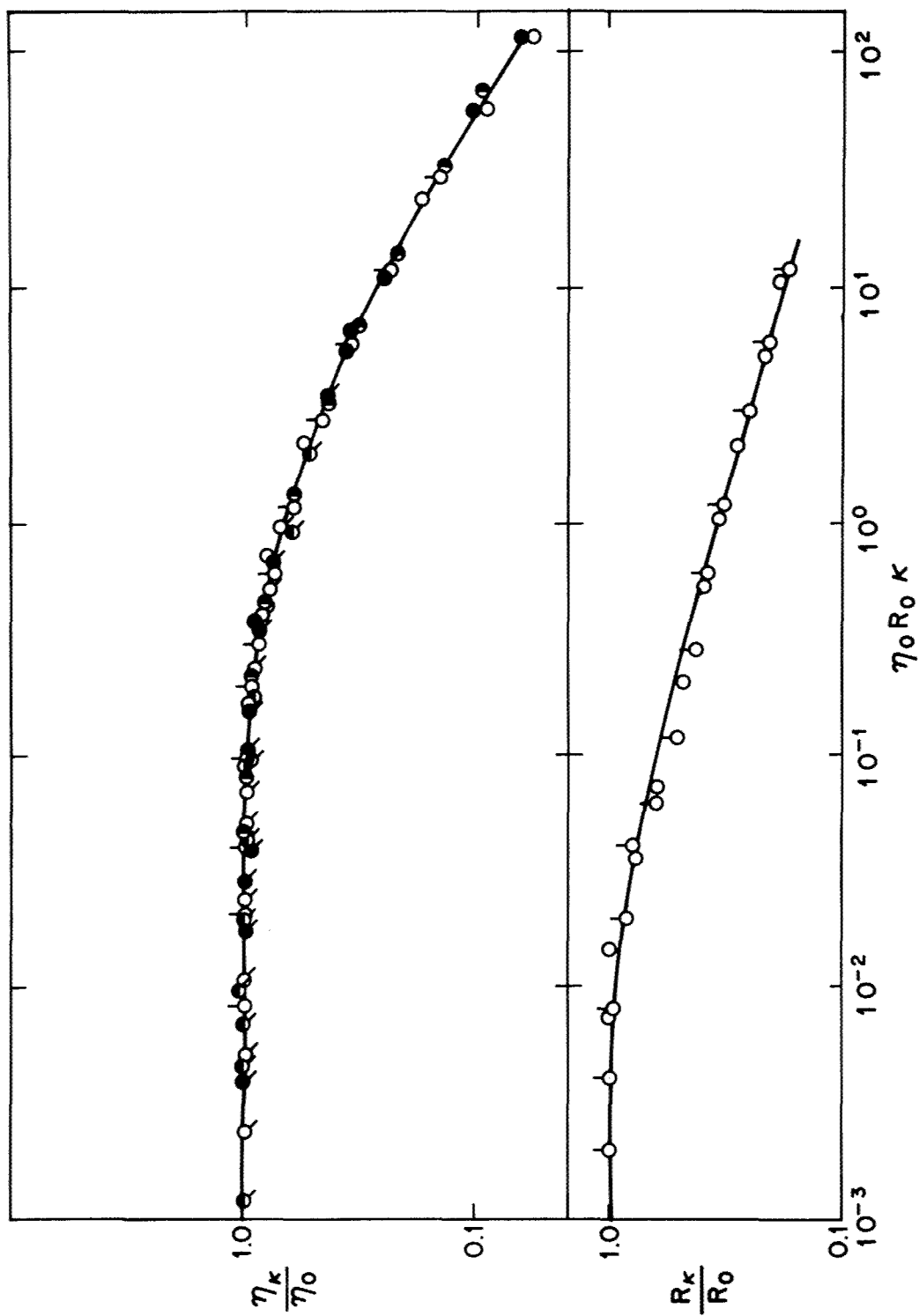


Figure 10 a) The reduced viscosity η_κ/η_0 versus reduced shear rate $\eta_0 R_0$ for PBT solutions with type I behavior.
 b) The reduced recovery R_κ/R_0 versus reduced shear rate $\eta_0 R_0$ for PBT solutions with type I behavior.

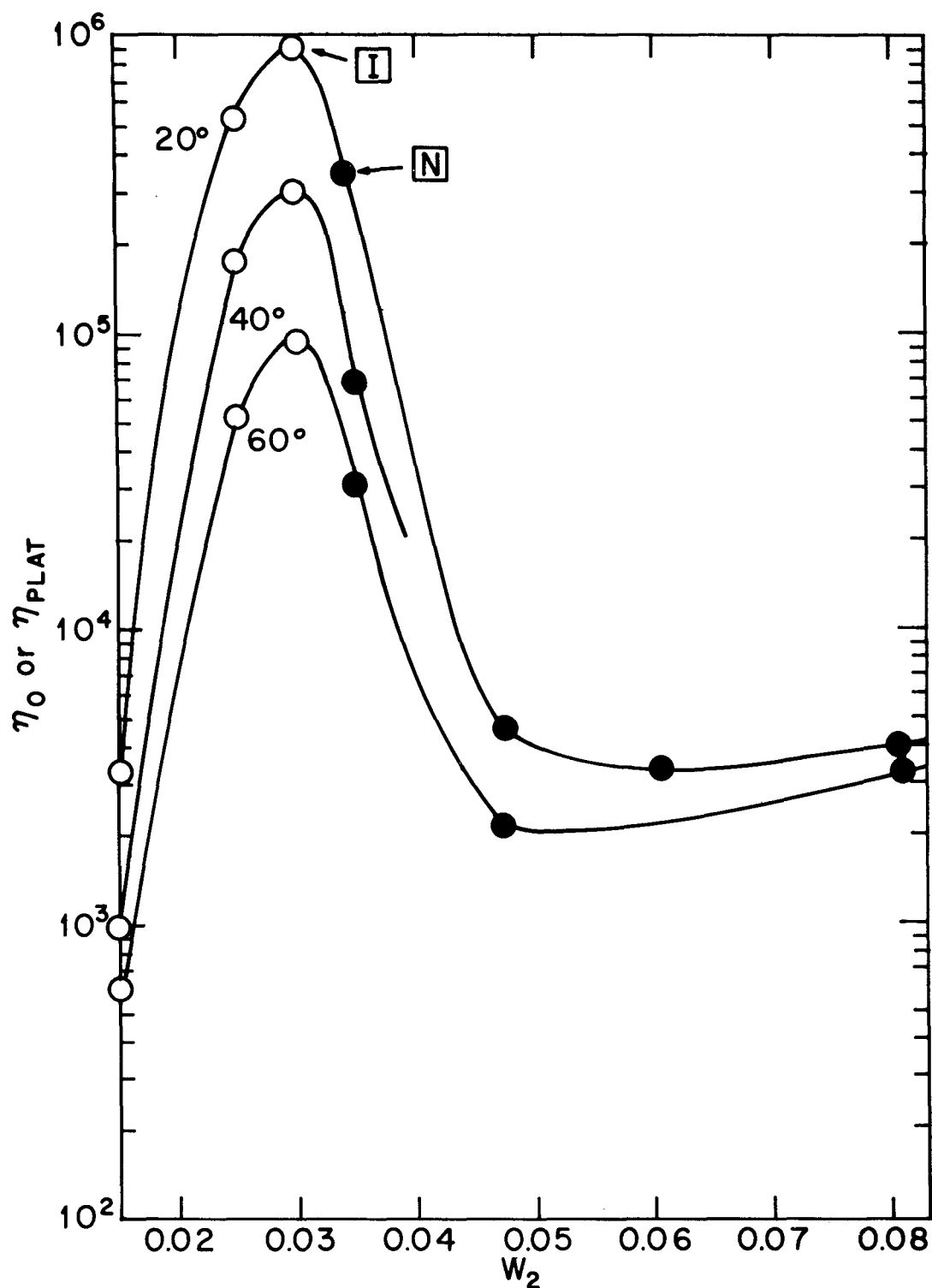


Figure 11

The viscosity versus temperature for PBT solution with the indicated w_2 . The limiting viscosity η_0 is used for solution with type I and II behavior. The plateau viscosity η_p is used for solutions with type III behavior.

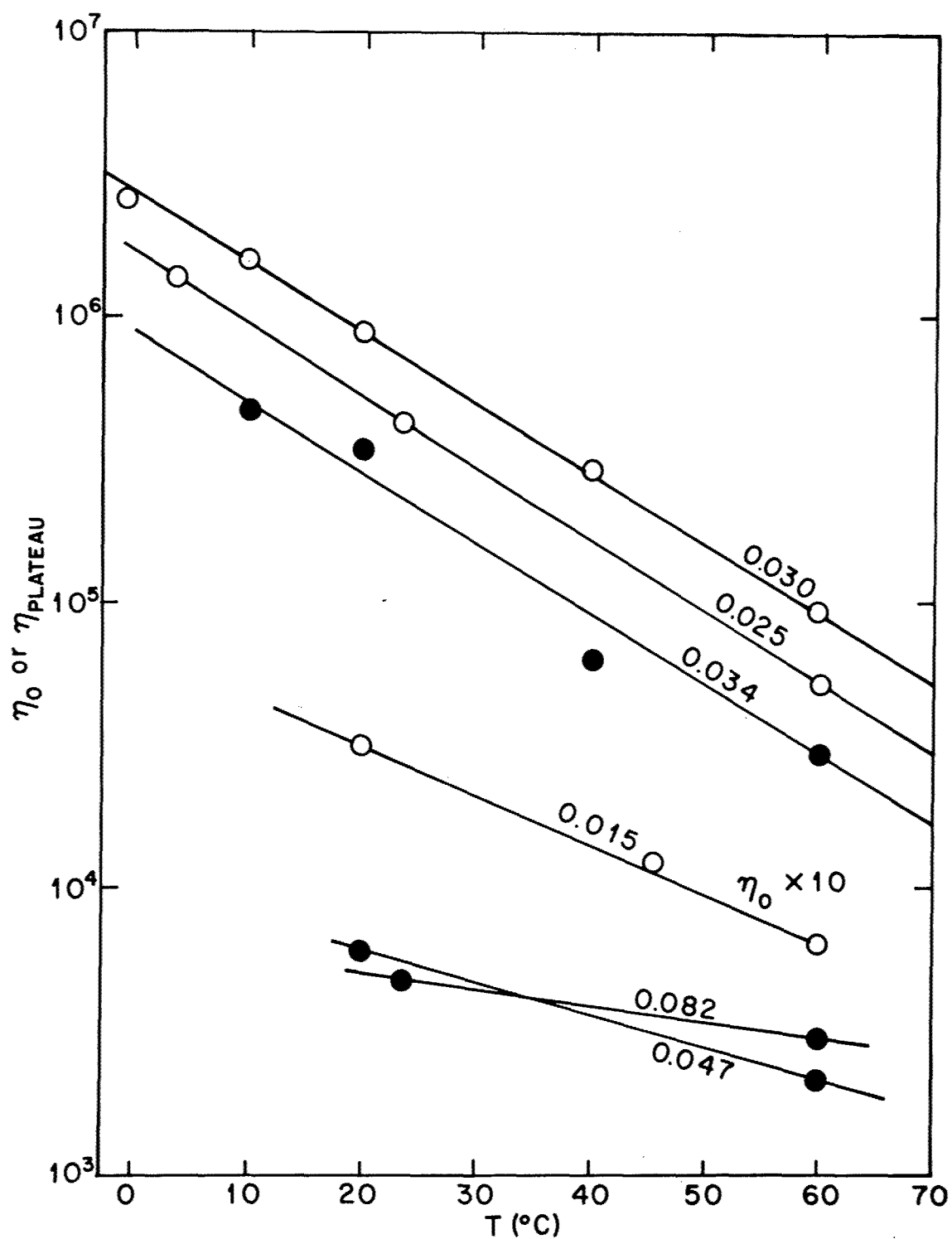


Figure 12

The viscosity η_0 or η_p (see Fig. Captions 1-5) versus temperature for PBT polymer solutions with indicated w_2 .

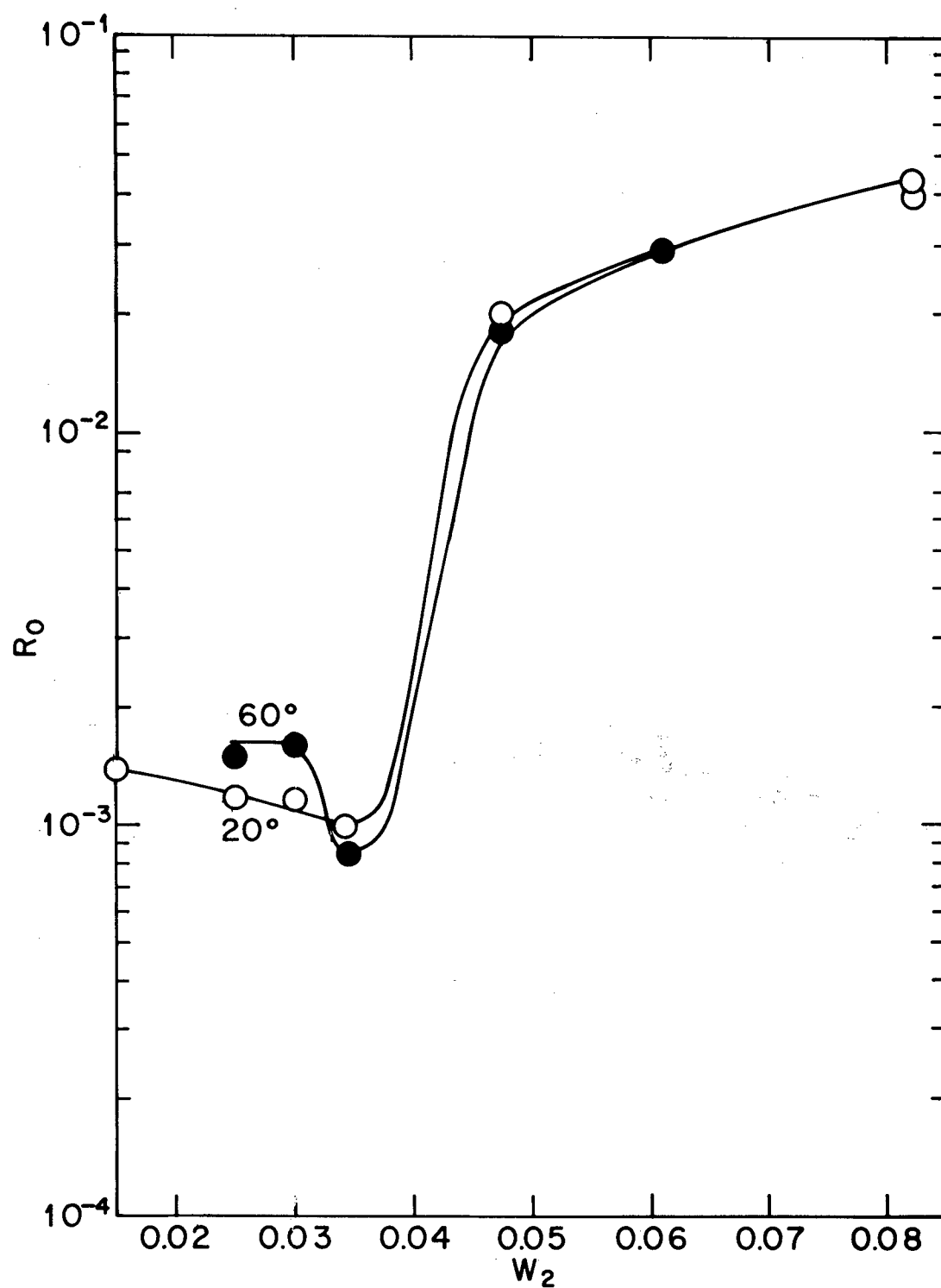


Figure 13 Limiting recoverable compliance R_0 versus weight fraction for PBT solutions with indicated temperature.

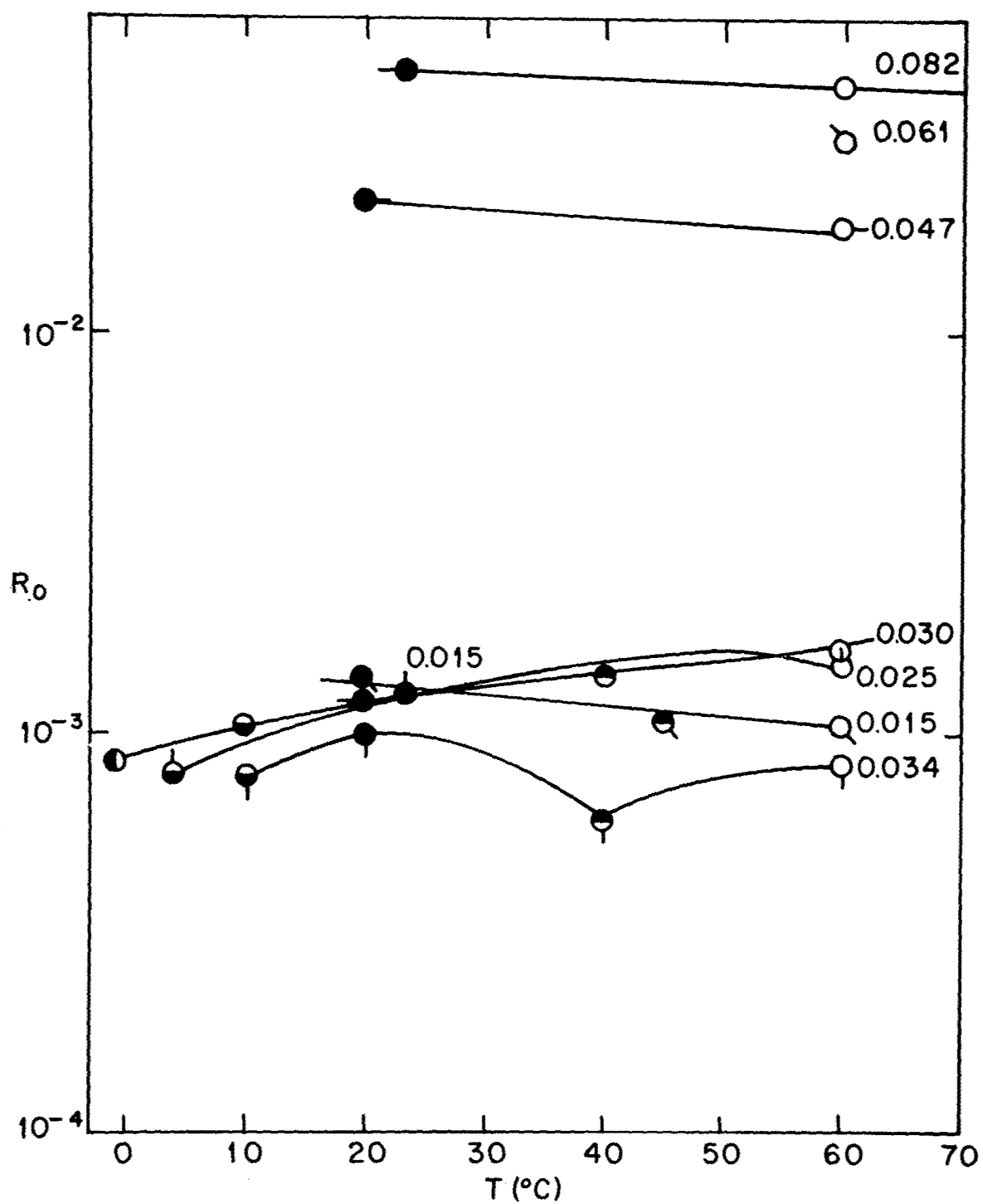


Figure 14 Limiting recoverable compliance versus temperature for PBT polymer solutions with indicated w_2 .

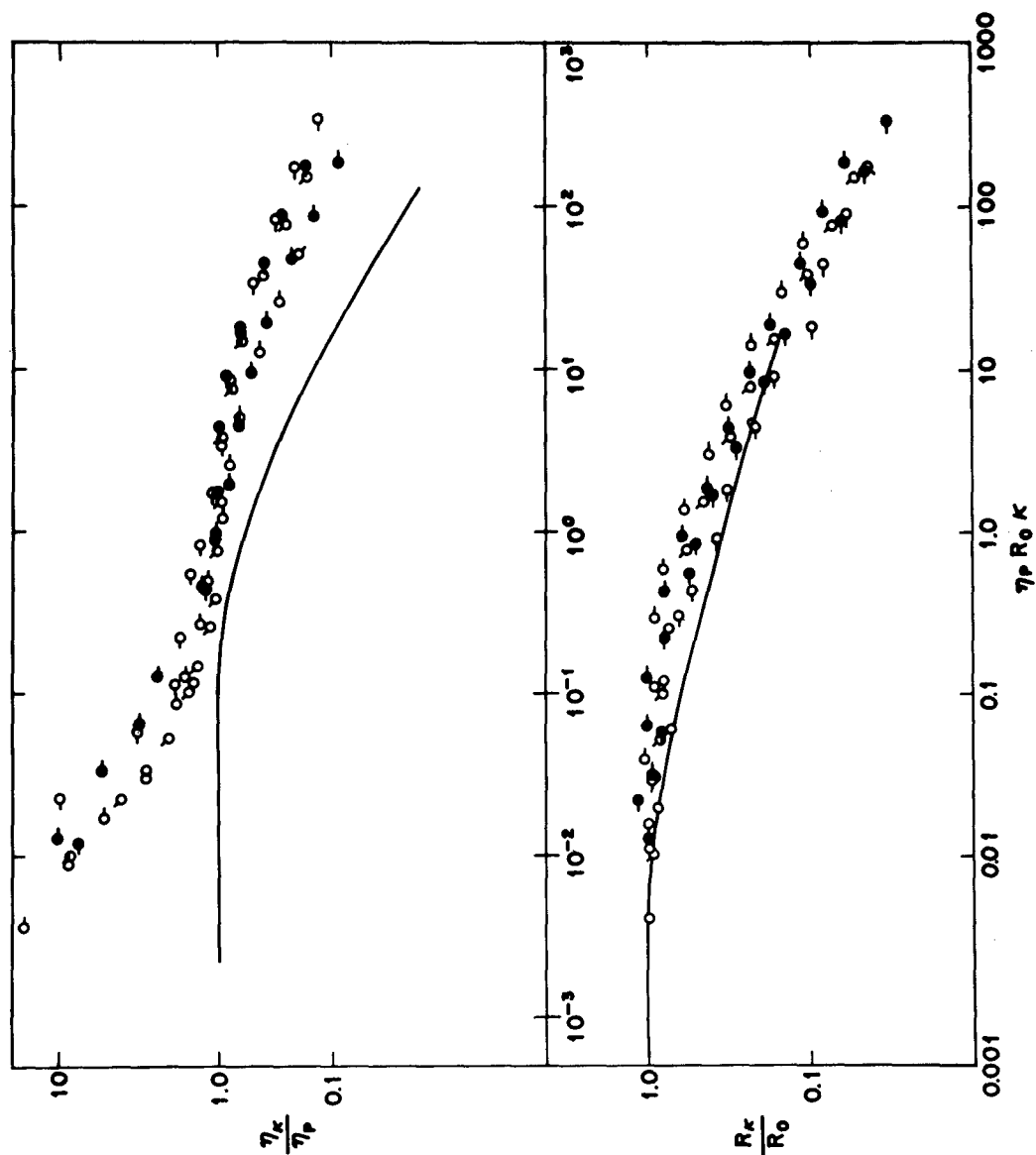


Figure 15 a) The reduced viscosity η_κ/η_p versus reduced shear rate $\eta_p R_0 \kappa$ for PBT solutions with type III behavior.
 b) The reduced recovery R_κ/R_0 versus reduced shear rate $\eta_p R_0 \kappa$ for PBT solutions with type III behavior.

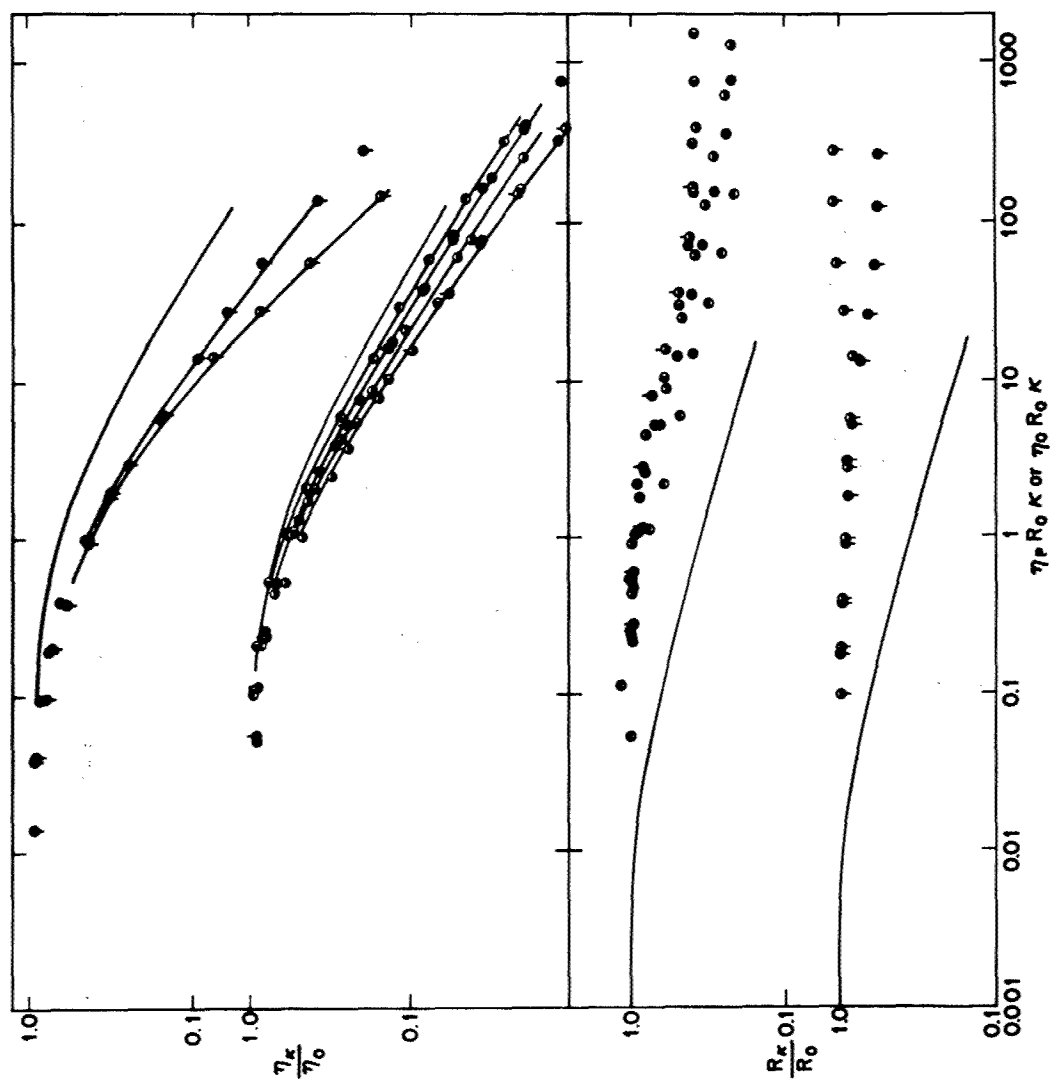


Figure 16 a) The reduced viscosity η_κ / η_0 versus reduced shear rate $\eta_0 R_0 \kappa$ for PBT solutions with type II behavior.
 b) The reduced recovery R_κ / R_0 versus reduced shear rate $\eta_0 R_0 \kappa$ for PBT solutions with type II behavior.

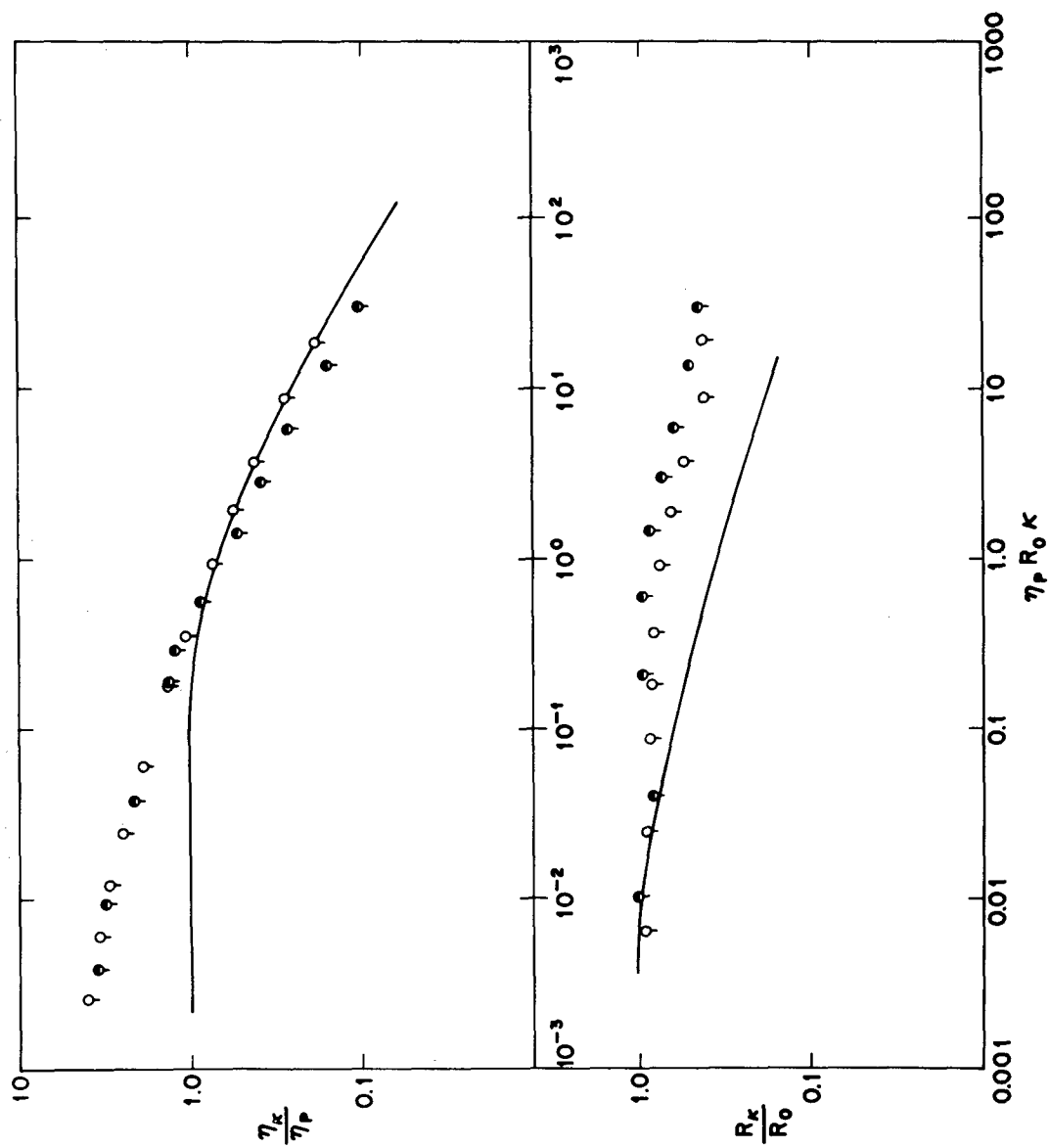


Figure 17 a) The reduced viscosity η_κ/η_p versus reduced shear rate $\eta_p R_0 \kappa$ for PBT solutions with type II behavior.
 b) The reduced recovery R_κ/R_0 versus reduced shear rate $\eta_p R_0 \kappa$ for PBT solutions with type II behavior.

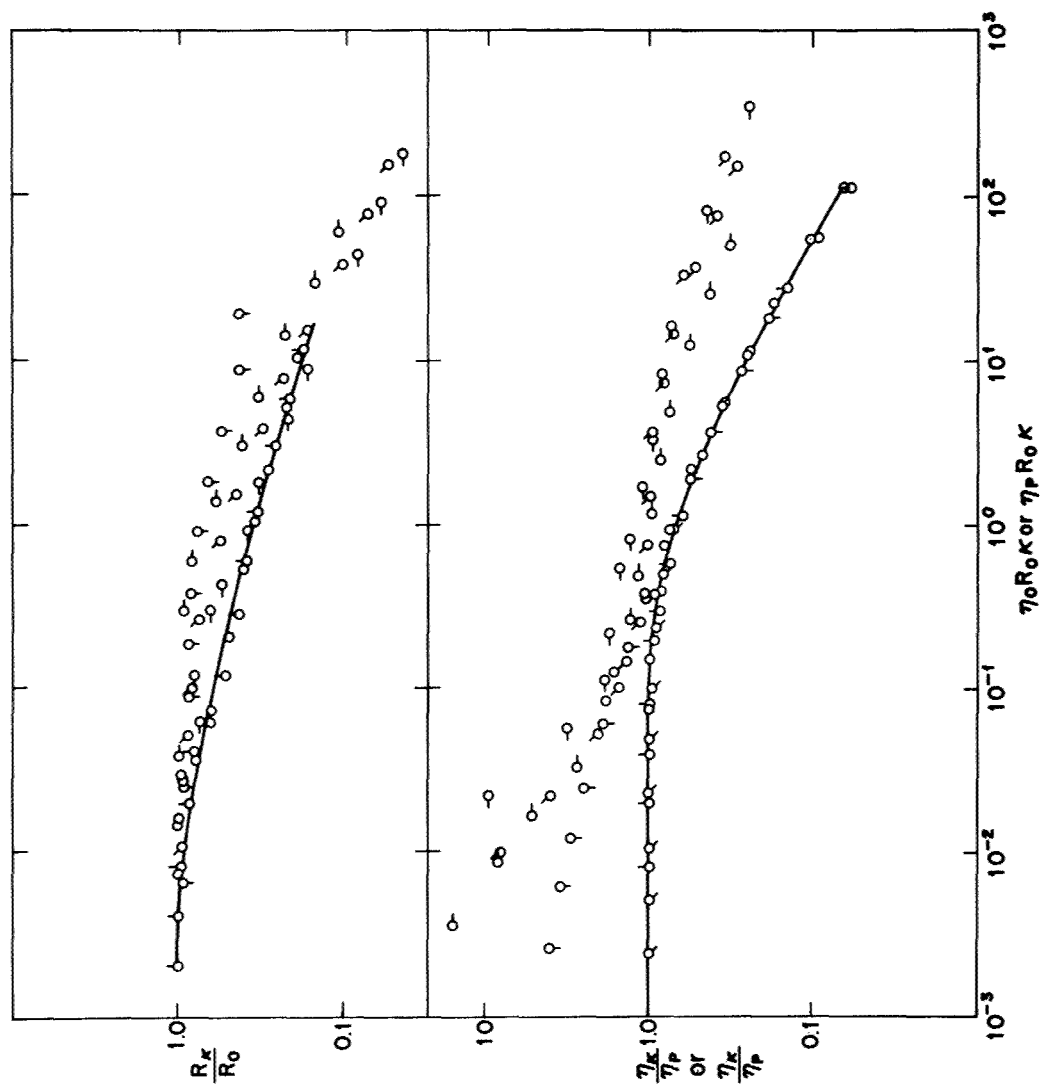


Figure 18 a) Composite curves of η_{sp}/η_{sp}^0 or η_{sp}/η_{sp}^0 versus $\eta_{sp}^0 R_0 c$, respectively, for data on PBT solutions with several concentrations at 60°C illustrating the range of behavior in types I, II and III.

b) Composite curves of R_w/R_0 versus $\eta_{sp}^0 R_0 c$, for data on PBT solutions with several concentrations at 60°C illustrating the range of behavior in types I, II and III.

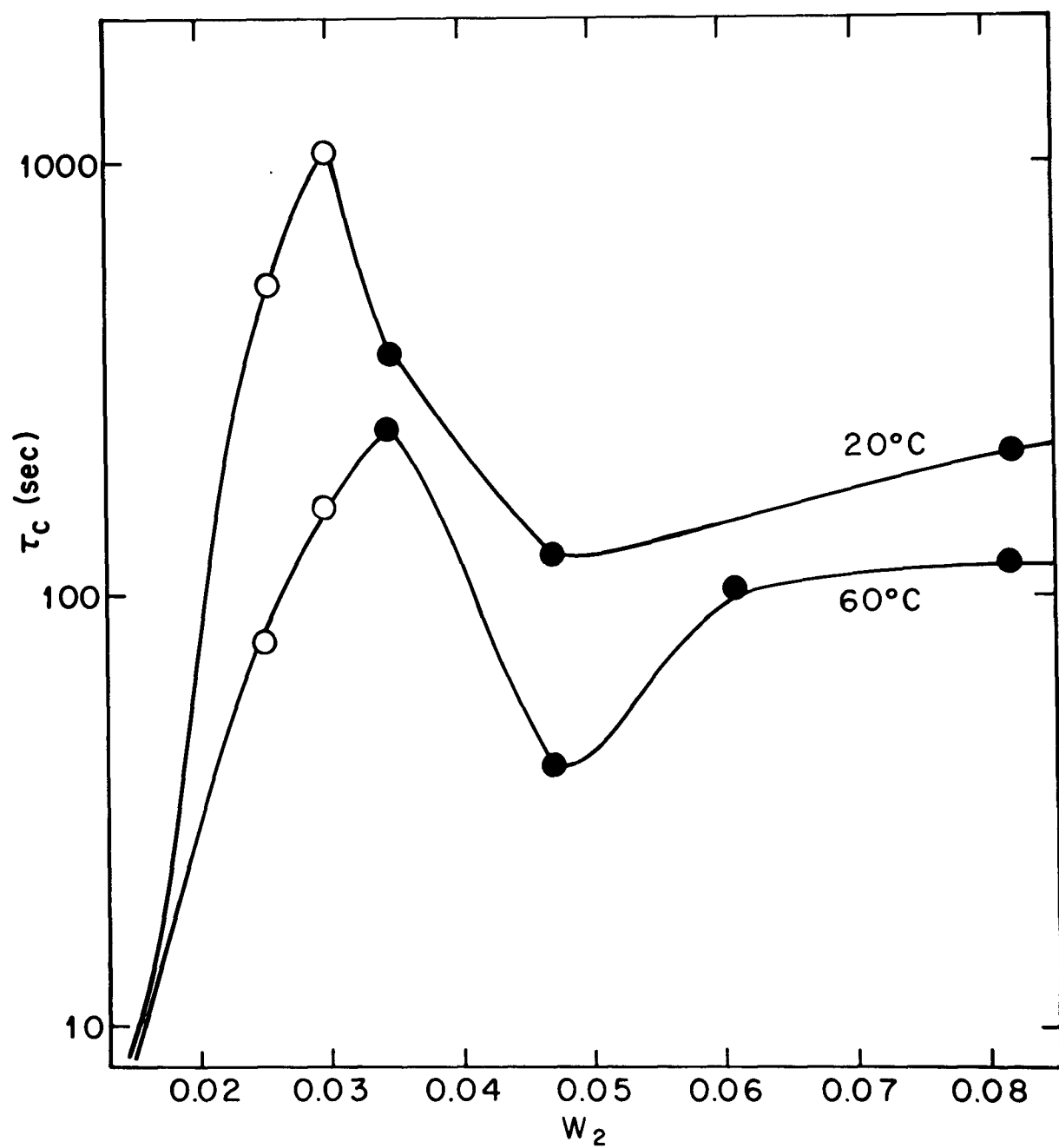


Figure 19

The rheological time constant $\tau_c = \eta_0 R_0$ or $\eta_p R_0$ versus w_2 for PBT solutions at two temperatures.

5. MOLECULAR ORIENTATION OF ROD-LIKE MOLECULES

5.1 Review Of Models For Representing PBT Polymer Solution.

In previous discussion of flow induced orientation of rodlike polymers, we have invoked the Bird dumbbell model for representation of the chain in solution. This model suffers from two defects:

(i) the frictional resistances are concentrated at the two ends of the rod, and (ii) the two beads are so far apart that the hydrodynamic interaction between them is assumed to be negligible.

The Kramers' method discussed above can be applied to a model composed of shishkebab of N beads. All results are the same for both models except the time constant τ_c for the latter is given by⁽¹⁷⁾

$$\tau_c = \frac{\pi \eta_s d L^2 N(N+1)}{40 k T (N-1)} \quad \text{for a shishkebab} \quad (61)$$

instead of

$$\tau_c = \frac{3\pi \eta_s d L^2}{20 k T} \quad \text{for a dumbbell} \quad (62)$$

where η_s is the solvent viscosity, d the diameter of the beads and L the length of the rod. (Note that Eqn. 61 reduces to Eqn. 62 if $N = 2$ for a dumbbell model). The shishkebab model takes care of the first defect but still assumes no hydrodynamic interaction among the beads, which is far from a realistic model for a solution of the rigid rodlike PBT polymer.

It came to our attention that in the treatment of a dilute

suspension of axisymmetric Brownian particles, Brenner⁽¹⁸⁻²⁰⁾ had shown that the rheological properties for such system for any homogeneous flow, steady or not, can be expressed in terms of five dimensionless fundamental material constants which depends only on the shape of the suspended particles. For convenience we have listed in Table 8 the values of these five constants for dumbbell, prolate ellipsoid and circular cylinder in terms of their aspect ratio r_p , in the limit of large r_p .

It has been shown that for a suspension of any axisymmetric particles under steady elongational flow, the orientational distribution function can be written as ⁽¹⁹⁾

$$\psi(\theta) = \frac{J}{4\pi} \exp(-\mu \sin^2 \theta) \quad (63)$$

where

$$J \equiv e^\mu / \int_0^1 e^{\mu z^2} dz$$

and

$$\mu \equiv B \bar{\kappa} / D_r \quad (64)$$

with $\bar{\kappa}$ being the elongation rate and D_r the rotating diffusion constant of the particle given by

$$D_r = kT/6 \eta_s V_p K_r$$

in which V_p is the volume of the particle and K_r is a geometric parameter dependent only on r_p (cf. Table 8).

Equation (63) is identical to the result obtained for rigid dumbbell reported previously if we put

$$\tau_c = \frac{B}{10D_r} \quad (65)$$

remembering that B is very close to unity for long slender bodies.

It is thus evident that the single most important material parameter governing the orientation of molecules in an elongational flow field is D_r , or τ_c as defined by Eqn. (65). Rigorous deviation of this parameter has been worked out for models of ellipsoid, cylinder and shishkebab of beads with hydrodynamic interactions by Perrin⁽²¹⁾, Broersma⁽²²⁾ and Yamakawa⁽²³⁾, respectively. In the limit of $r_p \gg 1$, their results reduce to

$$\begin{array}{ll} \text{for ellipsoid} & \tau_c = \frac{\pi \eta_s L^3}{30kT(\sigma - 0.5)} \\ \text{(Perrin)} & \end{array} \quad (66)$$

$$\begin{array}{ll} \text{for cylinder} & \tau_c = \frac{\pi \eta_s L^3}{30kT(\sigma - 1.02)} \\ \text{(Broersma)} & \end{array} \quad (67)$$

$$\begin{array}{ll} \text{and for shishkebab} & \tau_c = \frac{\pi \eta_s L^3}{30kT(\sigma - 0.466)} \\ \text{(Yamakawa)} & \end{array} \quad (68)$$

in which $\sigma \equiv \ln 2r_p$. Equation (66) is identical to the result presented in Table 8 for an ellipsoid. Equation (67) is considered to be more reliable than that given in Table 8 for a cylinder since Broersma took

end effects into account in his calculation.

The fact that τ_c is only weakly dependent on the aspect ratio r_p (inversely proportional to $[\ln 2r_p - \text{const}]$) when r_p is large, but strongly dependent upon the length L (proportional to L^3) suggests a strong dependence on molecular length and length distribution for molecular orientation since the parameter $\mu = \frac{15}{2} \tau_c \bar{\chi}$ enters the distribution function $\psi(\theta)$ exponentially.

Although the relations described in the preceding are intended to serve as guides in formulating process conditions for PBO and PBT, it should be recognized that the equations given were obtained without consideration for intermolecular interactions. Consequently, quantitative correlation of, for example, the molecular weight dependence of τ_c between experiment and the relations given above would not be expected. These relations may, however, prove helpful in understanding and predicting effects in concentrated solutions.

5.2 Elongational viscosity $\bar{\eta}$ and the time constant τ_c .

The elongational viscosity $\bar{\eta}$ as a function of elongation rate $\bar{\chi}$ has been calculated to be

$$\bar{\eta} = 3 \eta_s \left\{ 1 + \frac{5}{2} \phi \left[2Q_1 - \frac{1}{2} Q_2 (3F+1) + \frac{3}{4} (3Q_2 + Q_3) (3F-1) / \mu \right] \right\} \quad (69)$$

where $F(\mu) \equiv \frac{1}{2\mu} [J-1]$ and ϕ is the volume fraction of polymer. At the zero strain rate limit, $\lim_{\mu \rightarrow 0} F(\mu) = \frac{1}{3} + \frac{4}{45} \mu$ and

$$\bar{\eta}_0 = 3 \eta_s [1 + \phi (5Q_1 - Q_2 + 2Q_3)] \quad (70)$$

while at the high strain rate limit, $\lim_{\mu \rightarrow 0} F(\mu) = 1$ and the elongational viscosity goes to the value

$$\bar{\eta}_{\infty} = 3 \eta_s [1 + \phi(5Q_1 - 5Q_2)] \quad (71)$$

In the case of a solution of circular cylinders, Eqn. (69), (70), and (71) take the forms

$$\bar{\eta} = 3 \eta_s \left\{ 1 + \frac{5}{2} \phi \left[\frac{4}{5} + \frac{1}{45} \frac{r_p^2 (3F+1)}{(\ln r_p - 1.447)} + \frac{1}{10} \frac{r_p^2 (3F-1)}{\mu (\ln r_p + 2.06)} \right] \right\} \quad (72)$$

$$\bar{\eta}_0 = 3 \eta_s \left\{ 1 + \phi \left[2 + \frac{8r_p^2}{45(\ln r_p - 0.132)} \right] \right\} \quad (73)$$

$$\bar{\eta}_{\infty} = 3 \eta_s \left\{ 1 + \phi \left[2 + \frac{2r_p^2}{9(\ln r_p - 1.447)} \right] \right\} \quad (74)$$

The change of elongational viscosity due to strain rate is small.

For example, for moderately concentrated or concentrated solutions,

$\bar{\eta}_{\infty} / \bar{\eta}_0 = 1.58, 1.77$ and 2.74 for $r_p = 10^3, 10^2$ and 10 respectively.

This is similar to the value $\bar{\eta}_{\infty} / \bar{\eta}_0 = 2$ cited above for non-interacting dumbbells.

As the time constant τ_c plays an important role in the orientation process, we would like to examine it in more detail. The value of τ_c can usually be obtained from rheological measurements in simple shear flow as the product of viscosity η_0 and recoverable compliance R_0 in the limit of zero shear rate (dominant Brownian motion limit). We shall designate this value as τ_c' :

$$\tau_c' = \eta_0 R_0 \quad (75)$$

It has been shown that for a simple fluid⁽²⁴⁾

$$R_0 = \lim_{\kappa \rightarrow 0} \frac{T_{22} - T_{11}}{2T_{21}^2} \quad (76)$$

where $T_{22} - T_{11}$ and T_{21} are the primary normal stress difference and the shear stress respectively in a simple shear flow with shear rate κ . For a solution of axisymmetric particles⁽¹⁹⁾

$$\lim_{\kappa \rightarrow 0} T_{21} = \eta_s \kappa [1 + \phi(5Q_1 - Q_2 + 2Q_3)] \quad (77)$$

and

$$\lim_{\kappa \rightarrow 0} T_{22} - T_{11} = \frac{\phi}{5} \eta_s B^2 \kappa^2 K_r / D_r \quad (78)$$

Substitution of these into (75) and (77) yields

$$\tau_c' = \frac{B}{10D_r} \frac{\phi B K_r}{1 + \phi(5Q_1 - Q_2 + 2Q_3)} \quad (79)$$

or

$$\tau_c' = \frac{BK_r}{5Q_1 - Q_2 + 2Q_3} \tau_c \quad (80)$$

for moderately concentrated or concentrated solution. The constants in the front factor in Eqn. (69) can be found in Table 3.

On the other hand for cylinders, which better represent the PBT species, evaluation of the front factor results in

$$\tau_c = \frac{4}{5} \left(1 + \frac{0.464}{\ln 2r_p} \right) \tau_c' \quad (81)$$

Typical values of the front factors are 0.80, 0.85, 0.87 and 0.92 for $r_p = \infty, 10^3, 10^2$ and 10^1 respectively. Therefore, τ_c' , as measured from shear viscosity and recovery experiments slightly overestimate (10-20%) the effective time constant τ_c that determines the angular distribution function in elongational flow.

5.3 Effect of length distribution.

The actual molecular alignment in a fiber spinning operation is a time dependent process instead of the idealized steady state flow. For the situation of unsteady state Brenner has shown that the stress relaxes exponentially, with time with the relaxation time being $\frac{5}{3} \tau_c$ for stress relaxation after cessation of steady flow⁽¹⁹⁾. If the solution is composed of rods with a distribution of lengths, since $\tau_c \sim L^3$, the total stress will be dominated by the contribution from the longer species, especially at long times. As an example, the constant τ_{mix} of a mixture of equal fraction of two kinds of rods with length $L_1 = L$ and $L_2 = \frac{1}{2} L$ is calculated to be

$$\tau_{mix} = (\sum_i \phi_i \tau_i^2) / (\sum_i \phi_i \tau_i) = 0.9 \tau_1 \quad (82)$$

not too far from the longer time constant τ_1 .

Since the material cannot be deformed faster than it responds, the maximum attainable strain rate would be roughly bounded by τ_{mix}^{-1} (Hyan and Ballman have shown that the elongation rate $\bar{\kappa} = \tau_c + \frac{2\eta_0}{FV}$ for an isothermal melt spinning of a Maxwell fluid⁽²⁵⁾). Although the system under investigation is not exactly a Maxwell fluid, it seems reasonable to assume that the maximum $\bar{\kappa}$ is of the same order of magnitude of τ_{mix}^{-1} . Thus the attainable elongation rate $\bar{\kappa}$ that can orient the longer species with length L will not be able to orient the shorter species with length $\frac{1}{2}L$ or shorter. For example, suppose we have achieved an elongation rate $\bar{\kappa}$ which for $L_1 = L$ makes $\tau_1 \bar{\kappa} = 6$ with the Herman's orientation parameter $h = 0.99$ (orientable). Then for $L_2 = \frac{1}{2}L_1$, we have $\tau_2 \bar{\kappa} = 0.22$ and $h = 0.24$ (hardly oriented). The orientation effect rapidly decreases with decrease of the lengths of the species in the solution.

Table 8

Material Constants for Rod-like Models

Material Constants	Dumbbell*	Prolate Ellipsoid	Circular Cylinder
B (shape factor)	1	$1 - \frac{2}{r_p}$	$1 - 1.30 \frac{\ln r_p}{r_p}$
K_r (dimensionless rotary time constant)	$\frac{3}{4} r_p^2$	$\frac{r_p^2}{3(\ln r_p + 0.193)}$	$\frac{2}{9} \left[\frac{r_p^2}{\ln r_p + 0.307} + 0.65 \right]$
Q_1	$\frac{1}{5} e_z$ $e_z = 2.4 \sim 2.5$	$\frac{2}{5} - \frac{6 \ln 2r_p}{5r_p^2}$	$\frac{2}{5}$
Q_2	$-\frac{3}{10} r_p^2$	$-\frac{r_p^2}{15(\ln r_p - 0.81)} + \frac{2}{5}$	$-\frac{2r_p^2}{45(\ln r_p - 1.447)}$
Q_3	$\frac{9}{40} r_p^2$	$\frac{r_p^2}{10(\ln r_p + 0.193)}$	$\frac{3}{10} B^2 K_r$
D_r (rotatory diffusion cons.)	$\frac{2kT}{3\pi \eta_s d L^2}$	$\frac{3kT(\ln 2r_p - 0.5)}{\pi \eta_s L^3}$	$\frac{3kT(\ln 2r_p - 0.386)}{\pi \eta_s L^3}$

Where $r_p = L/d$ aspect ratio

L Length of dumbbell or cylinder, or
twice the semi-major axis of the
ellipsoid

d diameter of the bead or the cylinder,
or twice the semi-minor axis of the
ellipsoid

* Dumbbell with non-interacting spheres.

6. FLOW BIREFRINGENCE OF SOLUTIONS OF ROD-LIKE POLYMERS

An important aspect of the processing of rodlike polymers into oriented solids is the orientation induced by flow. One is interested in the extent of this orientation and the "time constants" associated with its development during flow and relaxation after cessation of steady flow. In recent work in our laboratory, we have used the rheological time constant $\tau_c = \eta_0 R_0$ to estimate the latter quantities, and have assumed that orientation is substantial if the shear rate $\dot{\gamma}$ in flow is large enough that $\tau_c \dot{\gamma} > \text{ca. } 10$. Flow birefringence measurements offer a means for a more direct assessment of the degree of orientation induced, and another means to estimate relaxation times by application of the Maxwell optico-dynamical effect⁽²⁷⁾. In the following, a flow birefringence apparatus constructed in our laboratory is described, and preliminary data are reported for some PBT solutions.

6.1 Flow Birefringence Apparatus.

The schematic diagram of an instrument designed for optical studies of flow induced orientation is given in Figure 20. A detail of the solution chamber is shown in Figure 21. The device is designed to subject a fluid to shearing flow between glass parallel plates. The induced orientation may be determined by examining the light transmitted between crossed polaroids. With solutions of the rodlike polymers of interest here (PBO or PBT), it is not difficult to induce a degree of orientation such that the extinction angle χ is nearly zero degrees, indicating a high degree of orientation of the rodlike chains

with their long axis parallel to the flow streamline. That is, if ψ is the orientation angle between the rodlike chain axis and the streamline, it is relatively easy to achieve a flow condition such that ψ is nearly zero, see below.

The apparatus is equipped with two light sources: 1) a He-Ne laser, about 5 mw intensity, and 2) a Xe arc lamp. The latter provides a source of parallel light to illuminate the entire area of the parallel plates. This is convenient for qualitative flow visualization and assessment of the extinction angle χ , which provides a measure for ψ . The laser source can be used to determine the transmission T for selected small (ca. 2 mm dia.) regions of the flow field. This can be used to evaluate the retardation δ , and hence the difference Δn of the principal components n_1 and n_2 ($n_1 > n_2$) of the refractive index ellipsoid:

$$\delta = 2\pi \ell \Delta n / \lambda \quad (83)$$

(δ in radians) where ℓ is the optical path length and λ the wavelength of the incident light. Thus, if the transmission is viewed between crossed polaroids, with γ the angle between the axis of the polarizer and the unique axis (n_1) of the refractive index ellipsoid,

$$T = \frac{1}{2} \sin^2 \frac{\delta}{2} (1 - \cos 4\gamma) \quad (84)$$

Equation (84) describes the "extinction cross" visualized with a well oriented fluid in flow, with the slow axis inclined at an angle ψ to

the flow lines. This extinction cross results from the fourfold symmetry in T as one traces around a flow line, with the result $\chi = \psi$. For example, suppose n_1 is oriented along the flow streamlines at angle ψ . Consider a path traced out along a streamline through the azimuthal angle Ω , measured with $\Omega = 0$ or π along the polarizer direction. Then, $\gamma = \psi + \Omega + \pi/2$ and, the extinction bands will appear at azimuthal angles corresponding to $\gamma = 0, \pi/2, \pi$ and $3\pi/2$. The extinction angle χ is defined as the smallest value of Ω . Maximum transmission occurs with fourfold symmetry, for $\gamma = \pi/4$, etc., with transmission equal to $\sin^2(\delta/2)$, providing a method to determine δ if transmission measurements are made quantitatively, see below.

A $1/4$ -wave plate is sometimes placed between the fluid and the analyzer, oriented with its slow direction parallel to the electric vector transmitted by the polarizer. With β the angle between the polarizer and analyzer axes ($\beta = \pi/2$ for crossed polaroids), the transmission is given by

$$T = \cos^2 \beta + \frac{1}{2} \sin 2\beta \sin \delta \sin 2\gamma - \frac{1}{2} \cos 2\beta \sin^2 \frac{\delta}{2} (1 - \cos 4\gamma) \quad (85)$$

Of course, with $\beta = \pi/2$, Eqn. (85) reduces to Eqn. (84). With appropriate values of β , Eqn. (85) can exhibit twofold symmetry. For example, for $\gamma = \pi/4$ or $5\pi/4$,

$$T_{\gamma = \pi/4} = \frac{1}{2} + \frac{1}{2} \cos (\delta - 2\beta) \quad (86)$$

Consequently, if β is adjusted to the value β_m such that $T_{\gamma=\pi/4}$ is zero, then $\delta = \pi + 2\beta_m$ gives the retardation, and hence Δn . Positive values of δ indicate positive Δn , and negative values indicate negative birefringence. This method for evaluating δ may be applied after the orientation angle ψ is determined by observation of the extinction according to Eqn. (84) as described above, since the azimuthal angle Ω required is just $\pi/4 - \psi$. It may be noted that for $\delta - 2\beta = \pi$, Eqn. (85) reduces to

$$T_{\delta-2\beta=\pi} = \frac{1}{2} + \frac{1}{2} \cos \delta (1 - \sin^2 2\gamma) - \frac{1}{2} [\sin^2 \delta \sin 2\delta + \cos^2 \delta \sin^2 2\gamma] \quad (87)$$

Equation (87) exhibits twofold symmetry, with extinction for $\gamma = \pi/4$ and $5\pi/4$, and maximum transmission $T = 1/2$ for $\gamma = 3\pi/4$ and $7\pi/4$. Use of Eqn. (86) provides a method for determining δ without quantitative transmission measurements. Other methods, based on photoelectric determination of T , have been proposed based on Eqn. (85). These have the advantage of greater sensitivity and resolution. One procedure, due to Zimm,⁽²⁸⁾ is readily adaptable with our apparatus, and may be used if needed in future work.

In the method currently used with the flow birefringence apparatus, the average orientation angle $\langle\psi\rangle$ is evaluated by visual determination of Ω_e for the fourfold extinction predicted by Eqn. (85) [or Eqn. (84)] for $\beta = \pi/2$. Since this occurs for $\gamma = 0, \pi/2$, etc., and $\gamma = \psi + \Omega$, evaluation of Ω_e gives $\langle\psi\rangle$ directly. If ψ is not independent of shear rate, κ , then the extinction will not occur at the same Ω for all radii, since $\kappa = \omega r/\ell$ increases with increasing r .

Under these circumstances the "extinction cross" will be deformed. The average birefringence $\langle \Delta n \rangle$ at any r is evaluated either by measurement of the transmission between crossed polaroids at a particular r with $\gamma = \pi/4$, or by the use of the $1/4$ -wave plate and visual determination of β_m for use to determine δ with Eqn. (86).

In addition to the values of $\langle \psi \rangle$ and $\langle \Delta n \rangle$ in steady-state flow, the transmission through crossed polaroids at some particular r and Ω is monitored following cessation of flow. According to Eqn. (84), the transmission will change as Δn and γ change, both of these being dependent on the distribution of the orientation angle ψ . If the quiescent fluid is isotropic, T will decrease to zero over the entire illuminated field, and it is convenient to monitor T as a function of r for the Ω for which γ was $\pi/4$ for the oriented fluid in flow. For this case, T will decrease from $(\sin \delta/2)^2$ to zero as a function of time. Conversely, if the quiescent fluid is nematic, T will increase to some constant value over the entire illuminated field, and it is convenient to monitor T as a function of r for the Ω for which γ was 0 for the oriented fluid in flow. For this case, T will increase from zero to the value for the uniform fluid. The transmission is monitored with a photodiode placed to receive the transmitted light from an aperture over the upper plate. The aperture serves to define r and Ω . The light is chopped at 400 Hz, and the photodiode current is dropped across a resistor to produce a 400 Hz modulated voltage. The latter is monitored with a voltmeter tuned to 400 Hz (a Hewlett-Packard Wave Analyzer, Model 302A).

The range of rotational velocity ω covered with the present instrument is from 10^{-4} to about 1 radian per second. The rotational velocity is varied by control of the speed of a high-torque servomotor. The shear rate $\kappa = \omega r/l$ depends on the plate separation l and the radius r . The former is usually in the range $0.002 < l < 0.1$ cm, and the plate radius is 1.8 cm. Consequently, the observable range of κ is $2 \times 10^{-4} < \kappa < 10^3 \text{ sec}^{-1}$.

6.2 Results

The flow birefringence behavior of several solutions of PBT in methane sulfonic acid has been observed. These include nematic solutions as well as one isotropic solution at a concentration (and temperature) near the phase boundary, see Table 9. These have been observed for κ down to about 10^{-3} sec^{-1} . In every case, a well defined extinction cross was observed between crossed polaroids, giving $\langle \psi \rangle = 0$, even for the lowest κ used. This result indicates that the disorienting effect of Brownian motion is quite small, or that the ratio κ/D_R must be very large, where D_R is the rotational diffusion constant of the solute (at the concentration used). Even though $\langle \psi \rangle$ was zero for the entire range of κ studied, $\langle \Delta n \rangle$ did reveal the effects of increased orientation with increasing ω . Thus, the transmission increased with increasing κ , showing the increase of δ , and hence Δn , with increasing κ as $f(\psi)$ becomes more sharply peaked about the mean value $\langle \psi \rangle$.

According to Eqn. (84), T should be zero for all γ when $\delta = 2\pi$, or $\Delta n = \lambda/l$. This condition corresponds to a circular dark interference ring. Since no such ring was observed with the isotropic

solution of PBT-53 in CSA ($w_2 = 0.019$), it appears that $\Delta n/1 < \text{ca. } 0.006$ for that solution. Application of Eqn. (86) permits estimation of the variation of Δn with χ . With isotropic solutions, for fixed ω , δ was observed to increase with increasing r , revealing the increase of Δn with increasing χ for the isotropic fluid. An attempt was made to determine δ for the same solution by transmission measurements through application of Eqn. (84) for $\gamma = \pi/4$. The transmission was estimated from measurements of the photodiode response G_χ with $\beta = \pi/2$ for $\omega > 0$, and G_0 with $\beta = \pi/2 - \alpha$ for the quiescent fluid ($\omega = 0$). Then, neglecting dichroic effects, preferential photodiode response to light of one polarization, etc., T is given by

$$T = \sin^2(\delta/2) \quad (88)$$

$$\frac{G_\chi}{G_0} \sin^2 \delta = \sin^2(\delta/2) \quad (89)$$

the latter equality coming from Eqn. (84). Application of Eqn. (88) resulted in a value of $\delta = 1.5$ rad., or Δn of 0.0003 for the isotropic solution in one steady-state flow with an isotropic solution with $\varphi = 0.02$.

The steady-state transmission was observed for the nematic fluids listed in Table 9. These fluids exhibited a zero degree extinction cross at steady-state, with the cross requiring a longer time to develop as the polymer concentration was increased.

Transmission measurements have also been used to follow orientation relaxation after cessation of steady-state flow. As mentioned above, relaxation was observed for $\gamma = 0$ for nematic fluids.

These relaxation times ranged from 30 to 600 s for the fluids studied, see Table 9. During the relaxation, the extinction cross broadens and becomes diffuse, but remains oriented at zero degrees.

6.3 Discussion

$$\langle \psi \rangle = \frac{\int_{-1}^1 \psi f(\psi) d \cos \psi}{\int_{-1}^1 f(\psi) d \cos \psi} \quad (90)$$

$$\langle \Delta n \rangle = \frac{\int_{-1}^1 \Delta n_{\psi} f(\psi) d \cos \psi}{\int_{-1}^1 f(\psi) d \cos \psi} \quad (91)$$

Of course, Δn_{ψ} depends on both optical and hydrodynamical parameters, e.g., the intrinsic refractive index difference $n_1 - n_2$ of the rodlike solute (with cylindrical symmetry of the polarizability tensor), the form birefringence, which for rigid molecules involves differences between the refractive index n_s of the solvent and each n_1 and n_2 and the orientation angle ψ , the latter being controlled by hydrodynamics and diffusion. For an orientation with axial symmetry about the preferred direction, Δn_{ψ} is given by

$$\Delta n_{\psi} = \varphi \frac{2\pi}{n_s} (g_1 - g_2) \left[\frac{3 \cos^2 \psi - 1}{2} \right] \quad (92)$$

where φ is the volume fraction of polymer, and

$$4\pi g_i = \frac{n_i^2 - n_s^2}{1 + (n_i^2 - n_s^2)L_i / 4\pi n_s^2} \quad (93)$$

Here, L_i is a form factor, with $L_1 = 0$ and $L_2 = 2\pi$ for rods. With neglect of second-order terms, $g_1 - g_2$ is approximately given by the relation

$$\frac{2\pi}{n_s} (g_1 - g_2) \approx n_1 - n_2 + (L_2 - L_1)(n_1 - n_2)(n_2 - n_s)/4\pi n_s \quad (94)$$

the second term accounting for the form birefringence, with the form factor $L_2 - L_1 = 2\pi$ for rodlike molecule.

The g_i also appear in optical properties such as the refractive index increment dn/dc and the overall anisotropy $\underline{\delta}$ measured by light scattering (not to be confused with the retardation δ):

$$\frac{dn}{dc} = \frac{\bar{v}}{3} (g_1 + 2g_2) \frac{2\pi}{n_s} \quad (95)$$

$$\underline{\delta} = \frac{g_1 - g_2}{g_1 + 2g_2} \quad (96)$$

where \bar{v} is the partial specific volume of polymer. In terms of these parameters,

$$\Delta n_\psi = \varphi(3/\bar{v}) \underline{\delta} (dn/dc) \left[\frac{3 \cos^2 \psi - 1}{2} \right] \quad (97)$$

If the orientation exhibits two-fold symmetry in the plane of the parallel plates, then the factor $(3 \cos^2 \psi - 1)/2$ should be replaced by $2 \cos^2 \psi - 1$. In the following, we will consider only the axially

symmetric case since this probably obtains in the parallel plate geometry of interest here when orientation is nearly along the flow lines.

With the use of Eqn. (97), $\langle \Delta n \rangle$ is given in terms of $\langle \cos^2 \psi \rangle$:

$$\langle \Delta n \rangle = \Delta n_{\infty} (3 \langle \cos^2 \psi \rangle - 1) / 2 \quad (98)$$

where $\Delta n_{\infty} = \varphi K$, with constant $K = (2\pi/n_s)(g_1 - g_2)$, depends only on intrinsic properties of the solute (and solvent) and not on κ . Thus, the flow birefringence experiment provides information on $f(\psi)$ through $\langle \psi \rangle$ and $\langle \cos^2 \psi \rangle$. Both of these measurable parameters should depend on the ratio of the rate of strain κ to the effective rotational diffusion constant D_R , with $f(\psi)$ becoming more sharply peaked about $\psi = 0$ as κ/D_R increases. For example, with steady-state elongational flow with shear rate $\bar{\kappa}$, the orientational distribution is given by the relation(1b)

$$f(\psi)/f(0) = \exp\left[-\frac{15}{2} \tau_c \bar{\kappa} \sin^2 \psi\right] \quad (99)$$

Note, that with this $f(\psi)$, $\langle \psi \rangle$ is equal to zero for any $\bar{\kappa}$, but the span of the distribution of ψ increases with decreasing $\bar{\kappa}$. Values of $\langle \Delta n \rangle / \Delta n_{\infty}$, equal to $(3 \langle \cos^2 \psi \rangle - 1) / 2$ calculated with this $f(\psi)$ are given by

$\tau_c \bar{\kappa}$	$\frac{\langle \Delta n \rangle / \Delta n_\infty}{= (3 \langle \cos^2 \psi \rangle - 1) / 2}$
0.01	0.0004
0.1	0.0356
1	0.653
10	0.961
25	0.984
∞	1

These data reveal the very rapid increase in the orientation that obtains for values of $\tau_c \bar{\kappa}$ near unity.

It is sometimes convenient to expand $f(\psi)$ in terms of Lengdre Polynomials $P_\ell(x)$, with $x = \cos \psi$:

$$f(\psi) = \sum_{\substack{\ell \\ \text{even}}} a_\ell P_\ell(\cos \psi) \quad (100)$$

$$a_\ell = \frac{2\ell + 1}{2} \langle P_\ell \rangle \quad (101)$$

$$\langle P_0 \rangle = 1 \quad (101)$$

$$\langle P_2 \rangle = (3 \langle \cos^2 \psi \rangle - 1) / 2 \quad (101)$$

$$\langle P_4 \rangle = (35 \langle \cos^4 \psi \rangle - 30 \langle \cos^2 \psi \rangle + 3) / 8 \quad (101)$$

etc.

The order parameters $\langle P_\ell \rangle$ then contain the dependence of $f(\psi)$ on shear rate, etc. If $f(\psi)$ is sharply peaked around $\psi = 0$, then it may be possible to represent $f(\psi)$ with only the first few terms in the expansion. Calculation with Eqn. (99) shows that several terms are

needed in Eqn. (100) to reproduce $f(\psi)$, even for $\tau\bar{\chi}$ as large as 25.

The most striking result observed with the flow birefringence experiments is the observation that $\langle\psi\rangle$ is essentially zero for all of the steady-state flows studied. This result shows that χ/D_R is large for all of the cases encountered so far. This is not too surprising since the substantial restrictions to rotational diffusion of the rodlike solute inherent for solutions near or over the critical concentration for formation of the nematic phase, render D_R small.

The observations $\langle\Delta n\rangle$ show that even though χ/D_R is large enough to give a zero degree average orientation of the chains to the flow direction, the values of χ/D_R are not necessarily large enough to force $\langle P_2 \rangle$ to its limiting value of unity. If the observed values of $\bar{s} = 0.5$, $dn/dc = 0.5$ ml/g, and $\bar{v} = 0.67$ ml/g are used to estimate K by use of Eqns. (95), (96) and (98), then $\Delta n_\infty = 0.02$, and the value of $\langle\Delta n\rangle = 0.0003$ observed with a solution with $\chi \sim 0.1$ would give $\langle P_2 \rangle = (3\langle\cos^2\psi\rangle - 1)/2$ equal to 0.015. This would appear to be a reasonable magnitude based on the product of χ and the observed "relaxation time" τ_R of $\tau_R\chi \sim 3$. In fact, however, the estimate for Δn_∞ is still too crude to be reliable. In future work $\langle\Delta n\rangle$ will be determined as a function of χ over a range wide enough to permit a reasonable assessment of $\langle\Delta n\rangle/\Delta n_\infty$, and hence $\langle\cos^2\psi\rangle$.

As mentioned above, relaxation of the orientation induced in steady-state flow has been monitored by the change in the transmission through the use of Eqn. (84). The average transmission at radius r and azimuthal angle Ω is

$$\langle T \rangle = \frac{\frac{1}{2} \int_{-1}^1 \sin^2 \frac{\delta}{2} [1 - 4 \cos(\psi + \Omega)] f(\psi) d \cos \psi}{\int_{-1}^1 f(\psi) d \cos \psi} \quad (102)$$

where

$$\delta = 2\pi \Delta n_{\psi} / \lambda$$

In the relaxation experiments with fluids that are isotropic in the rest state, $\Omega = \pi/4 - \langle \psi \rangle_{ss}$ and $\langle T \rangle$ decreases with increasing time following cessation of flow. With fluids nematic in the rest state, $\Omega = \langle \psi \rangle_{ss}$ and $\langle T \rangle$ increases with increasing time following cessation of flow. Here $\langle \psi \rangle_{ss}$ is the value of $\langle \psi \rangle$ during steady-state flow. It is evident from Eqn. (102) that the measured quantity $\langle T \rangle$ is related to $f(\psi)$ in a rather complicated way.

Relaxation of $\Delta n_{\psi} \propto (3 \cos^2 \psi - 1)/2$ appearing in Eqn. (2-18) has been discussed by Doi and Edwards¹⁵ for rod-like molecules in concentrations well below the nematic range. For such concentrations, these authors find that $(3 \langle \cos^2 \psi \rangle - 1)/2$ relaxes first rapidly with the time θ measured from cessation of flow, and then more slowly, the latter relaxation following the relation

$$(3 \langle \cos^2 \psi \rangle_{\theta} - 1)/2 = \exp(-\theta/\tau_c) \quad (103)$$

where τ_c is $(6D_R)^{-1}$, or the quantity $\eta_0 R_0$ used in our previous discussion of rheological behavior. For small θ , the alignment induced in flow acts to reduce interchain contacts, thereby enhancing rotational

relaxation. To treat this relaxation, the authors assume that $f(\psi, \theta)$ has a Gaussian form

$$f(\psi, \theta) = [2\pi g(\theta)]^{-1} \exp \left(-\frac{\sin^2 \psi}{2g(\theta)} \right) \quad (104)$$

with ψ small enough so that $\sin \psi \approx \psi$. The similarity to Eqn. (26) may be noted. The function $g(\theta)$ is found to be

$$g(\theta) = [2\alpha D_R \theta + g(0)]^{1/2} \quad (105)$$

where α is a numerical factor evaluated to be $1/3$, and

$$f(\psi, 0) \propto \exp \left(-\frac{\sin^2 \psi}{2g(0)} \right) \quad (106)$$

serves to evaluate $g(0)$. These relations lead to an initial relaxation

$$(3\langle \cos^2 \psi \rangle_\theta - 1)/2 = \exp [-3g(\theta)/2] \quad (107)$$

that exceeds then the relaxation rate at larger θ .

The data presently available are not sufficiently precise to assess the nature of the function $(3\langle \cos^2 \psi \rangle_\theta - 1)/2$. It has been found that $\langle \psi \rangle$ does not change during relaxation, and that $\langle T \rangle$ decays more-or-less exponentially. The former result is reasonable, since there is no reason

for any new preferential orientation to develop during relaxation of $f(\psi)$ to the rest distribution.

At this stage, rather than attempting to extract information on $\langle \cos^2 \psi \rangle$ from $\langle T \rangle$, we have defined an operational relaxation time τ_R such that $\langle T \rangle_{\theta=\tau_R} = 0.02 \langle T \rangle_0$ for fluids isotropic at rest, or $\langle T \rangle_{\theta=\tau_R} = 0.02 \langle T \rangle_{\infty}$ for fluids nematic at rest. Entries of τ_R given in Table 9 show that τ_R is similar to τ_c for the fluids studied. This is in accord with our previous suggestions that the orientation induced in flow should be expected to relax in a time comparable to the rheological time constant τ_c . In future work, the dependence of $\langle T \rangle$ on θ will be examined in more detail.

Table 9

Flow Birefringence Data Obtained with Some Solutions of Rodlike Polymers

Polymer	Solvents	φ	Temp. (°C)	Phase	$\langle\psi\rangle$ (deg)	Remarks ^(a)
PBT-53	CSA	0.0224	23	ISO	0	$\tau_R \sim 30-40$ s $\langle\Delta\rangle$ ca 3×10^{-4} for κ ca 0.1 s ⁻¹
"	"	0.029	40	ISO	0	
"	"	"	23	NEM	0	
PBT-62	MSA	0.0343	55	ISO	0	$\tau_R \sim 170$ s; $\tau_c = 300$ s
"	"	"	41	ISO	0	$\tau_R \sim 380$ s; $\tau_c = 300$ s
"	"	"	23	NEM		$\tau_R \sim 660$ s; $\tau_c = 400$ s
"	MSA	0.06.4	23	NEM	0	Extinction cross slow to form

(a) τ_R is the relaxation time for decay of birefringence on cessation of steady-state flow; τ_R is defined as the time required for the transmission to decrease to 2% of its steady-state value for the isotropic fluids. The entry for the nematic fluid is an estimate based on visual observations of the time for the extinction cross to vanish.

τ_c is the rheological time constant $\eta_0 R_0$.

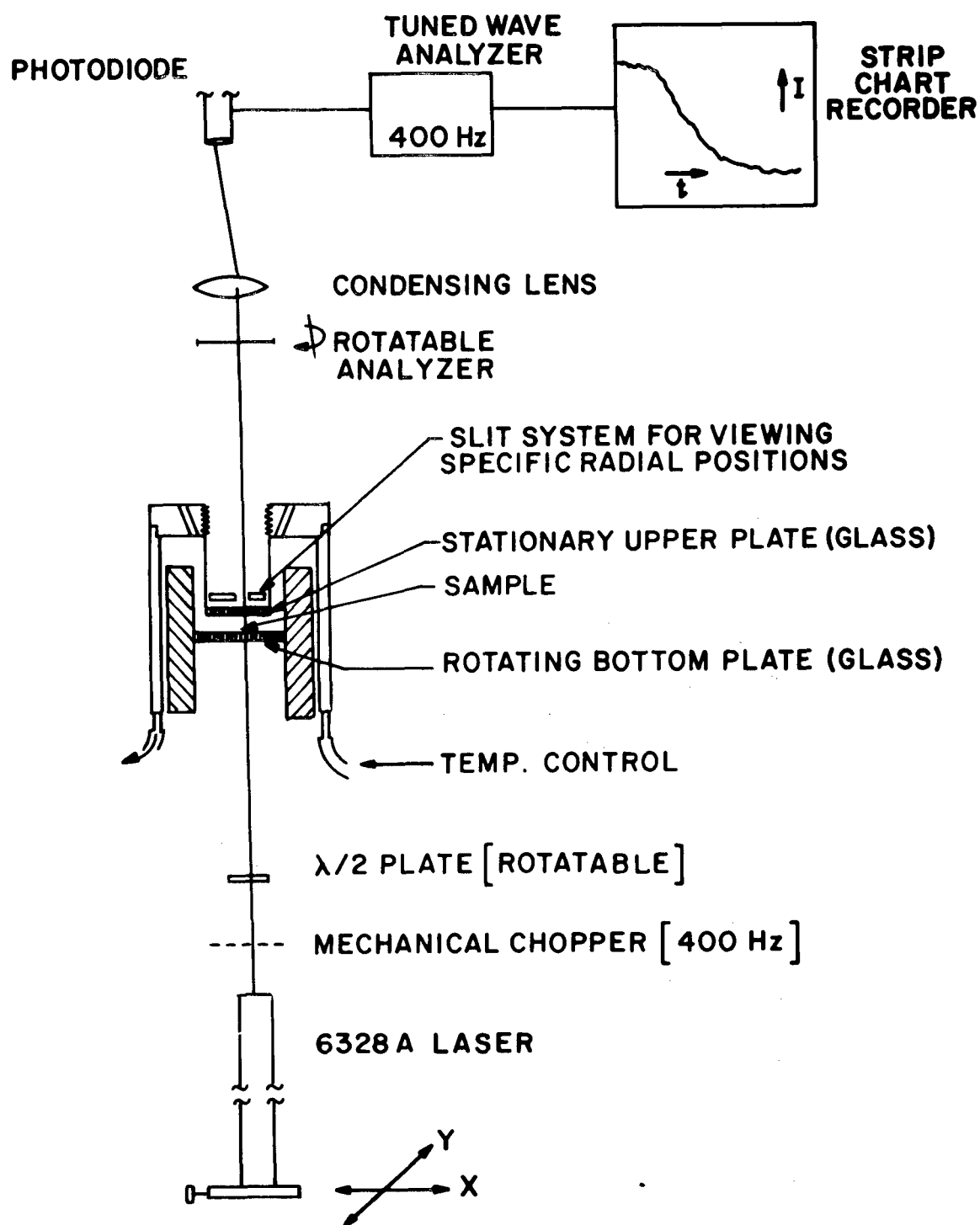


Figure 20

Overall schematic diagram of the flow birefringence apparatus.

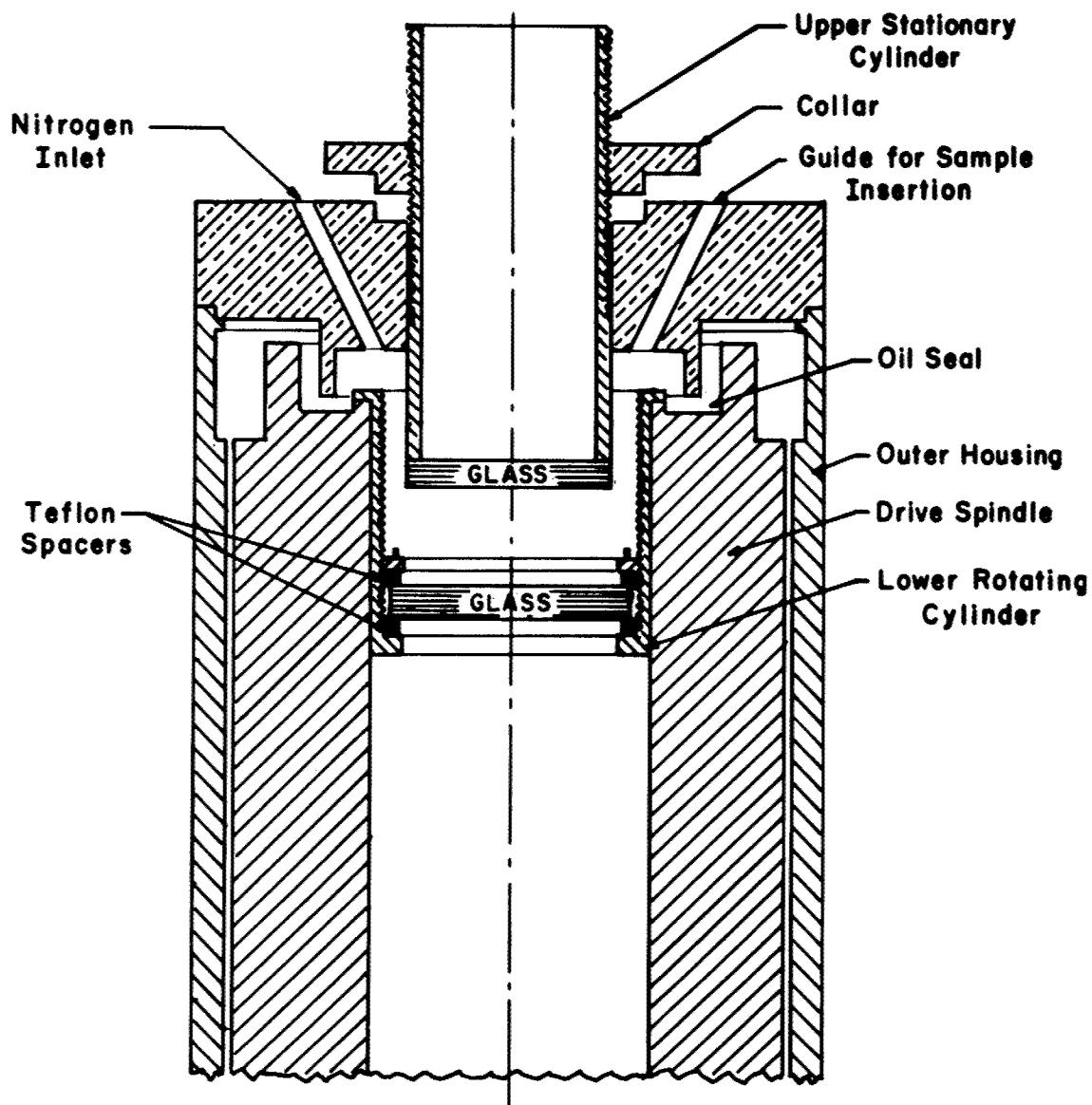


Figure 21

Detailed schematic drawing of the solution chamber of the flow birefringence apparatus.

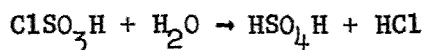
7. FIBER FORMATION BY SOLUTION PROCESSING

As emphasized above, the study of the fiber formation process affords a valuable means to assess methods to induce molecular orientation in solution processing, and a means to obtain oriented solid samples to permit the correlation of strength and modulus with molecular orientation. In preceding work⁽¹⁾, we initiated study of the wet-spin fiber formation process with PBO solution. In this study, we have pursued that topic, and expanded the study to induce dry-jet-wet spin fiber formation with solutions of both PBO and PBT. The following is divided into subsections dealing with wet-spin fiber formation with PBO, dry-jet-wet spin fiber formation of PBO, and dry-jet-wet spin fiber formation of PBT. These are accompanied by some remarks on the properties of the fibers prepared under various conditions.

7.1 Fiber Formation with PBO solutions

7.1.1 Solubility of PBO

The limited solubility of PBO in methane sulfonic acid has been a potentially serious concern. Attempts to achieve PBO concentrations in excess of ca. 9% (by weight) have nearly uniformly met with failure, the resultant mixture containing a substantial fraction of greenish aggregated component. In work with chlorosulfonic acid it was noted 1) that the greenish aggregated component was suppressed and 2) that considerable hydrogen chloride was generated over a long period of time during the dissolution process. Since HCl is a product of the hydrolysis of ClSO_3H :



the latter observation indicated the presence of water in the vacuum dried PBO or contamination by water during the dissolution process. The latter possibility is discounted since the solution was prepared in a well-sealed ampoule. Unfortunately, ClSO_3H is itself not a candidate as a solvent for fiber spinning since the HCl that would be evolved during coagulation could lead to the formation of voids in the fiber. It is possible, however, to use ClSO_3H to scavenge water in solutions prepared with $\text{CH}_3\text{SO}_3\text{H}$ and the PBO. Thus, the weight change due to HCl evolution can be used to determine the amount of water in $\text{CH}_3\text{SO}_3\text{H}$ (or PBO solutions in $\text{CH}_3\text{SO}_3\text{H}$). Experiments with $\text{CH}_3\text{SO}_3\text{H}$ available at CMU and Celanese gave the results in Table 10, showing small quantities of water in each. The water concentration in a solution prepared using a PBO dried at the Celanese laboratory and the $\text{CH}_3\text{SO}_3\text{H}$ from CMU are also given in Table 10.

TABLE 10

Water Content of $\text{CH}_3\text{SO}_3\text{H}$ and a PBO
Solution in $\text{CH}_3\text{SO}_3\text{H}$

<u>Material</u>	<u>%H₂O</u> <u>(By Weight)</u>
$\text{CH}_3\text{SO}_3\text{H}$ from CMU	0.12
$\text{CH}_3\text{SO}_3\text{H}$ from Celanese	0.16
PBO/ $\text{CH}_3\text{SO}_3\text{H}$ from CMU; 8.5% polymer	0.26

The analysis with the acids was as follows: let x be the initial weight of water in weight W of wet $\text{CH}_3\text{SO}_3\text{H}$. Then the weight loss Δw_0 due to the addition of w_A weight of ClSO_3H will be $\Delta w_0 = (36.5/18)x$, it being assumed that excess ClSO_3H is present. If, during the period required for all of the water initially present to react additional water is absorbed (e.g., during the period the HCl is vented to the atmosphere), then a weight loss $\Delta w'$ will also occur, leading to a total weight change Δw_T . When sufficient additional water has been absorbed to use up all of the ClSO_3H added, the sample will cease to lose weight, and will begin to gain weight as additional water is added from the atmosphere. At this point, the weight change Δw_T will reach a minimum $(\Delta w_T)_{\text{MIN}}$, and

$$\begin{aligned} (\Delta w_T)_{\text{MIN}} &= \Delta w^0 + \Delta w' \\ &= \frac{36.5}{18}x + \frac{18.5}{116.5} w_A - \frac{116.5}{18} x \end{aligned}$$

or

$$x = (\Delta w_T)_{\text{MIN}} - \frac{18.5}{116.5} w_A$$

Thus x can be calculated, independent of the effects of extraneous moisture absorption, giving the values in Table 10.

An attempt was also made to determine the moisture concentration in wet $\text{CH}_3\text{SO}_3\text{H}$ by measurement of the conductivity κ . Although the results on $\text{CH}_3\text{SO}_3\text{H}$ were in qualitative agreement with those listed in Table 10, the conductivity determination is not as accurate as the

gravimetric measurement owing to the low value of $d\kappa/dx$ in the concentration range of interest.

If allowance is made for the water in the solvent, then the data on the PBO solution indicate about one mole of water per mole of PBO repeat residue. More significantly, with the addition of the small amount of ClSO_3H required to react with the water, the greenish aggregate component disappeared and the solution took on the deep purple coloration observed with ClSO_3H solutions. We conclude that a small amount of water is held tenaciously by the polymer, and that this water has a deleterious effect on the solubility of the polymer in concentrated solutions, probably by prohibiting the dissolution process--it seems likely that the same amount of water could be tolerated by a solution once dissolution was complete. It is suggested that it may be essential to scavenge extraneous water during dissolution of PBO to achieve homogeneous solutions with polymer concentrations in excess of about 8%. The use of ClSO_3H may be one way to achieve this objective. Preliminary results at the Celanese laboratory suggest that the use of a slight excess of SO_3 in HSO_3 may be another way.

7.1.2 Fiber Wet-Spin Process

Solutions of PBO in $\text{CH}_3\text{SO}_3\text{H}$ in the concentration range 8-9% polymer are observed to be biphasic at room temperature, exhibiting both ordered and disordered regions. Since the solutions are thermotropic, they may be converted to fully ordered solutions by lowering the temperature. Fibers have been prepared at CMU with both biphasic solutions at room temperature and with full ordered solutions in the

temperature range 0-5°C.

Before discussing the fiber spinning results, it is convenient to consider an experiment in which a solution of PBO in $\text{CH}_3\text{SO}_3\text{H}$ (8.0% polymer by weight) was examined on the stage of a polarizing microscope as the temperature was varied from -2 to 120°C. During preparation, the temperature of the solution was alternated between 0 and 80°C to achieve more efficient dissolution--the lower temperature resulted in a reduced viscosity for the biphasic solution, and hence increasing mixing efficiency, whereas the higher temperature enhanced the dissolution process. Dissolution was effected in a sealed cell using a close fitting magnetic stirring bar for agitation. A portion of the solution was placed between cover slips in a special holder, protected from contamination by moisture by a mineral oil.

When first examined, the solution was biphasic (about 1/4 ordered phase by volume) and did not contain any obviously aggregated component. As the temperature was slowly (about 15°C/hr) increased to 120°C the ordered phase disappeared, so that the solution was completely optically isotropic at 120°C. On cooling to 25°C (about 20°C/hr), the sample returned to the biphasic state, but the fraction of ordered component was initially somewhat less than originally observed at 25°C. The fraction of the ordered component increased with time, returning to the original level after storage overnight at 25°C. The solution could be converted to a fully nematic structure by cooling to 15°C, and would return to the biphasic state immediately on heating to 25°C.

Solutions of PBO (received from AFML) were prepared in $\text{CH}_3\text{SO}_3\text{H}$. The former was used to prepare solutions with 8% and 9% polymer by weight. The solutions were deep blue in color.

Fibers were prepared using the bench scale apparatus described in previous reports.⁽¹⁾ Water was used as the coagulant and the fibers were prepared at spinning rates in the range 0.5 to 8 cm/sec (see Table 10). The as spun fibers exhibited a metallic blue hue under normal daylight.

A summary of fibers spun at the CMU and Celanese Laboratories is given in Table 10. Fibers have now been prepared from isotropic, biphasic and completely nematic solutions, and a variety of post treatments have been examined. The best as spun properties were obtained with a fiber prepared from a completely nematic solution exhibiting no gel or insoluble component (Fiber 10174). The x-ray diffraction pattern from the fiber showed diffuse equatorial arcing (see Fig. 22) and the scanning electron micrograph showed a convoluted surface with a smooth skin (see Fig. 22a and 22b). When scratched along its length, the fiber revealed a fibrillar structure, as shown in Fig. 23b.

As expected, the properties of the as spun fiber prepared with the nematic solution were superior to those from the biphasic solution. The latter produced better as spun fibers than the isotropic solution--compare properties for fibers 10174 (nematic), 09273 (biphasic) and 12010 (isotropic) in Table 10. The x-ray diffraction pattern for fiber 12010 prepared with the isotropic solution shows very little orientation (see Fig. 24). It may be noted that fibers prepared at

CMU and Celanese under similar conditions exhibit very similar properties: compare fibers 09273 and 36085-153, 04297 and 36085-162 and 09273-H2 and 36085-153H, for example.

The as-spun properties of fibers prepared with solution containing 9% PBO were inferior to those prepared with 8% solution, even though the former was nematic at room temperature. The difficulty is undoubtedly due to the presence of gel and undissolved material in the 9% solution--the latter components were evident on microscopic examination of the 9% solution. The x-ray diffraction pattern of the fiber showed no arcing (see Fig. 25a) indicating the lack of orientation evidenced by the low modulus of the as spun fiber, and the surface revealed a mottled, textured surface as shown in Fig. 25b. The fracture surface shown in Fig. 25b reveals a lack of the fibrillar structure seen with more well-oriented fibers (e.g., see Fig. 23b).

The properties of the as-spun fibers can be improved considerably by drawing at an elevated temperature. Stress-strain data for a fiber prepared from an isotropic solution are given in Fig. 26 for the as spun fiber (fiber number 12010) and the fiber after drawing to 17% at 400°C (fiber number 12010 H5). The drawing also increased the sharpness of the equatorial arcs somewhat. The effects of post spinning treatment are also beneficial with fibers prepared with biphasic solutions. The fibers with the highest modulus and tenacity so far obtained with PBO were so treated. For example, a modulus of 540 g/d about $7.3 \times 10^{10} \text{ N/M}^2$ or $1.1 \times 10^7 \text{ psi}$) was obtained with fiber 09273H2, with the stress-strain behavior shown in Fig. 5, and a tenacity of 4 g/d

(or ultimate strengths of about $5.4 \times 10^8 \text{ N/M}^2$ or $8.0 \times 10^4 \text{ psi}$) was obtained with fiber 36085-153H. The x-ray diffraction pattern of fiber 09273H2 shows a sharpening of the equatorial arcs, accompanying the improved properties (compared Figs. 23a and 23b). The exterior of the fiber was similar to that shown in Fig. 23 a for fiber 10174 exhibiting a convoluted texture with a smooth skin. When fractured at liquid nitrogen temperature by bending, the heat treated fiber 09273H2 displayed a very brittle fracture surface as shown in Fig. 27b. Fracture of the as-spun fiber 09273 appeared to be somewhat less brittle, as may be seen in Fig. 27a.

Attempts to improve the properties of the fiber spun from the 9% solution containing gel particles gave results similar to those obtained with the fiber prepared from the isotropic solution, as may be seen in Table 23 and Fig. 28. It is apparent that superior properties will only be obtained on post treatment if the as spun fiber is itself well oriented.

The results discussed above show the necessity of obtaining a substantial degree of orientation in the as spun fiber for the attainment of superior properties in the final fiber. The data show that the degree of orientation in the as spun fiber increases as the spinning solution is made nematic, but also reveal that a solubility limit is apparently reached with PBO in $\text{CH}_3\text{SO}_3\text{H}$ at a concentration somewhat less than 9% by weight. It appears that this solubility limit may be alleviated somewhat by the use of a water scavenger such as ClSO_3H . The best properties realized to date have come with a fiber prepared from a biphasic solution. The modulus and tenacity

of 540 and 4 g/d, respectively, are still below the target figures of 1000 and 20 g/d. Attention is now being focused on post spinning treatment of the fiber prepared with the nematic solution and the preparation of nematic solutions containing higher polymer concentrations. Since the as spun properties of the fiber prepared with the nematic solution are superior to those of the fiber mentioned above prepared with a biphasic solution, post spinning treatment of fibers prepared with nematic solutions should bring us closer to the target modulus and tenacity figures.

In wet spinning experiments at the Celanese Laboratory, a series of experiments were directed toward the effect of the coagulation bath on the properties of PBO fiber spun from solution in a methane sulfonic acid/chlorosulfonic acid solvent (97.5/2.5 percent by weight). The effect of methane sulfonic acid concentration in the aqueous coagulation bath was examined over the range 0 to 90 percent acid. Wet-spun fibers were examined by electron microscopy for void and surface smoothness. It was found that a coagulation bath with 30 percent acid in water produced wet-spun fibers with the least void fraction and the smoothest surface. A fiber spun from a solution with 8.6 percent PBO (I.V. of 2.78 dl/g) showed good properties:

As-spun	4.14 g/d	tenacity
	1.37 %	elongation at break
	502 g/d	modulus
	5.26	denier per filament

After drawing 1% at 425°C the properties improved, giving

Drawn:	4.8 g/d	tenacity
	0.7 %	elongation at break
	711 g/d	modulus
	4.8	denier per filament

The x-ray diffraction pattern of the heat drawn fiber showed significantly more orientation than with previous fibers of PBO.

Although the modulus is in the target range for PBO, the tenacity is still lower than our goal. It is hoped that improved orientation will be obtained with dry-jet wet spinning, as discussed elsewhere, in this report, and that this will lead to increased tenacity. However, it must be recognized that the tenacity may be limited by the limited solubility of PBO and/or the low molecular weights of the polymers so far available. The latter problem has been addressed at Celanese by attempts to gain increased molecular weight using terephthaloyldichloride as a replacement for terephthalic acid in the polymerization of PBO. Polymers prepared with this revision appear fibrous when precipitated in methanol, in contrast to the PBO prepared by the original procedure. Indeed, the fiber described above was prepared with polymer synthesized by the revised procedure. Synthetic efforts to prepare higher molecular weight polymers continue.

7.1.3 Dry-Jet-Wet-Spinning Of PBO Solution

It was reported previously⁽¹⁾ that with Kevlar solution, fibers could be dry-jet-wet spun easily whereas with PBO solutions, the fiber constantly ruptured in the dry jet region, failing to form a continuous filament. Now we have succeeded in dry-jet-wet spinning an 8.98% PBO solution to form continuous fibers with reasonable tensile

properties.

The PBO solution was prepared with PBO-25613-37 (I.V. = 2.3, furnished by Celanese Research Co.) using a mixed solvent of methane-sulfonic acid (MSA) containing 2.5% by weight chlorosulfonic acid (CSA). Standard dissolution process was followed, cycling the stirred solution between 0°C and 70°C. With a weak stirring magnet, it took about one week to complete the dissolution process. Under microscopic observation, the solution was completely nematic, and was highly stir-opalescent at room temperature. Dry-jet-wet spinning was accomplished at room temperature with Spinning Apparatus D⁽²⁾ with a vertical jet by gradually raising the glass needle above the coagulant (water) surface. No filament advancing roller pairs were used. The dry jet length x was approximately 0.7 cm. The solution was extended from the orifice of a glass needle with inner diameter $D_0 = 160 \mu$ at a speed V_0 of approximately 3 cm sec⁻¹. The take-up speed V_T was varied stepwise from 8.15 to 14.8 cm sec⁻¹, resulting in fibers of five different sizes and properties. Results are listed in Table 11. Besides the size S , tenacity T , initial modulus E_0 and elongations at break ϵ_b , we also include in the table the values of $T\epsilon_b^{1/2}$ and $E_0\epsilon_b^{1/2}$ for estimation of the superiority of tensile properties. The former quantity $T\epsilon_b^{1/2}$ was used by Rosenthal⁽²⁹⁾ and was referred to as the Tensile index. On the other hand Black⁽³⁰⁾ used an empirical relationship of $E_0\epsilon_b^{0.58} \geq 1000$ gpd as an indicator for super fibers. We found it more convenient to simply use the function $E_0\epsilon_b^{1/2}$ for correlating the data. It can be seen that, in

general, the higher the take-up speed V_T , the better the resulting fiber. Also it should be noted that, in contrast to wet spinning, a much higher take-up speed and draw ratio could be achieved in dry-jet-wet spinning. Detailed analysis of the process will be given in the following, including suggestions for development to permit further improvements.

In the analysis of the experimental data presented in Table 11, the average cross-sectional area A_d of the dried fiber will be calculated from

$$A_d = 74 S \quad (\mu^2) \quad (108)$$

the average radius of the dried fiber is then

$$R_d = 4.85 \sqrt{S} \quad (\mu) \quad (109)$$

with the density $\rho = 1.5 \text{ gm cm}^{-3}$.

Assuming complete solvent exchange in the coagulation bath and complete drying of the fiber on the take-up device, a mass balance yields

$$A_1 V_1 = A_d V_T / \phi \quad (110)$$

where V_T is the take-up speed and ϕ is the volume fraction of the polymer in the solution. Furthermore if the fiber contracted isotropically as demonstrated previously^(1c), the jet speed at quench can be

evaluated as

$$V_1 = V_T \phi^{-1/3} \quad (111)$$

The validity of these assumptions may be checked by in situ telescopic photography.

Based on the above, alignment conditions to induce molecular orientation are calculated for the fibers spun and are listed in Table 11. The residence times $t_1 - t_0$ do not vary much among the five fibers since the dry jet length remains the same. In Figure 29, the modulus index $E_0 \epsilon_b^{1/2}$ is plotted against the total elongational residence Re and the time average elongation rate $\langle \bar{\kappa} \rangle_t$. It increases rapidly with Re or $\langle \bar{\kappa} \rangle_t$. This is consistent with the picture described in section 3 that the degree of molecular alignment increases with elongation rate. As molecular alignment is perfected, the tensile properties of the fiber will be improved significantly. A naive projection of the modulus index to a value of 1000 (super fiber value) in Figure 29 results in $Re = 3$ or $\langle \bar{\kappa} \rangle_t = 23 \text{ sec}^{-1}$.

As stated in section 3, in a steady elongation flow, the Herman parameter h becomes 0.99 when $\tau_c \bar{\kappa} = 6$. Replacing $\bar{\kappa}$ with $\langle \bar{\kappa} \rangle_t$, we may approximately define an alignment condition for $\langle \bar{\kappa} \rangle_t$:

$$\langle \bar{\kappa} \rangle_t \geq 6/\tau_c \quad (112)$$

Sufficient time τ' must be allowed for the rodlike molecules

or the nematic regions to align under the elongational flow from their original random configurations. This leads to the condition for residence time

$$t_1 - t_0 \geq \tau'$$

Combining Eqns. (112) and (113), the required total elongational residence is therefore

$$Re \geq 6\tau'/\tau_c \quad (114)$$

in consistent with the condition suggested experimentally, provided that τ' and τ_c are the same order of magnitude.

In order to elucidate the nature of the dry jet alignment criteria suggested above (Re , $\langle \bar{\kappa} \rangle_t$, $t_1 - t_0$, and β), it is revealing to examine the effect of the experimental variables (R_0 , V_0 , V_T , X_1 , $\bar{\eta}$ and α) on such alignment criteria:

a) Effect of Re

According to Eqn. (12), Re is proportional to $2 \ln R_0$, or $(\ln V_1 - \ln V_0)$. A natural way to increase Re will be to increase the capillary radius R_0 , the take-up speed V_T or to decrease the initial speed V_0 . It will be shown, however, that we cannot increase V_T or decrease V_0 indefinitely without breaking the jet.

b) Effect of $\langle \bar{\kappa} \rangle_t$

Reduced elongation rate $\langle \bar{\kappa} \rangle_t \cdot \bar{\eta} R_0 / \alpha$ is plotted logarithmically

against the ratio R_0/R_1 for various reduced dry-jet-length $(x_1 - x_0)/b$ in Figure 30. The values are numerically calculated with Eqns. (11) and (12) after the values of a has been determined with Eqn. (18) (see below). It can be seen that a power relationship slightly greater than unity exists between $\langle \bar{\kappa} \rangle_t$ and R_0/R_1 .

c) Effect of $(t_1 - t_0)$

Reduced residence time $(t_1 - t_0)/(\bar{\eta} R_0/\alpha)$ is plotted against the reduced dry-jet length $(x_1 - x_0)/b$ for various values of R_0/R_1 in Figure 31. At low dry-jet length and especially high R_0/R_1 ratio, $(t_1 - t_0)$ increases only slowly with $(x_1 - x_0)$. On the other hand, at the high dry-jet length limit, $(t_1 - t_0)$ increases linearly with $(x_1 - x_0)$, as suggested by Eqn. (24b).

d) Effect of β

The spinnable condition Eqn. (39) dictates that the value of β be sufficiently small. In Figure 32, β is plotted against $(x_1 - x_0)/b$ for various values of R_0/R_1 according to Eqn. (18). Here it can be seen that an increase of $x_1 - x_0$ will increase the value of β and eventually leads to breakage of the jet. Less apparent is the effect of increasing the take-up speed V_T which effectively increases the ratio R_0/R_1 with R_0 fixed. Such an increase will result in a decrease of $(1 - \frac{\delta_0}{R_0} \cdot \frac{R_0}{R_1})^2$, the right hand side of Eqn. (39), more rapid than the decrease of β as indicated in Figure 32, and again leads towards the breakage condition. To decrease β , we have the option of increasing R_0 (with R_1 fixed) again, or increasing the parameter b which is proportional to the viscosity $\bar{\eta}$, the initial radius R_0 , the initial

velocity V_0 and inversely proportional to the surface tension α .

Besides increasing the viscosity of the solution, which is fixed by the concentration and temperature, two approaches may be adopted to circumvent the problem of jet breakage as we increase Re . In the first one, we have devised a spinneret with large R_0 , surrounded with a dry nitrogen sleeve. The nitrogen sleeve will prevent the large slow jet near the tip of the spinneret from premature coagulation by the surrounding moisture. An increase of V_0 can also diminish the value of β , but it also diminishes the residence time ($t_1 - t_0$). On the other hand, for a scaled-up process, this is advantageous as it speeds up the overall operation and should be born in mind. The second approach is similar in apparatus design, except we replace the nitrogen gas with a stationary inert liquid, such as polyphosphoric acid. The advantage is of two-fold: (1) the liquid-air surface tension is replaced by a liquid-liquid one, thus lowering α ; (2) the perturbation growth factor γ is also diminished according to Eqn. (33c) and (33d), thus improving the spinnability of the jet. However, this modification introduces complications in the analysis of data. On the one hand, as R_0 is increased, the total weight of the jet is increased making F_{grav} no longer negligible. A preliminary treatment of the equations is given in Appendix I. On the other hand, if β is made sufficiently small so that the effect of surface tension is negligible, a new set of equations can be written down (see Appendix II).

Finally study of the coagulation mechanism has been planned for potential candidate coagulants. It has been found that neither

methanol or water serves as a very satisfactory coagulant. A coagulant with appropriate diffusion constant so that it will quench the whole jet with radius R_1 in a short enough time so as to prevent thermal disorientation in the core, and that it will not disturb the molecular alignment during exchange of solvents, is needed for successful dry-jet-wet spinning.

7.1.4 Inert-jet wet spinning with a PBO solution

Inert-jet wet spinning has been attempted with a 8.41% PBO-37/MSA solution. The jet was formed in a glycerol fluid in the modified spinning apparatus. A coagulation bath containing 8% MSA/methanol was kept at 0°C.

The principle of inert-jet wet spinning has been discussed in Section 2.3. As compared with a dry-jet, the inert liquid jet has the advantage of decreased surface tension and increased jet stability, the latter resulting from enhanced viscous damping. Our experimental observations confirmed these predictions. For example, a jet was easily formed in the glycerine fluid, even with very low initial velocities--with the latter, the 'jet' in air would merely grow into a large bead suspended on the spinneret surface. With a viscosity of 1490 centipoise at 20°C, the glycerine fluid stabilized the jet as expected. However, the high viscosity of the inert fluid proved to be disadvantageous in the subsequent coagulation process. It was observed that a film of glycerine wrapped around that jet when it quenched into the coagulation bath. The rate of diffusion and convection of the glycerine was so low that coagulation was prevented from taking place in a time shorter than the relaxation time of the

molecules. As a result, the fiber was too weak to be taken up. The high viscosity of the glycerine fluid also resulted in a nonuniform film thickness, causing assymmetric coagulation around the jet.

Since glycerol has a higher density than the methanol based coagulant, an inverted configuration of inert jet spinning was also investigated. In this configuration, the spinneret pointed upward. It was immersed in a bath with a glycerine layer at the bottom and a layer of methanol based coagulant on the top. A thinner and more uniform film was formed around the jet upon reaching the coagulation fluid. The same slow coagulations persisted, preventing fiber take-up. It is concluded that with selection of an inert fluid with a viscosity and density chosen to optimize the balance between stability in the inert jet region and rate of diffusion in the coagulation region, a successful inert jet wet spinning may be achieved.

TABLE 11

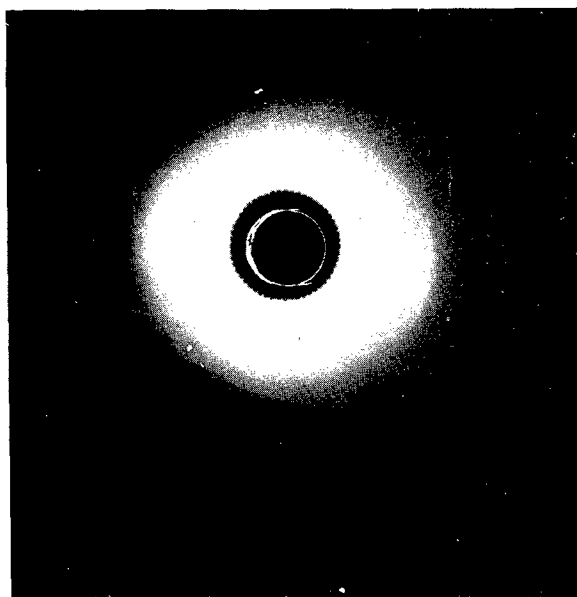
DATA ON PBO FIBERS

Number	Polymer Weight %	Material	Laboratory	Solution State	Fiber Treatment % Draw/Temp.	Fiber Area (Denier) ^c	Fiber Takeup Speed cm/sec	Modulus (g/d) ^d	Tenacity (g/d)
12010	5.4	PBO-30	CMU	Isotropic/24°C	As Spun	18.5	--	81	1.7
12010H5	"	"	"	"	17%/400°C	15.8	--	220	2.5
09273	8.0	PBO-5	CMU	Biphasic/24°C	As Spun	10.4	0.6	128	1.54
09273H2	"	"	"	"	6%/382°C	13.4	--	540	2.3
36085-153		PBO-50A	Celanese	Biphasic/5°C	As Spun	11	--	124	1.5
36085-153H	"	"	"	Biphasic/5°C	10%/470°C	--	--	254	4
10174		PBO-5	CMU	Nematic/8°C	As Spun	6.3	1.2	164	--
10176	"	"	"	"	As Spun	7.0	2.1	132	1.57
04297	9.0	PBO-2	CMU	Nematic ^a /24°C	As Spun	17.3	8.4	66	--
04297H	"	"	"	"	4%/450°C	--	--	204	1.6
36085-162		PBO-50	Celanese	? ^b /24°C	As Spun	13.3	--	81	0.8
36085-162H	"	"	"	"	6%/390°C	11	--	160	1.79
36085-163	"	"	"	"	As Spun	3.3	--	82	1.4

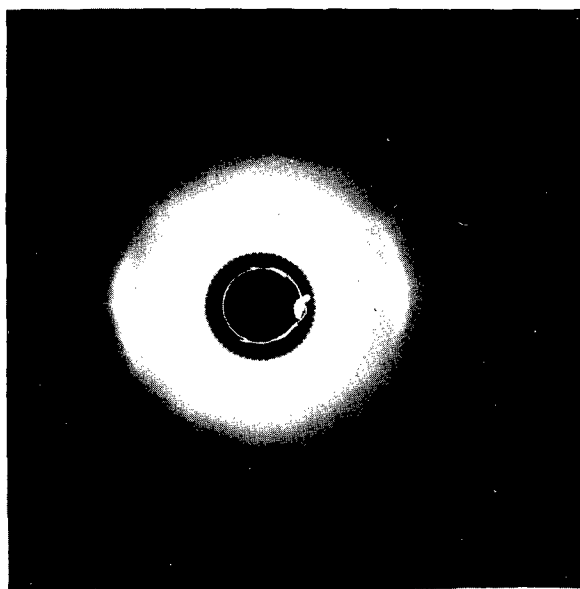
^a Solution contained a small fraction of gel.^b Solution contained undissolved material.^c Multiply by 1.11×10^{-6} / ρ to convert to cm^2 ; ρ is about 1.53g/ml for PBO.^d Multiply by $8.82 \rho \times 10^7$ to convert to N/M^2 , or by $1.30 \rho \times 10^4$ to convert to psi.

Table 12
Fibers Dry-Jet-Wet Spun From
8.98% PBO-37/MSA (2.5% CSA)

	PBO Fibers #				
	01277	01278	01279	012710	012711
<u>Properties</u>					
S (denier)	9.45	6.5	6.12	5.27	5.45
T (gpd)	1.06	1.23	1.31	1.90	1.65
E ₀ (gpd)	76	85	117.7	142	112.3
e _b (%)	3.02	3.43	2.2	3.12	3.6
E ₀ e _b ^{1/2}	132	157	175	251	213
T e _b ^{1/2}	1.84	2.28	1.94	3.36	3.14
<u>Alignment Conditions</u>					
V _T (cm/sec)	8.15	10.7	12.2	13.8	14.8
R ₀ /R ₁	2.39	2.88	2.97	3.21	3.15
e	5.72	8.32	8.83	10.3	9.95
γ	0.014	0.018	0.019	0.022	0.021
t ₁ -t ₀ (sec)	0.160	0.148	0.146	0.141	0.142
(x̄) _t (sec ⁻¹)	10.9	14.3	14.9	16.5	16.2
(x̄) _x (sec ⁻¹)	21.5	30.0	34.5	39.7	42.4
Re	1.74	2.12	2.18	2.33	2.30



a) Fiber 09273, as spun from a biphasic solution.



b) Fiber 09273H2, above after 6% draw at 382^oC.

Fig. 22 X-ray diffraction patterns of PBO fibers.

(Diffraction patterns courtesy of D. Wiff, AFML)



b) Fractured end of fiber 10174



a) Surface of fiber 10174, as spun from a nematic solution

Fig. 23 Scanning electron micrographs of a PBO fiber.
(Data obtained at Celanese Laboratory)



Fig. 24 X-ray diffraction pattern for PBO fiber 04297H.

(Diffraction pattern courtesy of D. Wiff, AFML)

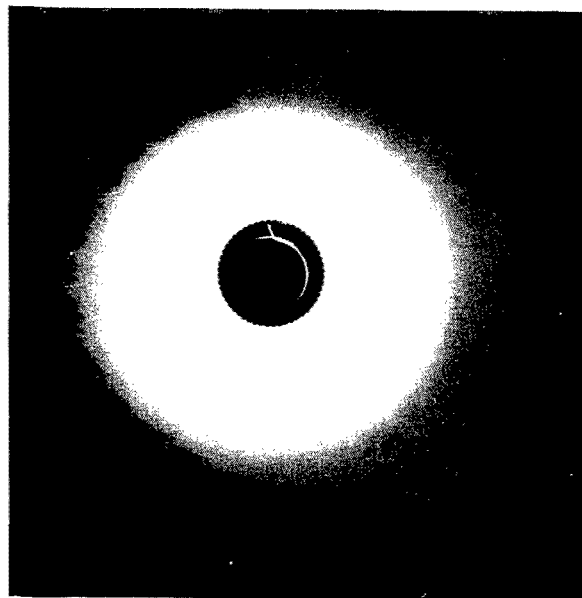


Fig. 25

a) X-ray diffraction pattern for as spun fiber 04297.



b) Scanning electron micrograph for a specimen of fiber 04297 fractured at liquid nitrogen temperatures.

(Diffraction pattern and micrograph courtesy of D. Wiff, AFML)

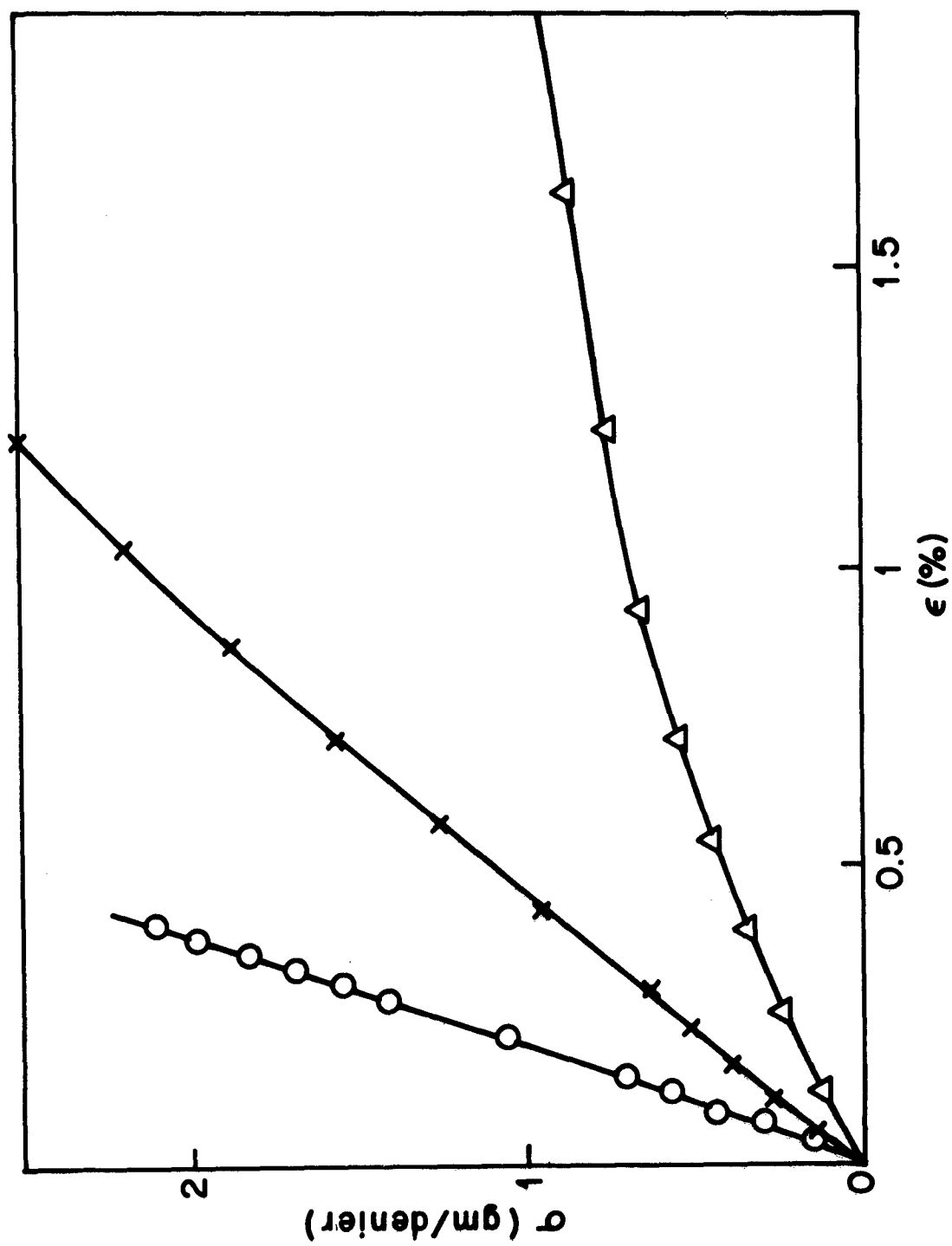
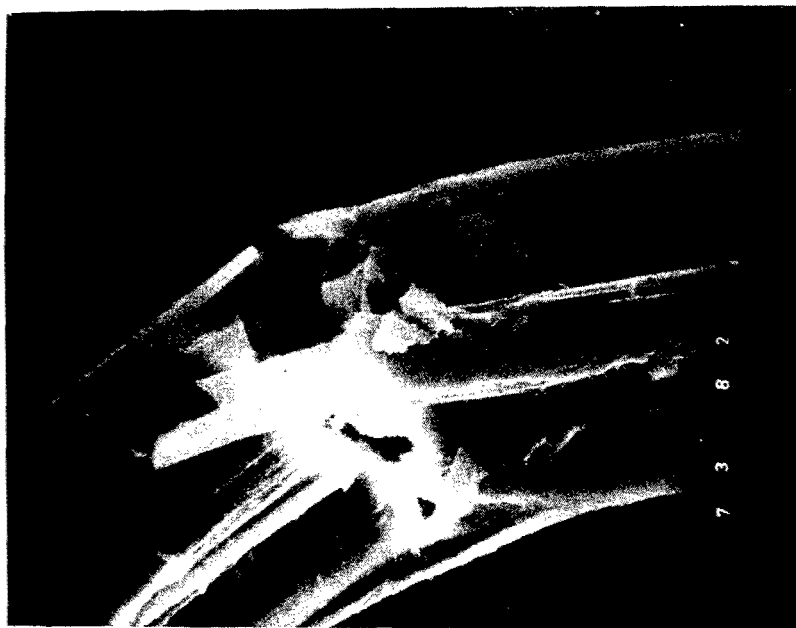


Figure 26 Stress-strain data for PBO fibers.
 Δ As-spun fiber 12010 prepared with an isotropic solution.
 \otimes Above after 17% draw at 400°C, fiber 12010HS.
 \circ Fiber 09273H2, spun from a biphasic solution.

Figure 27



a) Fiber 09273 as spun from a biphasic solution;
fractured in liquid nitrogen (x1000).



b) Fiber 09273H, above after 6% draw at 382°C ,
fractured in liquid nitrogen (x1000).

Fig.26. Scanning electron micrographs of PBO fiber.

(Micrograph courtesy of D. Wiff, AFML)

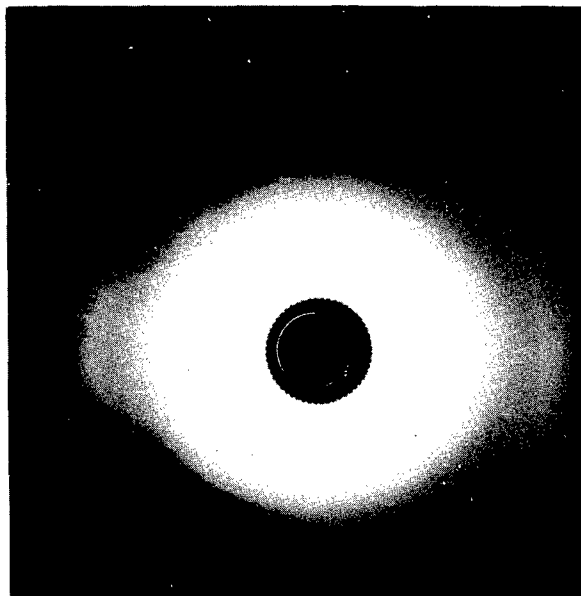


Fig.28 X-ray diffraction pattern of PBO fiber 12010 prepared from an isotropic solution.

(Diffraction pattern courtesy of D. Wiff, AFML)

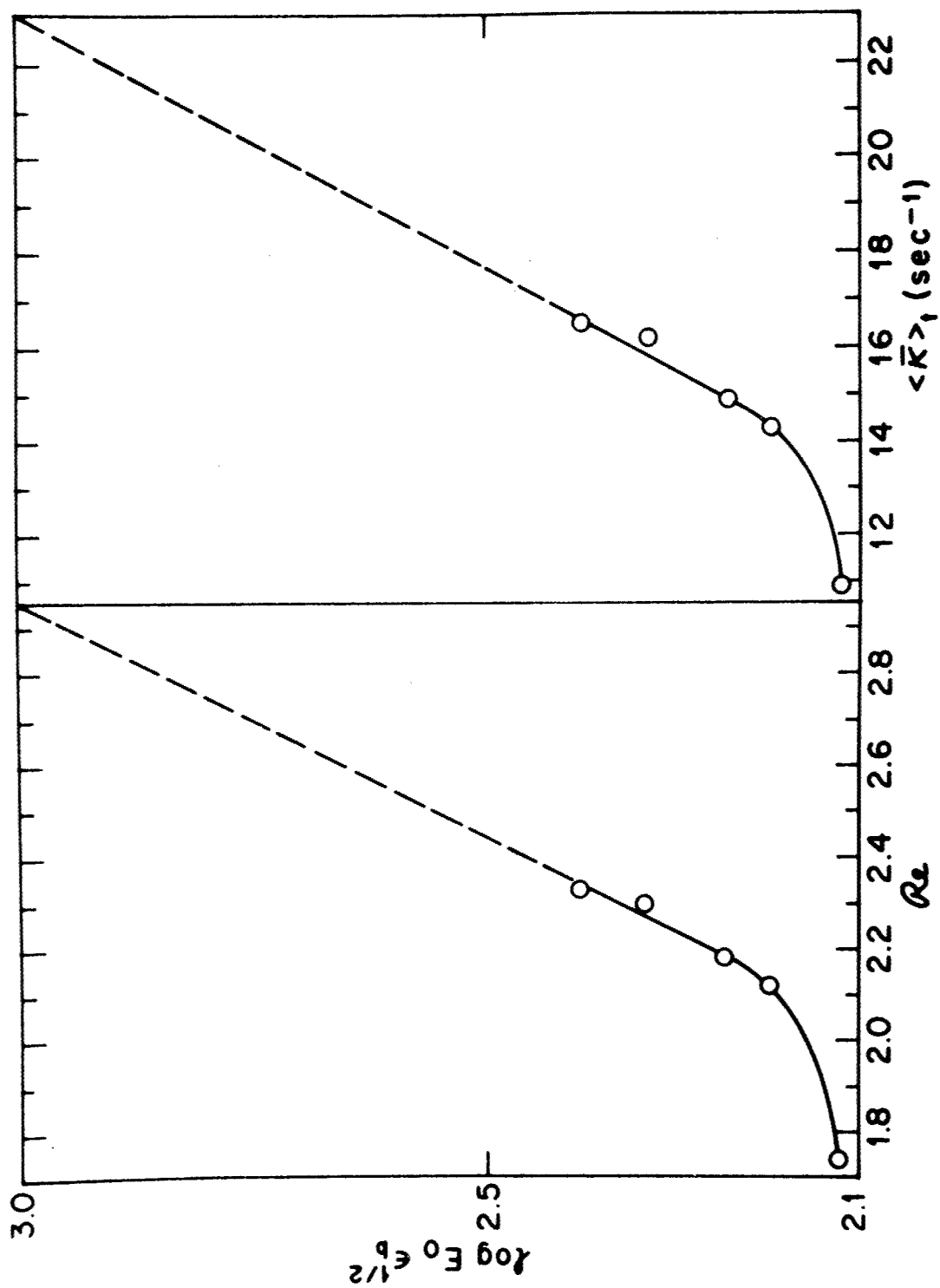


Figure 29 Logarithm of modulus $E_0^{1/2}$ plotted against elongational residence Re and time-average elongation rate $\langle \bar{K} \rangle_t$ for PBO dry-jet wet spun fibers.

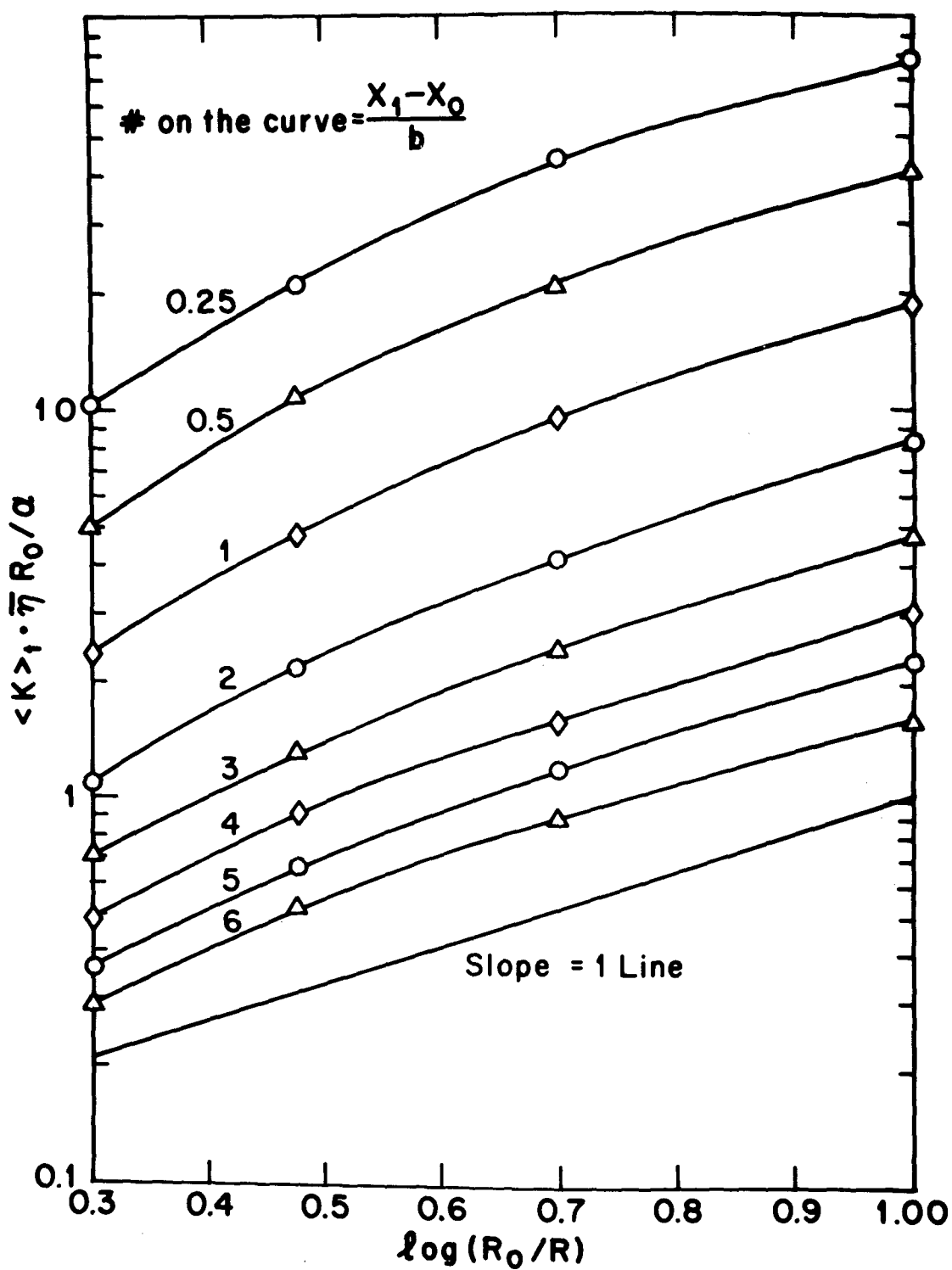


Figure 30

Reduced time-average elongation rate $\langle \bar{x} \rangle_t \cdot \bar{\eta} R_0 / \alpha$ plotted logarithmically against radius ratio R_0/R_1 for selected values of dry-jet length $(x_1 - x_0)/b$.

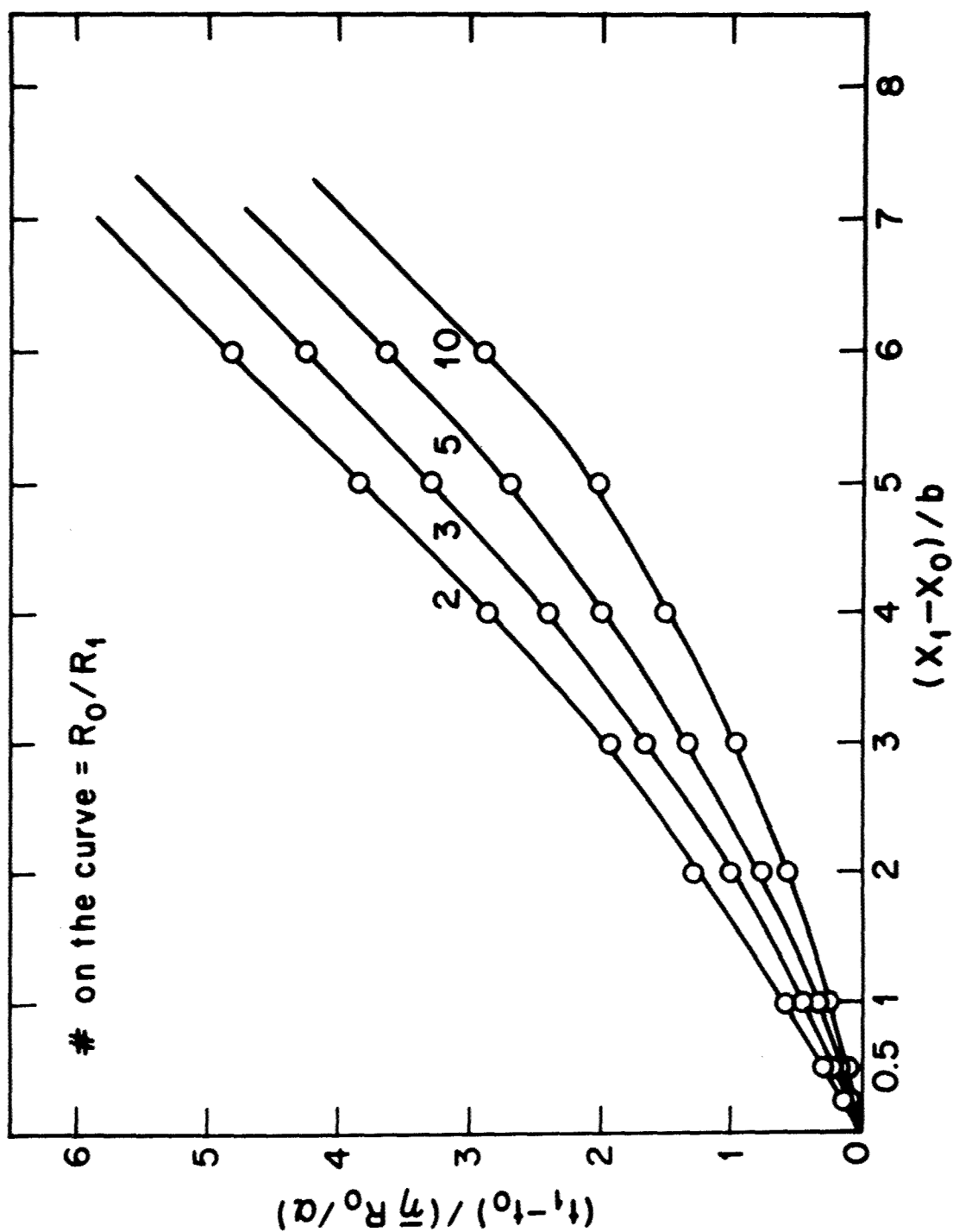


Figure 31 Reduced dry-jet residence time $(t_1 - t_0) / (\bar{\eta} R_0 / \alpha)$ plotted against dry-jet length $(x_1 - x_0) / b$ for selected values of radius ratio R_0/R_1 .

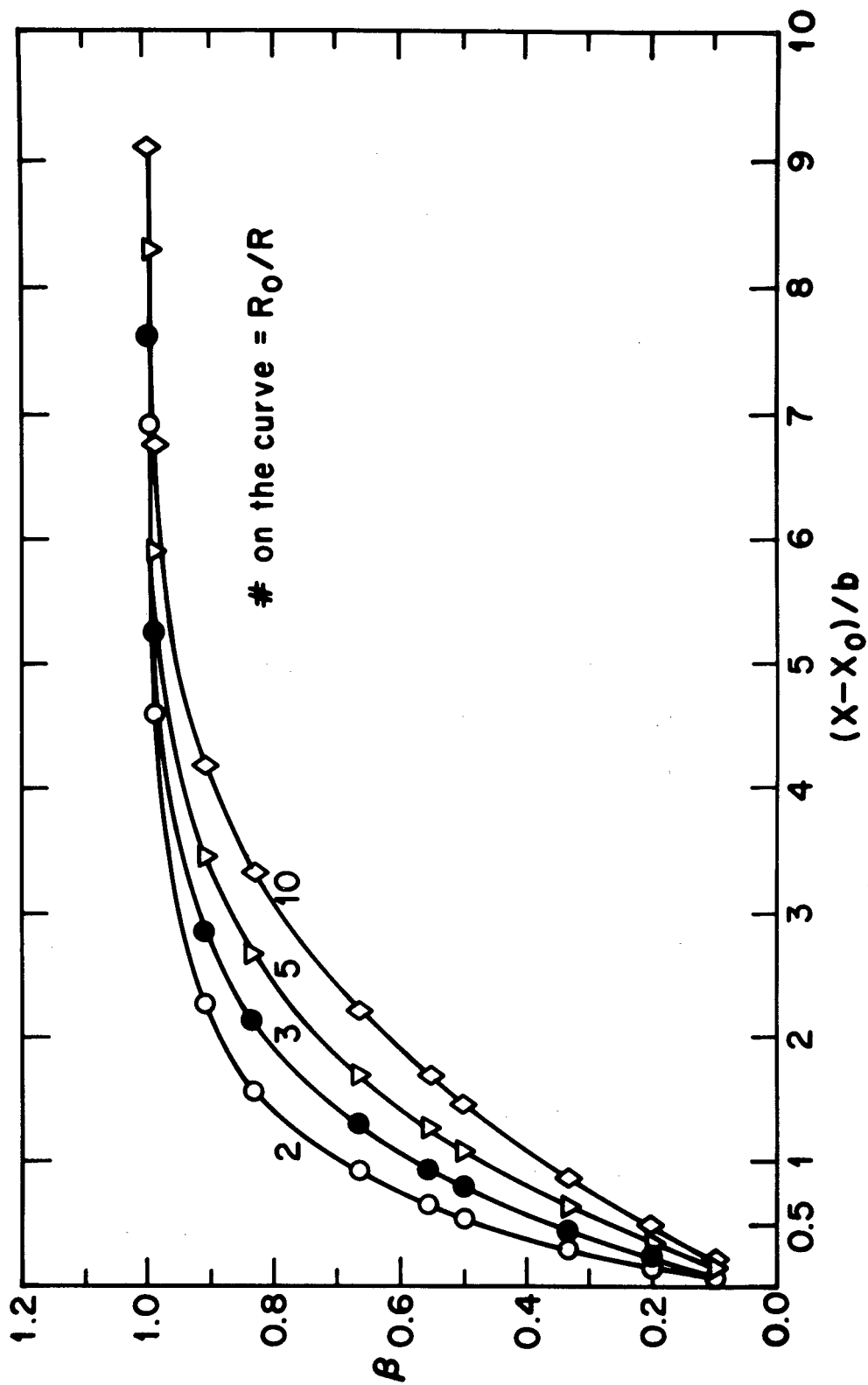


Figure 32 Contribution β of the force due to surface tension to the total force plotted against reduced dry-jet length $(x_1-x_0)/b$ for selected values of radius ratio R_0/R_1 .

7.2 Fiber Formation with Nematic Solutions of PBT

The formation of the available polybenzobisoxazoles (PBO) into well oriented solids has been hampered by what appears to be a low level of intermolecular association, preventing the attainment of well ordered solutions and hence well oriented solids. It appears that solutions of polybenzobisthiozole (PBT) exhibit much less inter-chain association, and in this section we will describe experiments leading to the formation of well oriented PBT fibers with a very high modulus (e.g. up to 1000 g/den or 2×10^7 psi). Rheological considerations for the orientation of rodlike polymers in a flow field used to design the fiber forming process are also discussed in the following.

7.2.1 Wet Spinning with a PBT-43 Solution

A 9.2% PBT solution was prepared with PBT-2122-43 (I.V. = 9 furnished by J. Wolf of the SRI) using the standard mixed solvent of methane sulfonic acid (MSA) containing 2.5% by weight chlorosulfonic acid (CSA). The polymer was first dried on a vacuum line for six days with a weight loss of 18%. The latter presumably is due to loss of absorbed water or residual terephthalic acid. The standard dissolution process was followed, with occasional release of the pressure built up in the dissolution tube caused by evolution of hydrogen chloride, as the solvent was hydrolyzed by residual water on the polymer. The solution was completed in four days and was stir-opalescent.

Spinning was performed at room temperature with the spinning apparatus described previously⁽¹⁾. Glass needle spinnerets of two diameters (385μ and 312μ) were used. The coagulation baths consisted

of a 50% methanol/ethyl sulfate quench bath and a pure methanol wash bath. Six fibers were obtained by a wet spinning process, with tensile properties listed in Table 12. Owing to the small amount of sample available, it was not possible to optimize the spinning parameters. Thus the fiber properties are not exceptional (modulus of 28 ~ 80 gpd and tenacity of 0.04 ~ 0.9 gpd). The possibility of dry-jet wet spinning was demonstrated with 312 μ spinneret, but no fiber was taken up due to shortage of sample.

7.2.2 Dry-jet Wet Spinning and Wet Spinning with a PBT-47 Solution

A 10.3% PBT solution was prepared with PBT-2122-47 (I.V. = 10.7 furnished by Dr. J. Wolf of SRI) using the standard technique. The weight loss of the as-received polymer in the vacuum line was 2.2%. The solution was completed in five days and was totally nematic at room temperature. Dry-jet wet spinning was successfully accomplished at room temperature with a modified spinning apparatus. The essential features of modification involved (a) a stabilizing sleeve surrounding the glass needle spinneret and (b) a V-shape coagulation tube instead of the conventional rectangular bath. The former stabilized the dry jet to an extent that more than 30 mm dry-jet length without rupture were attainable and the latter provided an easier start-up procedure. Wet spinning was also conducted with the same solution. Water, methanol and 70% methanol/sulfolane were used as the first coagulant. In all cases pure methanol was used in the second bath. The spinneret diameter was 265 μ . The resulting fibers are listed in Table 13. High modulus fibers were obtained in this series of experiment. In

particular, Fiber # PBT-071938 has an as-spun modulus of 820 gpd. An x-ray diffraction pattern is shown in Figure 33, indicating an extremely high orientation of the molecules in the fiber. The same fiber was heat drawn at 386°C to 0.9% with the procedure described in a previous report⁽¹⁾. The resulting fiber attained a modulus of ~ 1,000 gpd, the x-ray diffraction pattern of which is shown in Figure 34. Even higher orientation and crystallinity can be seen. The apparent tensile strength of the material is not very high (~ 5 gpd), although it is higher than any of the PBO fiber tested. It is believed that the apparent low value is due to the defects caused by incursion during coagulation. A much higher value would be obtained if we take into account the structural factor of the fiber. This will be discussed in detail below.

7.2.3 Dry-Jet Wet Spinning with a PBT-53 Solution

A series of thirteen PBT fibers were prepared by the dry-jet wet spinning process using the solvent system described above, with a coagulation bath of 50:50 methanol and sulfolane (along with a methanol wash bath) and PBT-2122-53 provided by Dr. J. Wolfe. The spinning solution contained 9.85% polymer. A 96 micron radius spinnerette was employed, together with a shield designed to protect the fresh exudate in the "air gap" from disturbance by drafts, etc. and to permit the operator to pass a slow flow of nitrogen through the air gap. Although not used in these experiments, the shield is also designed to permit the inert jet wet spinning process described in an earlier section.

The fiber spinning parameter of interest here are shown in Table 14. As in previous sections, the elongation number R_e is determined from the initial and final radii. R_0 and R_1 , respectively, of the jet:

$$R_e = 2 \ln \frac{R_0}{R_1}$$

The final radius R_1 is estimated from the radius of the dry fiber, using Eqns. 108-111. The initial modulus E_0 ; elongation at break ϵ_b (expressed as strain at break times 100, or percent strain), and the strength at break or tenacity T , were all determined with an Instron tester.

Elongation numbers ranging from 2.26 to 2.93 were achieved. As explained in previous sections, R_e must be large enough to insure sufficient coventionation in the jet, but not so large that small perturbations in the jet radius can be amplified to the point of jet rupture. The values of R_e achieved here are similar to those we have reported previously, but fall short of the range 5-6 that might be desirable for fabrication of very highly oriented fibers.

The modulus index $E_0 \epsilon_b^{1/2}$ (with ϵ_b in percent strain) varies from 610 to 1215 for the two fibers for which data are presently available. Fiber 5346 was heat treated at 450°C under nitrogen (at Celanese Research Center) resulting in a marked improvement in properties. The as-spun and heat treated fiber properties are as follows:

	T	ϵ_b	E_o	$E_o \epsilon_b^{1/2}$
	gpd	(%)	gpd	
As-Spun	6	11	366	1215
Heat Treated	11.5	1	1220	1220

It may be noted that modulus index $E_o \epsilon_b^{1/2}$ did not alter much on heat treatment, despite appreciable change in modulus, percent strain at rupture and tenacity.

7.2.4 Dry-Jet Wet Spinning with a PBT Solution

A series of eight PBT-62 fibers were prepared by the dry-jet wet spinning process using the solvent system described above, with a coagulation both of 50:50 water and sulfolane or 40:60 water and sulfolane followed by a methanol wash bath. The polymer, sample PBT-2122-62A, furnished by SRI, has an intrinsic viscosity of 26 dl/g. A preparation with 10% polymer by weight in MSA failed to become homogeneous, even after several weeks, but a homogeneous solution with 8.2% polymer by weight in MSA was obtained after three weeks dissolution time. The nematic solution was used to form fibers under the conditions given in Table 15. Values of R_e and some fiber properties are also listed. Samples of this fiber have been provided to Professor E. Thomas, University of Massachusetts, for additional physical characterization. It may be noted that the PBT-62 fibers do not seem to be superior to the PBT-53 fibers, despite the higher molecular weight of the PBT-62 polymers. The reduced solubility of the higher molecular weight polymer may account for the lack of marked

improvement in properties.

As with PBT-53 fibers, heat treatment at 450°C serves to increase the modulus and tenacity of the fiber:

	T	ϵ_b	E_o	$E_o \epsilon_b^{1/2}$
	gpd	(%)	gpd	
As-Spun	5.0	1.5	500	600
Heat Treated	8.1	1.0	920	910

7.2.5 Effects of Spinning Variables

a) Elongation Number and Dry-Jet Length

It has been established that the two most important processing parameters in a fiber spinning operation are the elongation number $R_e \equiv \int_0^{t_1} \bar{\kappa} dt$ and the reduced dry-jet length $X_r \equiv \pi 2 R_o \bar{\kappa} / \bar{\eta} Q^{(2)}$. The conditions for spinnability and orientation can be summarized as follows

$$2 \ln \frac{R_o}{\delta_o} \sqrt{1 - \beta} > R_e > \frac{3 R_o \bar{\eta}}{\alpha \tau_c} G(R_e, X_r) \quad (115a)$$

$$t_1 - t_o > \tau' \quad (115b)$$

(Spinnability)

(Orientation)

in which β is given implicitly by

$$R_e = 2 \ln \left[\beta + (1 - \beta) \exp\left(\frac{X_r}{\beta}\right) \right] \quad (116)$$

and the function $G(R_e, X_r)$ by

$$G(R_e, X_r) = \left\{ \beta \ln \frac{\beta}{\beta - 1} - 1 + \beta \ln \left[1 - \frac{1}{\beta} \exp \left(- \frac{R_e}{2} \right) \right] + \exp \left(- \frac{R_e}{2} \right) \right\} \quad (117)$$

(Here R_0 is the initial radius of the fiber, not to be confused with the zero shear recoverable compliance R_0). The parameter β is a measure of the force due to surface tension to that of the total, and

$$\lim_{\beta \rightarrow 0} G(R_e, X_r) = \ln \frac{1 - \exp \frac{X_r}{R_e}}{1 - \exp \frac{R_e}{2}} - 1 \quad (118)$$

In Figure 35, we plotted the modulus index of a series of PBT-47 fibers with the elongation number R_e . Although the data scattered a bit, the general trend is evident and is in accord with Eqn. (115b) if τ'/τ_c is the order of unity. In view of the simplicity of the model involved, its prediction for orientation of the molecules must be considered quite successful.

In Figure 36, we have plotted the modulus index against the dry-jet length with same take-up speed. The modulus index in general increases with the dry-jet length, but the effect tapers off as dry-jet length gets longer. This result is consistent with the time dependent behavior of the orientating species in the dry jet. Enough time has to be allowed for the orientation to reach its steady-state, and once the steady state flow has been established, any further increase of residence time (or dry-jet length) is not necessary.

In the preceding discussion, we have put aside the thermodynamic effect of liquid crystal formation for the sake of simplifying

mathematical treatment. The nematic mesophase formation in these systems undoubtedly plays an important role in the fabrication process. In fact Marrucci⁽²⁶⁾ have discussed the enhancement of liquid crystal formation due to elongational flow by modifying Flory's lattice theory. Under microscopic observation, a quiescent nematic solution of PBT polymer does not necessarily line up in one direction as a whole. The opposite is always true that they order themselves in local regions. It has been observed by the author that upon shearing, these local regions do not simply reorient themselves to the shearing direction, but break up into much smaller regions (or even molecular species) which oscillate at low shear rate but line up at higher shear rates. Although the molecular models discussed in Section 5 were developed for axisymmetric particles, their applicability to particles of arbitrary shapes is reasonably self-evident, provided that the rotatory diffusion constant D_r is adequately defined. It is quite possible that the orientating species upon imposition of flow are much smaller than the relaxing species when the imposed flow is removed for a nematic polymer solution. If such is the case, it remains important to find out the size and shape of these species under either situation using optical methods.

The values of $E_o \epsilon_b^{1/2}$ for the as-spun fiber are similar to those reported earlier for comparable R_e . We were unable to increase R_e in the present case as the fiber ruptured for $R_e > 3$. Thus, even though the decreased denier may be advantageous for uniform coagulation, it may be disadvantageous with respect to orientation since the

allowable R_e is necessarily reduces (see Table 14). The case of a multijet spinnerette may offset this effect somewhat.

The relative constancy of the modulus index $E_o \epsilon_b^{1/2}$ with heat treatment is encouraging. It may be possible to use coagulants with lower coagulation rates, and fewer problems with incursions, to produce fibers or films nearly free of voids. These may then be heat treated to improve E_o and T to the desirable levels. For example, fibers wet spun into sulfolane, with final coagulation in a water/sulfolane mixture are incursion free. Such a system may be used in our latter studies on film formation.

b) Incursion During Coagulation

It was mentioned above that incursions occur during coagulation of PBT/MSA solution on a glass slide. The same effect can be observed in the spun fiber in our experiment. In Figure 37, we show a picture of both fiber # PBT-47-071938 and PBT-47-071938H1 under optical microscope. The fiber axis are 45° with respect to the cross polars. The fibers are highly oriented everywhere except where incursions occurred which broke into the fiber and formed a short core as it is elongated. A scanning electron micrograph shown in Figure 38 confirms the defect that was created due to such incursion effect. The presence of these defects is explanatory of the high modulus but moderate tenacity of these fibers.

Suppose the fiber is composed of f fraction of defects per unit length, and in each defect section the ratio of area that contains well oriented molecules to the total cross-sectional area is q . Then

by simple geometric argument the idealized initial modulus of the fiber without defect is given by

$$E = E_{app} \left[1 + f \left(\frac{1}{q} - 1 \right) \right]$$

where E_{app} is the apparent initial modulus as measured. Based on the observation with optical microscope, $f \sim 1/10$ and $q \sim 1/3$, then $E \approx 1.2 E_{app}$, not too different from E_{app} . On the other hand, the fiber will break at its weakest point and the idealized tenacity is given by

$$T = \frac{T_{app} - E' \epsilon_b}{q_{min}} + E' \epsilon_b$$

where T_{app} is the apparent tenacity, ϵ_b the elongation at break, E' the tensile modulus of the defect (unoriented) region and q_{min} is q at the weakest point. Then the estimated tenacity is $15 \sim 20$ gpd for a fiber without incursion defect.

c) Conclusion

(1) Successful dry-jet wet spinning with PBT/MSA solution has been demonstrated to yield fibers with modulus 1,000 gpd and tenacity 5 gpd.

(2) The moderate tenacity is attributed to the defects caused by incursion during coagulation. Without such defects, the tenacity is estimated to be $15 \sim 20$ gpd.

(3) Stabilization of jet and easier jet starting has been

achieved with inert jet wet spinning (IJWS). Yet additional problems have to be overcome to put IJWS into practice.

(4) Molecular models for rodlike polymer have been reviewed in connection with orientation under elongational flow. The prime molecular parameter that determines orientation is its rotatory diffusion constant which depends on the third power of the length of the species.

(5) A broad distribution of molecular lengths is undesirable in the orientation fabrication processes as the orientation effect quickly deteriorates for shorter species.

(6) The significance of elongation number and the dry-jet length has been experimentally established in accord with theoretical prediction. It is desirable to make $R_e = 5 \sim 6$ for perfect orientation of molecules in an elongational flow.

(7) Additional rheological, optical and coagulation study are needed to elucidate the molecular mechanism involved in the fabrication process for refinement.

Table 13

Wet Spinning Of
9.2% PBT-43/MSA

Code	Size (denier)	T (gpd)	ϵ_b (%)	E_o (gpd)	$T\epsilon_b^{1/2}$	$E_o\epsilon_b^{1/2}$
PBT-06291	230	0.86	4.14	60	1.75	122
06292	119	0.78	1.7	72	1.02	94
06293	180	0.39	0.59	80	0.30	61
06294	151	0.09	0.16	55	0.04	22
06295	155	0.04	0.077	48	0.01	13.3
06296	80	0.35	3.7	28	0.67	52

Table 14
Wet Spinning and Dry Jet Wet Spinning
of 10.3% PBT/MSA

Code		Dry Jet (mm)	Take-up Speed (cm/sec)	Size (denier)	T (gpd)	ϵ_b (%)	E_o (gpd)	$E\epsilon_b^{1/2}$
PBT-071927	Wet Spinning	--	6.3	70.2	2	4.5	62	132
071935		--	4.4	58.9	2	5.7	87	208
071936		--	8.5	71.5	2	6	57	138
071937		--	6.65	131.4	0.23	2.3	11	16.7
071928	Dry Jet Wet Spinning	2	5.2	22.0	2.5	3.0	87	151
071929		3	6.8	18.4	3.3	2.9	145	247
071930		3.5	8.5	16.4	3.7	3.3	130	236
071931		5	8.5	14.9	3.5	2.64	185	301
071932		8	8.5	13.1	3.8	2.4	220	341
071933		10	8.5	14.9	3.76	1.01	432	432
071934		12	8.5	5.9	3.73	1.53	390	482
071938		11	31.9	4.0	5.2	1.1	820	800
071939		20	9.3	21.4	4	3.5	160	299
071940		20	11.9	17.1	4.4	2.9	193	329
071941		20	17.1	11.9	2.5	1.6	270	338
071942		30	18.9	9.75	4.9	2.1	250	313
071943		30	17.1	9	3.55	1.35	323	375
071945		--	(free fall)	31.5 132	3.8	5.4	130	302

Table 15

Dry-jet Wet Spinning of 9.85% PBT-53/MSA

Code	Dry-jet (mm)	P (psi)	Take-up Speed (cm/sec)	Size (denier)	T (gpd)	ϵ_b (%)	E_o (gpd)	R_e
PBT-5346	15 ~ 20	180	11.3	8.8	6	11	366	2.26
47	"	200	"	6.5				2.57
48	12	200	14.5	9.9				2.15
49	20	200	20.3	6.2				2.61
50	20	200	23.3	4.5				2.93
51	10	200	26.3	4.8				2.87
52	10	200	31.9	6.8				2.52
53	15	200	20.3	5.9				2.66
54	10	200	31.9	5.1				2.80
55	15	200	31.9	5.1	4.9	1.3	535	2.80
56	15	200	20 ~ 26	6.5				2.56
57	15	200	31.9	7.1				2.48
58*	23	50	82.5					

* PBT-5358 were spun from a spinnerett with $d = 481 \mu$.

TABLE 16

Dry-jet Wet-spinning of 8.2% PBT-62/MSA

Code	Dry-jet (mm)	P (per)	Take-up (cm/sec)	Size (den)	T g/d	ϵ_b (%)	E_0 g/d
PBT-6260	22	70	1.98	28.0			
61	22	70	2.96	18.1	7.6		
62	22	70	3.96	11.5			
63	22	100	5.14	20.8	5.0	1.5	500
64	22	100	6.72	15.7	6.1	1.9	530
65	20	100	7.9	14.6	7.7	0.9	580
66	20	70	4.74	12.4			
67	35	70	4.74	11.3			

Figure 33 X-ray diffraction pattern for a dry
jet wet spun fiber #PBT-071938.
(Courtesy of D. Wiff, Univ. Dayton)

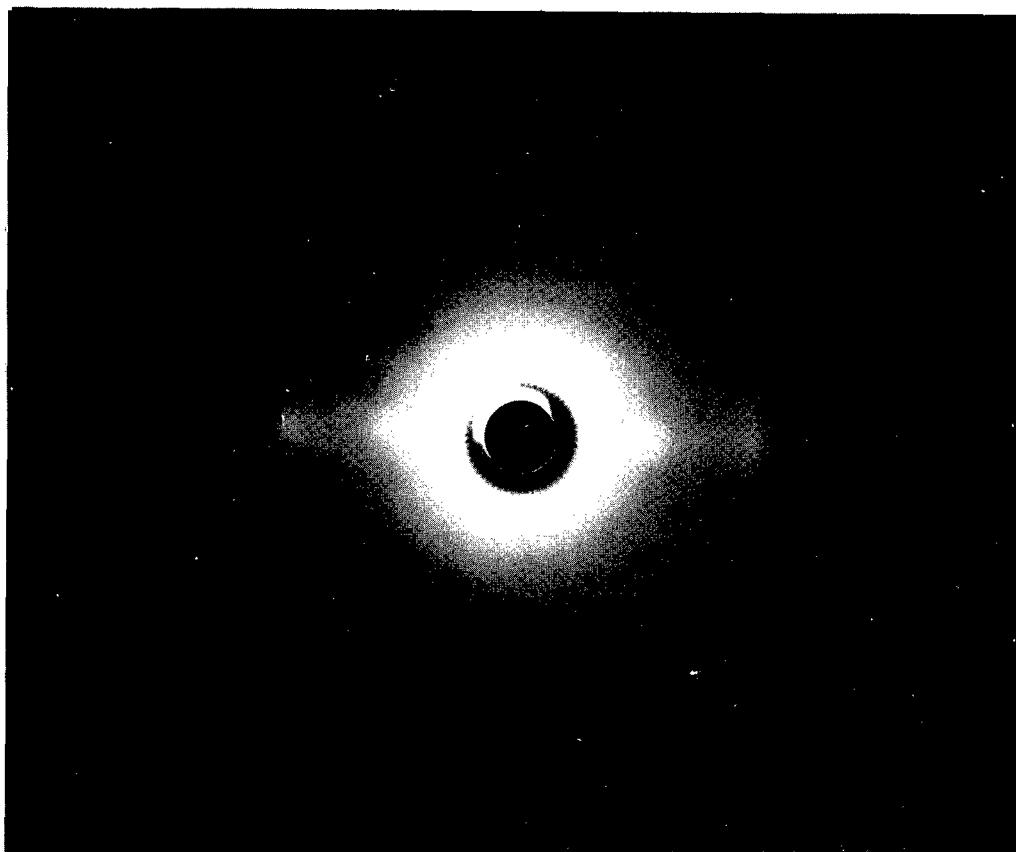
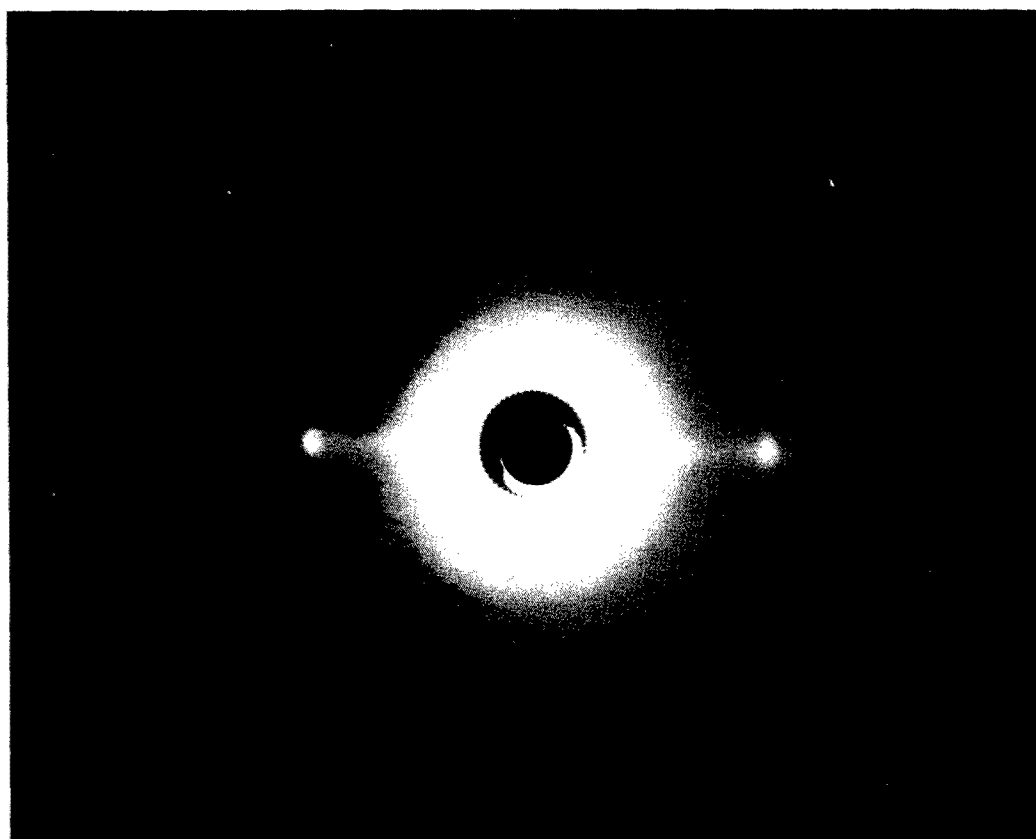


Figure 34 X-ray diffraction pattern for heat drawn fiber #PBT-071938H2. (Courtesy of D. Wiff, Univ. Dayton)



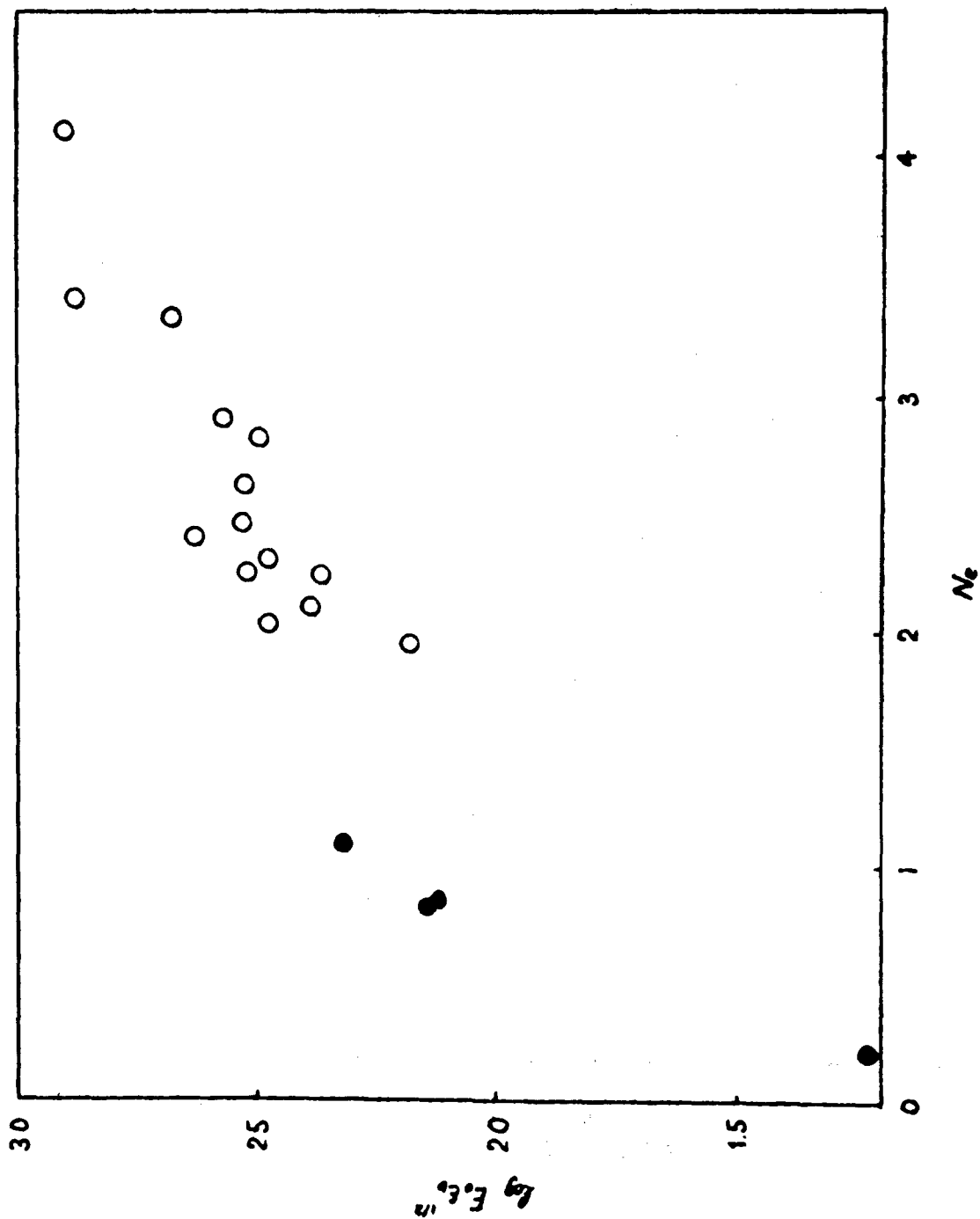


Figure 35 Logarithm of modulus index plotted against the elongation number N_e for a series of wet-spinning (filled circles) and dry-jet wet spinning (open circles) experiment with PBT-47/MSA solutions.

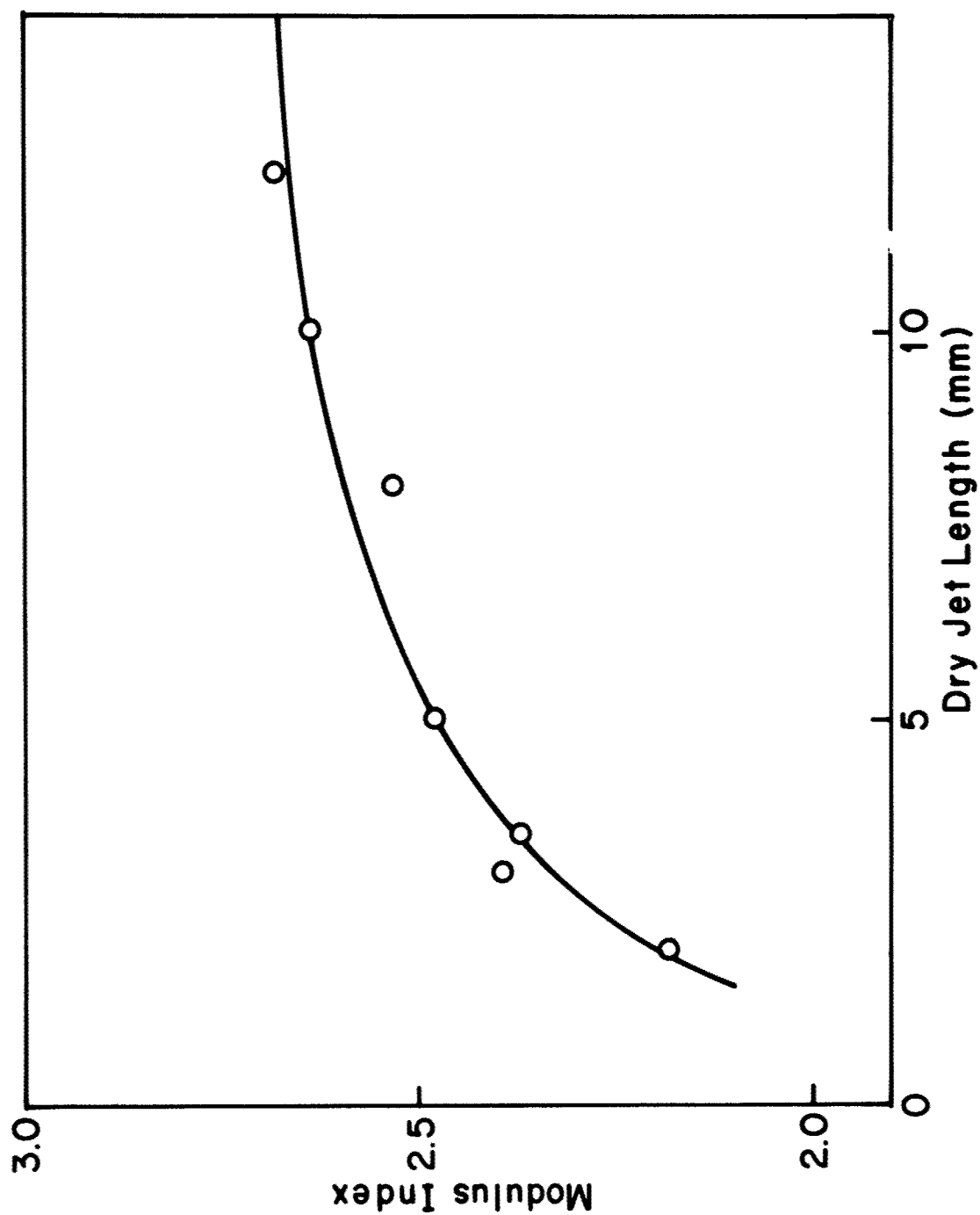


Figure 36 Logarithm of modulus index plotted against the dry-jet length for a series of dry-jet wet-spinning experiments with same take-up speeds, with PBT-47.

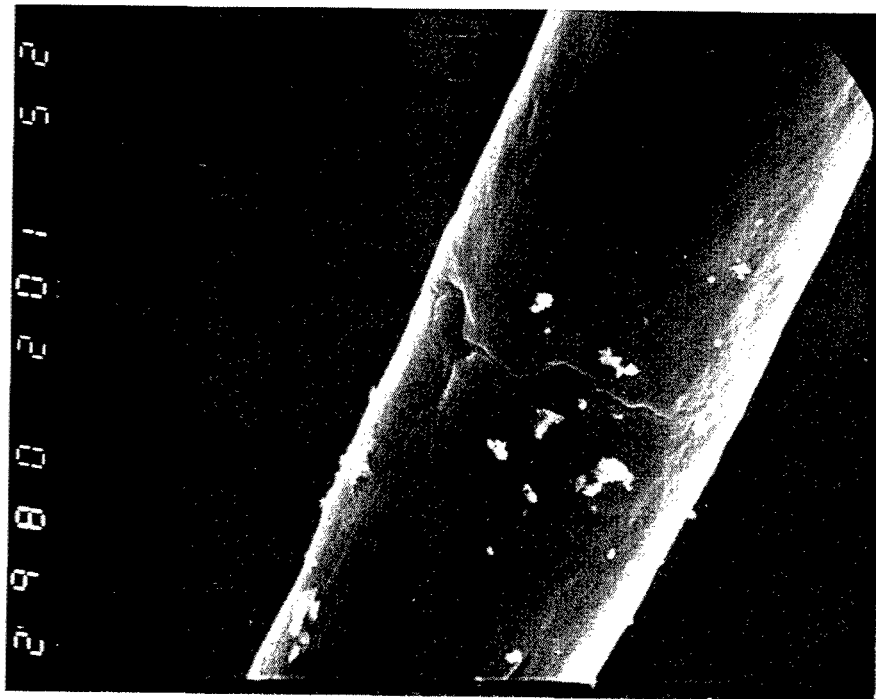


(a)

(b)

Figure 37 Optical microscopy of (a) PBT-071938
and (b) PBT-071938H1, fiber axis 45°
to the cross polars, fiber diameter
~ 10 μ .

Figure 38 Scanning electron microscopy of PBT-071930, showing defects due to incursion 1,000X. (Courtesy of D. E. Laughlin, Dept. of Metalurgy and Material Science, CMU).



8. TENSILE CREEP AND THERMAL-MECHANICAL CONDITIONING

8.1 Creep and Recovery

Tensile creep and recovery experiments at room temperature have been performed on single filaments of fibers PBO-0429-7, PBO-0429-8 and PBO-1201-0. (See Table 10). The tensile creep compliance $D(t)$, defined as the strain $\epsilon(t)$ divided by stress σ is shown as a function of the cube root of time in Figure 39 for a PBO-0429-8 fiber. In this case, we employ the specific stress in grams per denier, gpd, since the average size of the fiber is better expressed in denier rather than in terms of the cross-sectional area, especially for nonuniform fibers or fibers of unknown density. Curves (a), (b) and (c) represent consecutive first, second and third loadings of the sample after previous creep and recovery. The stress σ here is 0.735 gpd. After the third loading (c) the fiber became "mechanically conditioned" so that further tests yielded the same curves. The creep data for $t > 15$ sec are fitted by the Andrade cube root relation:

$$D(t) = D_{NR}(t) + D_A(1 + \beta_R t^{1/3}) \quad (119)$$

where $D_{NR}(t)$ is the nonrecoverable compliance and the second term is recoverable.

The recovery compliance $D(\theta, t_c)$, the corresponding viscoelastic function at recovery time θ after creep of duration t_c is shown in Figure 40. If the sample under investigation is linear viscoelastic, The Boltzmann superposition principle yields

$$D(\theta, t_c) = D_{NR}(t_c) + D_A \beta_R R(\theta, t_c) \quad (120)$$

where

$$R(\theta, t_c) \equiv (\theta + t_c)^{1/3} - \theta^{1/3} \quad (121)$$

Plots of $D(t)$ versus $t^{1/3}$ from creep and $D(\theta, t_c)$ versus $R(\theta, t_c)$ from recovery should have identical slopes $D_A \beta_R$; the former curve has intercept of $D_{NR}(t_c) + D_A$ at $t = 0$ and the latter an intercept $D_{NR}(t_c)$ at $R(\theta, t_c) = 0$ (or $\theta = \infty$). The initial modulus E_0 is given by D_A^{-1} , the reciprocal of the difference of the two intercepts. Curves (b) and (c) of the second and third run follow the behavior described above within experimental error. Values of relevant parameters are listed in Table 16. Curves (a) of the first run, however, do not yield the same slopes for creep and recovery plots although they can be fitted by the cube root relations. One can empirically assume that

$$D_{NR}(t) = D_A (\beta_c - \beta_R) t^{1/3} + D_{NR}'(t) \quad (122)$$

where the first term is the cube-root contribution to the non-recoverable compliance. Substituting Eqn. (122) into Eqn. (119), we have for the creep compliance

$$D(t) = D_{NR}'(t) + D_A (1 + \beta_c t^{1/3}) \quad (123)$$

The intercept, $D_{NR}'(t) + D_A$, at $t = 0$ cannot be used directly to evaluate the initial modulus. The value of D_A , instead, can be obtained by subtracting Eqn.(120) from Eqn.(123), at $t = t_c$ and $\theta \rightarrow 0$:

$$D_A = D(t = t_c) - D(\theta = 0, t_c) \quad (124)$$

the second term being the extrapolated value of Eqn. (120) at $\theta = 0$. The initial recoverable compliance D_A obtained in this manner is however not a property of the virgin fiber but that of the fiber after irreversible creep has occurred for time t_c under a stress σ . The ideal value of initial compliance D_A of the virgin fiber must, therefore, be obtained at a stress level σ_0 low enough to ensure linear viscoelastic behavior. For fibers that have been subjected to a stress $\sigma > \sigma_0$, we arbitrarily define an apparent initial compliance D'_A equal to the value $D(t)$ at $t = 15$ sec. This value is in general within 5% of the value D_A determined more elaborately by the infinitesimal stress method. The apparent initial modulus E'_0 is calculated as $(D'_A)^{-1}$ and is entered in the last column in Table 17.

The Andrade creep behavior of PBO is reminiscent of the behavior of BBB polymer. Indeed, the polymers have similar Andrade cube-root coefficients β_R . The initial modulus is however much higher for PBO than for BBB ($E_0 \approx 25$ gpd for the as-spun BBB fiber or film). Even at room temperature, the fiber PBO can be mechanically conditioned to attain an initial modulus of 10^2 gpd as indicated by our experiments.

8.2 Thermal-Mechanical Annealing

Extensometry at increasing temperatures has been carried out on a PBO-1201-0 fiber previously subjected to one cycle of creep and recovery at room temperature. The fiber was installed in the tensile creep apparatus with a constant load of 1 g (or a specific tensile stress of 0.055 gpd). The apparatus was evacuated and then heated from room temperature to 600°C over 7 hours. The extension of the fiber was monitored and is plotted against temperature in Figure 41. Since temperature equilibrium was not reached except at the beginning and the end of the experiment, there might be some error ($\pm 10^\circ\text{C}$) in the temperature, but the general features are not affected. For comparison, the dashed curve in the figure indicates the extension of the fiber that would have been incurred in the time required to reach temperature. Up to 130°C specimen contracted with increasing temperature due to thermal annealing. The maximum contraction is even larger than the nonrecoverable strain (ca. 0.16%) incurred in the previous creep experiment. As the temperature increased about 130°C, the effect of the load took over and the specimen extended up to 1.4% (or $\epsilon/\sigma = 0.259$ denier/g) at 530°C. Thereafter, it contracted drastically, probably due to oxidative degradation.

Another thermal mechanical measurement was made on an as-spun PBO-0429-7 fiber equilibrated at elevated temperatures. A single filament of the fiber was loaded with a 5 g weight (or $\sigma = 0.368$ gpd) in the tensile creep apparatus which was then evacuated and heated stepwise to 460°C. After equilibration at each intermediate temperature,

tensile recovery and creep measurements were performed. After the 460°C measurement, the instrument was cooled to room temperature and the cycle was repeated for a load of 10 g weight up to 350°C.

Figure 42 shows the result of the first heating cycle. The nonrecoverable strain ϵ_{NR} was measured after the recovery experiment at each temperature. Again behavior similar to that of the PB0-1201-0 fiber can be observed. The nonrecoverable extension is about 0.004% per °C below 160°C, changing to 0.012% above this point. This indicates that enhanced intermolecular mobility is achieved in fibers as-spun or mechanically conditioned at room temperature beginning at ca. 130 to 160°C. On the other hand, the initial recoverable tensile modulus E_0 decreases to a minimum at 390°C; thereafter, it increases more rapidly upon further increase of temperature under the 5 gm load. The increase in E_0 is probably due to molecular rearrangements facilitated by the enhanced mobility.

It took 25 hours to complete the first temperature cycle. In the second cycle, however, essentially no nonrecoverable strain was observed up to 350°C under a load twice as high ($\sigma = 0.76$ gpd). The specimen even underwent a slight contraction (-0.05%). Thus, it appears that well-annealed fibers do not display the enhanced mobility. The specimen so treated was drawn to a permanent extension of 4% and the initial tensile modulus was measured to a 204 gpd. These results indicate that hot-drawing at 390°C could be used in post-spinning treatment of PB0 fibers.

Similar effects were found with a PBT-62 fiber (PBT-62-63).

The fiber was held at 450°C under vacuum for 15 hr. under a tensile stress of 1 g/d. The instantaneous modulus E_0 was then determined over the temperature range from 30 to 430°. In addition, creep and recovery was studied at 30° and 400°C. The data on E_0 as a function of temperature show that E_0 is only weakly affected by temperature for the thermally annealed fiber, with $E_{APP} \equiv \partial \ln E_0 / \partial (RT)^{-1}$ equal to 300 cal/mol. The creep and recovery data on the fiber could be fitted by Eqns. 119-121 with $D_{NR}(t)$ equal to zero at both 30 and 400°C for the thermal-mechanically conditioned fiber. The time constant $\tau_A = \beta_R^{-1/3}$ for Andrade creep decreased about eight-fold over the range 30 to 400°C, being about 3.6×10^6 sec at 30°.

TABLE 17

CREEP AND RECOVERY PARAMETERS FOR
PBO FIBERS

Sample	Run	$D_{NR} (t)$ (denier/g)	D_A	D_A'	β_c (sec ^{-1/3})	β_r	E_o (gm/denier)	E_o'
PBO-0429-8	1st	0.0281	0.0107	0.0182	0.0314	0.0101	93	55
	2nd	0.0012	0.0110	0.0112	0.0080	0.0082	91	89
	3rd	0.0010	0.0106	0.0108	0.0075	0.0072	94	93
PBO-0429-7	1st	0.0066	0.0112	0.0151	0.0326	0.0277	89	66
	2nd	0.0088	0.0098	0.0124	0.0194	0.0094	102	81
PBO-1201-0	1st	0.0030	0.0120	0.0123	0.0160	0.0063	83	81

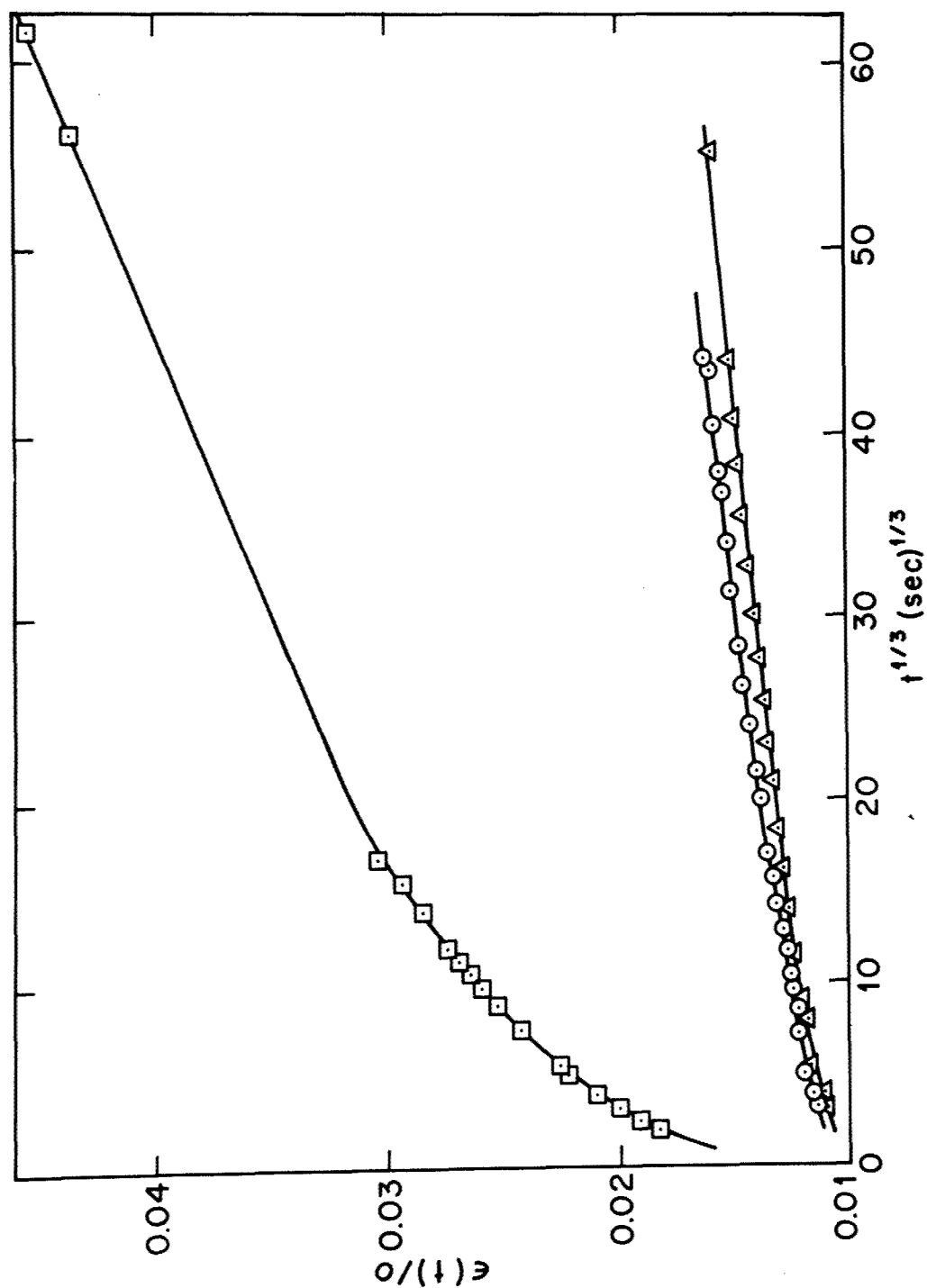


Fig. 39 Tensile creep compliance $D(t)$ versus the cube root of time $t^{1/3}$ under a stress of 0.735 gpd for PBO-0429-8 fiber at room temperature.
(a) square, (b) circle and (c) triangle refer to first, second and third loading cycles.

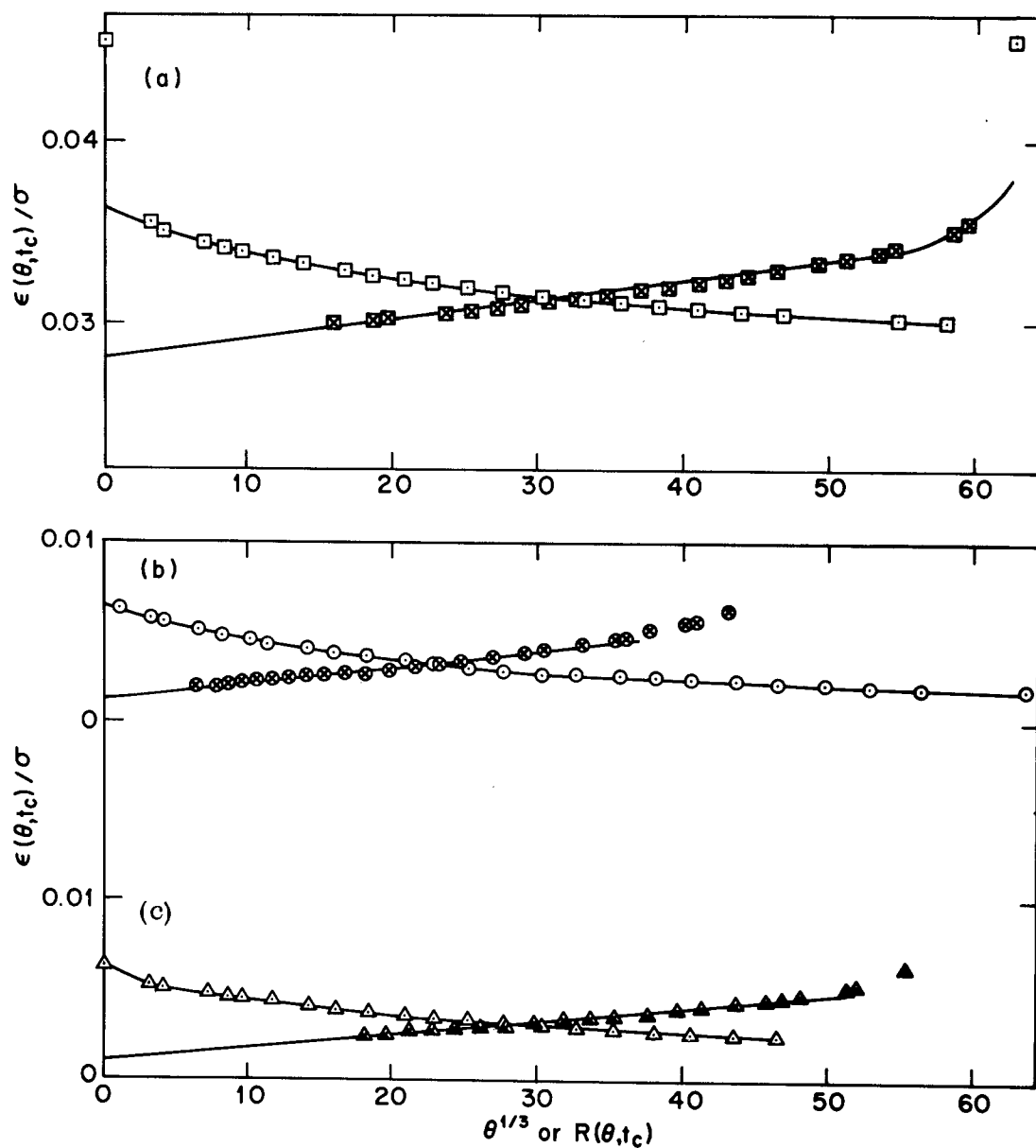


Fig. 40 Recovery compliance $D(\theta, t_c)$ versus cube root of recovery time (dotted points); and the function $R(\theta, t_c)$. (Crosses); (a) square, (b) circle and (c) triangle, refer to recovery from the first, second and third loading.

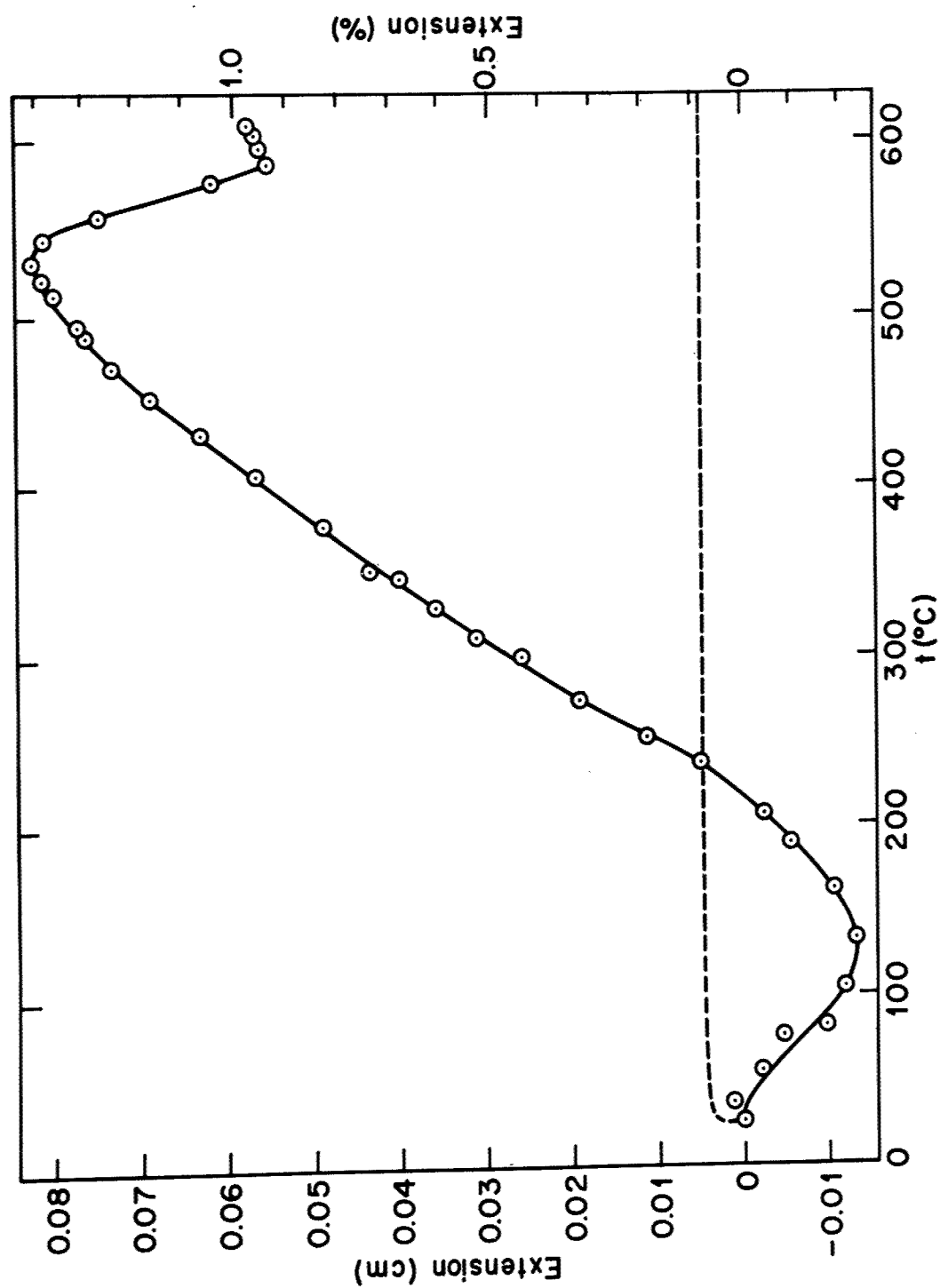


Fig. 41 Extension of PBO-2101-0 fiber under a stress of 0.055 gpd.

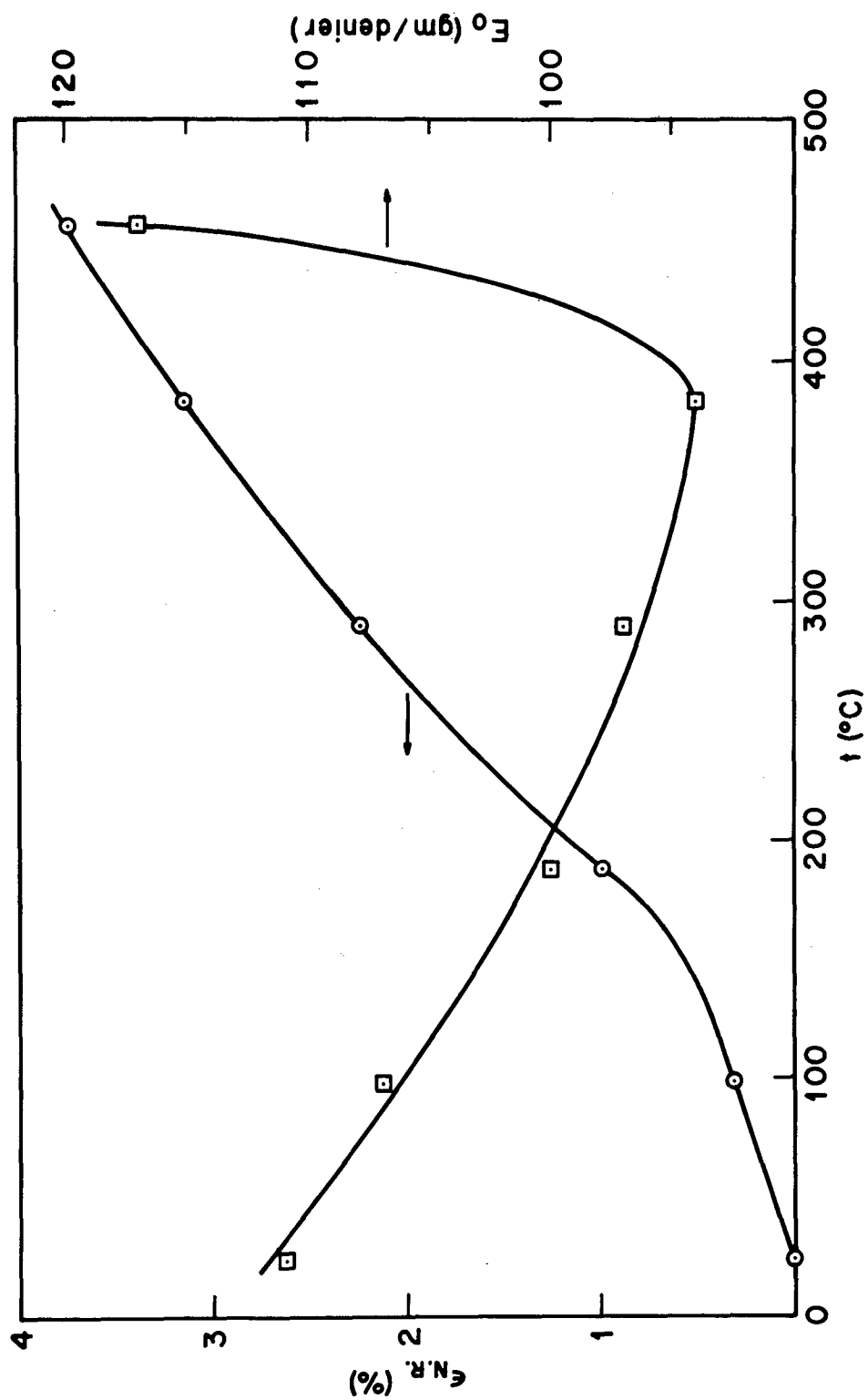


Fig. 42 Nonrecoverable strain ϵ_{NR} and initial modulus E_0 of PBO-0429-7 fiber under a stress 0.368 gpd.

9. Scale-up of Fiber Formation Process

Under subcontract arrangement, the fiber formation of PBO and PBT under larger scale operation has been investigated by the Celanese Research Company. The principal effort has involved three separate tasks:

- 1) synthesis of PBO for use at Celanese and elsewhere in the AFML program
- 2) fiber formation by solution processing of PBO prepared by Celanese
- 3) fiber formation by solution processing of PBT prepared by SRI International

The results of this work are given in detail in report prepared by the Celanese Research Company, included herein in its entirety in the Appendix. In addition, the results have been included, in part, in the preceding text, and have, of course, substantially influenced the course of the overall investigation.

In summary, the synthesis effort identified some problems with the original PBO preparation as concerned the scale-up monomer and polymer synthesis. These included the method used to reduce intermediates in the monomer synthesis, and the corrosion of reaction components in the polymerization. Problems were overcome to permit preparation of PBO at the 6 Kg batch level. Samples of this polymer were used by Celanese, and provided to other AFML designated research groups.

Although the results of the processing studies on PBO completed by Celanese have been included in part in the preceding discussion, the details of their work were not described. These details, which may be

found in the appended Celanese report, include additional scanning electron microscopy, some x-ray diffraction, and the study of coagulation bath composition. Since these results were included in the overall presentation made above, and may be found in the Appendix, we will not repeat them here in detail. In summary, the Celanese study showed:

- 1) PBO solution are difficult to process by the dry-jet wet spin method.
- 2) Homogeneous PBO solutions have not been prepared at concentrations of about 12 percent by weight.
- 3) Wet spun fibers appear to have voids created in the coagulation process.
- 4) Post fiber spinning heat treatment increases the modulus of PBO fibers. (The highest modulus achieved for PBO was 710 g/d).
- 5) The coagulation created voids limit the tenacity.

In addition to these conclusions, the Celanese workers observed that a PBO solution could be formed into a ribbon by extrusion--the preliminary process did not produce good orientation. The work on PBO fiber formation indicated the need for an apparatus capable of working with solution volume of the order 50 ml. A suitable instrument was designed and constructed.

Work at Celanese also included fiber formation of PBT obtained from SRI International. As indicated in the previous report, experience shows that PBT is easier to work with than PBO.

The Celanese study showed that

- 1) PBT solutions could be processed by the dry-jet wet spin method.

- 2) The coagulation process creates voids that diminish the overall tenacity. (The highest overall tenacity achieved was 12.3 g/d).
- 3) Post fiber spinning heat treatment increase the modulus of PBT fibers. (The highest modulus achieved was 1530 g/d).

In addition, some preliminary data showed the evolution of SO_2 from some PBT fibers heated to 200-300°C. This occurred despite the thermal-mechanical evidence that the fibers are stable at temperatures up to 400°C, as discussed in section 9 of this report. The origin magnitude and reproducibility of the SO_2 evolution should be explored further. Flammability studies by Celanese showed that both PBT and PBO are intrinsically noncombustible.

As with PBO, preliminary data were obtained on the formation of PBT ribbon by extrusion of a solution through a slit die. Reasonable results were obtained, but the overall orientation was low with the preliminary data.

10. CONCLUSIONS AND RECOMMENDATIONS

The preceding report has described the solution processing of PBO and PBT to form oriented fibers. An analytical discussion of the fiber formation process showed that dry-jet wet spinning is the preferred process, largely because it effects a separation of the orientation and coagulation steps in the formation process. Although the molecular orientation and disorientation time constants appear to be satisfactory for this two-step process with both PBO and PBT, only the latter is readily processed by the dry-jet wet spin process.

The relative difficulty of processing PBO by the dry-jet wet spin process may relate to the state of aggregation of its solution, intermolecular association being more pronounced with PBO solutions than with PBT solutions. Since PBO is less easily processed than PBT, and also appears to be no more thermally stable, or easily synthesized than PBT, it is recommended that any further effort on the formation of oriented, thermally stable polymers be directed toward PBT as opposed to PBO.

The formation of solutions of PBT into oriented fibers has resulted in fibers with high modulus (ca 1530 g/d, or 3×10^7 psi), but with an overall tenacity (ca 12 g/d or 2.3×10^5 psi) that is decreased by voids incurred during the coagulation step. Calculations show that the inherent tenacity of the flow-free fiber is about 20 g/d (or $r \times 10^5$ psi) or greater. The importance of these voids in determining fiber tenacity warrents some additional study of methods to

suppress their formation. Two methods can be suggested based on prior experience:

- 1) Decreased temperature of the coagulation bath to suppress both the disorientation time of the solution and the coagulation rate--the latter should suppress void formation.
- 2) Prepare mixtures of PBT containing high and low molecular weight components. The former will permit orientation, whereas the latter may permit higher overall concentration, thereby suppressing void formation.

The latter recommendation is based partly on the observation that increased molecular weight of PBT does not bring increased modulus or tenacity in the processed fiber, probably because it is necessary to use lower concentrations in the processing solution to obtain solution homogeneity. The latter is essential to obtain the needed high orientation in the processed material.

The results of the solution processing of PBO and PBT indicate that a film formation device discussed previously³¹ should be useful in the formation of PBT films by solution processing. It is recommended that further attention be given to the design and use of this apparatus to develop oriented PBT films. Some work along these lines is presently underway at CMU.

Additional thermal-mechanical and thermal stability data will be required on well oriented PBT materials as these become available, and these results should be evaluated in term of the AFML objectives for PBT materials.

Finally, the overall results with PBT can be considered

good--well oriented, high modulus fibers with reasonable tenacity have been prepared, and the physical properties appear to be good up to about 400°C. Nonetheless, additional work is needed to bring the solution processing to a useful level, and it is recommended that this effort be carried out.

REFERENCES

1. C. P. Wong and G. C. Berry, "Physical Properties of Complex Aromatic-Heterocyclic Polymers," Technical Report AFML-TR-71-2, Part VII, May 1977, a) p 61, b) p.37-40, c) p.66.
2. A. Ziabicki, Physical Fundamentals of the Fiber-Spinning Process, in Man-Made Fibers, edited by H. F. Mark, et al. Vol. 1, Interscience Publisher, New York (1967).
3. R. B. Bird, M. W. Johnson, Jr., and J. F. Stevenson, Proc. Fifth Int. Congress Rheology, 4, 159 (1970).
4. D. R. Paul, J. Applied Polymer Sci., 12, 2273 (1968).
5. C. D. Han, Rheological Acta, 9, No. 3, 355 (1970).
6. J. L. White and Y. Ide, Appl. Polymer Symposium, No. 27, 61 (1975).
7. A. Ziabicki, R. Takserman-Krozer, (a) Roczniki Chemii, Ann. Soc. Chim. Polonorum, 37, 1503 (1963); (b) 37, 1607 (1963); (3) 38, 465 (1964); (d) Kolloid-Z Polymere, 198, 60 (1964).
8. C. Z. Weber, angew Math. Mech. 11, 136 (1931).
9. S. Tomotika, Proc. Roy. Soc. (London) A 150, 322 (1935).
10. G. C. Berry and C.-P. Wong, J. Polymer Sci., Polymer Phys. Ed., 13, 1761 (1975).
11. W. W. Graessley, Adv. Polymer Sci., 16, 1 (1974).
12. G. C. Berry, B. L. Hager and C.-P. Wong, Macromolecules, 10, 361 (1977).
13. C.-P. Wong, H. Ohnuma and G. C. Berry, J. Polymer Sci., Symp. No. 65, 173 (1978).
14. C.-P. Wong and G. C. Berry, Polymer, 20, 229 (1979).
15. M. Doi and S. F. Edwards, J. Chem. Soc., Farad Trans. II, 74, 560 (1978).
16. M. Doi and S. F. Edwards, J. Chem. Soc., Farad Trans. II, 74, 918 (1978).
17. R. B. Bird, R. C. Armstrong and O. Hassager, "Dynamics of Polymeric Liquids," Vol. 1, John Wiley & Sons, N. Y. 1976, p. 81.
18. H. Brenner, Chem. Eng. Sci., 27, 1069 (1972).

19. H. Brenner, *Int. J. Multiphase Flow*, 1, No. 2, 195 (1974).
20. H. Brenner and D. W. Condiff, *J. Coll. Interface Sci.*, 47, 199 (1974).
21. F. Perrin, *J. Phys. Radium*, [7], 1 (1936).
22. S. Broersma, *J. Chem. Phy.* 32, No. 6, 1626 (1960).
23. H. Yamakawa and J. Yamaki, *J. Chem. Phy.*, 58, No. 5, 2049 (1973).
24. B. D. Coleman and H. Markovitz, *J. Appl. Phys.*, 35, 1 (1964).
25. J. C. Hyun and R. L. Ballman, *J. Rheology*, 22, 369 (1978).
26. G. Marrucci and A. Ciferri, *J. Polymer Sci., Polymer Letters*, 15, 643 (1977).
27. J. Maxwell, *Proc. Royal Soc.* A22, 46 (1873).
28. B. H. Zimm, *Rev. Scientific Instr.*, 29, 360 (1958).
29. A. J. Rosenthal, *Texile Res. J.*, 36, No. 7, 593 (1966).
30. W. B. Black, J. Preston et al. *J. Macromol. Sci. Chem.* A7 (1) 137 (1973).
31. G. C. Berry and C.-P. Wong, "Physical Properties of Complex Aromatic-Heterocyclic Polymers," Part VI, October 1976, p. 48.

Appendix I

COMMENTS ON THE USE OF EQUATION 7

A few words should be said about the approximation of Eqn. (1) with Eqn. (7). In this approximation, we have neglected the term F_{grav} which has a time average value ranging from 0.064 to 0.072 dynes. The term F_{rheo} ranging from 0.31 to 0.38 dynes is retained in the equation. A closer look at their initial values shows the opposite. According to Eqn. (22)

$$\bar{\kappa}_0 \approx 2V_0 \gamma / b \quad (\text{I-1})$$

and the initial contribution of F_{rheo} is

$$F_{\text{rheo}}^0 = 2Q \bar{\eta} \gamma / b \quad (\text{I-2})$$

the value of which ranges from 0.018 to 0.027. On the other hand the initial value of F_{grav} is given by

$$F_{\text{grav}}^0 = g\rho Q(t_1 - t_0) \quad (\text{I-3})$$

the value of which ranges from 0.13 to 0.14 dynes. Therefore a closer approximation to Eqn. (1) should instead be

$$F = A\bar{\eta}\bar{\kappa} + 2\pi\Omega R - g\rho Q(t_1 - t) \quad (\text{I-4})$$

This equation can be solved to yield an implicit function of

t for R:

$$q_1 \ell n \frac{u - q_1}{u_0 - q_1} + q_2 \ell n \frac{u - q_2}{u_0 - q_2} = - \ell n \frac{R}{R_0} \quad (I-5)$$

where

$$u_0 = [F + g\rho Q(t_1 - t_0) - 2\pi\alpha R_0]/2\pi\alpha R_0 \quad (I-6)$$

$$u = [F + g\rho Q(t_1 - t) - 2\pi\alpha R]/2\pi\alpha R \quad (I-7)$$

$$q_1 = [1 + \sqrt{2g\rho Q\eta/\pi\alpha^2}] / 2 \quad (I-8)$$

and

$$q_2 = [1 - \sqrt{2g\rho Q\eta/\pi\alpha^2}] / 2 \quad (I-9)$$

Interpretation of this function is complicated as the value of F is yet to be determined.

However, in the initial stage of the jet ($t \approx t_0$), the rheological contribution can be neglected and Eqn. (I-4) solved to yield

$$R = R_0 - \frac{g\rho Q}{2\pi\alpha} t \quad (I-10)$$

The initial elongation rate is given by Eqn. (8)

$$\bar{\chi}_0 = \frac{g\rho Q}{\pi\alpha R_0} \approx 0.7 \text{ sec}^{-1}$$

twice the value given by Eqn. (I-1). This initial gravitational effect, however, decreases rapidly as the elongation rate increases exponentially according to Eqn. (10). We can approximate Eqn. (I-4) stepwise: firstly with Eqn. (I-10) up to a time t_g , and then with Eqn. (7) by considering t_g, R_g, V_g, X_g , as its t_0, R_0, V_0 and X_0 .

Appendix II

USE OF EQUATION 7 WITH A 'POWER LAW FLUID'

In case of $\beta \ll 1$, Eqn. (7) is reduced to

$$F = A \bar{\eta} \bar{\kappa} \quad (\text{II-1})$$

This equation can be solved explicitly for a fluid obeying the power law

$$\bar{\eta} = \bar{\eta}_0 (\bar{\kappa}/\bar{\kappa}_0)^m \quad (\text{II-2})$$

where m is the power which makes $\bar{\eta} = \text{constant}$ at $m \rightarrow 0$ and $\bar{\kappa} = \text{constant}$ at $m \rightarrow \infty$. Solution to Eqn. (II-1) are listed in Table 3 for the general m and particular $m = 0, \infty$ and 0.2 .

Table 18

Equations for Power-law Fluid with Constant Tension

General Case		Special Cases	
	(a)	(b)	(c)
Power-law fluid	$\bar{\eta} = \bar{\eta}_0 (\bar{x}/\bar{x}_0)^m$	$m = 0$	$m = 0.20$
Equation of Force-Balance	$F = \bar{\eta} \bar{x} A$	constant $\bar{x} = \bar{x}_0$	This may be a realistic case for dumbbell, $0.1 \leq \bar{x} \leq 2$
Equation of steady-state	$Q = AV$	$\xi = \frac{1}{\bar{x}_1} \left(\frac{A_0}{A_1} - 1 \right) = b$	$\xi = \frac{6}{\bar{x}_1} \left[\left(\frac{A_0}{A_1} \right)^{1/6} - 1 \right]$
Parameters	$\xi = \frac{1}{\bar{x}_1} \cdot \left(\frac{m+1}{m} \right) \left[\left(\frac{A_0}{A_1} \right)^{m/(m+1)} - 1 \right]$	$Re = \frac{A_0}{\eta_0} \frac{\bar{x}_0}{A_1}$	$b = \frac{1}{6} \xi$
	$b = \frac{1}{\bar{x}_1} \left[\left(\frac{A_0}{A_1} \right)^{m/(m+1)} - 1 \right] = \frac{m}{m+1} \xi$		
Viscosity profile	$\bar{\eta} = \bar{\eta}_0 (1 + \frac{m}{m+1} \xi x) = \bar{\eta}_0 (1 + bx)$	$\bar{\eta} = \bar{\eta}_0 (1 + \xi x)$	$\bar{\eta} = \bar{\eta}_0 (1 + \frac{1}{6} \xi x)$
Streaming profile	$A = A_0 (1 + bx)^{-(m+1)/m}$	$A = A_0 / (1 + bx)$	$A = A_0 (1 + bx)^{-6}$
Velocity profile	$V = V_0 (1 + bx)^{(m+1)/m}$	$V = V_0 (1 + bx)$	$V = V_0 (1 + bx)^6$
Elongation rate	$\bar{x} = \bar{x}_0 (1 + bx)^{1/m}$	$\bar{x} = \bar{x}_0$	$\bar{x} = \bar{x}_0 (1 + bx)^5$
Initial Elongation rate	$\bar{x}_0 = V_0 \xi = \frac{m+1}{m} \cdot \frac{V_0}{\bar{x}_1} \left[\left(\frac{A_0}{A_1} \right)^{m/(m+1)} - 1 \right]$	$\bar{x}_0 = \xi V_0 = b V_0$	$\bar{x}_0 = V_0 \xi$
External Force	$F = Q \bar{\eta}_0 \xi$	$F = Q \bar{\eta}_0 \xi = Q \bar{\eta}_0 b$	$F = Q \bar{\eta}_0 \xi$
Residence time	$t_1 = (1+m) \left[\frac{1}{\bar{x}_0} - \frac{1}{\bar{x}_1} \right] = (1+m) \cdot \frac{1}{\xi Q} \left[A_0 - (1+bx_1) A_1 \right] = (1 - \frac{A_1}{A_0}) / \bar{x}_0$	$t_1 = Re / \bar{x}_0$	$t_1 = 1.2 \left(\frac{1}{\bar{x}_0} - \frac{1}{\bar{x}_1} \right) = \frac{1.2}{\xi Q} (A_0 - (1 + bx) A_1)$
Travelling distance	$x = \frac{1}{b} \left[\left(1 - \frac{1}{1+m} \bar{x}_0 t \right)^{-m} - 1 \right]$	$x = \frac{1}{b} \left[e^{-\bar{x}_0 t} - 1 \right]$	$x = \frac{1}{b} \left[(1 - 0.85 \bar{x}_0 t)^{-0.2} - 1 \right]$
Travelling area	$A = A_0 \left[1 - \frac{1}{1+m} \bar{x}_0 t \right]^{-(m+1)}$	$A = A_0 e^{-\bar{x}_0 t}$	$A = A_0 (1 - 0.85 \bar{x}_0 t)^{1.2}$
Travelling velocity	$V = V_0 \left[1 - \frac{1}{1+m} \bar{x}_0 t \right]^{-(m+1)}$	$V = V_0 e^{-\bar{x}_0 t}$	$V = V_0 (1 - 0.85 \bar{x}_0 t)^{-1.2}$
Travelling along rate	$\bar{x} = \bar{x}_0 \left[1 - \frac{1}{1+m} \bar{x}_0 t \right]^{-1}$	$\bar{x} = \bar{x}_0$	$\bar{x} = \bar{x}_0 / (1 - 0.85 \bar{x}_0 t)$
Travelling viscosity	$\bar{\eta} = \bar{\eta}_0 \left[1 - \frac{1}{1+m} \bar{x}_0 t \right]^m$	$\bar{\eta} = \bar{\eta}_0 e^{-\bar{x}_0 t}$	$\bar{\eta} = \bar{\eta}_0 (1 - 0.85 \bar{x}_0 t)^{-0.2}$

Appendix III

SYNTHESIS AND PROCESSING OF ROD-LIKE AROMATIC HETEROCYCLIC POLYMERS: PARA-PHENYLENE-POLYBENZBISOXAZOLES AND PARA-PHENYLENE-POLYBENZBISTHIAZOLES. A REPORT FROM THE CELANESE RESEARCH COMPANY.

The following is a report in its entirety submitted to CMU by the Celanese Research Laboratory as required by subcontract with CMU on AF Contract No. F33615-76-C-5165. The results of this study are also to be found in the text of the CMU report.

SYNTHESIS AND PROCESSING OF RODLIKE
AROMATIC HETEROCYCLIC POLYMERS:
PARA-PHENYLENE-POLYBENZOBIS-
OXAZOLES AND PARA-PHENYLENE-POLYBENZOBIS-
THIAZOLES

CELANESE RESEARCH COMPANY
SUMMIT, NEW JERSEY 07901

MAY 1979

Final Report for Period April 1977-April 1979

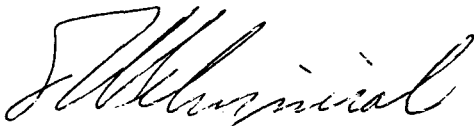
AIR FORCE MATERIALS LABORATORY
AIR FORCE WRIGHT AERONAUTICAL LABORATORIES
AIR FORCE SYSTEMS COMMAND
WRIGHT-PATTERSON AIR FORCE BASE, OHIO 45433

NOTICE

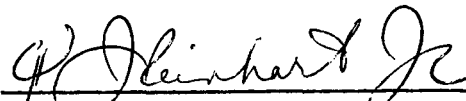
When Government drawings, specifications, or other data are used for any purpose other than in connection with a definitely related Government procurement operation, the United States Government thereby incurs no responsibility nor any obligation whatsoever; and the fact that the Government may have formulated, furnished, or in any way supplied the said drawings, specifications, or other data, is not to be regarded by implication or otherwise as in any manner licensing the holder or any other person or corporation, or conveying any rights or permission to manufacture, use, or sell any patented invention that may in any way be related thereto.

This report has been reviewed by the Information Office (OI) and is releasable to the National Technical Information Service (NTIS). At NTIS, it will be available to the general public, including foreign nations.

This technical report has been reviewed and is approved for publication.



Dr. T. Helminiak
Project Scientist



T. J. REINHART, JR., Chief
Composites, Adhesives & Fibrous Matls Br
Nonmetallic Materials Division

J. M. Kelble, Chief
Nonmetallic Materials Division

REPORT DOCUMENTATION PAGE		READ INSTRUCTIONS BEFORE COMPLETING FORM
1. REPORT NUMBER AFML-TR	2. GOVT ACCESSION NO.	3. RECIPIENT'S CATALOG NUMBER
4. TITLE (and Subtitle) Synthesis and Processing of Rod-like Aromatic Heterocyclic Polymers: Para-Phenylene-Polybenzobisoxazoles and Para-Phenylene-Polybenzobisthiazoles		5. TYPE OF REPORT & PERIOD COVERED Final Technical Report April 1977-April 1979
7. AUTHOR(s) Dr. E. W. Choe Dr. S. N. Kim		6. PERFORMING ORG. REPORT NUMBER
9. PERFORMING ORGANIZATION NAME AND ADDRESS Celanese Research Company 86 Morris Avenue Summit, New Jersey 07901		8. CONTRACT OR GRANT NUMBER(s)
11. CONTROLLING OFFICE NAME AND ADDRESS		10. PROGRAM ELEMENT, PROJECT, TASK AREA & WORK UNIT NUMBERS
14. MONITORING AGENCY NAME & ADDRESS (If different from Controlling Office)		12. REPORT DATE June 1979
		13. NUMBER OF PAGES
		15. SECURITY CLASS. (of this report) Unclassified
		15a. DECLASSIFICATION/DOWNGRADING SCHEDULE
16. DISTRIBUTION STATEMENT (of this Report) Approved for public release; distribution unlimited.		
17. DISTRIBUTION STATEMENT (of the abstract entered in Block 20, if different from Report)		
18. SUPPLEMENTARY NOTES		
19. KEY WORDS (Continue on reverse side if necessary and identify by block number) Para-ordered Polymers High Modulus Fibers and Films Polybenzobisoxazoles Polybenzobisthiazoles		
20. ABSTRACT (Continue on reverse side if necessary and identify by block number) The synthesis of poly-(para-phenylenebenzobisoxazoles) (PBO) and the processing of poly-(para-phenylenebenzobisthiazole) (PBT) and PBO into high modulus organic fibers and films are described. The monomer, 4,6-diaminoresorcinol was polymerized with terephthaloyl dichloride in polyphosphoric acid at 90 to 210°C to attain fibrillar poly-(p-phenylenebenzobisoxazole). PBO and PBT in methanesulfonic acid with a small amount of chlorosulfonic acid were spun into high modulus fibers and films.		

DD FORM 1 JAN 73 1473

UNCLASSIFIED

SECURITY CLASSIFICATION OF THIS PAGE (When Data Entered)

FOREWORD

This report was prepared by the Celanese Research Company, 86 Morris Avenue, Summit, New Jersey 07901, under a subcontract to Contract No. F33615-77-C-5061, "Solution Processing - Rodlike Polymers", granted by Carnegie-Mellon University. It was administered by the Air Force Materials Laboratory, Air Force Systems Command, Wright-Patterson Air Force Base, Ohio, with Dr. Thaddeus Helminiak (MBC) as Project Scientist, and Carnegie-Mellon University with Dr. Guy Berry, subcontract monitor.

The work described in this report was conducted by Drs. E. W. Choe, Project Leader and S. N. Kim. Dr. Joseph R. Leal, served as Contract Administrator. Appreciation is expressed to Dr. Ronald DeMartino for assistance in polymerization; Mrs. Ana Bercovici for spinning; Dr. Ian Hay for x-ray analysis.

This technical report covers the work conducted from April 1977 to April 1979.

TABLE OF CONTENTS

SECTION	Page
I. INTRODUCTION	178
II. RESULTS AND DISCUSSION	179
A. Synthesis of Monomers and Intermediates.....	179
B. Rodlike Polymer Preparation.....	191
1. Poly-(p-phenylenebenzobisoxazole) from 4,6-Diaminoresorcinol and Terephthalic Acid	191
2. Poly-(p-phenylenebenzobisoxazole) from 4,6-Diaminoresorcinol and Terephthaloyldichloride	203
C. Fabrication of Rodlike Polymers	213
1. PBO Fabrication	213
a. Dope Preparation and Characterization..	213
b. Fabrication and Properties of PBO Fiber	215
c. Fabrication and Properties of Film.....	219
2. PBT Fabrication	237
a. Dope Preparation and Characterization..	237
b. Fabrication and Properties of PBT Fibers	237
c. Fabrication and Properties of PBT Film	240
III. EXPERIMENTAL SECTION.....	255
IV. CONCLUSIONS AND RECOMMENDATIONS	264
REFERENCES	271

LIST OF ILLUSTRATIONS

<u>Figure</u>	<u>Title</u>	<u>Page</u>
1	C^{13} MR Spectrum of Resorcinol Diacetate.....	186
2	Temperature and Time vs. Yield of 4,6-Dinitroresorcinol.....	187
3	C^{13} NMR of 4,6-Dinitroresorcinol in DMF and DMF-d7.....	188
4	C^{13} NMR Spectrum of 2,4,6-Trinitroresorcinol in DMSO-d6.....	189
5	C^{13} MR Spectrum of 4,6-Diaminoresorcinol Dihydrochloride in water, external DMSO-d6 Lock.....	190
6A	TGA in N_2 For PBO Polymer 25613-37 Prep'd from Terephthalic Acid.....	195
6B	TGA in N_2 for PBO Polymer 26273-9A prep'd from Terephthaloyl Dichloride.....	196
7A	TGA in Air for BPO Polymer 25613-37 Prep'd from Terephthalic Acid.....	197
7B	TGA in Air for PBO Polymer 26273-9A Prep'd from Terephthaloyl Dichloride.....	198
8	Spiral Stirrer.....	200
9	PBO Polymerization Apparatus.....	202
10	FTIR Spectra of PBO.....	209
11	FTIR Spectra of PBO.....	210
12	SEM Micrograph of PBO Polymer 26273-9 Prep'd from Terephthaloyl Dichloride.....	211-212
13	Critical Concentration Curve for PBO.....	226
14	X-RAY Diffraction Pattern for PBO Ppt'd from 100% H_2SO_4	227

LIST OF ILLUSTRATIONS Cont'd.

<u>Figure</u>	<u>Title</u>	<u>Page</u>
15	X-Ray Diffraction Pattern-11% PBO in 100% H ₂ SO ₄	228
16	X-Ray Diffraction Pattern-11% PBO Dope in Methanesulfonic Acid.....	228
17	Sem Micrographs of PBO Fibers.....	229-233
18	X-Ray Diffraction Pattern of Wet Spun PBO Fibers.....	234
19	Tenacity and Modulus vs. Polymer I.V.....	235
20	Fiber Properties vs. Spin Draw Ratio.....	236
21	Schematic Diagram of PBT Spinning Apparatus.	250
22	As-Spun PBT Fiber Properties vs. Spin Draw..	251
23	Effect of Heat Treatment on PBT Fiber Tenacity.....	252
24	Effect of Heat Treatment on PBT Fiber Modulus.....	253
25	Effect of Gauge Length on PBT Fiber Tenacity.....	254
26	Schematic Diagram of PBO Spinning Apparatus.	263

LIST OF TABLES

<u>Table</u>	<u>Title</u>	<u>Page</u>
I	Nitration of Resorcinol Diacetate.....	183
II	Temperature and Time vs. Dinitro- & Trinitroresorcinol.....	184
III	Preparation of 4,6-Diaminoresorcinol Dihydrochloride.....	185
IV	PBO Polymers.....	193
V	Elemental Analysis.....	194
VI	PBO Polymers form Terephthalic Acid and 4,6-Diaminoresorcinol.....	201
VII	PBO Polymers from Terephthaloyl Dichloride and 4,6-Diaminoresorcinol.....	207
VIII	Polymerization Time and Temperatures vs. PBO I.V.....	208
IX	PBO Polymer Supply.....	221
X	Principle Spacings of PBO.....	222
XIA	Spinning Conditions.....	223
XIB	PBO Fiber Properties as Wet-Spun.....	224
XII	Heat Treatment of PBO Fibers.....	225
XIII	PBT Polymer Supply.....	242
XIVA	Spinning Conditions.....	243
XIVB	PBT Fiber Properties as Dry Jet--Wet Spun..	244
XV	Properties of Heat-Treated PBT Fibers.....	245
XVI	Properties of Heat-Treated PBT Fibers.....	246
XVII	Gauge Length vs. PBT Fiber Properties.....	247

LIST OF TABLES Cont'd.

<u>Table</u>	<u>Title</u>	Page
XVIII	Fiber Flammability--Critical Oxygen Concentration.....	248
XIX	PBT Ribbon Properties.....	249

LIST OF APPENDICES

<u>Appendix</u>	<u>Title</u>	<u>Page</u>
1	Major Component Safety Data Statement	272
2	List of PBT Samples Forwarded to University of Massachusetts	273
3	Orientation in PBO Samples	274
4	Structure of PBO Films	275

SECTION I

INTRODUCTION

This report covers work carried out in support of the Air Force effort on the synthesis and solution processing of the high molecular weight rodlike polymer, poly-(para-phenylenebenzobisoxazole) (PBO) and poly-(para-phenylenebenzobisthiazole) (PBT). These polymers are characterized by a high degree of molecular order and fabricated shaped items of high strength and modulus⁽¹⁾.

This work encompassed an improvement in the polymerization of linear high molecular weight poly-(para-phenylenebenzobisoxazole), and the synthesis of its intermediates and monomers. The preparation and characterization of spinning dopes of PBO and poly-(p-phenylenebenzobisthiazole) was accomplished along with conversion into fibers and films. The PBO and PBT fibers exhibited fiber properties of 4.8 g/d tenacity, 0.7% elongation, 711 g/d modulus, and 12.3 g/d tenacity, 0.9% elongation, and 1527 g/d modulus, respectively.

SECTION II

RESULTS AND DISCUSSION

A. Synthesis of Monomers and Intermediates

The initial procedures for the preparation of 4,6-diaminoresorcinol monomer and intermediates were provided by the Air Force Materials Laboratory (2). The monomer was prepared by nitration of resorcinol diacetate to dinitroresorcinol which was subsequently reduced to the monomer. Because poor yields of dinitroresorcinol and excessively long catalytic reduction periods were experienced, the initial procedures were modified to improve the yields and efficiency. Resorcinol diacetate was prepared in a quantitative yield in a 20 gallon glass-lined distillation reactor by heating resorcinol and acetic anhydride at 118-145° for 6.5 hours with a small amount of sodium acetate as a catalyst. The product was collected by distillation through a 6m x 0.125m tower or through a Nester/Faust spinning band column (0.9m x 10mm) with a monel spinning band. Two batches of resorcinol diacetate totaling 66 kg (145 lbs) were prepared in the pilot plant. The C¹³MR spectrum of resorcinol diacetate is shown in Figure 1.

The nitration of resorcinol diacetate was carried out at 10°C with a 1:1 mixture of fuming and concentrated nitric acids, according to the AFML procedure,

to accumulate about 2kg of 4,6-dinitroresorcinol in 12 batches (500 g. scale). An overall yield of 33% of the desired 4,6-dinitroresorcinol was obtained. The results are summarized in Table I. A by-product was isolated and identified as 2,4,6-trinitroresorcinol.

The 2,4,6-trinitroresorcinol, commonly known as styphnic acid, explodes on rapid heating to decomposition with the evolution of oxides of nitrogen. A derivative of styphnic acid, lead styphnate, explodes at 260-310°C and is used as a primer in explosives. A major component safety data statement obtained from the Army for trinitroresorcinol is attached as Appendix I. Extreme caution should be taken during the nitration step in controlling the reaction temperature.

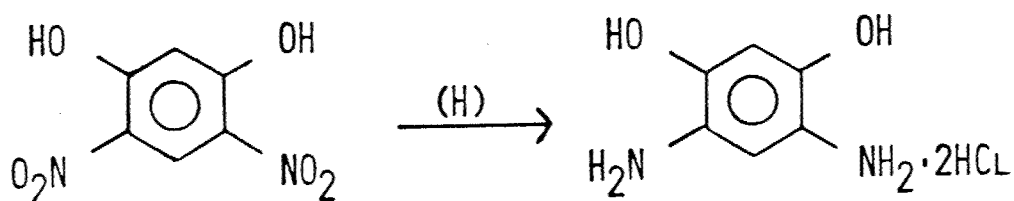
A study of the effect of reaction temperature and time on the yield of 4,6-dinitroresorcinol during the nitration of resorcinol diacetate was undertaken in the hope of increasing the yield. The results showed that a significant improvement in the yield of 4,6-dinitroresorcinol from 30% to 52% is possible and that the reaction time can be shortened to one hour from 24 hours.

A series of nitration reactions was run at four temperatures: 0°, 15°, 25°, and 35°C, and for various reaction periods ranging from one hour to 24 hours. The results, summarized in Table II, indicate that the formation of

the desired 4,6-dinitroresorcinol is favored at 25°C. Under these conditions, an approximately 50% yield is obtained. The nitration is essentially complete within one hour at 25°C, and prolonged reaction period does not alter the ratio of dinitro- to trinitroresorcinol. At temperatures greater than 35°C, the nitration reaction became somewhat difficult to control.

A graphical representation of the effect of temperature and time on the yield of 4,6-dinitroresorcinol during the nitration of resorcinol diacetate is shown in Figure 2. The C^{13} MR spectra of 4,6-dinitroresorcinol and 2,4,6-trinitroresorcinol are shown in Figures 3 and 4, respectively. Seven moderate size (500 g) nitration reactions were carried out under the best conditions (25°C, 2½ hours), identified from the above study, to prepare about 1.4 kg of 4,6-dinitroresorcinol.

The small scale reduction of 4,6-dinitroresorcinol to the 4,6-diaminoresorcinol monomer in a Parr Hydrogenator according to the AFML procedure proceeded well at 345 kPa (50 psi) hydrogen and 25°C over a 26 hour period to provide a 72-77% yield. However, when the catalytic hydrogenation was scaled-up and carried out in a 10 gallon glass-lined pressure reactor, the hydrogenation took 7 days at 345-550 kPa (50-80 psi) hydrogen over 10% palladium/charcoal. Two pilot plant batches were run by this method.



Since the catalytic hydrogenation of 4,6-dinitroresorcinol required an exceptionally long reaction time, other reduction methods were investigated in order to improve and speed up the productivity of the monomer. Significant improvements in the yield and the reaction time were made by reducing the 4,6-dinitroresorcinol with tin and hydrochloric acid at 80-90°C. The reduction was complete after about 3 hours. Three batches of 4,6-diaminoresorcinol were prepared in the laboratory by this process. The C^{13}MR analysis (Figure 5) showed that this sample is identical with that prepared previously by the catalytic hydrogenation. The fast rate of reduction is attributed to the increased solubility of 4,6-dinitroresorcinol in hydrochloric acid solution at elevated temperature.

Approximately 1 kg of the monomer was prepared in the pilot plant by this process. After the purification and characterization of the monomer, it was polymerized to PBO. The results are summarized in Table III.

TABLE I

NITRATION OF RESORCINOL DIACETATE

<u>EXPERIMENT NUMBER</u>	<u>REACTION CONDITIONS</u>		<u>DINITRO-</u>		<u>M.P. (°C)</u>
	<u>T°C</u>	<u>HOURS</u>	<u>WT. (g)</u>	<u>YIELD* (%)</u>	
25613-18	10-15	24	23	25	223-226
25613-19B 11 Batches	10-15	24	1667	33	221-225
25613-43 7 Batches	25	2½	1347	42	211-214

* After recrystallization.

Analysis: DSC, PMR, C¹³MR, IR

TABLE II

TEMPERATURE AND TIME VS. DINITRO- & TRINITRORESORCINOL

<u>EXPERIMENT NUMBER</u>	<u>T°C</u>	<u>HOURS</u>	<u>DINITRO YIELD* (%)</u>	<u>M.P. (°C)</u>	<u>TRINITRO YIELD (%)</u>	<u>RATIO DI/TRI</u>
25613-48-1	0	1	3.8	215-224		
-2	0	2	7.2	215-224		
-3	0	3	10.4	215-224		
-4	0	4	18.5			
-5	0	5	21.8			
25613-48-6	15	4	33.7	215-222		
-7	15	5	42.7	210-215	35.97	1.18
-8	15	6	33.7	218-224	61.87	0.54
-9	15	7	34.2	217-224	49.49	0.69
-10	15	24	33.8	223-226	10.80	
25613-48-11	25	1	52.3	212-223	33.65	1.55
-12	25	2	49.17	213-223	31.34	1.56
-13	25	4	48.96	218-223	31.78	1.54
-14	25	7	47.2		30.98	1.52
-15	35	1	44.6		30.98	1.34

* Before Recrystallization

TABLE III

PREPARATION OF 4,6-DIAMINORESORCINOL DIHYDROCHLORIDE

<u>EXPERIMENT NUMBER</u>	<u>METHOD</u>	<u>YIELD %</u>		
25613-20B	A (Lab)			
25613-20C	A (Lab)			
25779-1 ^e	A (Pilot Plant)			
25779-8	A (Pilot Plant)			
25613-44 ^e	B (Lab)	81.4 ^a		66.1 ^c
" -45	B (Lab)	87.6 ^a	79.3 ^b	68.8 ^c
" -46	B (Lab)	87.6 ^a	(497.4g)	64.7 ^c
25779-36	B (Pilot Plant)	97.5 ^a	(571.4g) ^a	74.6 ^b (380g)
" -37	B (Pilot Plant)		(261.2g) ^a	83.5 ^b (426g)
" -38	B (Pilot Plant)		(-261.2g)	76.5 ^b (195g)

^aCrude, ^bAfter first recrystallization, ^cAfter second crystallization, ^eC¹³ MR and H¹ NMR chemical shifts are identical.

Method A: Lab; Parr Hydrogenator,
50 psi H₂, Pd/C, 25°C, 26 hours, shaking
Pilot Plant; 10 gals. glass-lined pressure reactor
50-80 psi H₂, Pd/C, 7 days, 55 RPM agitation

Method B: Lab; Sn, HCl, 90-100°C, 2.5 hours
Pilot Plant; 20 gals. glass-lined reactor
80-90°C, 3-1/2 hours

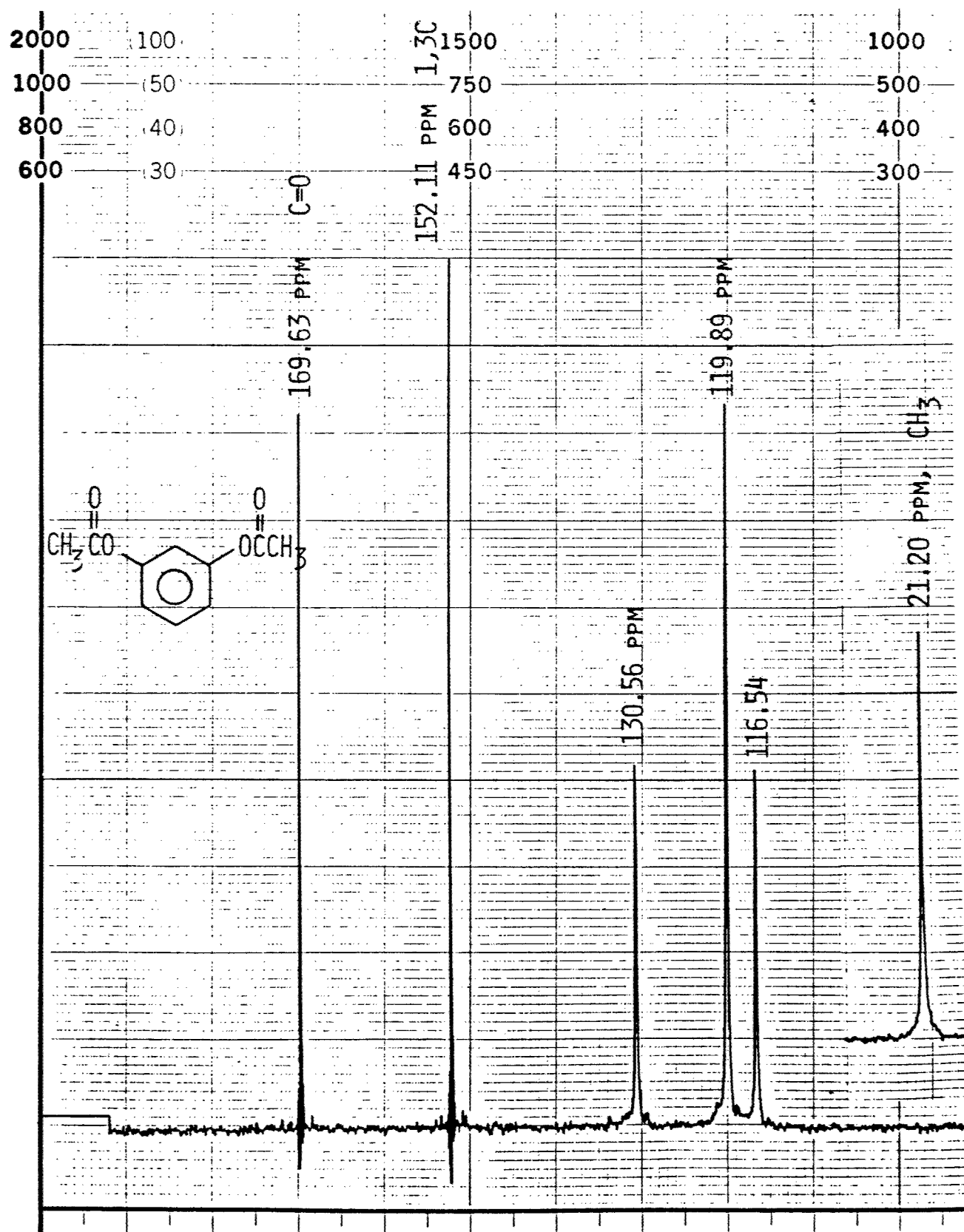


FIGURE 1. ^{13}C MR SPECTRUM OF RESORCINOL DIACETATE

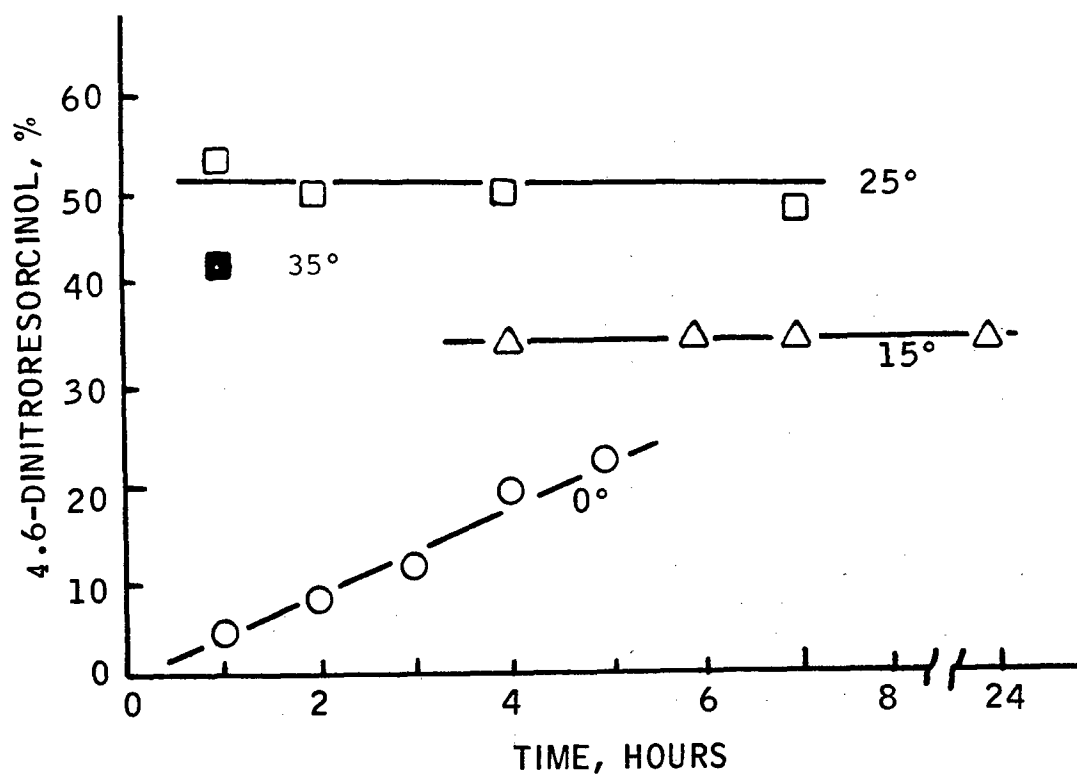


FIGURE 2. TEMPERATURE AND TIME VS. YIELD OF 4,6-DINITRORESORCINOL

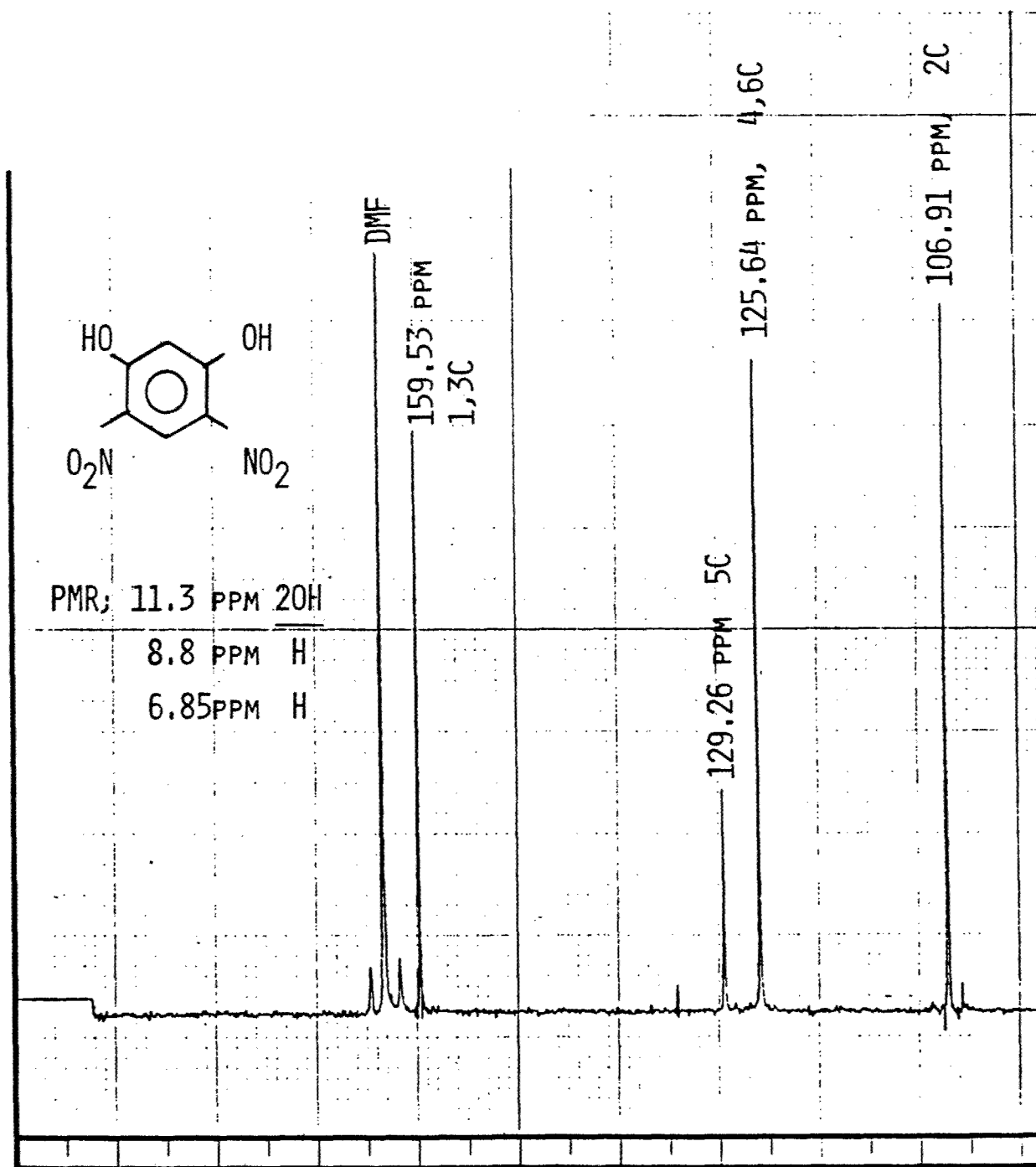


FIGURE 3. ^{13}C NMR OF 4,6-DINITRORESORCINOL IN DMF AND DMF- D_7

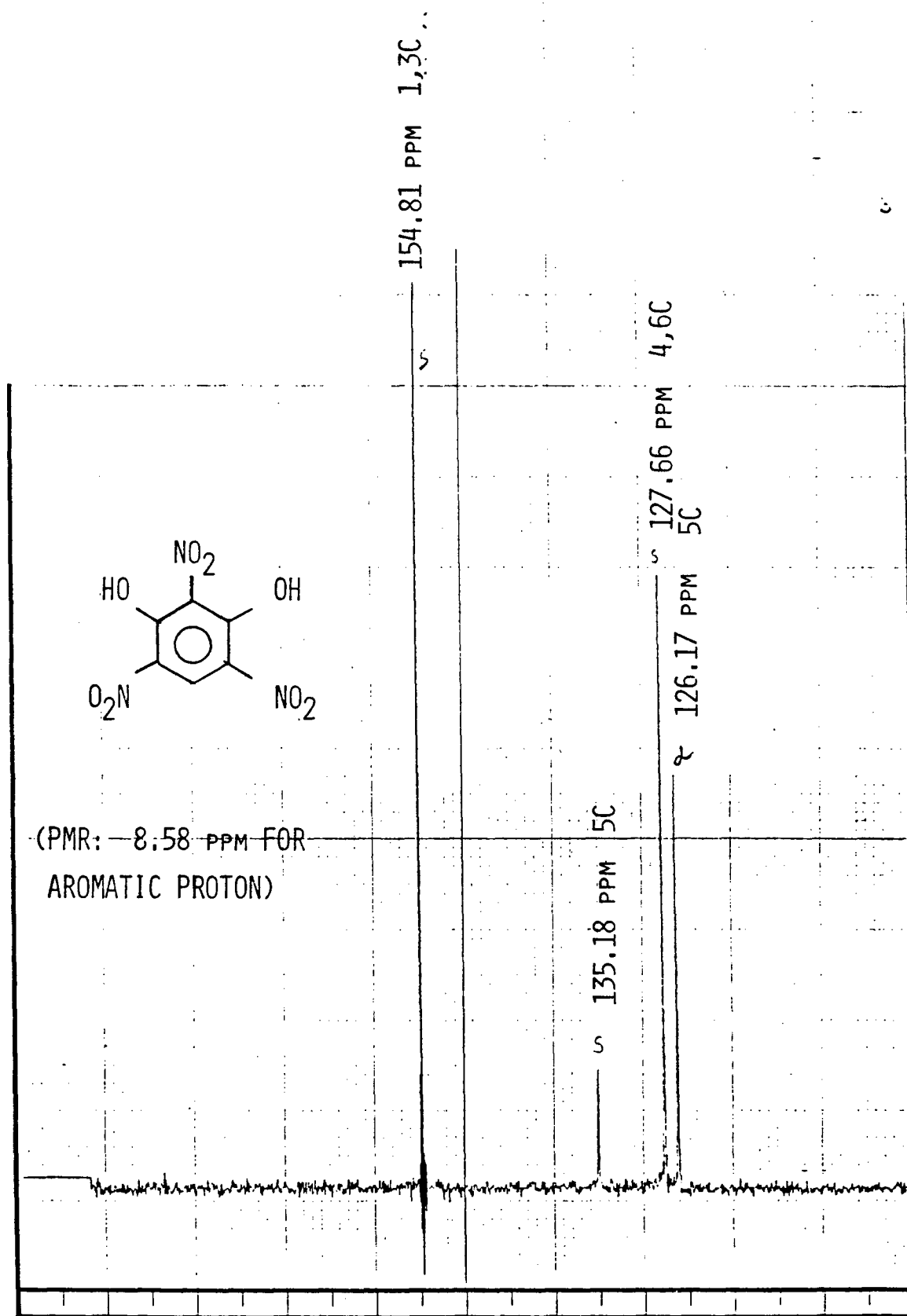


FIGURE 4. ^{13}C NMR SPECTRUM OF 2,4,6-TRINITRORESORCINOL IN $\text{DMSO}-d_6$

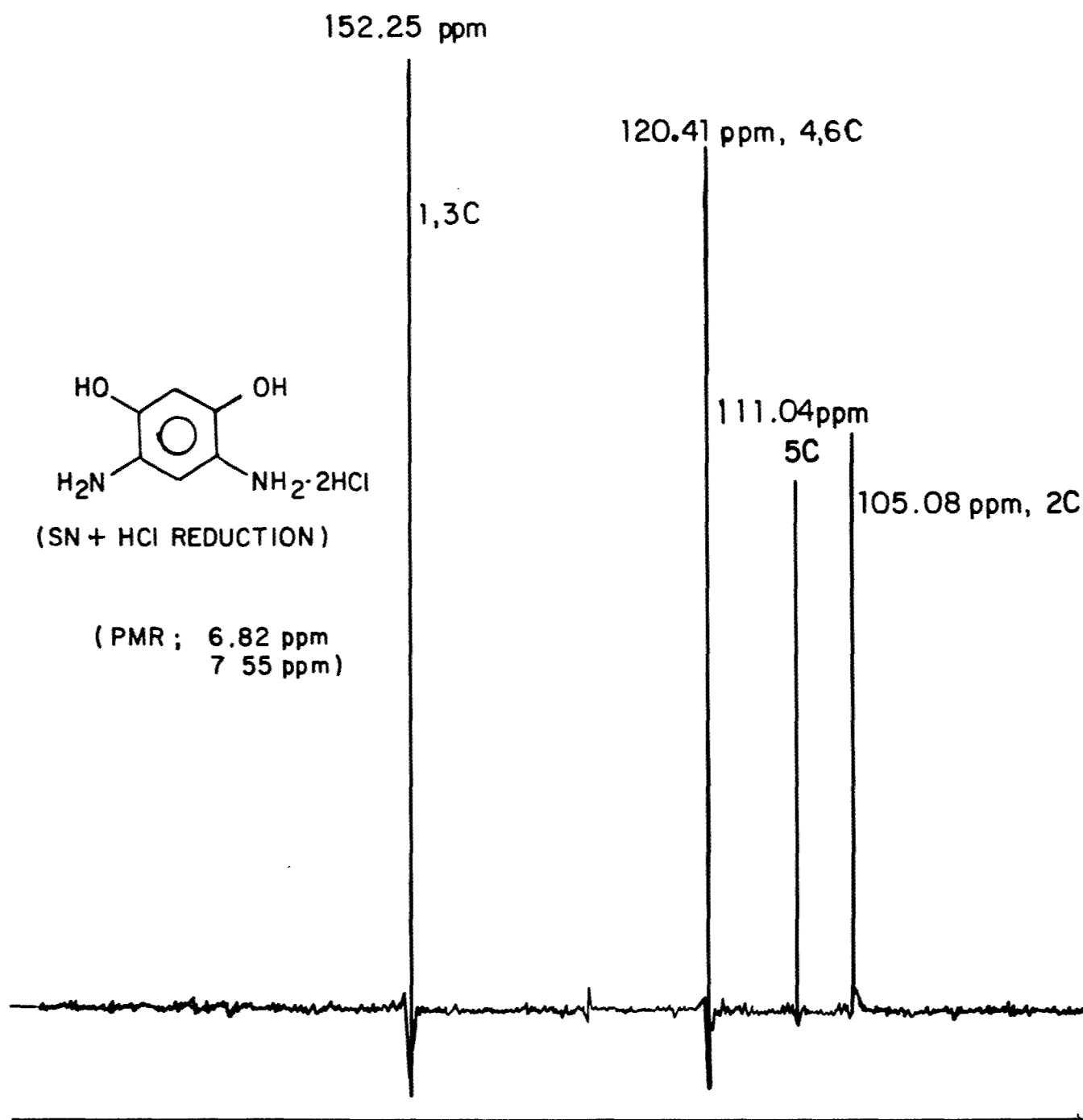
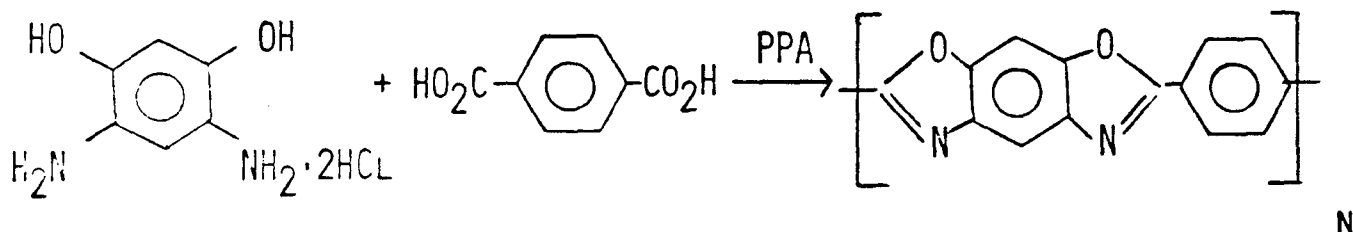


FIGURE 5. C^{13} MR SPECTRUM OF 4,6-DIAMINORESORCINOL DIHYDRO-
CHLORIDE IN WATER, EXTERNAL DMSO- d_6 LOCK

B. Rodlike Polymer Preparation

1. Poly-(para-phenylenebenzobisoxazole) (PBO) from 4,6-Diaminoresorcinol and Terephthalic Acid

Poly-(para-phenylenebenzobisoxazole) (PBO) was prepared by the Air Force procedure as well as a modified procedure from fiber grade terephthalic acid and 4,6-diaminoresorcinol dihydrochloride in 115% polyphosphoric acid (PPA).



The initial polymerizations were carried out at two concentrations, 1.219% on a 0.32 molar scale and 1.918% on a 0.474 molar scale. The inherent viscosities and ash content are shown in Table IV, and elemental analysis in Table V. TGA curves for PBO polymers are shown in Figures 6 and 7.

The results of the quantitative determination of ash and metals on several PBO polymers showed that four polymers contain excessive amounts of iron and phosphorus due to the corrosion of the agitator used in hot PPA.

In order to eliminate the iron and phosphorus contaminants and the corrosion problem of metal agitators, several agitators resistant to hot PPA were fabricated: four glass turbine type agitators for 2-liter and 5-liter flasks; two Hastelloy B spiral agitators for 2-liter and 5-liter flasks; and one tantalum spiral agitator. The design of the spiral agitators is shown in Figure 8. These corrosion resistant agitators were found to be satisfactory and resistant to PPA at 210°C when used to prepare PBO polymers (Table VI). The turbine type glass agitator appeared to be somewhat less efficient in shearing the reaction mixture than the spiral agitator.

The existing polymerization equipment was also modified to gain ten times greater torque than before. This power is necessary to agitate the very viscous PBO polymer solutions in polyphosphoric acid. A drawing of the modified equipment is shown in Figure 9.

The PBO polymers prepared from 4,6-diaminoresorcinol and terephthalic acid in PPA showed inherent viscosities ranging from 1.1 to 2.11 dl/g as determined at 0.2% in methanesulfonic acid. The moderately low viscosities of PBO polymers were of concern, and the research effort was directed toward the achievement of higher molecular weight. One approach to this end was by reaction of the diamine with the acid chloride of terephthalic acid.

TABLE IV

PBO POLYMERS

<u>POLYMER NO.</u>	<u>% POLYMER SOLIDS</u>	<u>PPA</u>	<u>I.V.* (dl/g)</u>	<u>ASH (%)</u>
25613-32F	1.219	600g	2.42	1.34
25613-35	1.219	6kg	1.71	34.7
25613-36	1.219	6kg	1.13	54.8
25613-37 ^b	1.817	6kg	3.71 ^a , 2.27 2.44 ^d	1.64
25613-38	1.219	6kg	2.7 ^a , 2.18	2.03
25613-39 ^c	1.817	6kg	2.39 ^a	18.94
25613-40 ^c	1.817	6kg	2.83	32.9
AFML PBO #2			3 ^a , 2.40	4.51

TYPICAL POLYMERIZATION CONDITIONS: Temp °C/Hours; 60°/16, 90°/5, 130°/3, 150°/16, 170°/3, 185°/3, 205°/24.

* The inherent viscosities were determined at 0.2% concentration in methanesulfonic acid at 25°C.

^a After precipitation from PPA.

^b 205°/48 hours

^c 205°/72 hours

^d Intrinsic viscosity

TABLE V

ELEMENTAL ANALYSIS

		<u>FOUND</u>					
	<u>THEORY</u>	<u>25613-37</u>		<u>25613-38</u>		<u>26273-9A</u>	
C	71.795	68.47	68.70	68.33	68.09	70.29	70.30
H	2.582	2.79	2.88	2.76	2.76	2.77	2.96
N	11.960	11.42	11.29	11.37	11.59	11.64	11.59

PART NO. 990449

DU PONT Instruments
MEASURED VARIABLE

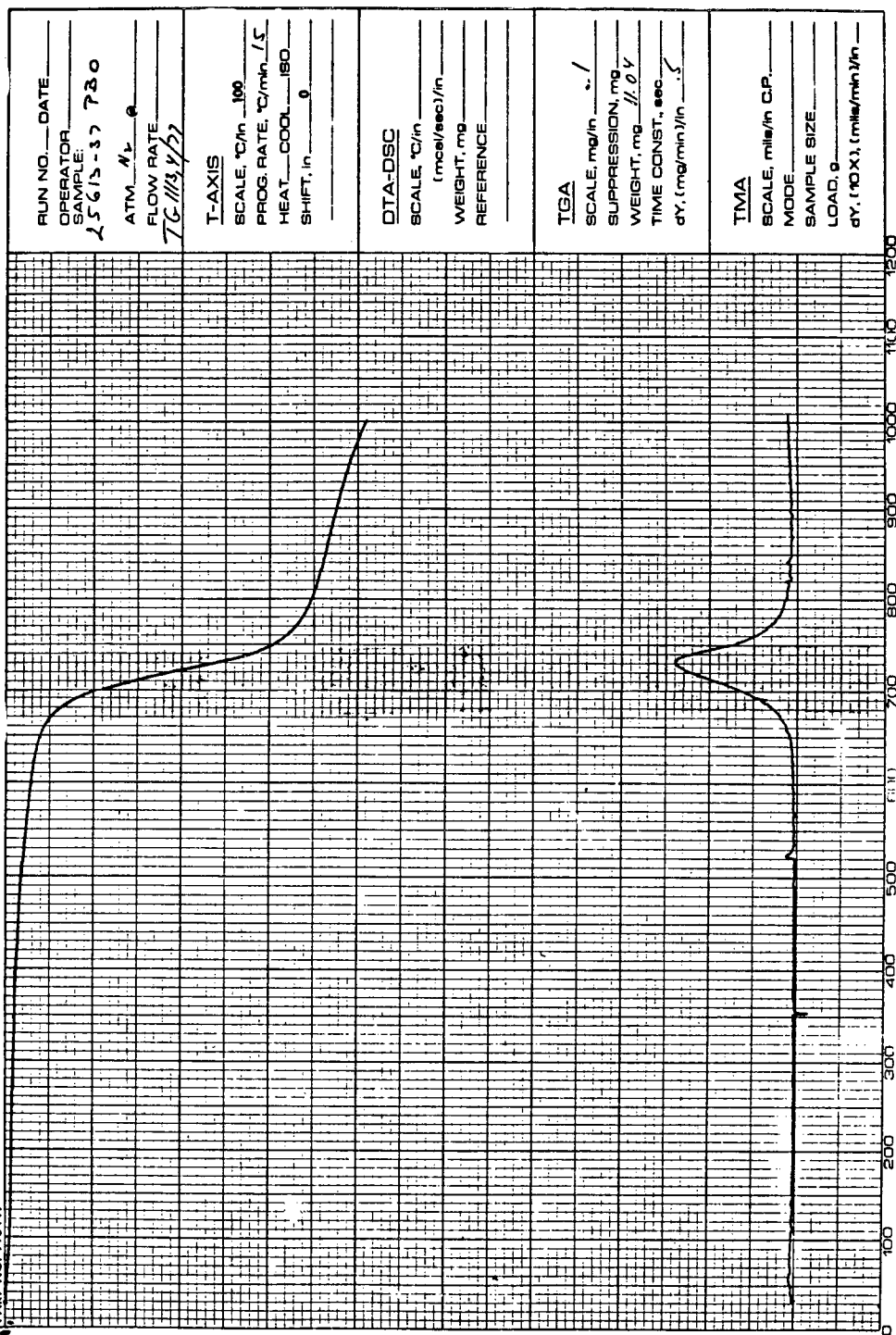


FIGURE 6A. TGA IN N₂ FOR PB0 POLYMER 25613-37 PREP'D FROM TEREPHTHALIC ACID

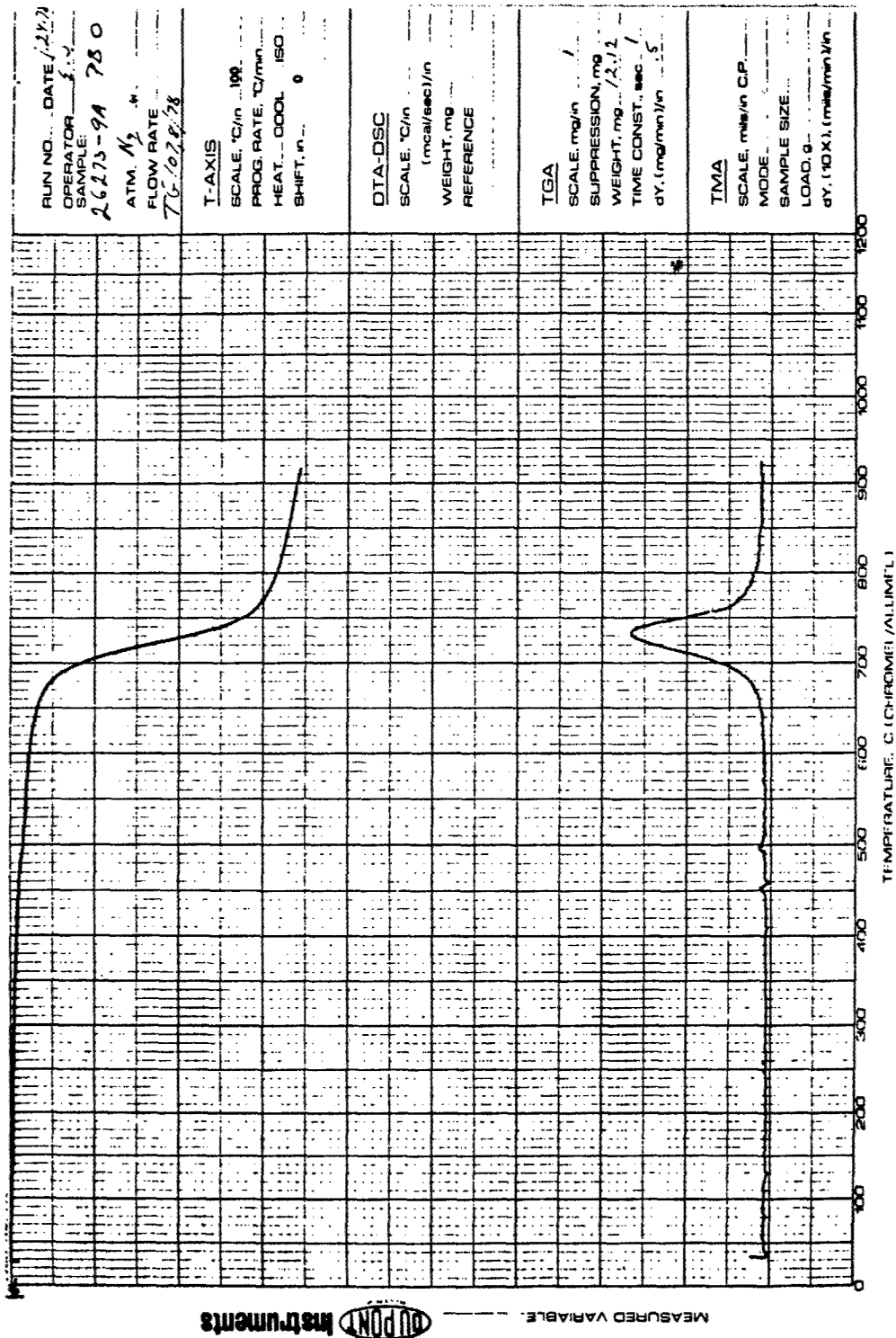


FIGURE 6B. TGA IN N₂ FOR PB0 POLYMER 26273-9A PREP'D FROM TEREPHTHALOYL DICHLORIDE

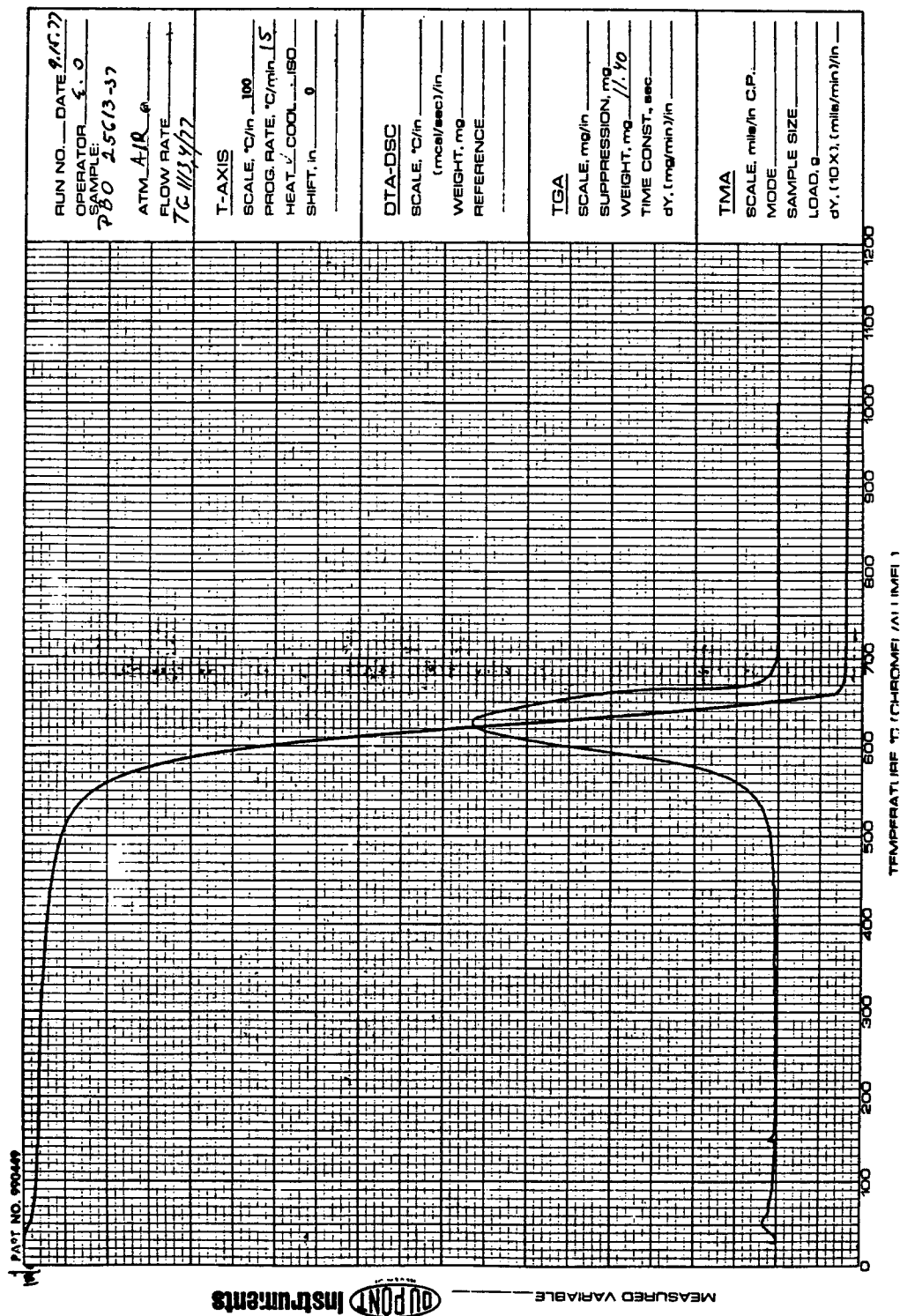


FIGURE 7A. TGA IN AIR FOR BPO POLYMER 25613-37 PREP'D FROM TEREPHTHALIC ACID

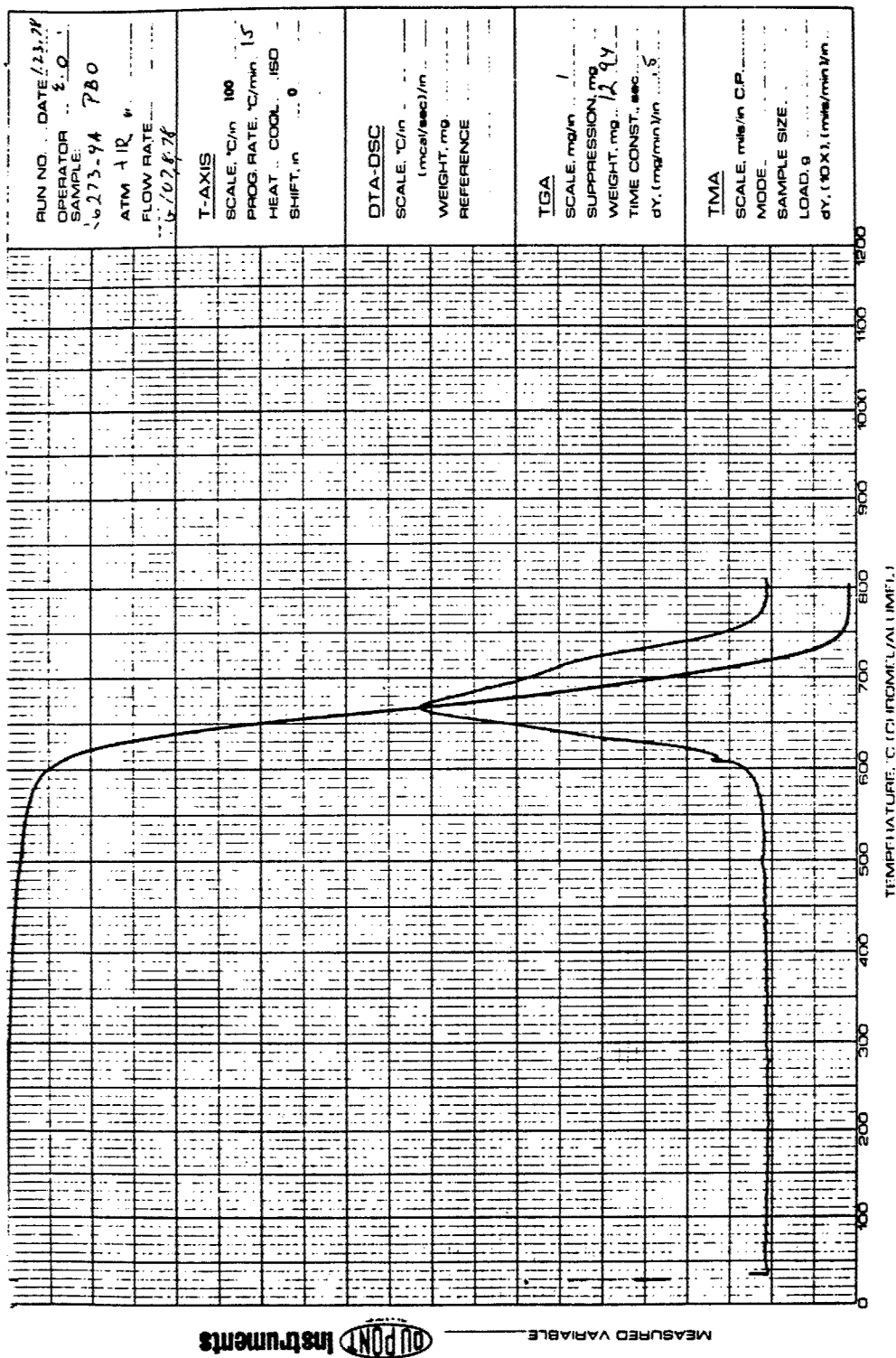


FIGURE 7B. TGA IN AIR FOR PBO POLYMER 26273-9A PREP'D FROM TEREPHTHALOYL DICHLORIDE.

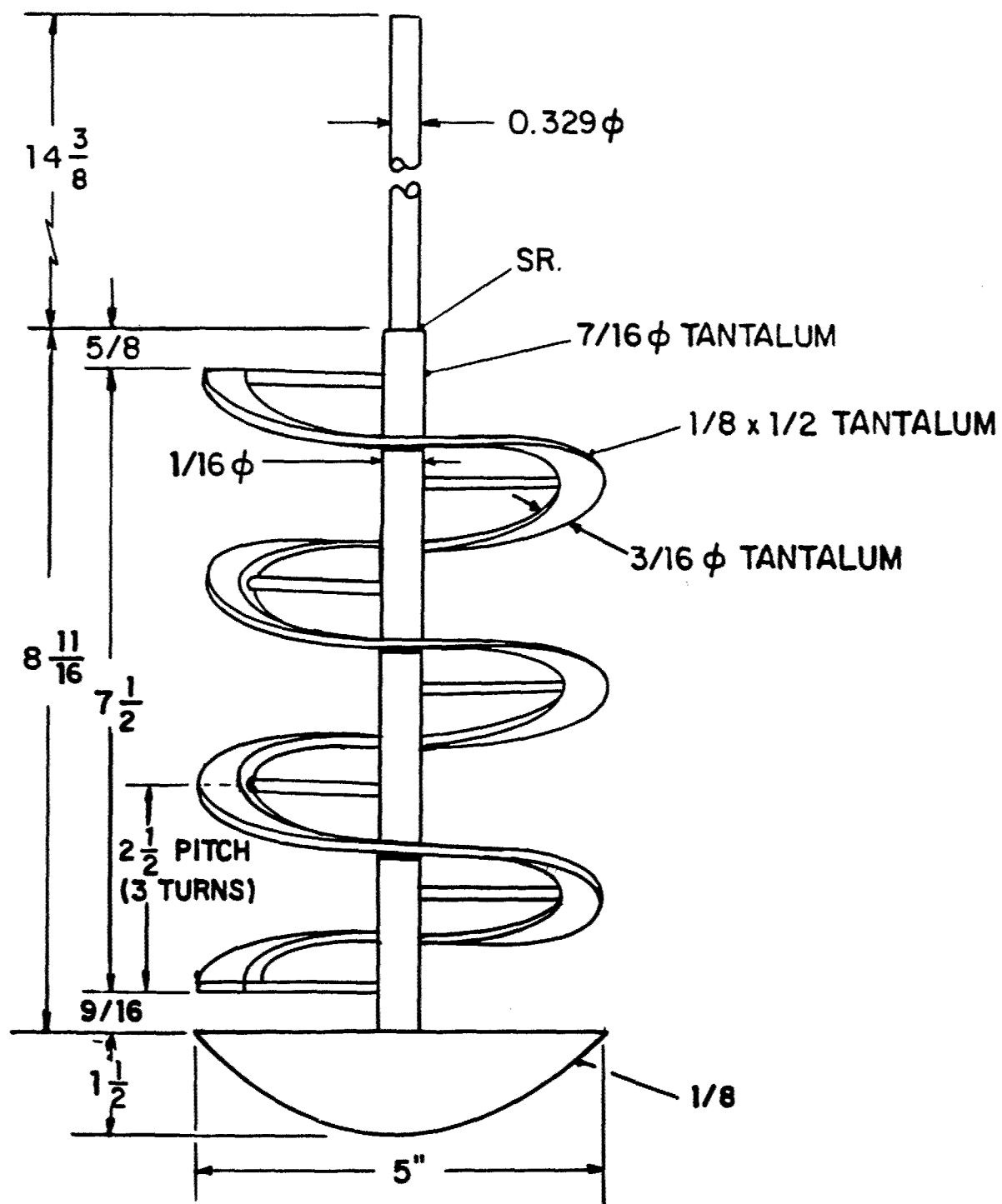


FIGURE 8. SPIRAL STIRRER

TABLE VI

PBO POLYMERS FROM TEREPHTHALIC ACID
AND 4,6-DIAMINORESORCINOL

<u>POLYMER NO.</u>	<u>PPA^b (kg)</u>	<u>I.V.^c (dl/g)</u>	<u>STIRRER</u>	<u>ASH (%)</u>
25612-17	2	1.96 ^d	GLASS	0.91, Ca, P.
25613-50	6	2.11	TANTALUM	0.71, Pb, Cd.P.
25612-18	6	1.10	TANTALUM	
26273-2	2	1.64	HASTELLOY B	
26273-4 ^a	2	1.92	HASTELLOY B	
26290-2	2	2.11	HASTELLOY B	
26290-3	2	2.06	HASTELLOY B	

a 210°C/48 hours

b 1.817% Polymer Solids

c 0.2% in methanesulfonic acid

d I.V. = 1.7 in 100% H₂SO₄

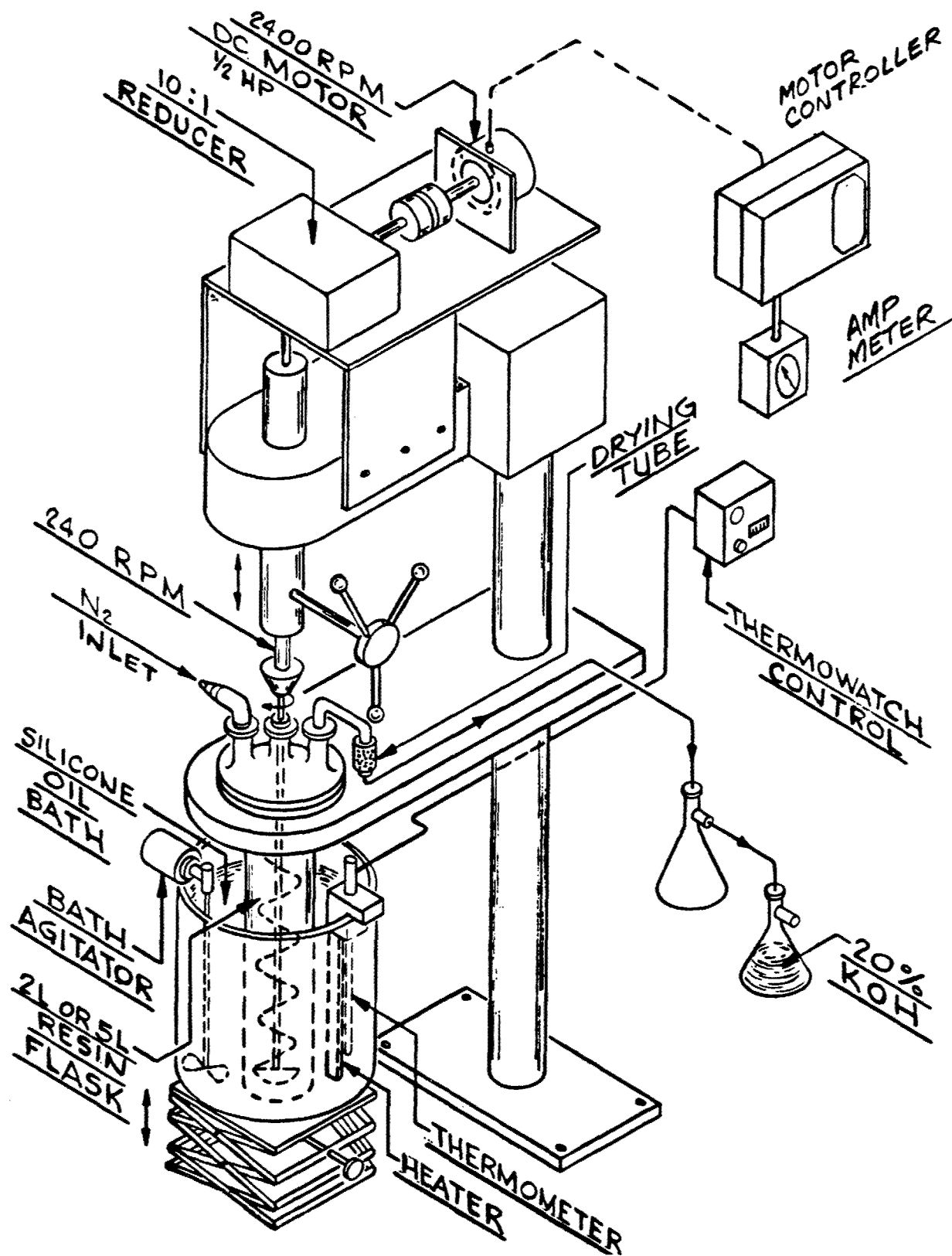


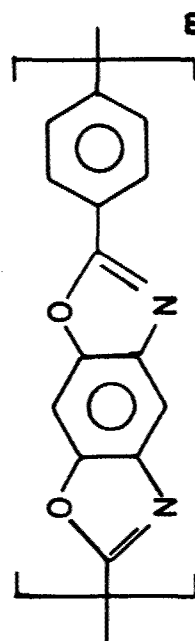
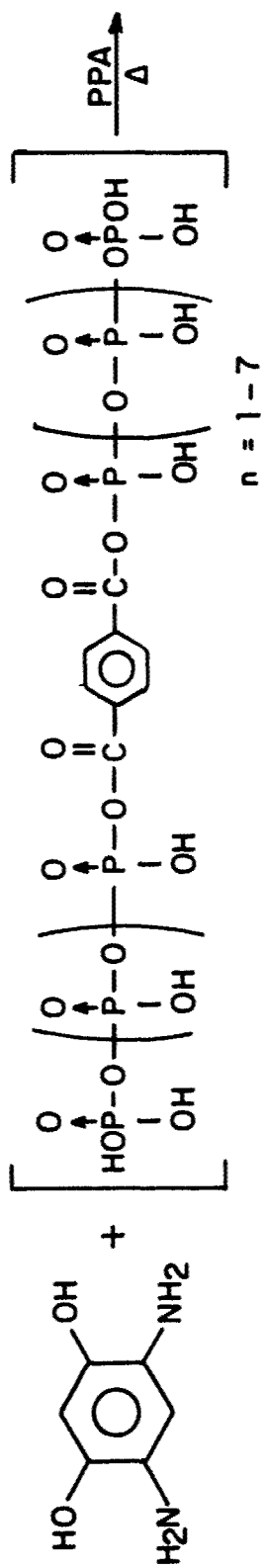
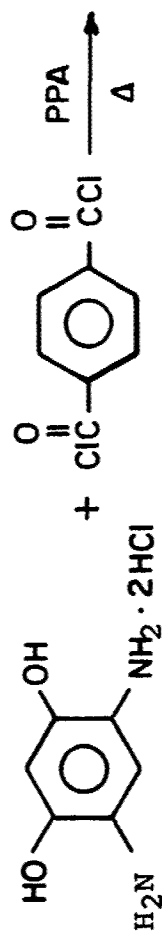
FIGURE 9. PBO POLYMERIZATION APPARATUS

2. Poly-(para-phenylenebenzobisoxazole) from
4,6-Dinitroresorcinol and Terephthaloyl Dichloride

In an attempt to produce a higher I.V. polymer, PBO was prepared from diaminoresorcinol and terephthaloyl dichloride in a two-step polymerization; the formation of polyamide in DMAc-LiCl, followed by the cyclization of the amide to PBO in PPA. The I.V. of this polymer was extremely low; therefore, this two-step method was not pursued further.

In another attempt to produce a higher I.V. polymer, a small quantity of PBO was synthesized directly in PPA from diaminoresorcinol and terephthaloyl dichloride. It was noticed during the work-up that the polymer was fibrous and formed a tough film. The inherent viscosity was 2.04 dl/g as determined at 0.2% in methanesulfonic acid. This new process was scaled-up successfully to produce I.V. 2.8 dl/g (in MSA) PBO polymer (EWC 26273-9A) in a sufficient quantity (35 grams) for a spinning experiment and other characterizations. The infrared spectrum of this polymer film is identical to that of the authentic sample. The TGA thermograms in air and/or nitrogen were satisfactory and are shown in Figures 6 and 7. Fourier Transform Infrared Spectra of PBO's prepared from terephthalic acid and/or terephthaloyl dichloride are shown in Figures 10 and 11. As observed in the previous batch, the polymer is fibrillar.

PBO FROM TEREPHTHALOYL DICHLORIDE AND 4,6-DIAMINORESORCINOL



ADVANTAGES: MOL. WT. DISTRIBUTION ?

HIGHER I.V.

NO SUBLIMATION

A fibril about one inch long was produced and isolated during the precipitation of the polymer into methanol from the PPA polymerization mixture. This fibril was photographed in a scanning electron microscope to obtain some information as to the general morphology of its surface. The micrographs at 100X to 5000X (Figure 12 a-d) exhibit the fiber with a longitudinal fibrillar texture and with many loose strands or fibrils.

It appears that terephthaloyl dichloride reacts with polyphosphoric acid to form a dipolyphosphoric acid ester of terephthalic acid with evolution of hydrochloric acid. The white milky ester reacts with 4,6-diaminoresorcinol to give a clear amber solution at 160°C, and polymerizes to PBO. Two advantages for the use of terephthaloyl dichloride in the polymerization are that no sublimation occurs at the end of the reaction, and the formation of PBO polymer with a higher I.V.

The PBO polymers prepared by this method are summarized in Table VII. The inherent viscosities were in the range from 2.10 to 3.88 dl/g as determined at 0.2% in methanesulfonic acid when the polymers were precipitated directly into methanol, isolated, washed and dried. Some decrease in viscosity is apparent when the polymer was dissolved first in methanesulfonic acid, precipitated into methanol, isolated, washed and dried.

A study on the effect of polymerization time and temperature on the PBO I.V. was carried out by determination of the I.V. of polymer samples removed after several time intervals (24, 48 and 120 hours) at 210°C and 250°C. Preliminary results showed some evidence for a slight decrease in inherent viscosity on heating at 210° or higher for a period greater than 48 hours. The results are shown in Table VIII.

TABLE VII

PBO POLYMERS FROM TEREPHTHALOYL DICHLORIDE
AND 4,6-DIAMINORESORCINOL

<u>POLYMER NO.</u>	<u>PPA^c</u> <u>(kg)</u>	<u>I.V.^d</u> <u>(dl/g)</u>	<u>I.V.^e</u> <u>(dl/g)</u>
26273-5 ^a	0.5	--	2.04
26273-9 ^a	2	3.88	2.78
26273-38 ^b	2	3.57	2.44
26290-4 ^a	2	2.10	2.06
26290-5 ^a	2		1.71
26290-9 ^a	2		

a 210°/48 hours

b 210°/24 hours

c 1.817% Polymer Solids

d After precipitation from PPA

e After precipitation from MSA

TABLE VIII

POLYMERIZATION TIME AND TEMPERATURES VS. PBO I.V.

<u>TEMP., °C</u>	<u>HOURS</u>	<u>I.V.^a (dl/g)</u>	<u>I.V.^b (dl/g)</u>
210	24	3.14	2.55
210	48	3.06	2.42
210	120	2.88	2.01
250	24	0.84 ?	

Experiment No. 26290-8, Terephthaloyl Dichloride and
Diaminoresorcinol.

a After precipitation from PPA

b After precipitation from MSA

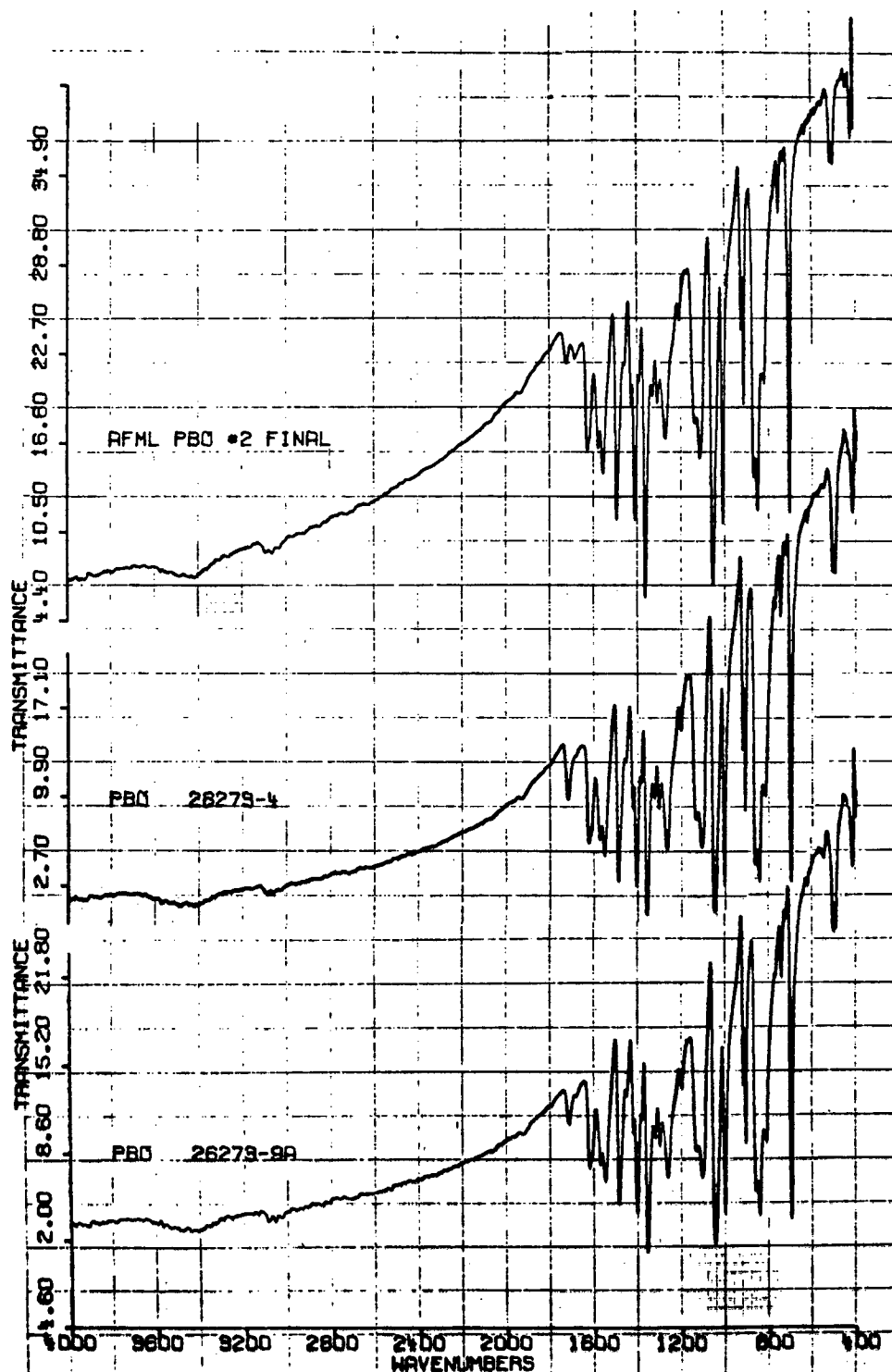


FIGURE 10. FTIR SPECTRA OF PBO

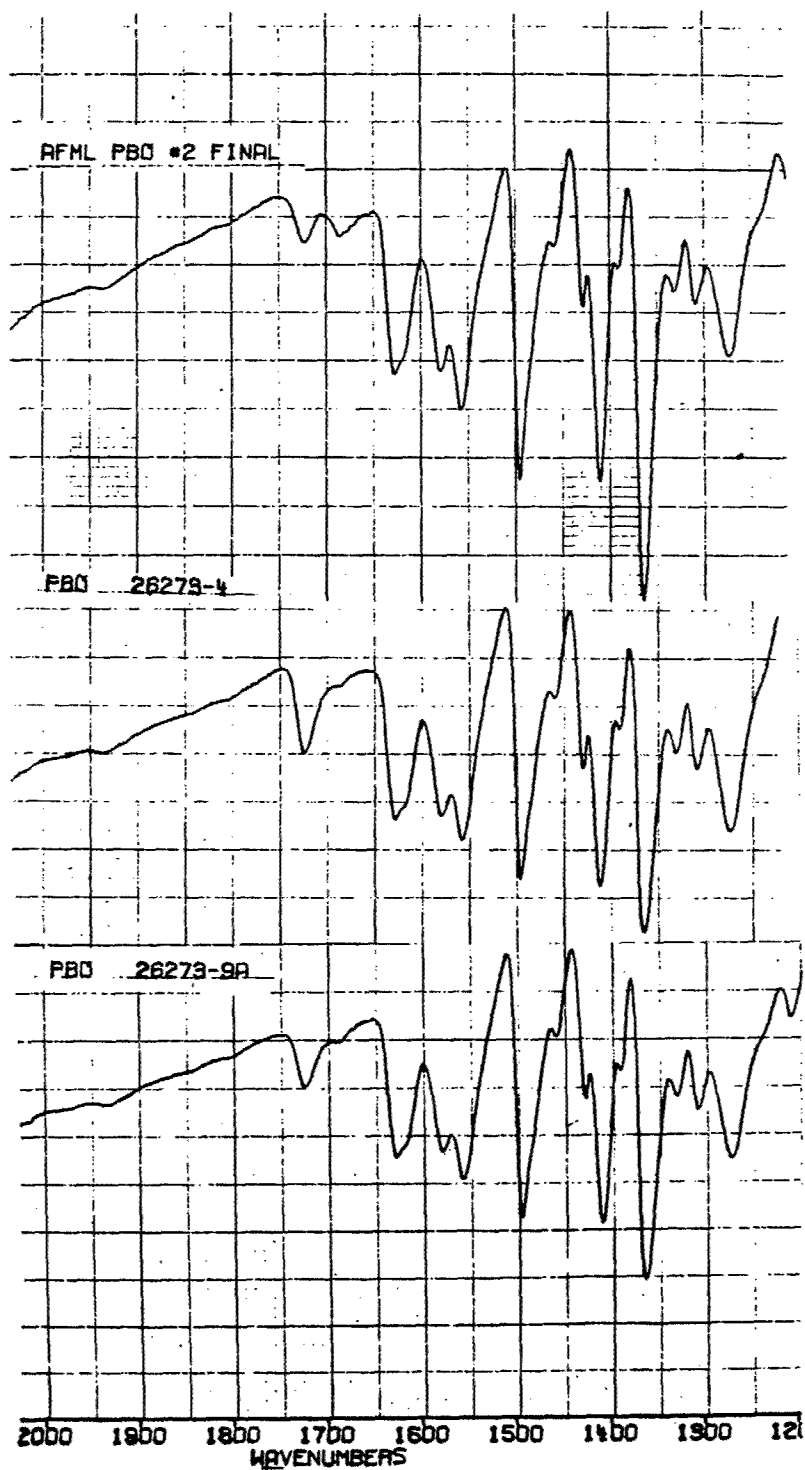
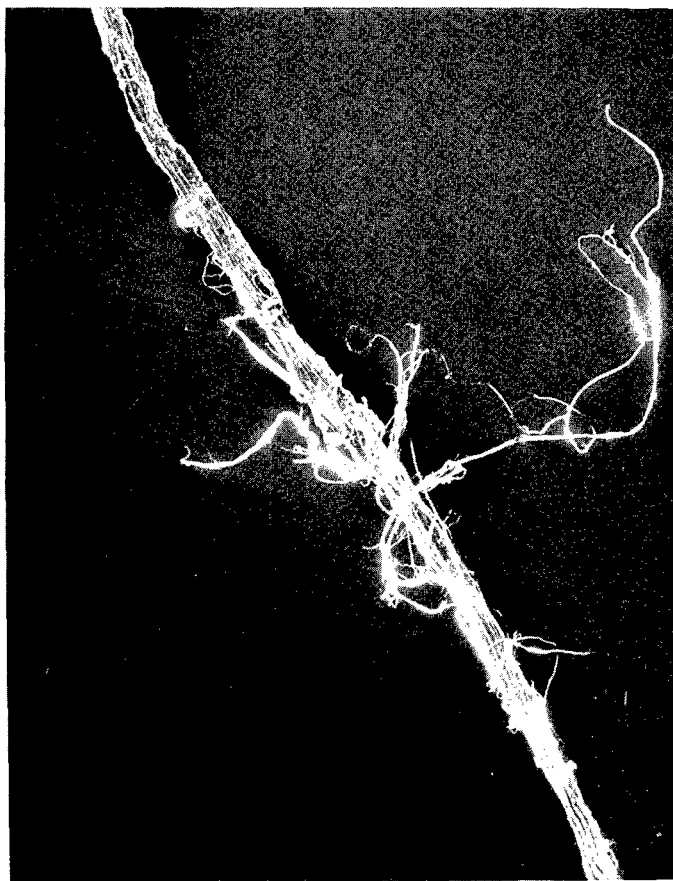


FIGURE 11. FTIR SPECTRA OF PBO

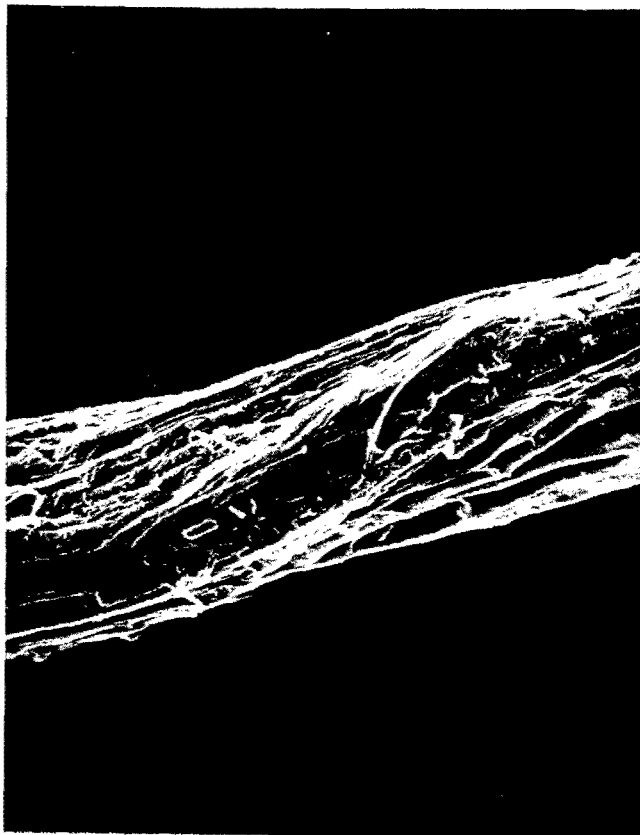


a. 100X

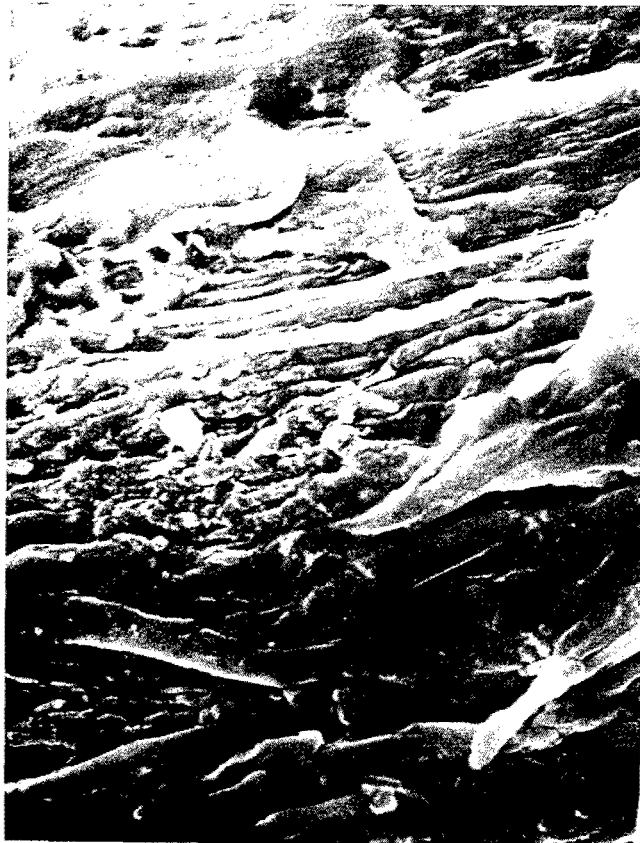


b. 1000X

FIGURE 12. SEM MICROGRAPH OF PBO POLYMER 26273--9 PREP'D FROM TEREPHTHALOYL DICHLORIDE



c. 1000X



d. 5000X

FIGURE 12. SEM MICROGRAPH OF PBO POLYMER 26273-9 PREP'D FROM TEREPHTHALOYL DICHLORIDE

C. Fabrication of Rodlike Polymers

1. PBO Fabrication

a. Dope Preparation and Characterization

An attempt to prepare a 15% solids PBO/MSA dope was made under nitrogen by adding the polymer solid (No. 25613-40) to MSA at 80°C with agitation. The dope was stirred for 24 hours. Although the particle count indicated the dope to be fairly clean, it was not possible to spin it successfully under the conditions known to work well for a related polymer. It could not be filtered through a 50 μm filter at conditions as extreme as 27.6 MPa (4000 psi) and 120°C. The 15% dope was diluted with MSA to 12% but filtration remained impossible. Careful examination of the 12% dope revealed that it contained undissolved particles (polymer aggregates or foreign matter). Further dilution to 10% solids did not improve the spinnability. When a 10% dope was prepared from another PBO batch (25613-37), it wet-spun well.

The color of PBO/MSA-CSA dope was slightly different from batch to batch. Also, it seemed to depend on the solids level and the moisture contaminant. It was reported that moisture causes the formation of polymer aggregates. The 8% dope (25613-50A, I.V. 2.1) was bluish, the 10% dope was greenish and at 9%, it was an intermediate shade between the other two. If the bluish dope is left in the ambient atmosphere, it turns green quickly.

With respect to the dope preparation, the PBO prepared from diaminoresorcinol and terephthaloyl dichloride and PBT polymers behaved very similarly to that of the PBO polymer prepared from diaminoresorcinol and terephthalic acid. Microscopic examination of PBO/MSA dopes show them to be in an anisotropic nematic liquid crystal state at room temperature. The list of PBO polymer batches is given in Table IX.

PBO dopes in sulfuric acid (100%) were prepared and characterized. A typical critical concentration curve for the rodlike polymers was observed for the PBO (I.V. 2.1 dl/g) in 100% H_2SO_4 at 70°C and the curve is shown in Figure 13. The PBO dopes in 100% H_2SO_4 at concentrations greater than 8% solids exhibit crystalline structures (x-ray). They are semi-solid at ambient temperature and lyotropic liquids at temperatures above 70°C. The x-ray diffraction patterns of the dopes were different from that of PBO itself, showing

some crystallinity and similarity to that of 16% Kevlar dopes in 100% H_2SO_4 . This might be probably due to both or either of the formation of a PBO/sulfuric acid complex or the sulfonation of the aromatic rings. X-ray diffraction patterns for the PBO- H_2SO_4 complex is shown in Figure 14. When the dope was slowly precipitated, PBO crystallized out. The x-ray diffraction patterns of the crystals were extremely well defined, indicating a very high degree of orientation. The principal spacings are listed in Table X and the x-ray diffraction patterns in Figure 15. A PBO dope in MSA also showed some crystallinity (x-ray) at 11% solids, with the diffraction pattern shown in Figure 16. This is different from those of PBO itself and PBO/ H_2SO_4 dopes.

b. Fabrication and Properties of PBO Fibers

There are many process variables in fiber spinning and their relative importance depends on the spinning method chosen (i.e., wet, dry, melt spinning, etc.) which in turn is dictated by inherent polymer properties such as meltability, solubility, I.V., etc. In the case of PBO polymer, it does not melt and is only soluble in strong acidic solvents such as 100% sulfuric acid or methane sulfonic acid.

An initial approach to the PBO spinning was to try a wet spinning system known to work well for a Kevlar/ H_2SO_4 dope, and then try a dry-jet wet spinning system to increase the spin draw ratio (SDR) and the orientation. Generally

speaking, dry-jet wet spinning, by extruding the polymer dope into the air or other gas medium briefly before it touches the coagulating liquid, allows higher SDR and consequently higher molecular ordering than does wet spinning. In this way, higher fiber mechanical properties are realized.

A 10% dope was prepared (25613-37) and wet spun into a water bath at 5°C. The spinning parameters and the PBO fiber properties are listed in Table XIA. Subsequently, 8% and 9% dopes were prepared from another polymer batch (25613-50A, I.V. 2.1) and spun into a 5°C water coagulation bath. The one time data showed that the fiber from the 8% dope yielded a slightly higher tenacity than the fiber from 9% dope.

Scanning electron micrographs of the fibers showed the fiber surfaces to be convoluted and rugose with a small amount of surface debris. They also showed a coarse longitudinal stranded texture which tends to separate into individual strands at the fiber ends (Figure 17). The poor surfaces were probably due to a violent coagulation reaction caused by an incursion phenomenon at the acid-water interface. Such finger-like diffusion phenomena at the acid-water interface is frequently observed when a dope containing strong acid is spun into water. The low solids level (9%) probably contributed to the formation of a rough fiber surface-- Kevlar type polymers are normally spun from 20% solids dope.

When the fiber was heat treated, it improved the properties to 4.8g/d/0.7%/711g/d, which was significantly higher than the previously reported levels for the PBO polymer prepared from terephthalic acid.

The effect of MSA concentration in the coagulation bath on the fiber surface morphology and the fiber mechanical properties was evaluated over the acid concentration from 0 to 90% in water. The SEM micrographs of the fiber are given in the Figures 17-a to 17-h. The smoothest and void free fiber was obtained from the 30% MSA concentration. Fiber coagulated from this MSA concentration also yielded the highest property levels. The wide angle x-ray diffraction patterns showed a significantly higher degree of orientation than those for the previous PBO polymers prepared from terephthalic acid (Figure 18). Subsequently, three more batches of PBO polymers (I.V. 2.2, 2.1, and 2.4) were wet spun. Results are given in Table XIB. The physical properties obtained were lower than those from the 2.8 I.V. polymer, presumably because of the lower molecular weight. The PBO polymer from the terephthaloyl dichloride spun better than did the polymers made from terephthalic acid but they still could not be dry-jet wet spun. The effects of I.V. and SDR are given in Figures 19 and 20. When the I.V. 2.8 fibers (highest I.V. available) were heat treated at temperatures from 425 to 500°C, the properties, particularly the modulus, increased significantly (Table XII).

The spin draw is key to the molecular orientation leading to high fiber mechanical properties. The fibers wet spun from PBO polymers prepared from terephthalic acid were so weak that they could not be spin stretched and could be taken up only in the relaxed state. The weak wet filament strength is probably attributable to the low I.V. Due to the lack of cohesive strength of the dope, numerous attempts to dry-jet wet spin were not successful.

Sulfuric acid (> 100%) was evaluated as a solvent for PBO spinning dope. Two PBO-H₂SO₄ dopes at 11% and 9% solids were prepared at 70°C. The dope viscosities were very high and the dopes did not flow at room temperature. It was not possible to spin the 11% dope, because it could not be filtered, even when the dope was heated to 150°C. The 9% dope broke clean at the spinneret face but the extruded filament was too weak to take up. SEM micrographs (1,500X to 10,000X) showed the 9% fiber surfaces to be lumpy with a random pattern, much more so than the fiber spun from MSA solvent. The cross sectional view appears to be round with large internal voids (Figure 17-j).

A PBO prepared from terephthaloyl dichloride (batch 26273-9A, I.V. 2.8) made an 8.6% dope (97.5/2.5 methane-sulfonic acid/chlorosulfonic acid solvent ratio) was spun into 30% MSA/70% water coagulation bath. The filaments were slightly spin stretchable (up to ~ 50%) and the best as-spun properties (T/E/M) obtained were 4.2g/d/1.4%/502g/d.

c. Fabrication and Properties of PBO Ribbon

The feasibility of PBO film casting was evaluated with an 8.6% dope (polymer 26273-9A, I.V. 2.8). When a film (10 mil wet thickness) was cast onto a glass plate (13 x 25cm) with a drawing knife and coagulated in water, it shrank substantially. The high shrinkage in turn caused the film to split in the direction parallel to the draw. As the film dried, it shrank further. The dried film was brittle and too weak for measurement of its mechanical properties. As a control, a chlorinated poly-(p-phenyleneterephthalamide) film (10% solids in DMAc) was cast in a similar manner. It shrank much less and the tear strength was much higher than the PBO film. In attempts to reduce the PBO film coagulation rates, various baths (MSA/H₂O, concentrations varying from 0 to 70%, and isopropanol) and different quenching geometries (from one side, only from side edges, etc.) were evaluated. Despite a reduced coagulation rate, the film could not be prevented from splitting. It may be that the excessive shrinkage is due primarily to the low solids level.

A ribbon was extruded through a 6mm x 0.25mm (0.25 in. x 10 mil) slit die utilizing the spinning equipment. In the process of coagulation (in 30% MSA in water) and drying, the ribbon shrank to 3mm (1/8 in.) but it did not split. A tensile strength of 103 MPa (15,000 psi) and a modulus of

TABLE X

PRINCIPAL SPACINGS OF PBO

POLYMER	3.35Å	5.55Å	11.35Å
FIBER	3.27Å	3.52Å	5.52Å
POLYMER RECRYSTALLIZED FROM 10% DOPE IN 100% H ₂ SO ₄			
	1.20Å (VW),	1.329Å (VW),	1.38Å (VW),
	1.94Å (M-S),	2.38Å (M-S),	2.76Å (M-S),
	3.24Å (VVS),	3.51Å (VS),	3.92Å (VW),
			4.14Å (VW),
			4.38Å (VW),
		5.50Å (VVS)	11.19Å (M-S)
POLYMER RECRYSTALLIZED FROM 8.6% SOLUTION IN MSA			
	2.39Å (VW),	2.52Å (VWV),	2.86Å (VWV),
	3.36Å (S. Broad),	5.53Å (S),	9.16Å (VW),
			11.26Å (W)

TABLE XI A

SPINNING CONDITIONS^a

<u>SAMPLE SPIN NO.</u> 26085-	<u>POLYMER NO.</u>	<u>I.V.</u>	<u>SPINNERET (μm)</u>	<u>COAG. BATH COMP.</u>	<u>JET VEL. m/min.</u>	<u>SPIN DRAW RATIO</u>
-7-3 ^b	25613-37**	3.7	10 x 50	Water	10	1
-15-3 ^c	25613-50A**	2.2	10 x 100	Water	10	1
-16-2 ^d			10 x 100	Water	10	<1
-3 ^d			10 x 50	Water	10	1
-25-1	26273-9A*	2.8	10 x 100	30/70	4.5	1.4
-2				50/50	6.3	<1
-3 ^e				50/50	6.3	<1
-4				40/60	6.3	1
-5				40/60	6.3	1.1
-27-1	26290-2*	2.2	10 x 100	30/70	6.3	1
-2				30/70	6.3	1
-3				30/70	6.3	1
-29-1	26290-4*	2.1	10 x 75	30/70	6.3	1.1
-2				30/70	6.3	1
-3				30/70	6.3	<1
-4				30/70	5.3	1.2
-5				30/70	4.4	1.43
-46-3	26273-38*	2.4	10 x 100	30/70	6.3	<1
-4					6.3	1.2
-5				Iso-pro- panol	6.3	<1
-6				Iso-pro- panol	6.3	<1

a Dope concentrations: 8.6% in 97.5% MSA/2.5% CSA,
dope and bath temp @RT unless otherwise noted.

b Dope concentration: 10% in 100% MSA

c Dope concentration: 8% in 100% MSA

d Dope concentration: 9% in 97.5% MSA/2.5% CSA

b, c, d, e Dope and bath temp: 5°C

* PBO from Terephthaloyl Dichloride

** PBO from Terephthalic Acid

TABLE XI B
PBO FIBER PROPERTIES AS WET-SPUN

SAMPLE SPIN NO.	POLYMER NO.	I.V.	FIBER PROPERTIES (n = 10)				
			DPF	ELONG. %	TEN. (g/d)	TE $\frac{1}{2}$	MODULUS (g/d)
26085-							
-7-3 ^b	25613-37**	3.7	3.1	1.4	1.0	1.2	103
-15-3 ^c	25613-50A**	2.2	11.0	3.9	1.5	3.0	124
-16-2 ^d			13.3	2.4	0.8	1.3	81
-3 ^d			3.3	3.9	1.5	3.0	82
-25-1	26273-9A*	2.8	5.3	1.4	4.2	4.9	502
-2			13.4	8.7	1.3	3.8	81
-3 ^e			9.4	3.5	2.1	4.0	172
-4			9.2	6.6	2.3	5.8	132
-5			5.5	2.4	3.4	5.3	340
-27-1	26290-2*	2.2	11.1	2.9	1.2	2.0	102
-2			11.0	3.1	1.2	2.2	91
-3			10.8	2.5	1.3	2.1	110
-29-1	26290-4*	2.1	8.3	2.2	2.1	3.1	200
-2			9.1	3.4	1.8	3.3	122
-3			9.5	3.4	1.5	2.7	120
-4			7.2	2.5	2.2	3.5	198
-5			6.5	1.7	2.6	3.3	269
-46-3	26273-38*	2.4	12.0	5.0	1.4	3.1	114
-4			8.4	3.0	2.0	3.4	160
-5			14.1	2.2	0.9	1.2	68
-6			12.0	2.2	1.2	1.2	97

a Dope concentrations: 8.6% in 97.5% MSA/2.5%CSA,
dope and bath temp @RT unless otherwise noted.

b Dope concentration: 10% in 100% MSA

c Dope concentration: 8% in 100% MSA

d Dope concentration: 9% in 97.5% MSA/2.5%CSA

b, c, d, e Dope and bath temp: 5°C

* PBO from Terephthaloyl Dichloride

** PBO from Terephthalic Acid

TABLE XII

HEAT TREATMENT OF PBO FIBERS*

SPIN NO.	POLYMER NO.	TREATMENT TEMP. C.	SINGLE FILAMENT FIBER PROPERTIES			
			DPF	ELONG %	TEN. (g/d)	TE ^{1/2} MODULUS (g/d)
26085-25-1	26273-9A (I.V.=2.8)	As Spun	5.3	1.4	4.2	4.9 502
"	"	425	4.8	0.7	4.8	4.0 711
"	"	450	4.9	0.6	4.4	3.4 723
"	"	475	5.2	0.5	3.3	2.3 584
"	"	500	5.2	0.9	4.5	4.3 559

* The fiber was grabbed in the Instron and held for three minutes at the test temperature. Then it was drawn at a 10% strain rate until broken. The broken sample was tested at room temperature. The elongation to break at temperature was less than 1%.

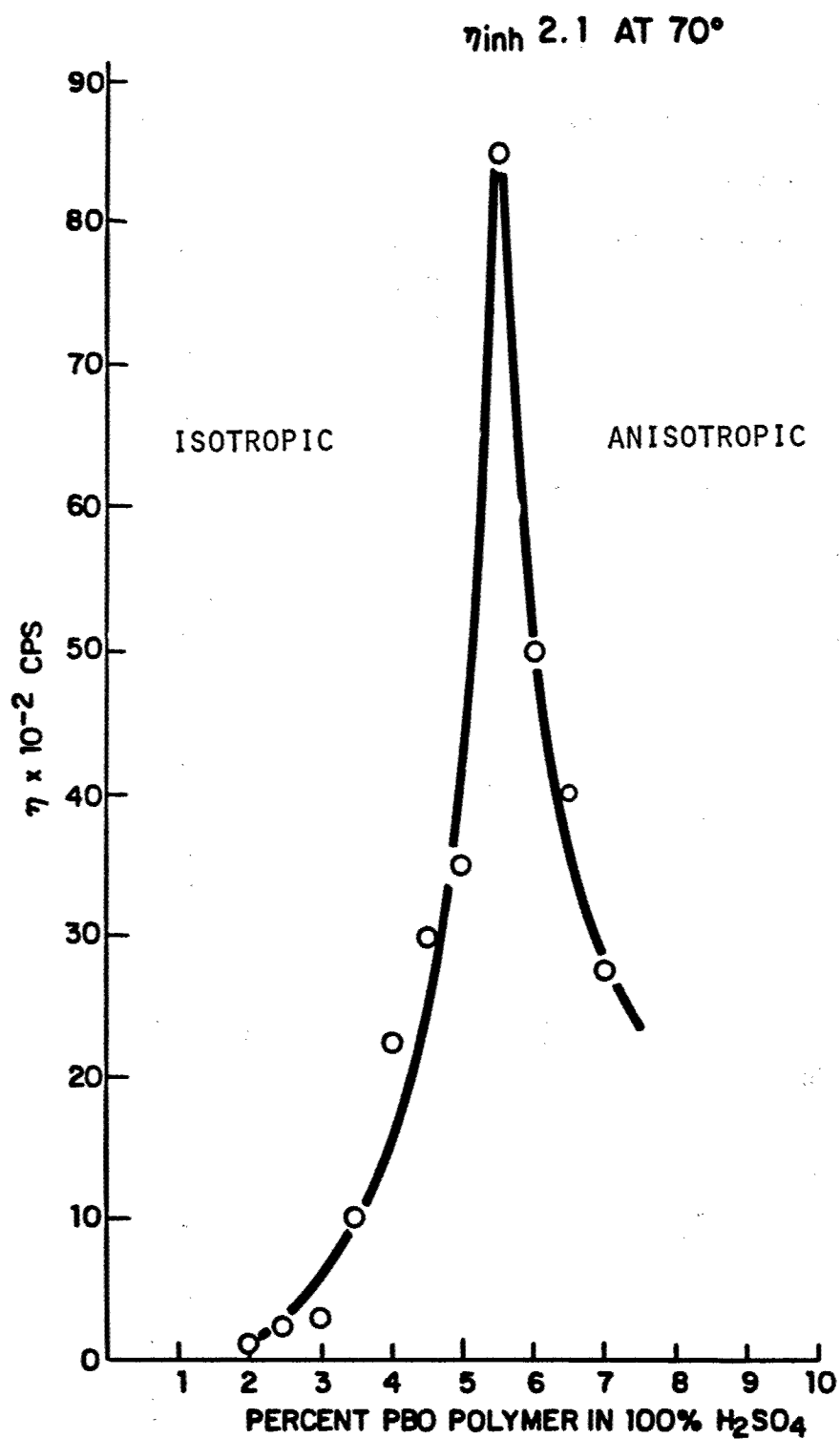


FIGURE 13. CRITICAL CONCENTRATION CURVE FOR PBO

of 7.6 GPa (1.1×10^6 psi) at 0.8% elongation were measured. The ribbon denier was calculated to be 346. The extrusion continuity (wet extrusion) was good but the properties obtained were significantly lower than the properties obtained with fibers from the same polymer.

A PBO solution (batch No. 25613-50, I.V. 2.11) in methanesulfonic acid was cast between two glass plates and one of the two plates removed in such a way as to induce a shearing action and an orientation. The resulting film was coagulated in water and dried first at room temperature and then at 80°C. In conoscopic observation, both films show a centered acute bisectrix figure which indicates they are well oriented. Wide-angle x-ray patterns for these films show a planar orientation. (Appendix 3 and 4).

TABLE IX

PBO POLYMER SUPPLY

<u>SPIN NO.</u>	<u>POLYMER NO.</u>	<u>I.V.</u> <u>(dl/g)</u>	<u>SPINNABILITY</u>		<u>COMMENTS</u>
			<u>WET</u>	<u>DRY-JET-WET</u>	
26085-2	25613-40 ^a	1.8	No	No	Dope, not filterable at 4000 psi & 80°C
26085-7	25613-37 ^a	3.7	Yes	No	
26085-15	25613-50A ^a	1.89	Yes	No	
26085-21	25613-17 ^a	2.17	No	No	Dope, not filterable at 4000 psi & 170°C
26085-23	26274-4 ^a	1.92	No	No	" " "
26085-25	26273-9A ^b	2.78	Yes	No	
26085-27	26290-2 ^b	2.15	Yes	No	
26085-29	26290-4 ^b	2.1	Yes	No	
26085-45	26273-30 ^b	2.4	Yes	No	

^a PBO from Terephthalic Acid^b PBO from Terephthaloyl Dichloride

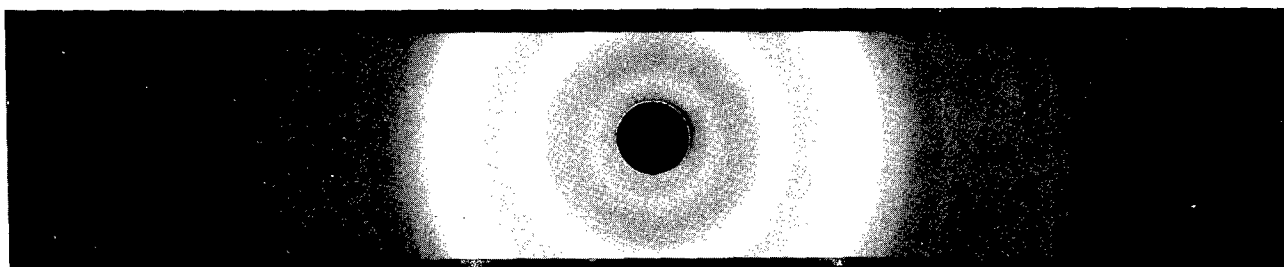


FIGURE 14. X-RAY DIFFRACTION PATTERN FOR PBO
PPT'D FROM 100% H_2SO_4

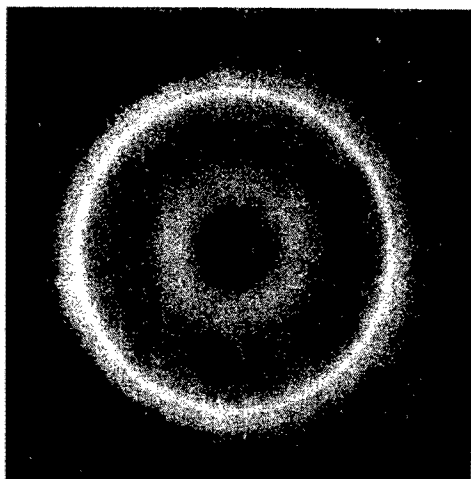


FIGURE 15. X-RAY DIFFRACTION PATTERN-
11% PBO in 100% H_2SO_4

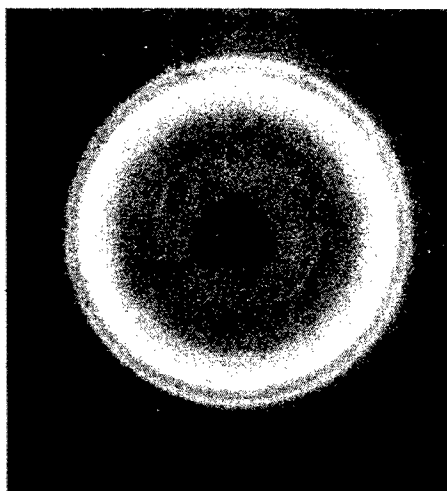


FIGURE 16. X-RAY DIFFRACTION PATTERN- 11% PBO
DOPE IN METHANESULFONIC ACID



101 004 18178
a. POLYMER 26085-25 (I.V. 2.8)
COAGULATED IN 30/70 MSA/H₂O

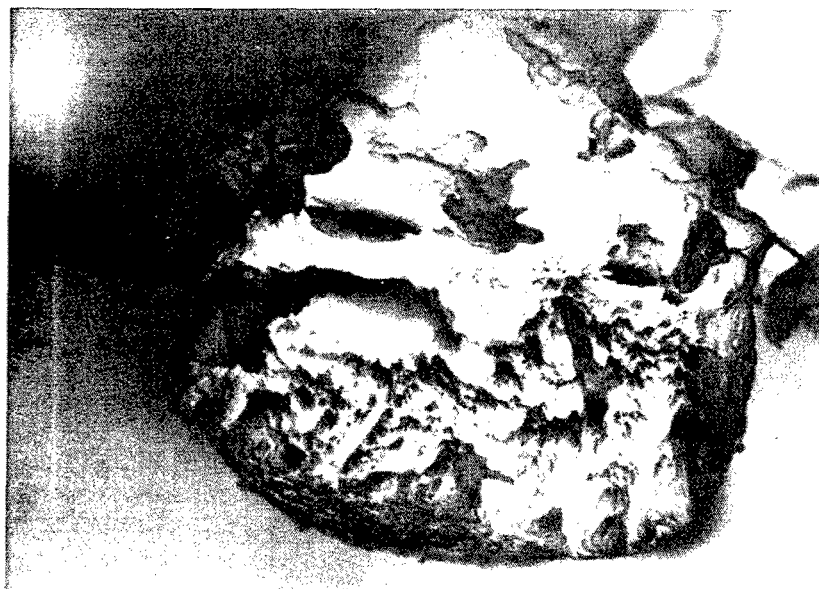


05KV X1960 10U 003 18278 CRO
b. POLYMER 26085-25 (I.V. 2.8)
COAGULATED IN 40/60 MSA/H₂O

FIGURE 17. SEM MICROGRAPHS OF PBO FIBERS

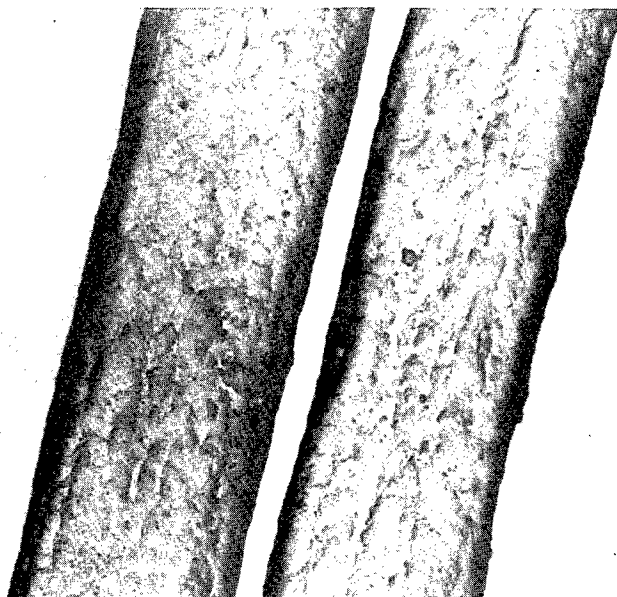


c. POLYMER 26085-25 (I.V. 2.8)
COAGULATED IN 30/70 MSA/H₂O



05KV X3360 100 003 18278 CRO
d. POLYMER 26085-25 (I.V. 2.8)
COAGULATED IN 40/60 MSA/H₂O

FIGURE 17. SEM MICROGRAPHS OF PBO FIBERS



10KV X1000 10U 002 17278 CRC

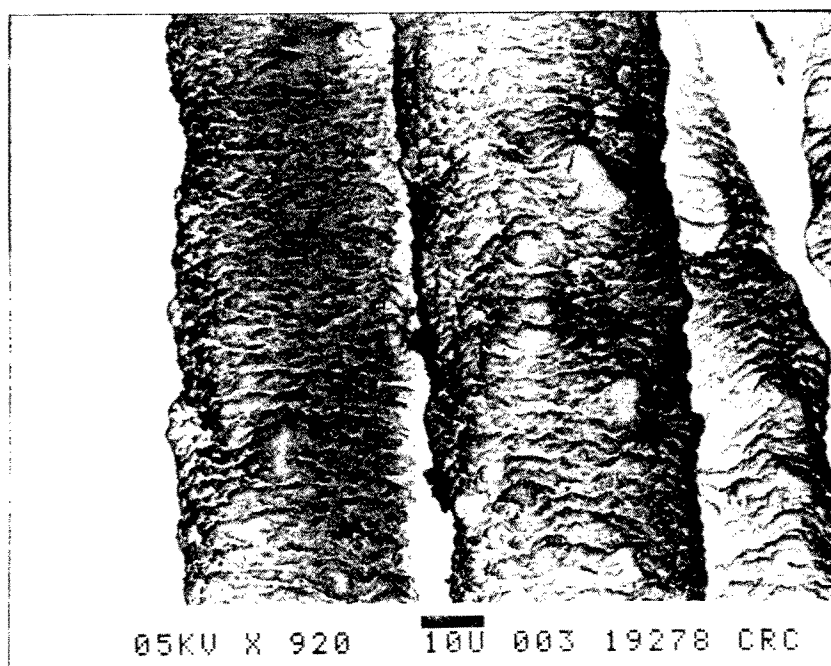
- e. POLYMER 26085-25 (I.V. 2.8)
COAGULATED IN 50/50 MSA/H₂O



20KV X1210 10U 002 20278 CRC

- f. POLYMER 26085-25 (I.V. 2.8)
COAGULATED IN 70/30 MSA/H₂O

FIGURE 17. SEM MICROGRAPHS OF PBO FIBERS

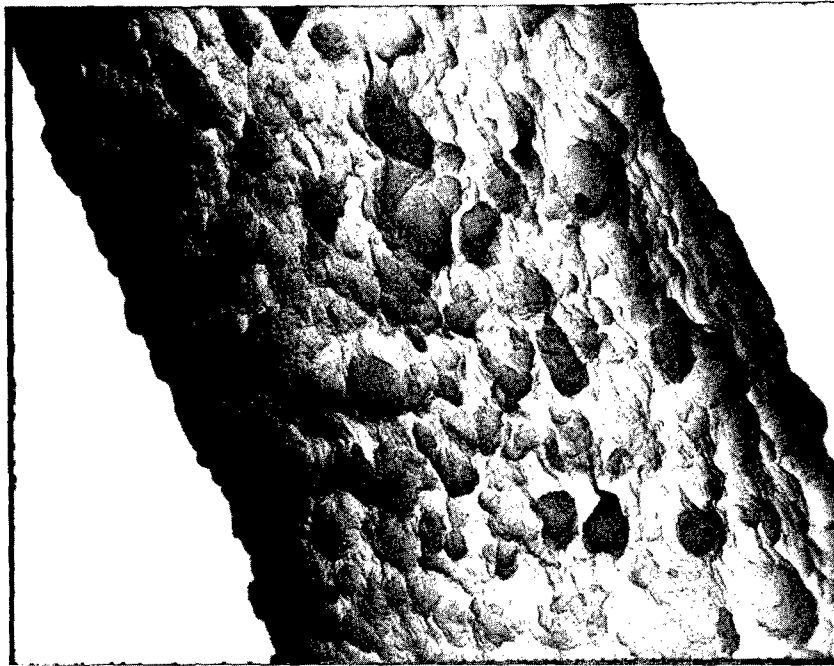


g. POLYMER 26085-25 (I.V. 2.8)
COAGULATED IN 0/100 MSA/H₂O

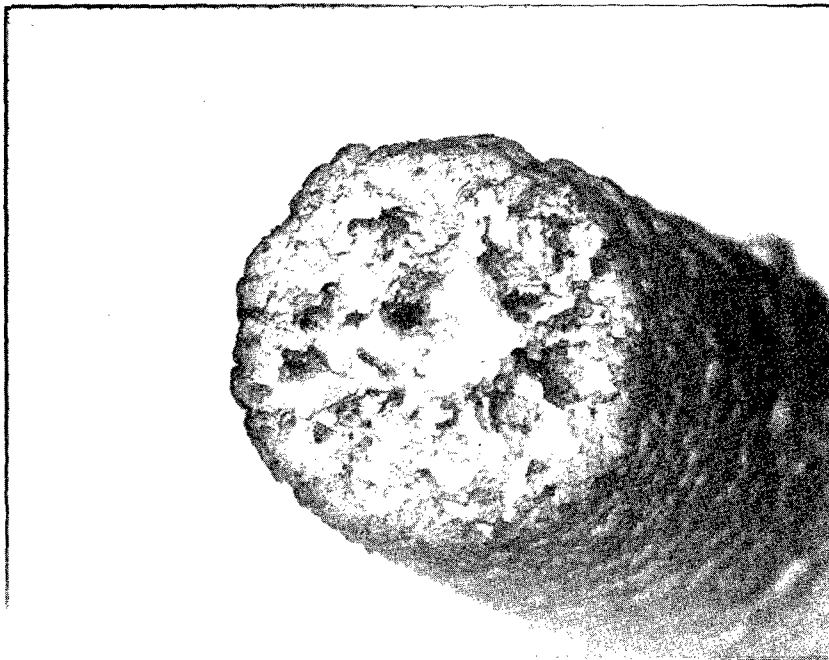


h. POLYMER 26085-25 (I.V. 2.8)
COAGULATED IN 90/10 MSA/H₂O

FIGURE 17. SEM MICROGRAPHS OF PBO FIBERS

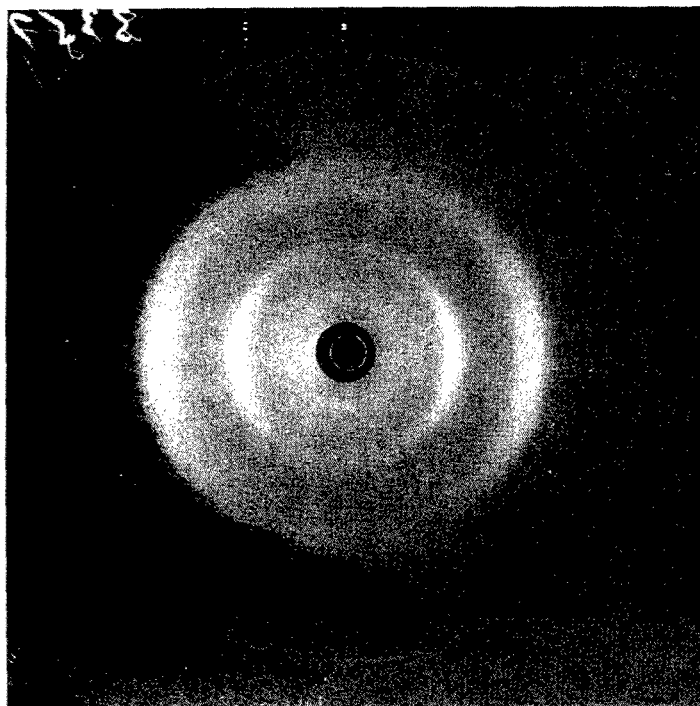


i. POLYMER 26085-23 (I.V. 1.9)
 H_2SO_4 DOPE COAGULATED IN H_2O

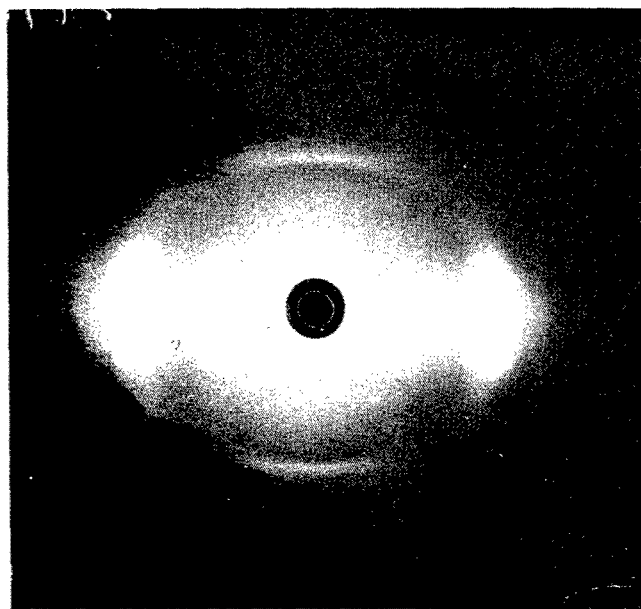


j. X-SECTION OF i

FIGURE 17. SEM MICROGRAPHS OF PBO FIBERS



a. FIBER 26085-16-2 PREP'D FROM
TEREPHTHALIC ACID



b. FIBER 26085-25-1 BEFORE HEAT-DRAWING PREP'd
FROM TEREPHTHALOYL DICHLORIDE, PKV 50,
MAMP 100, EXPOSURE 3 HOURS, RADIATION CuK_α

FIGURE 18. X-RAY DIFFRACTION PATTERN OF WET SPUN
PBO FIBERS

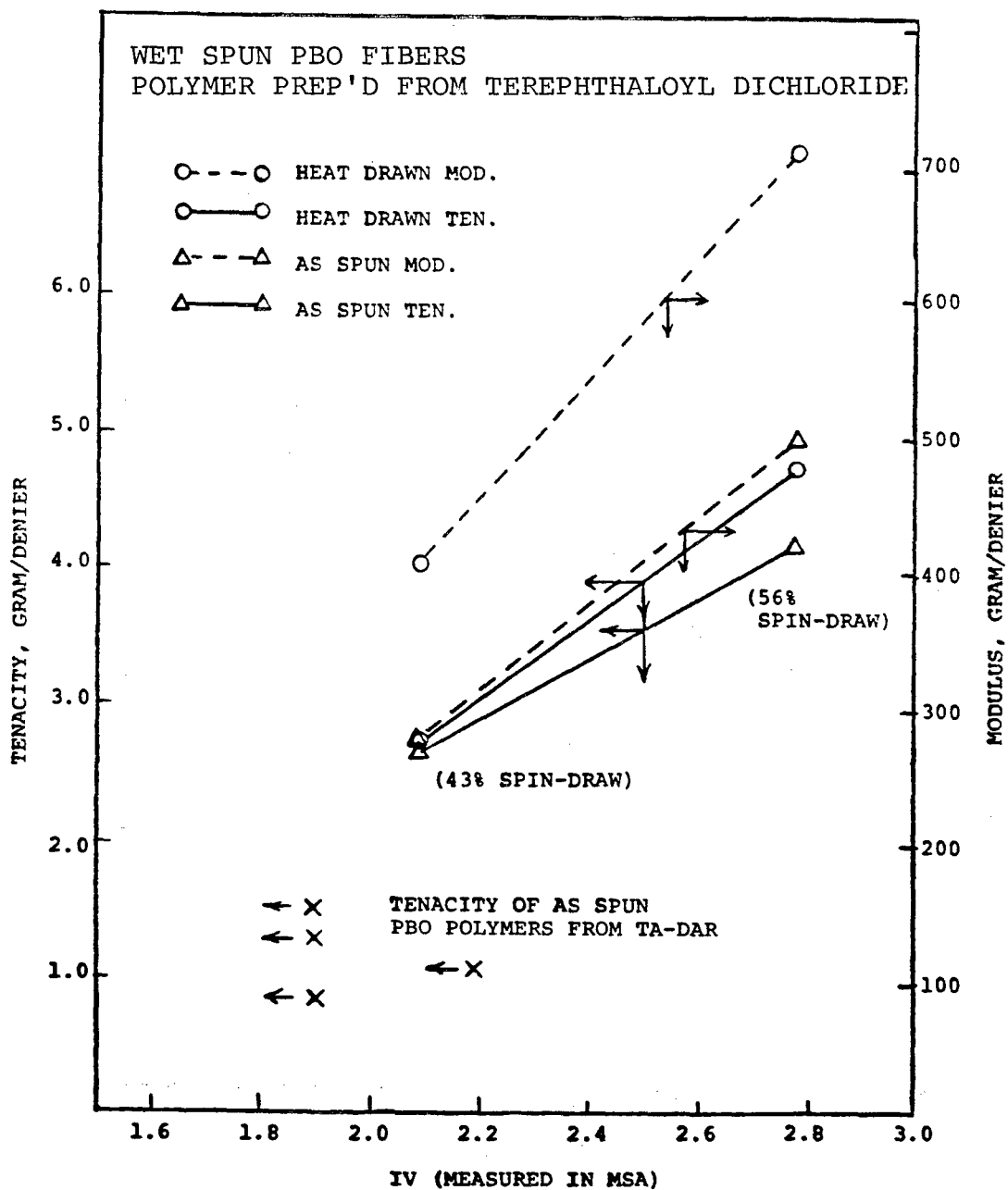


FIGURE 19. TENACITY AND MODULUS VS POLYMER I.V.

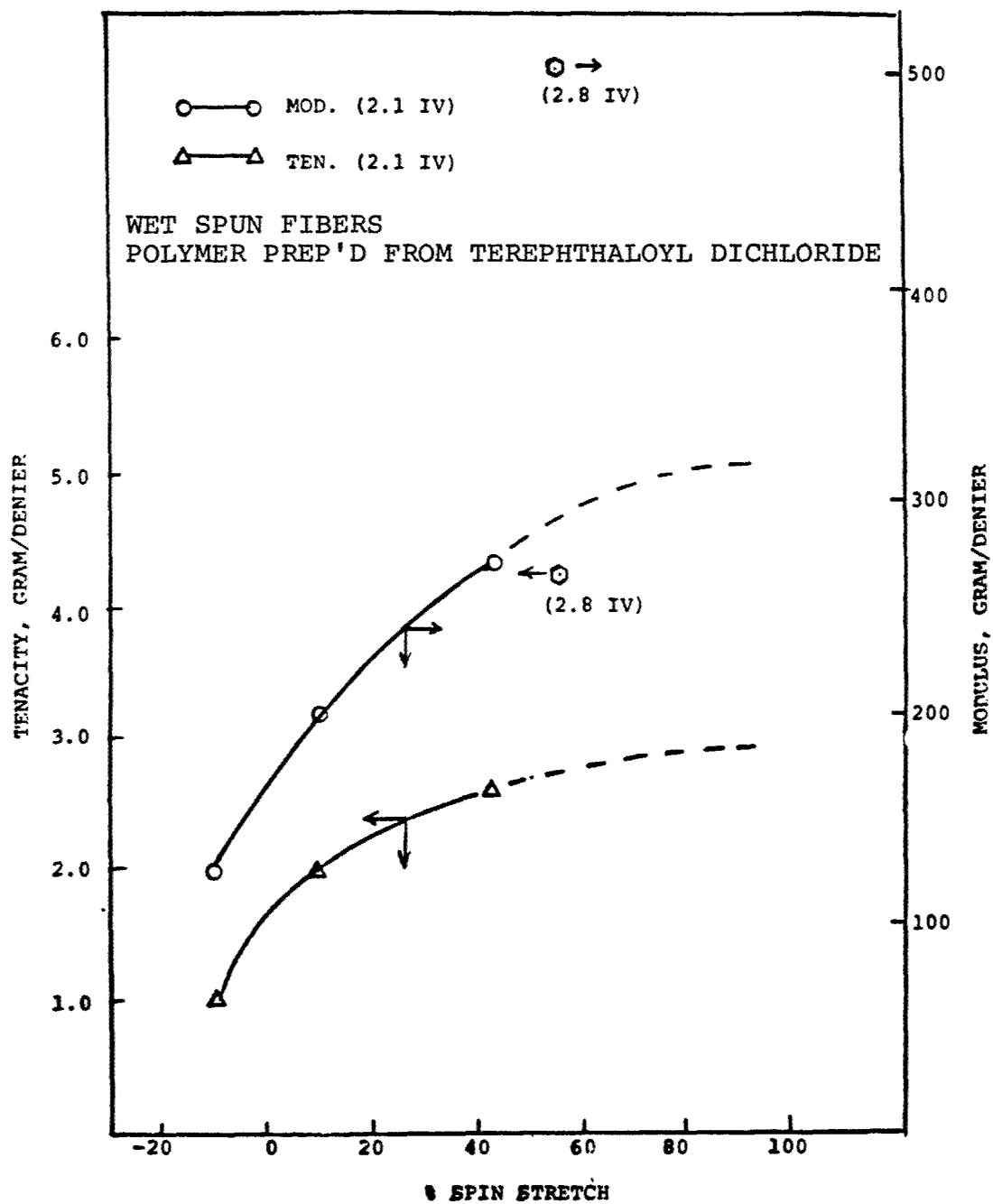


FIGURE 20. FIBER PROPERTIES VS SPIN DRAW RATIO

2. PBT Fabrication

Three batches of poly-(para-phenylenebenzobisthiazole) (PBT) (65gm total, I.V. 14, 18 and 23) were received from AFML (Table XIII). The preparative method for PBT is described elsewhere (3).

a. PBT Dope Preparation and Characterization

The PBT dopes (mostly 9.5% solids in 97.5 MSA/2.5 CSA) were prepared under nitrogen in a 200 ml glass flask at a temperature between 80 to 85°C in a manner similar to that previously described for PBO dope preparation.

b. Fabrication and Properties of PBT Fiber

Due to limited polymer availability, a new spinning apparatus requiring only 50 ml for a full charge and 15 ml dead volume was made of Hastelloy C, and used for the PBT spinning (Figure 21). A tantalum jet, 5 x 100 μ m was used throughout the experiments. Unlike the PBO, the PBT dopes (9.5% solids in 97.5/2.5 MSA/CSA) prepared from the I.V. 14 and 18 polymers had strong cohesive strengths and were successfully dry-jet wet spun. Spin draw ratios up to 4.0 with good spinning continuity were demonstrated. The fiber properties are given in Table XIV. The I.V. 18 polymer showed better spinnability and higher fiber properties. As-spun properties of 9.3 g/d tenacity, 1011 g/d modulus and 2.9% elongation were obtained. After heat-treating, the properties were 12.3 g/d tenacity, 1527 g/d modulus and 0.9% elongation.

Of the spinning variables evaluated, (MSA concentration in the coagulation bath, air gap, spin draw ratio), the SDR showed the strongest effect on as-spun fiber properties. As the SDR increased, the modulus increased more than did the tenacity. Three levels of MSA concentrations, (25, 37.5, 500 in water) were evaluated with the 50% bath yielding the best overall properties. The air gap (6, 13, 19mm) (0.25, 0.5, 0.75 in.) showed no significant effect. The effect of SDR on the as-spun fiber tenacity and modulus is given on Figure 22.

Attempts to spin I.V. 23 polymers were not successful. The 9% dope contained gel-like undissolved particles and could not be filtered through 50 μ m filter even under conditions as severe as 27.6 MPa (4000 psi) and 130°C. Such particles were also observed in a 0.5% solids solution in MSA. The polymer was regenerated by reprecipitation of a 0.5% solids solution but its I.V. dropped to 6 from 23. The regenerated polymer was not dry jet-wet spinnable because the solution lacked sufficient cohesive strength. When wet spun, it yielded fibers with 1.5 g/d tenacity, 0.6% elongation and 24 g/d modulus, the levels of properties observed for PBO fibers.

When the as-spun fibers were heat-treated in a nitrogen atmosphere at temperatures varying from 425°C to 525°C, the highest properties (Tables XV & XVI) were obtained at 500°C. The heat-treatment increased the modulus more than it did the tenacity. (Figures 23 & 24).

The PBT fiber spun from the I.V. 18 polymer was evaluated for the effect of gauge length on properties (6, 13, 25, 76mm) (0.25, 0.5, 1.0 and 3.0 in.). The tenacity decreased as the grab length increased due to the presence of flaws in the fiber. SEM micrographs show evidence of microvoids in the fiber. The magnitude of the tenacity decline with gauge length is quite similar to that of carbon or graphite fibers (Figure 25). The data is displayed in Table XVII.

Flammability was measured on the I.V. 18 PBT fiber (Table XVIII). The PBT fiber is intrinsically non-combustible in air (i.e. will not maintain a flame without heat input from an extraneous source). The critical oxygen concentration of PBT fiber is 35.7 TW/22.6 BW. A critical oxygen index of 32.5 TW/21 BW signifies noncombustibility. By comparison, Nomex (26.7 TW/18.0 BW) is flammable and PBI (46.5TW/28.0 BW) is not.

Mass spectral analysis showed that as-spun PBT fibers (coagulated, washed, neutralized, washed and dried) give off SO_2 at 200-300°C. The source of the SO_2 may be residual acid or the salt formed during the neutralization or even the polymer itself (incompleted ring closure, etc.). Such contaminants can lower the fiber mechanical properties, especially at elevated temperatures. Various means of washing the fiber were tried to identify the SO_2 source. Normally, the PBT bobbins (taken up after coagulation and washing) are

neutralized without delay in a NaHCO_3 /water bath for at least 2 hours, washed overnight in deionized water and dried. In the tests, one bobbin was washed in the water overnight, then neutralized, washed again and dried. Another bobbin was washed in the water for 2 days without the neutralization. The mass spec data of the three samples, including a normally processed control, all showed SO_2 traces of comparable magnitude. The results suggest that the neutralization step or the salt (if any) is not the only source of SO_2 . More work is obviously required to identify the origin of this effluent.

Scanning electron micrographs of even the best PBT fibers so far showed signs of internal voids in them. Surface flaws and internal voids can lower fiber mechanical properties, especially at high temperatures and the elimination or reduction in the number of such flaws will improve the fiber properties significantly.

c. Fabrication and Properties of PBT Ribbon

Due to the limited polymer supply, no film casting experiments were conducted. However, PBT ribbons were successfully extruded through 6mm x 0.25mm (0.25 in. x 10 mil) and 13mm x 0.25mm (0.5 in. x 10 mil) slit jets from a 9.5% solids dope made with the I.V. 18 polymer. The extrusion continuity was good.

The ribbons shrank to narrow widths (1.6mm to 3mm) (1/16 to 1/8 in.) during the coagulation and drying mostly due to the low solids content in the dope. The best ribbon properties obtained in this first trial are 272 MPa (39,400 psi) tenacity, 0.6% elongation and 19.3 GPa (2.8×10^6 psi) modulus. (See Table XIX).

TABLE XIII

PBT POLYMER SUPPLY
(SOURCE: SRI)

<u>CODE</u>	<u>I.V.</u> <u>(dl/g)</u>	<u>QUANTITY</u> <u>(GRAMS)</u>
2122-53	14	29
2122-57	18	25
2122-62B	23	<u>13</u>
TOTAL		67

TABLE XIV A

SPINNING CONDITIONS^a

<u>SAMPLE SPIN NO. 27554-</u>	<u>POLYMER NO.</u>	<u>COAG. BATH COMP. (MSA/H₂O)</u>	<u>SPIN DRAW RATIO</u>	<u>AIR GAP (Inch)</u>
-6-1	2122-53 ^b	37.5/62.5	---	0.5
-2			2	0.5
-3			2	0.5
-4		50/50	---	0.25
-5		25/75	---	0.5
-6			---	0.5
-9-1	2122-57 ^c	50/50	2	0.5
-2			2	0.75
-3			2	0.25
-4			---	0.5
-5			3.9	0.5
-6		37.5/62.5	16	0.5
-7			2	0.5
-8			DB	0.25
-9		25/75	DB	0.75
-10			2	0.5
-11			2	0.5
-12			DB	0.5
-17-1	2122-57 ^c	50/50	2	0.5
-2A			4,2	0.5
-2B			3,4	0.5
-2C			4,2	0.5

^aDope concentration: 9.5% in 97.5% MSA/2.5% CSA
Dope and bath temperature: RT
Jet Velocity: 6.3 mpm.

^bI.V., 14

^cI.V., 18

TABLE XIV B

PBT FIBER PROPERTIES AS DRY JET--WET SPUN

SAMPLE SPIN NO. 27554-	POLYMER NO.	FIBER PROPERTIES (n=10)				
		DPF	ELONG (%)	TEN. (g/d)	TE $\frac{1}{2}$	MODULUS (g/d)
-6-1	2122-53 ^a	5.1	3.9	9.0	17.7	595
-2		4.2	3.8	8.9	17.3	566
-3		4.3	3.2	10.0	18.1	941
-4		4.3	2.9	9.4	16.0	780
-5		8.1	3.7	7.5	14.5	475
-6		6.2	3.2	7.6	13.5	614
-9-1	2122-57 ^b	5.4	3.7	9.1	17.3	749
-2		5.4	3.5	8.8	16.6	741
-3		5.3	3.3	8.5	15.4	720
-4		2.2	1.9	8.9	12.4	1054
-5		3.3	2.9	9.3	15.8	1011
-6		6.5	3.5	8.0	15.0	586
-7		5.2	3.4	8.2	15.1	645
-8		2.4	2.3	8.7	13.1	925
-9		2.9	2.3	9.3	14.2	1073
-10		5.3	2.7	7.0	11.5	591
-11		6.3	3.0	7.4	12.7	555
-12		5.6	2.7	6.8	11.2	591
-17-1	2122-57 ^b	5.4	3.4	9.0		800
-2A		2.4	2.1	9.8		1010
-2B		3.7	2.8	9.2		898
-2C		2.1	2.0	10.3		1170

^aI.V., 14^bI.V., 18

TABLE XV

PROPERTIES OF HEAT-TREATED PBT FIBERS

SPIN NO.	POLYMER NO.	TREAT TEMP (C°)	FIBER PROPERTIES (n=10)				
			DPF	ELONG (%)	TEN. (g/d)	TE _{1/2}	MOD. (g/d)
27754-							
-6-2	2122-53*	None	4.2	3.8	8.9	17.4	566
	"	425	4.1	0.9	10.6	10.1	1330
	"	450	4.1	0.8	10.3	9.2	1320
	"	475	3.9	0.9	11.0	10.4	1340
-6-3	2122-53	None	4.3	3.2	10.0	17.9	941
	"	425	3.6	0.7	7.6	6.4	1100
	"	450	3.8	0.7	9.3	7.8	1350
	"	475	4.3	0.8	11.1	9.9	1450

27754-6-2 : Coagulated in 37.5/62.5 MSA/H₂O; Spin Draw Ratio = 2

27754-6-3 : Coagulated in 50/50 MSA/H₂O; Spin Draw Ratio = 2

*I.V., 14

TABLE XVI

PROPERTIES OF HEAT-TREATED PBT FIBERS

SPIN NO.	POLYMER NO.	TREAT TEMP (C°)	FIBER PROPERTIES (n=10)					DEN. (g/ml)
			DPF	ELONG (%)	TEN. (g/d)	TE _{1/2}	MOD. (g/d)	
27554-								
-9-1	2122-57*	None	5.4	3.7	9.1	17.3	749	1.557
	"	425	4.9	0.9	11.2	10.6	1419	
	"	450	5.2	0.8	9.2	8.2	1319	
	"	475	5.5	0.9	9.6	9.1	1366	1.581
	"	500	4.7	0.7	9.4	7.9	1424	
	"	525	5.0	1.0	12.3	12.3	1458	
-9-5	2122-57	None	3.3	2.9	9.3	15.8	1011	
	"	425	3.0	0.9	12.0	11.4	1568	
	"	450	3.2	0.8	10.4	9.3	1421	
	"	475	3.1	0.8	11.1	9.9	1497	
	"	500	3.1	0.9	12.3	11.7	1527	
	"	525	3.0	0.8	11.9	10.6	1602	
-9-7	2122-57	None	5.2	3.4	8.2	15.1	645	
	"	425	4.8	0.7	8.3	6.9	1277	
	"	450	4.5	0.7	8.5	7.1	1260	
	"	475	4.5	0.6	8.0	6.2	1395	
	"	500	4.5	1.0	10.9	10.9	1283	
	"	525	4.5	0.9	11.8	11.2	1469	

27554-9-1 : Coagulated in 50/50 MSA/H₂O; Spin Draw Ratio = 2

27554-9-5 : Coagulated in 50/50 MSA/H₂O; Spin Draw Ratio = 3.9

27554-9-7 : Coagulated in 37.5/ 62.5 MSA/H₂O; Spin Draw Ratio = 2

*I.V., 18

TABLE XVII

GAUGE LENGTH VS PBT FIBER PROPERTIES

<u>FIBER CODE</u>	<u>GAUGE LENGTH (inches)</u>	<u>DPF</u>	<u>TEN. (g/d)</u>	<u>ELONG. (%)</u>	<u>MOD. (g/d)</u>
27554-9-5 *	0.25	3.2	12.3	1.7	959
"	0.50	3.1	12.3	1.1	1368
"	1.0	3.0	12.1	0.9	1595
"	3.0	3.2	7.7	0.5	1522

*I.V., 18

TABLE XVIII

FIBER FLAMMABILITY
CRITICAL OXYGEN CONCENTRATION

	<u>COC (TW)</u>	<u>COC (BW)</u>
PBO	36.1	22.8
PBT	35.7	22.6
PBI	46.3	28.0
NOMEX	26.5	18.0

Note: COC-TW 32.5 and COC-BW 21 signifies a material which is "intrinsically non-combustible".

TABLE XIX

PBT RIBBON PROPERTIES

RIBBON CODE	SLIT DIE	HEAT TREAT	TENACITY		ELONG. (%)	MODULUS	
			(MPa)	(PSI)		(GPa)	(PSI)
27554-15-2	1/4" x 10 mil	No	231	33,500	6.5	8.9	1.29 x 10 ⁶
27554-15-2	1/4" x 10 mil	Yes	165	24,000	1.5	10.4	1.51 x 10 ⁶
27554-15-3	1/2" x 10 mil	No	267	38,700	5.0	11.2	1.62 x 10 ⁶
27554-15-3	1/2" x 10 mil	Yes	272	39,400	1.6	19.4	2.82 x 10 ⁶

2% Strain rate

Dried widths 1/16 to 1/8"

Note: Unless otherwise stated, the fibers were tested at room temperature and 1 inch gauge length.

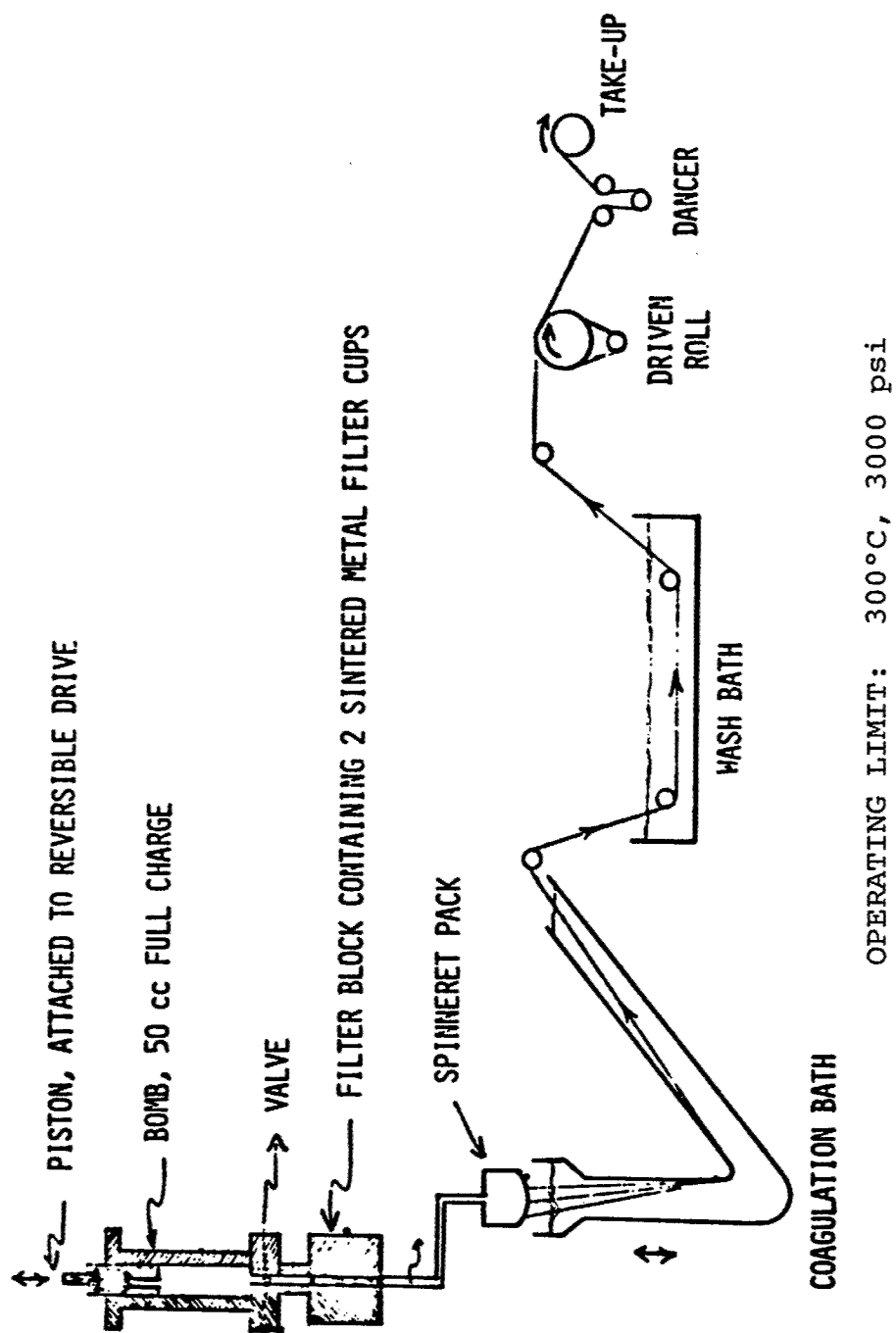


FIGURE 21. SCHEMATIC DIAGRAM OF PBT SPINNING APPARATUS

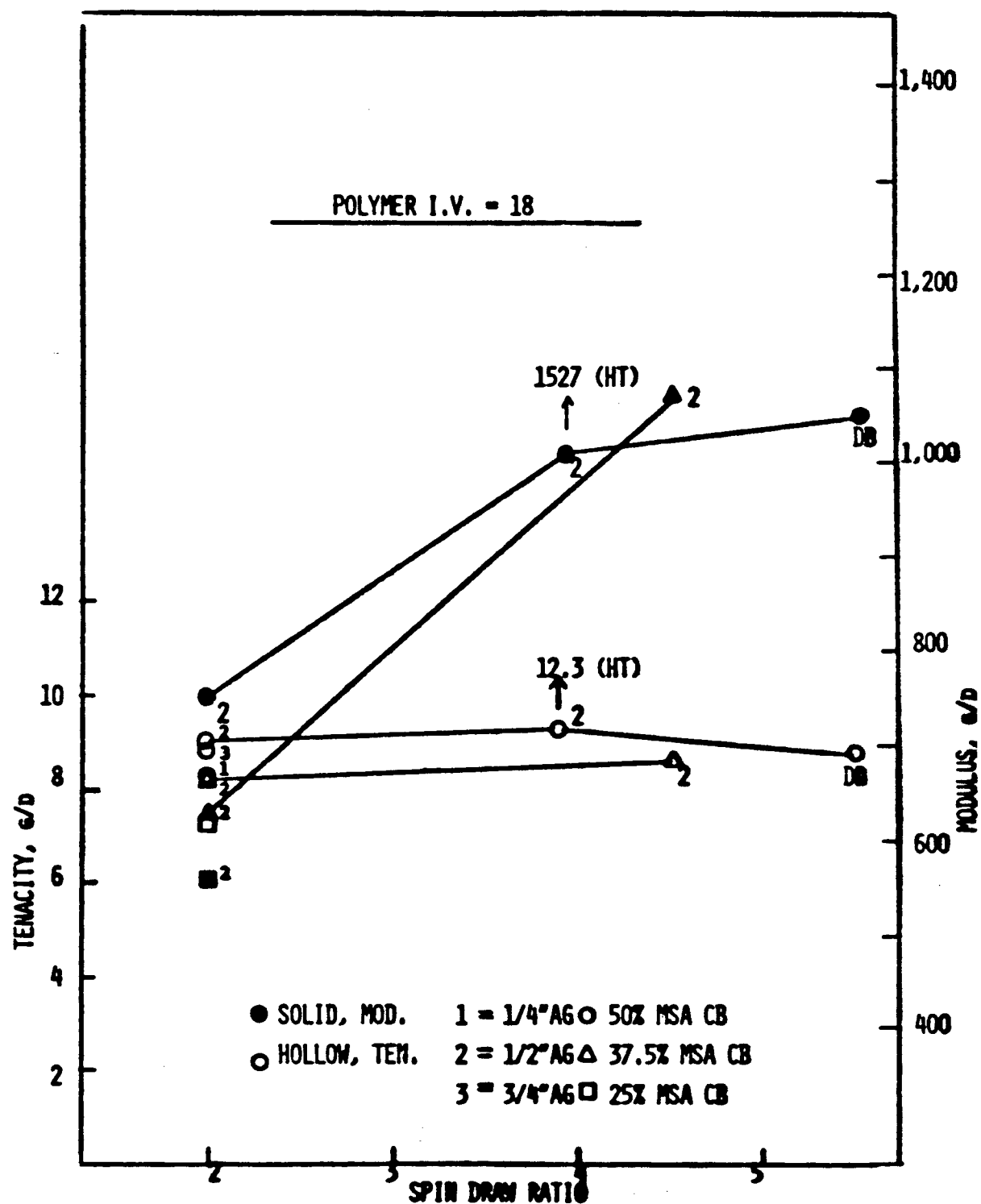


FIGURE 22. AS-SPUN PBT FIBER PROPERTIES VS. SPIN DRAW

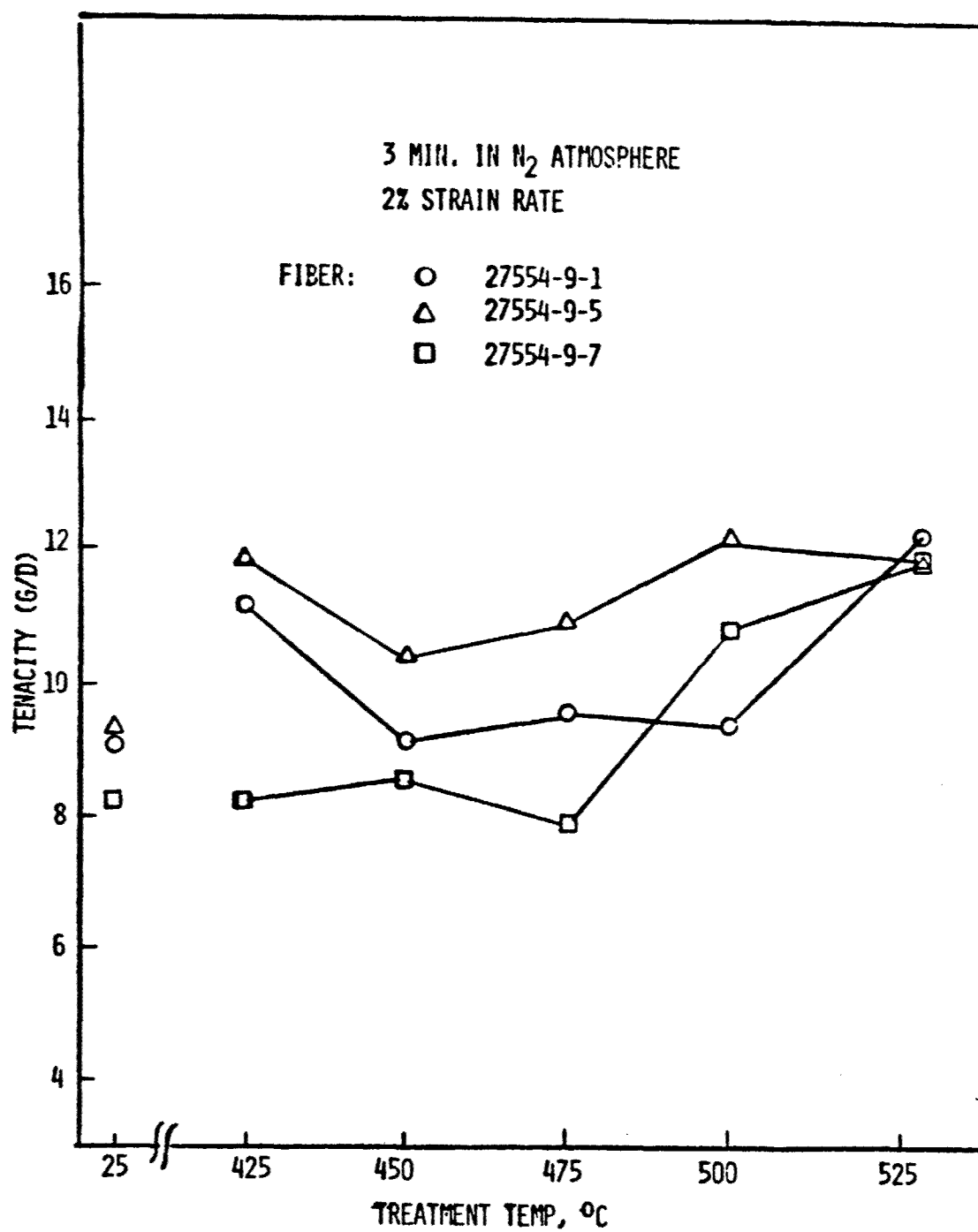


FIGURE 23. EFFECT OF HEAT TREATMENT ON PBT FIBER TENACITY

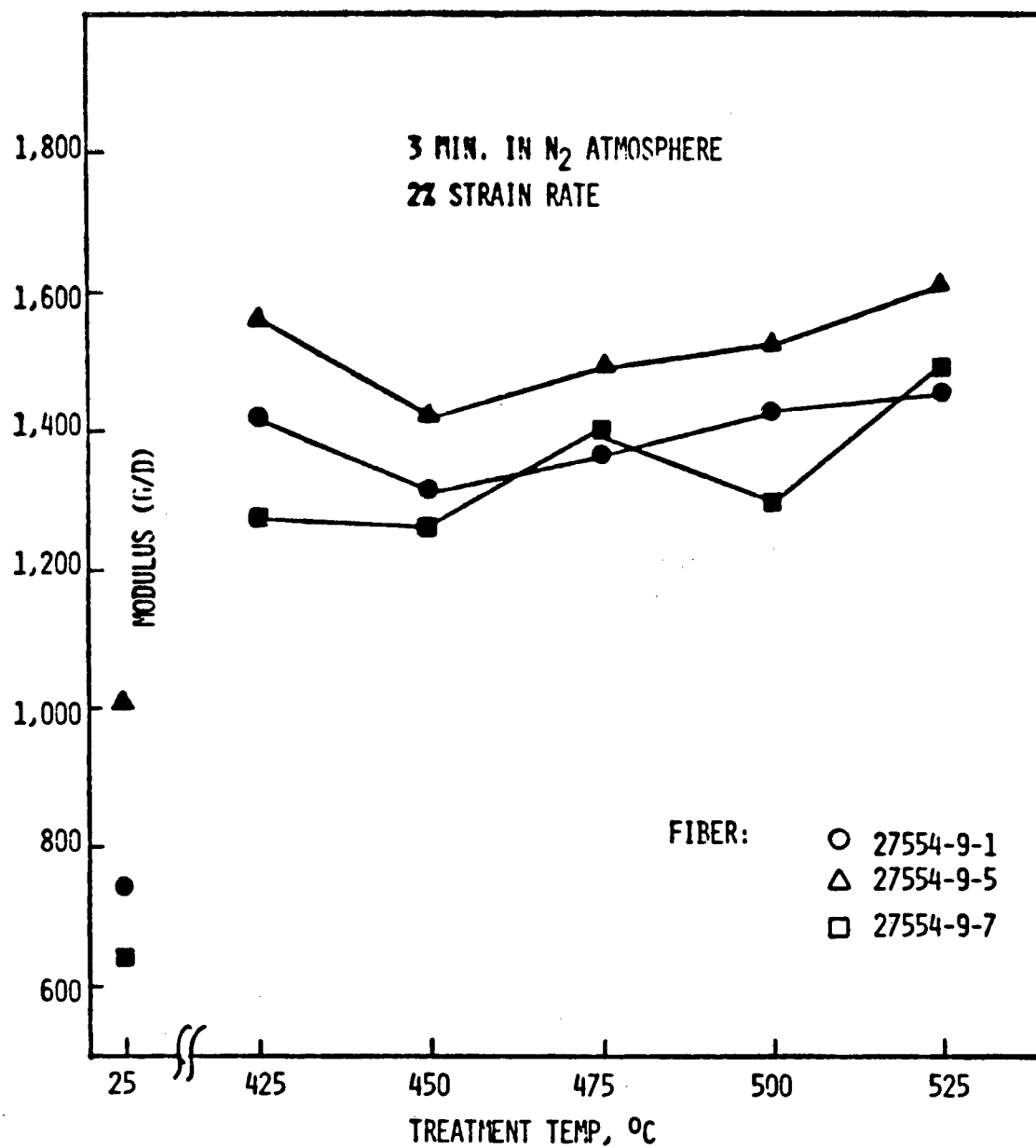


FIGURE 24. EFFECT OF HEAT TREATMENT ON PBT FIBER MODULUS

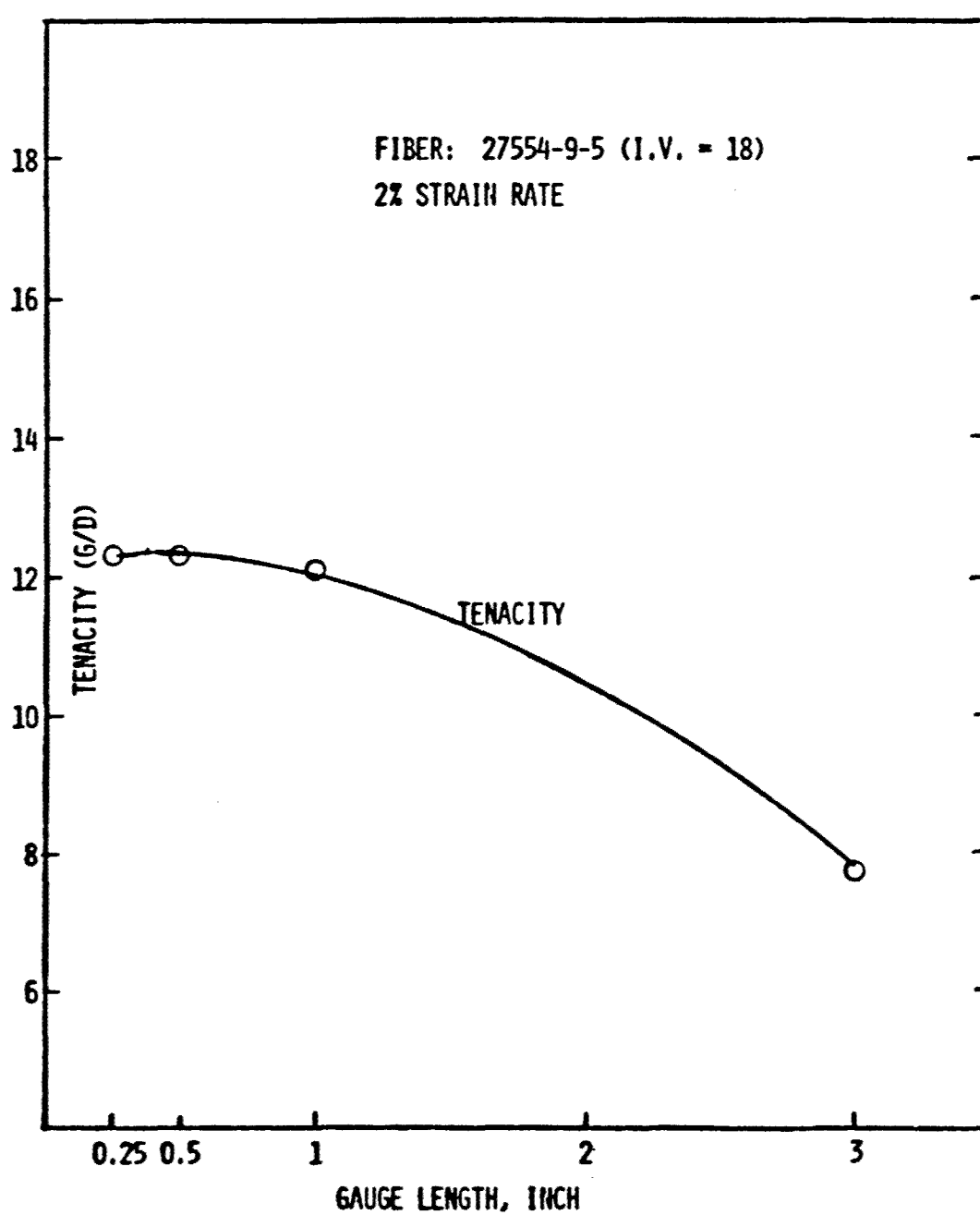


FIGURE 25. EFFECT OF GAUGE LENGTH ON PBT FIBER TENACITY

SECTION III

EXPERIMENTAL

IR spectra were measured on a Nicolet 7199 Fourier Transform Infrared Spectrometer in the phases noted. NMR spectra were measured on a Varian EM 360 and CMR spectra were measured on a Varian CFT-20. Microanalytical work was performed by Schwarzkopf Microanalytical Laboratory. All inherent viscosities were determined at 25°C using methanesulfonic acid as solvent and at a polymer concentration of 0.2 g/100 ml.

1. Resorcinol diacetate

In a 20-gallon glass-lined reactor with agitator, distillation column and condenser, were charged 43.6 kg (96 lbs) of acetic anhydride, 18 kg (40 lbs) of resorcinol and 222.4 grams of sodium acetate. The reactor was purged with nitrogen. The reaction mixture was heated to 137°C. The acetic acid by-product (18.9 kg) (41.5 lbs) was distilled and collected over 6 hours. The reaction temperature rose gradually to 145°C by the end of the distillation. The reaction temperature was then raised to 200°C over 4.5 hours to collect an additional 9 kg (20 lbs) of acetic acid and excess acetic anhydride. The crude resorcinol diacetate weighed 33 kg (72.9 lbs). NMR analysis showed a 97:3% ratio of resorcinol diacetate and resorcinol monoacetate.

Resorcinol diacetate was distilled through a distillation tower (13cm x 6m) (5 in. x 20 ft.) or through a Nester/Faust Spinning band.

Another batch was prepared to yield 33.2 kg (73.1 lbs) of resorcinol diacetate.

2. 4,6-Dinitroresorcinol

This compound was prepared in small batches by the nitration of diacetylresorcinol according to the following general procedure.

To a mixture of 1300 ml of fuming nitric acid and 1300 ml of concentrated nitric acid maintained at a designated temperature with an ice or water bath was added 500 g (2.6 mole) of diacetylresorcinol in 30 min. The reaction mixture was stirred at the designated temperature and time period, and then poured into ice water. The precipitate was collected by filtration and washed with water. The solid was digested with boiling water and filtered. Recrystallization of the insoluble material from ethyl acetate (8.5 l) gave 4,6-dinitroresorcinol with a melting point and yield described in Tables I and II.

Evaporation of ethyl acetate on a rotary evaporator gave crude styphnic acid. Recrystallization from toluene (1.0 l) provided yellow plates of pure 2, 4, 6-trinitroresorcinol, mp 178°C and T_x 98°C. A total of 18 batches at the scale described above were run, with the results shown in Tables I and II.

3. Reduction of 4,6-Dinitroresorcinol: Preparation of 4,6-Diaminoresorcinol Dihydrochloride

a. Parr Hydrogenator

This procedure was provided by AFML. In a Parr bottle is placed 10 g of 4,6-dinitroresorcinol, 1 g of 10% palladium on charcoal, wet and 275 ml of 6.2% hydrochloric acid (40 ml concentrated hydrochloric acid and 235 ml water). The bottle is purged with nitrogen, placed in a Parr Pressure Reaction apparatus, purged with hydrogen and then shaken under approximately 345 kPa (50 psi) of hydrogen for 26 hr. The reaction mixture is then filtered through a 50mm pad of Celite (using a glass frit which can be stoppered to minimize air contact) into 800 ml of cold, stirring tetrahydrofuran which had been saturated with hydrogen chloride gas. (Gaseous hydrogen chloride is bubbled into the tetrahydrofuran for 15 min. while stirring and cooling with an ice-water bath.) The light pink precipitate is allowed to stand in a refrigerator for 1 hour and is then collected by filtration.

The dihydrochloride is recrystallized by dissolving in 150 ml of water containing 1 g of stannous chloride and heating to boiling for 5 min. The cloudy mixture is gravity filtered while hot and, with stirring, 150 ml of concentrated hydrochloric acid is added to the filtrate all at once.

Crystallization begins rapidly and is completed by cooling in an ice-water bath. The crystals were filtered and dried at 60°/0.1 torr overnight to obtain 72.3-77% yield of 4,6-diaminoresorcinol dihydrochloride.

b. Reduction of 4,6-Dinitroresorcinol with Tin and Hydrochloric Acid

In a flask under nitrogen were placed 10.65 grams (0.05 mole) of 4,6-dinitroresorcinol, water (300 ml) and concentrated hydrochloric acid (900 ml). The resulting mixture was heated to 90°C. Tin sheets (30 grams) were added over 2.5 hours. The hot solution (100°C) was filtered to remove excess tin. The filtrate was allowed to cool to room temperature to precipitate the 4,6-diaminoresorcinol dihydrochloride. The product was filtered. The mother liquor was chilled in an ice-bath to obtain a second crop of the product. Recrystallization of the product, as described under 3.a, provided 9.8 grams of 4,6-diaminoresorcinol dihydrochloride. The results of several batches prepared are summarized in Table III.

The following procedure was used for a large scale reduction of 4,6-dinitroresorcinol with tin and hydrochloric acid.

In a 20 gallon glass-lined reactor fitted with a vent to atmosphere, and an acid scrubber which is connected to a sodium hydroxide neutralization tank, were charged under nitrogen 40 l (10.7 gal) of concentrated reagent grade hydrochloric acid, 13.6 l (3.6 gal) of deionized water, and 479.25 grams of 4,6-dinitroresorcinol.

The reaction mixture was heated to 90°C and maintained at that temperature throughout the reaction period. Tin was added at the rate of 120 grams every 4 minutes until 2700 grams of tin were consumed. The addition of tin was complete in 1.5 hours. The reaction mixture was maintained at 90°C for an additional hour, and cooled to ambient temperature. The solid (497.4 g, 97.5% yield), crude product was filtered under nitrogen, and purified as described earlier to obtain 380 grams (74.6%) of 4,6-diaminoresorcinol. The results are given in Table III.

4. Preparation of Poly[1,7-Dihydrobenzo (1,2-d:4,5-d') - Dioxazole-2,6-diyl]-1,4-Phenylene] (PBO)

a. From Terephthalic Acid and 4,6-Diaminoresorcinol Dihydrochloride

A modified Air Force Materials Laboratory procedure was used, as described generally below:

Polyphosphoric acid (115%) (PPA) was acquired from FMC or MCB, and was deoxygenated by heating under nitrogen at 150°C overnight. The polymerizations were carried out under nitrogen at 1.219% or 1.817% concentrations in 2-liter or 5-liter resin flasks, equipped with a spiral agitator. Agitators made of glass (turbine type), Hastelloy B, teflon coated steel, or tantalum were available.

4,6-Diaminoresorcinol (100.99 g, 0.474 mole) and pulverized terephthalic acid, fiber grade (78.75 g, 0.474 mole) were placed under nitrogen in a 5-l resin flask. The deoxygenated PPA (6 kg) was transferred under nitrogen into the flask. The mixture was stirred at 60°C for 16 hours, and then at 90°C for 5 hours to dehydrochlorinate. The following heating stages were used for the polymerization:

130°C for 3 hours
150°C for 16 hours
170°C for 3 hours
185°C for 3 hours
200°C for 24 - 48 hours

At the end of the polymerization, the polymer was scooped out of the flask and precipitated into 11.4 l (3 gal) of methanol. The polymer was filtered, washed with methanol and dried at 100°C.

The polymer was dissolved in methanesulfonic acid and filtered. The filtrate was poured into methanol to precipitate the polymer. The polymer was filtered, washed consecutively with water, dilute ammonium hydroxide, water and finally methanol, before being dried at 100°/0.1 torr. Results are shown in Tables IV, V and VI.

b. From Terephthaloyl Dichloride and
4,6-Diaminoresorcinol Dihydrochloride

The same procedure as described in Section 3.a was used with one exception. The terephthalic acid was

replaced with terephthaloyl dichloride. Results are given in Table VII.

5. Preparation and Spinning of Dopes

The PBO and PBT dopes were prepared in a 200 ml glass flask fitted with a helical agitator (Hastelloy B) and immersed in an 85°C oil bath. The polymer granules were added slowly to the solvent at 85°C. The agitator speed was controlled between 45 to 50 rpm. To protect the dope from atmospheric moisture, the flask was maintained under a nitrogen blanket at all times. The dope was maintained hot until all undissolved particles disappeared. The test counts of undissolved polymer or foreign materials in the dope were conducted with an optical microscope (up to 500 X). Methanesulfonic acid (Eastman 98% min. Assay) and chlorosulfonic acid (MCB practical grade) were used as solvents. The chlorosulfonic acid was added to remove moisture contaminants, if any, by forming highly volatile HCl.

A wet spinning apparatus developed previously for research on poly-(p-phenyleneterephthalamide) was used for the PBO spinning. The dope is metered by a piston connected to a ram. The ram speed was accurately controlled by a variable speed motor with a micro-meter (Figure 26). The dope was then filtered in 2 stages before it reached the spinneret. Temperatures and pressures at various key points are continuously indicated and recorded. The operating limits

of the spinning assembly is 300°C and 21 MPa (3000 psi). The apparatus requires 200 ml for a full charge and its dead volume is 25 ml. Tantalum spinnerets of 10 x 50 μ m, 10 x 75 μ m and 10 x 100 μ m were initially evaluated. Due to low filament strength and the low solids level in the dope, most spinning, except the initial evaluation, was done with the 10 x 100 μ m spinneret. The coagulation bath trough was 56 cm (22 in.) long.

Because only 67 gm of PBT was available, a smaller spinning assembly was fabricated. This apparatus was constructed of a more acid resistant material (Hastelloy C). In contrast to the other spinning instrument, this required only 50 ml full charge, with 15 ml dead volume. A V-tube coagulation bath was used, 56 cm (22 in.) long. The operating principle of the new 1/4 scale apparatus was the same as the initial one. For ribbon spinning, slit jets 6mm x 0.25mm (0.25 in. x 10 mil) and 13mm x 0.25mm (0.5 in. x 10 mil) were used.

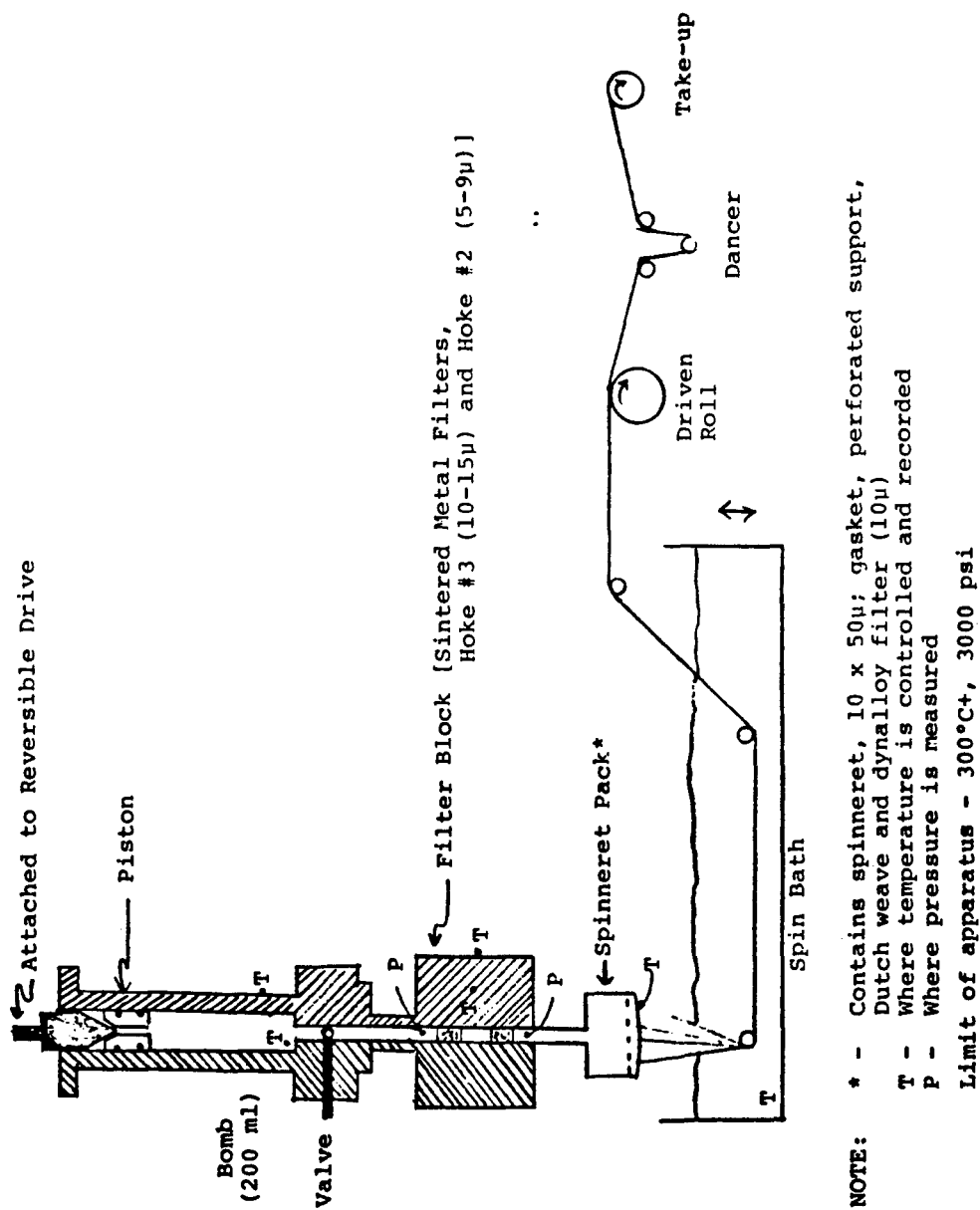


FIGURE 26. SCHEMATIC DIAGRAM OF PBO SPINNING APPARATUS

SECTION IV

CONCLUSIONS AND RECOMMENDATIONS

A. PBO

PBO polymer could only be wet spun. Because of low dope cohesive strength (low I.V.), it could not be dry-jet-wet-spun. The spinnability of the PBO prepared from terephthaloyl dichloride and diaminoresorcinol was slightly better than that for the PBO prepared from terephthalic acid and diaminoresorcinol. The best overall fiber properties demonstrated for PBO were 4.8 g/d tenacity, 0.7% elongation and 711 g/d after heat treatment. Final denier of this sample was 4.8. The dope of PBO from the dichloride could be spin stretched up to about 45% but that of the polymer from terephthalic acid could not be spin stretched.

A PBO ribbon was successfully extruded through a 6mm x 0.25mm (0.25 in. x 10 mil) slit jet but it shrank to 3mm (1/8 in.) during the coagulation and drying. The as-spun ribbon properties were 346 denier, 103 MPa (15,000 psi) tenacity, 7.6 GPa (1.1×10^6 psi) modulus and 1.6% elongation. When PBO films were cast onto a glass plate, they cracked and split badly due to excessive shrinkage during the coagulation and drying. Various coagulation baths and coagulation geometry were investigated to minimize this but all attempts

failed. The PBO fiber properties as demonstrated in this work are considered to be relatively low. It appears that higher I.V. PBO polymers are necessary to attain significant improvements in spinnability and fiber properties.

B. PBT

The PBT polymers used had I.V.'s of 14, 18 and 23. The I.V. 14 and 18 polymers dry-jet wet spun well, and spin draw ratios (SDR) as high as 4.5 with good spinning continuity were achieved. Fiber properties of 12.3 g/d tenacity, 0.9% elongation and 1527 g/d modulus were measured. The 1527 g/d modulus is impressive for an organic fiber. Of the spinning variables tested (air gap, coagulation bath, SDR) the SDR has the strongest effect on the as-spun fiber properties. The data suggests that the higher the as-spun fiber properties, the higher the heat-treated properties. I.V. 18 polymer yielded higher fiber properties than I.V. 14 polymer. On the other hand, I.V. 23 polymer contained insoluble gel-like materials and could not be spun. The gauge length data and SEM showed that even the best fibers appear to contain surface flaws and internal voids. Mass spec data showed the evolution of SO_2 between 200 to 300°C. It is probable that if the flaws and contaminants are eliminated (or minimized), the fiber properties may increase significantly.

PBT and PBO fibers are intrinsically non-combustible, with the flammability being better than Nomex but not quite as good as PBI.

PBT ribbons were successfully extruded using 6mm x 0.25mm (0.25 in. x 10 mil) and 13mm x 0.25mm (0.5 in. x 10 mil) slit jets. The best overall ribbon properties obtained were 272 MPa (39,400 psi) tenacity, 1.6% elongation and 19.3 GPa (2.82×10^6 psi) modulus.

REFERENCES

1. T.E. Helminiak, F.E. Arnold, and C.L. Bennev, Amer. Chem. Soc., Prepr. Div. Polym. Chem., 16 (2), 659 (1975).
2. Fred E. Arnold and T. Helminiak, Private Communciation.
3. James F. Walfe, Bock H. Loo and F.E. Arnold, Am. Chem. Soc., Prepr. Div. of Polym. Chem. 19 (2). 1. (1978);
James F. Wolfe, AFML-TR-78-32 Vol. I, 1978.

APPENDIX 1

MAJOR COMPONENT SAFETY DATA STATEMENT (ARMCCM Suppl 1 to AMCR 385-17)		DATE 4 Oct 1976	
MATERIAL/COMPONENT/ASSEMBLY TRINITRORESORCINOL (TNR)		NUMBER 10153	REVISION
APPLICABLE ASPR SAFETY CLAUSE 7-104.79			
SENSITIVITY			
PA FRICTION TEST/FIBER SHOE UNKNOWN		PA FRICTION TEST/STEEL SHOE UNKNOWN	
IMPACT TEST (For comparison - Lead Azide 3", TNT 14", RDX 8") >36" 2kg wt		BUREAU OF MINES TEST ELECTROSTATIC DISCHARGE (For comparison - Lead Azide 0.0075 joules; igniter comp 0.21 joules; black powder >12.5 joules) >13.8 Joules	
HAZARDS			
FIRE Moderate		FLASH POINT SOLVENTS	
AUTO IGNITION TEMPERATURE Melts at 175°C		PARTICLE SIZE	
COMBUSTION PRODUCTS Toxic. When heated to decomposition evolves highly toxic oxides of nitrogen.			
FLAMMABLE LIMITS	VAPOR-AIR MIX	LOWER PERCENT	UPPER PERCENT
EXPLOSION Moderate to high depending on confinement.			
EXPLOSIVE LIMITS	VAPOR-AIR MIX	LOWER PERCENT	UPPER PERCENT
EXPLOSIVE TEMP (5 Sec)	TOXIC		
UNKNOWN	Toxic. Avoid inhalation, ingestion and skin contact.		
IN-PROCESS HAZARD CLASSIFICATION Class F 1.1			
SPECIAL REQUIREMENTS (Continue on reverse if necessary) 1. Is an amber to reddish brown powder. 2. Toxic - absorbed chiefly through the skin and through inhalation of the dust or vapor when these materials are heated. Effect on body is reduction of the oxygen-carrying power of the blood and depression of the nervous system. Chronic poisoning occurs more frequently than acute, in the form of anemia, moderate cyanosis, fatigue, slight dizziness, headache, insomnia and loss of weight. 3. May cause irritation of the nose and throat, nausea and vomiting and complaints related to the nervous system. Prolonged chronic exposure may result in damage to the liver and kidneys.			
SHIPPING/STORAGE CLASSIFICATION OF ITEM WHEN PACKAGED IN ACCORDANCE WITH APPROVED PACKING DRAWINGS			
AMC HAZARD CLASS F 1.1		AMC COMPATIBILITY GROUP D	
DOT BILL OF LADING CLASS Class A Explosive		DOT CONTAINER MARKING High Explosives - Dangerous D.O.T	

APPENDIX 2

LIST OF PBT SAMPLES SENT TO THE UNIV. OF MASS.

Polymer Code	Fiber Sample Code	Good Sample ⁽¹⁾ (Sample Length /No. of Fil)	Transient ⁽²⁾ Sample (gm)
PBT2122-53 (IV = 14)	27554-6-1	18 Meter/5 Fil	0.160 gm
"	27554-6-2	15 " /5 "	0
"	27554-6-3	11 " /5 "	0.149 gm
PBT2122-57 (IV = 18)	27554-9-1	10 " /5 "	0.131 gm
"	27554-9-3	5 " /4 "	0.030 gm
"	27554-9-5	36 " /5 or 4"	0.119 gm
"	27554-9-6	17 " /4 "	0.051 gm
"	27554-9-7	21 " /4 "	0.037 gm
"	27554-9-10	17 " /4 "	0.113 gm
"	27554-9-11	7 " /4 "	0.056 gm

Notes: (1) Good samples mean that they were taken after the spinning conditions reached steady states.

(2) Transient samples mean that they were taken before spinning conditions reached steady states during changes of the parameters, and the properties are not evaluated.

Interoffice Memorandum

APPENDIX 3

TO (Name and Location)	DATE
Dr. Eui W. Choe	Nov. 4, 1977
FROM (Name and Location)	REFERENCE NO.
M. A. Sieminski	MAS-77-171

Sanction: 09070-17
Samples: 37-39 10/77

Subject: Orientation in PBO Samples

The following samples

26085-9 11.5% PBO/MSA fibers
25613-50 Film dried @ room temp.
25613-50 Film dried @ 80°C

were received for microscopical examination to determine whether they showed signs of orientation.

The following observations were made:

26085-9. Fibers are opaque. Give no indication of orientation.
25613-50. In conosopic observation, both films show a centered acute bisectrix figure which indicates they are well oriented.


M. A. Sieminski

MAS:cad

Interoffice Memorandum

APPENDIX 4

TO (Name and Location)	DATE
E. W. Choe	Nov. 4, 1977
FROM (Name and Location)	REFERENCE NO.
Ian L. Hay	ILH-77-42

Subject: Structure of PBO Films

Project: #09070

W.R.: #21554

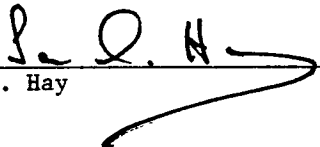
Samples: 25613-50 Room Temp dried
25613-50 80°C dried

X-Ray: 313-317C

Wide-angle X-ray patterns were taken of the two films in three mutually perpendicular directions namely normal to the film plane and in two directions parallel to the film plane. With the X-ray beam normal to the film plane a completely unoriented pattern was obtained while with the beam parallel to the film plane the equivalent of a fiber pattern was observed in each case.

These patterns are those typically obtained from a film which has so called planar orientation. The best analogue to this orientation is a mat of oriented fibers in which all of the fibers lie in the plane of the film but have no preferred direction in this plane. Although the paucity of reflexions from PBO make it difficult to interpret the patterns completely unambiguously they are consistent with the molecular axis lying preferentially in the plane of the film. It is more difficult to make an estimate of the degree of orientation, (i.e., in the fiber mat analogy how well oriented individual fibers are), but the room temperature film is closer to that of the Carnegie Mellon fibers (see ILH-77-29) and that of the 80°C film closer to that of our wet spun fibers (ILH-77-23).

(Note. Sample #26085-9 11.5% PBO/MBA Fibers was not examined.)


Ian L. Hay

ILH:cad